University of Bath

UNIVERSITY OF BATH

PHD

An inertial sensor system for analysing human movement

Fogg, Erica J.

Award date:
2006

Awarding institution:
University of Bath

Link to publication

An Inertial Sensor System for Analysing Human Movement

Submitting by

Erica J. Fogg

for the degree of PhD

of the University of Bath

2005

COPYRIGHT

Erica J. Fogg

Abstract

The introduction of micro-electro-mechanical systems (MEMS) in recent years has shown the potential to revolutionise everything from cell biology to car airbags. The second largest sales volume among MEMS devices is the accelerometer. These accelerometers are typically small, light, inexpensive, and provide measures of tilt, motion, vibration and shock of an object to which it is attached. An inertial sensor system (INS) is typically comprised of accelerometers and gyroscopes, and measures accelerations and orientations. This type of motion analysis system may be a viable alternative to mainstream motion capture systems. An investigation was conducted into the design and development of an MEMS inertial sensor system with regard to gaining an understanding of the potential to measure human movements.

A MEMS inertial sensor system was designed and built which met a number of the required specifications. It measured accelerations and angular rates in three dimensions with adequate measurement ranges, at a bandwidth of 50 Hz. A rigorous procedure for calibrating all of the sensors was developed and the resultant calibration parameters were verified through a series of experiments.

The performance and potential of the MEMS inertial sensor system was demonstrated through a number of experiments. The response of the accelerometer and gyroscope sensors were characterised and the performance of the gyroscope with respect to time and temperature was investigated. More importantly, an understanding of the potential of the system to measure a number of kinematic parameters that describe human movement was demonstrated. The parameters investigated were the points of contact and take off, contact frequency, horizontal velocity and distance travelled. Although the movements investigated in this study were basic locomotive movements, it was suggested that with further work, the system would have the potential to measure the technical aspects of athletic events such as the short sprints.

Acknowledgements

For their valued contribution to this thesis, I would like to thank the following:

My supervisors: Dr Robert Watson for the opportunity to study for this degree and for the experiences gained in the process, for constant support, ideas and solutions, and for his ability to keep my spirits high, always; and Dr Aki Salo for his dedication to the project, for his meticulous supervision, and his guidance with my practical experiments.

Mr Michael Thomas for his continuous assistance throughout, for his kind words of encouragement and his genuine belief that I could do it.

My friends during my time in Bath, particularly my training partners for providing valued companionship and a means of escape from the rigours of my work.

My family for their love and interest; Julian for love, support, tolerance and encouragement; and Nana, I dedicate this to you and wish you were here to celebrate.

Table of Contents

List of Figures

Chapter 5

Chapter 6

Appendix A

Appendix B

List of Tables

List of Abbreviations

AC	alternating current
A/D	analog to digital converter
CCD	charge couple device
CODA	Cartesian opto-electronic dynamic anthropometer
CoM	centre of mass
DC	direct current
DGPS	differential global positioning system
DLT	direct linear transform
EiMU	embedded inertial measurement unit
EKF	extended kalman filter
EMG	electromyography
EMI	electromagnetic interference
FES	functional electrical stimulation
FOG	fibre optical gyroscope
FS	full scale
FSR	force sensitive resistors
GNSS	global navigation satellite systems
GPS	global positioning system
GRF	ground reaction force
HMD	head mounted display
IC	integrated circuit
IMU	inertial measurement unit
INS	inertial navigation system
LCD	liquid crystal display
LED	light emitting diode
MARG	magnetic, angular rate and gravity sensors
MEMS	micro-electro-mechanical systems
NED	north east down
PC	personal computer
PCB	printed circuit board
PIC	programmable integrated circuit

PWM	pulse width modulation
RLG	ring laser gyroscope
RMS	root mean square
RTD	resistive temperature detector
SF	scale factor
SPKF	sigma points kalman filter
ToF	time of flight
UKF	unscented kalman filter
WSLR	weighted statistical linear regression

Chapter 1 Introduction

1.1 Introduction

This chapter introduces the research study. Firstly, a brief description of the evolution of the micro-electro-mechanical systems (MEMS) devices, the various types available, and some examples of their uses are presented. The virtues of the MEMS accelerometer sensor are characterised, and following this, the motive for carrying out the research study is outlined. It is clear that MEMS inertial sensors have the potential for capturing human movements and in particular are proposed to be used to analyse sprinting technique. The second section reviews the current motion analysis techniques that are used to capture human movements. The limitations of these techniques are highlighted against the merits of an inertial sensor system. The contribution of this research in the form of the main aim of the thesis is defined along with the objectives required to achieve this aim. Lastly, a brief description of the thesis layout is presented.

1.2 Background

Interest in the development of MEMS devices has increased rapidly since the early 1990s. In the most general sense, MEMS attempts to exploit and extend the fabrication techniques developed for the integrated circuit (IC) industry. This typically involves sensors or actuators containing mechanical elements such as beams, gears, diaphragms, and/or springs being added to the electrical, optical, fluidic and/or chemical elements [1]. The result is an integrated microsystem for the perception and control of the physical world. The resulting products can respond to numerous types of input such as chemical, light, pressure, vibration and acceleration. These devices are smaller, faster, cheaper and consume less power than conventional machines used, making their applications virtually unlimited. The first commercialised MEMS device appeared in the automotive industry as a sensor to activate the deployment of an airbag under crash conditions [2, 3]. These devices are now driving revolutionary changes in other industries such as communications, aerospace, defence, electronic, medical, consumer and exploited further in the automobile industry. For example, every time an ink jet printer is used, an MEMS device containing microscopic chambers connected to ink filled chambers pumps the ink to create a high-definition

print [1, 4]. If you visit someone in hospital, their blood pressure might be monitored by a disposable MEMS pressure transducer or their drugs delivered by an MEMS based system [5]. Today's high definition television and compact computer display projectors are outfitted with millions of microscopic MEMS mirrors that provide higher resolution pictures [6]. Fiber optic MEMS components have been utilised as optic switches offering the advantages of being five times smaller and up to 20 times faster than traditional optical relay-switches [7]. In the future, MEMS will be used to shrink the electronics of a mobile phone to fit inside a wrist watch, to enable implantable human monitoring devices and reduce the size and expense of diagnostic and therapeutic equipment such as microfluidic devices for blood and DNA analysis.

The second largest sales volume among MEMS devices after pressure sensors is the micromachined accelerometer [8]. As with all MEMS devices the accelerometer has several attractive attributes which makes them applicable to a vast array of applications [9-11]. The sensors require a low voltage supply and offer a low current drain, which enables them to be powered by batteries. They are small, light and inexpensive and are capable of measuring a wide bandwidth and have a low noise floor, which enables small acceleration signals to be resolved. The integrated electronics onboard the chip provides a more stable and robust signal output and reduces the amount of signal processing circuitry required. An inertial accelerometer can potentially measure the tilt, motion, vibration and shock of the object to which it is attached [12]. The large volume demand for accelerometers is driven by the automotive industry [13]. These sensors are used to activate safety systems such as stability systems and electronic suspension, antitheft, occupant detection as well as airbags. Their uses have extended to biomedical applications for activity monitoring; numerous consumer applications such as active stabilization of picture in camcorders, head mounted displays and virtual reality, joysticks, laptops, two dimensional mouse [14], sports equipment and personal navigators; in industrial applications such as robotics and machine and vibration monitoring [15]; in the shipping industry for tracking and monitoring mechanical shock and vibration during transportation and handling of equipment or goods [16]; several military applications, including impact and void detection, safing and arming in missiles. Further applications include the use of high precision accelerometers in self-contained inertial navigation and guidance systems [17], seismometry for oil exploration and earthquake prediction, and

microgravity measurements and platform stabilization in space [18]. These devices are also fast becoming viable alternative to mainstream motion analysis systems for the use in the field of biomechanics for human movement measurement.

The fascination of the understanding of human movement has given rise to speculation and discussion in a variety of biomechanical research activities. Much of the work can be categorised although not exclusively into the following research interests of orthopaedic, clinical, and sports. The field of orthopaedic includes the monitoring of the rehabilitation and recovery of patients after strokes, surgery, injuries or accidents [19], the understanding of the mobility abnormalities of patients with disorders, the development of prostheses and orthoses for amputee patients [20], and the understanding of physical behaviour [20]. Clinical research can involve for example, gait analysis [21], the understanding of the sequences of movement that constitute trips and falls, activity monitoring [22], the understanding of the mobility problems of the elderly [23] and posture and balance [24]. The research interest in sports largely involves monitoring muscle activity, research and design of materials and equipment, the simulation modelling of particular movements, gaining insight into the prevention of injury, and analysis of sports techniques to help improve sports performance [25-27].

The analysis of sports technique is where the interests of this thesis lie. It is widely understood that sports technique substantially affects performance. Technique can be defined as the pattern and sequence of movements that the athletes use to perform a sport skill [28]. The purpose of analysing technique is to reveal trends such as movement timings and key sequences, to monitor skill progression, to highlight physical limitations, to highlight fundamental principles within the sport, and to illustrate the critical factors that are associated with optimising performance and preventing injury [29]. The majority of the best athletes in the world, no matter what their sport, use a technique which appears smooth, coordinated, graceful and is an extremely efficient use of their physical abilities. Although a sports coach plays a vital role in analysing technique the human eye cannot see enough and the brain cannot remember enough information to provide the valuable feedback to strive towards improving technique. Therefore, various motion analysis systems that capture human movement are being utilised frequently and widely today.

Inertial sensor systems using MEMS sensors are gaining in reputation of being a viable alternative to the more popular, well established motion analysis systems. The small size and light weight means they are suitable as body worn sensors, being easily attached to athletes and without cumbrance. The sensors offer the potential to be portable since they can be battery powered enabling data collection to be carried out in a natural training environment. The size and potentially the latency of the MEMS sensors are reduced by the on-board conditioning circuitry increasing the possibility of real-time feedback. This provides the ability to analyse training during or soon after completion. The rich information supplied by the sensors offers the potential to provide adequate measurements of the majority of the human movements that describe the techniques in sports, for example, sprinting. All of these characteristics contribute to an advantageous motion analysis system.

1.3 Review of Current Kinematic Motion Analysis Technology

1.3.1 Introduction

The majority of the biomechanical research activities listed above involves experimental work that requires motion analysis techniques. There are many measuring techniques available today which are highly developed and allow the quantification of kinematic, kinetic and other aspects of human movement such as pressure distribution, strain measurement and electromyography (EMG). The interest of this research is concerned with the kinematic measurements of human movement. The main motion analysis techniques for measuring the kinematics of movements are reviewed with respect to a number of parameters. These are their accuracy and resolution (smallest change detected), responsiveness in terms of sample rate and latency, robustness as a measure of the system's susceptibility to noise and interference from outside sources, usability in terms of range of operation, working volume and ease and time to set up, and finally the cost of the systems.

1.3.2 Acoustic Systems

Acoustic systems such as Logitech trackers (VR Depot) and the Gesture and Media System (GAM) (Acoustic Position Research (APR)) [30, 31], use the transmission and sensing of high frequency ultrasonic sound waves to determine position. These systems are based on the principle of time of flight (ToF) of signals travelling at the speed of sound through the air to determine the distance between transmitters and receivers. The systems are limited by multipath reflections due to hard surfaced objects such as walls and floors within or near by the tracking area. The emitters need to be omni-directional so that they can be positioned and orientated arbitrarily within the tracking area and a line of sight between emitter and receivers is required. They suffer noise interference, which can be reduced by resonating at high frequencies, offering the possibility of higher resolution. However, this reduces the range due to an increase in transducer size and frequency attenuation of sound in air after 40 kHz depending on humidity [32]. The performance can be affected by environmental factors such as wind, temperature, humidity and air currents causing uncertainty in the speed of sound [33]. Therefore the system operates more reliably in a laboratory environment. The sampling rate and latency of the systems are limited by multipath reflection, tracking volume, frequency and the environment.

1.3.3 Magnetic Systems

Magnetic (or electromagnetic) systems such as MotionStar (Ascension Technology Corporation) and Liberty (Polhemus) [34, 35], rely on sensor measurements of the local magnetic field vector to track position and orientation. Typically, a fixed source unit generates three orthogonal electromagnetic fields by actively inducing excitations of three orthogonal coils of wire wound around a common core in sequence. The system can either have an active alternating current (AC) or static direct current (DC) source [32, 36]. An AC source emits continuously changing magnetic fields producing circulating currents (eddy currents) which in turn produces a secondary magnetic field that distorts the emitter field pattern. A DC source emits a sequence of pulses. The sensor units contain electromagnetic coils and three orthogonal magnetic sensors (such as magneto-resistive, magneto-inductive, micro-mechanical and hall-

effect sensors) for AC or DC systems, respectively, and provide a three dimensional vector defining the position and orientation with respect to the excitation. Pulsed DC systems are preferred over AC systems because of the reduction in transient distortions (since eddy currents are created only when the magnetic field is changing i.e. at the beginning when the pulse is sent) but the system must wait for the initial transient to subside and the field to reach its steady state. The major disadvantages of these systems are ferromagnetic disturbances, limited range and volume, latency and slow update rate [32]. The effects of ferromagnetic and conductive material within close proximity to the source induce eddy currents that act as unwanted source units and cause disturbance to the magnetic field. The most common approach to address these distortions is to ensure that the working volume contains no offending objects. The system may require frequent recalibration in new testing environments. The range of operation (typically 3 m) and volume is severely limited by the strength of the magnetic field which diminishes with distance [32, 36]. The latency and low update rate are caused by the time required in waiting for the magnetic field to reach its steady state after a pulse is sent. Typically, the receivers are sampled at rates approaching 240 Hz for 16 sensors with a latency of 3.5 ms [34]. The sensors are normally tethered to the host computer which may be cumbersome to the user and restrict movements. Despite these problems, there are some noteworthy advantages to using a magnetic approach for tracking human movements. Firstly, the size of the user-worn component can be quite small. Secondly, the magnetic fields pass right through the human body, eliminating line-of-sight requirements. Thirdly, you can use a single source unit to simultaneously excite and thus track multiple sensor units. The type of motion analysis system using this technique claims to provide accurate and reproducible six dimensional tracking of the body in real time to the resolution of 0.0012° and 0.04 mm and accuracy of 0.15° and 0.76 mm [34]. They are simple to set up and operate, they have no moving parts and so are very durable. The systems typically cost around £21,000. Ascension technology also offers the Minibird 500 which is the smallest available magnetic tracker with a size of 10 x 5 x 5 mm [35]. However, it has to be wired and the base unit is fairly cumbersome.

1.3.4 Mechanical Systems

Mechanical systems such as body tracker II (Puppetworks) and X-IST Fullbody tracker (nodna) [37, 38], typically involves some form of a direct physical linkage of rigid mechanical pieces interconnected with electromechanical transducers such as potentiometers or shaft encoders. These are often incorporated into a re-sizable exo-skeletal suit and the sensors are adjusted so that they are positioned about the joints of interest. The amount of deformation is proportional to the change in angular displacement, which is measured during movements and can be sent wirelessly to a host computer. The mechanical system offers the advantages of simplicity, are precise and responsive to user inputs, no external source is required, no interference from external sources such as light or magnetic fields and an increase in capture range is achievable (such as cameras or wires). However, they only measure rotations and thus absolute positions in three dimensions are required to be derived through appropriate software, the equipment must be adjusted regularly and suffers from wear, is heavy and cumbersome [32, 36]. Typical resolution of the systems is 0.15° with an update rate of 240 Hz [37]. The system can measure up to 18,000°s^{-1} and a standard system costs roughly £24,000 [37].

1.3.5 Optical Image Based Systems

Optical systems can be initially categorised by the type of acquisition. The two types of acquisition are manual and automatic. Manual acquisition involves cinefilm [39, 40] or video-based [41-43] systems that capture and record images in either analogue or digital format. The majority of cameras comprise of a lens system (lens, aperture and shutter), a charge couple device (CCD) containing an array of photosides to convert the intensity of the light entering the camera into electronic signals and a recording medium. Analogue cameras use recording formats such as VHS, S-VHS, 8mm or Hi-8 and store the information as a magnetic pattern on the tape with a horizontal resolution from 240 to 400 lines. Digital cameras (DV or Digital-8) store information on tape, DVD or directly into memory via Firewire Port or Ethernet with an increased horizontal resolution of over 500. The standard sampling rate for video cameras is generally fixed at 50 Hz or 60 Hz, for Europe and US, respectively,

although high speed cameras can also be used. The movement can be recorded without markers [44, 45] or with passive (reflective spheres or tape) markers. Passive markers reflect external ambient light. Recording with suitable lighting gives a good contrast between the markers and the rest of the objects i.e. the human limb in the images. Once the images are recorded, they are digitised (if not already) and the coordinates of the marker locations can be identified either manually or by a semi-automatic image analysis software application such as Peak Performance (Vicon Peak), Target and WinAnalyse (Mikromak). The marker locations are reconstructed within the reference frame of the movement space normally by the direct linear transformation (DLT) [46] or scaling. This technique requires the synchronised digitised coordinates of body landmarks from images obtained from one camera or at least two cameras for two and three-dimensionally analysis, respectively [47]. A typical calibration routine involves the collection of static and/or dynamic data of a calibration object such as frame, wand or cube with markers at known coordinates. Synchronisation of multiple cameras can be achieved by genlocking or by using a timing device in the field of view of each camera. More information regarding the equipment and procedures can be found in the literature [48, 49] and reviews of camera systems can be found in [50-52].

Alternatively, an automatic system may be used. This involves a detection system which tracks the location of markers automatically providing three-dimensional movement information in real time. The two types of detection systems available are a camera based system such as Eagle or Hawk system (Motion Analysis Corporation), Mac or ProReflex (Qualisys) [53] and Vicon MX (Vicon Peak) [54-56] or a scanner unit system containing a number of sensors such as CODA (Charnwood Dynamics), SELSPOT (Innovision Systems Inc) [57] and OptoTrak (Northern Digital). The camera based system tracks passive markers and follows the requirements with regards to the number of cameras, calibration, synchronisation and lighting conditions mentioned above. The availability of specialised camera units allow greater number of pixels and higher frame rates in excess of 50Hz due to reductions in data processing within the camera and transfer rates via ethernet ports. A scanner unit, such as CODA, typically contains a linear array of three sensors in fixed positions that receive the signals from active markers. Active markers are infrared light emitting diodes (LED's), which are triggered and pulsed sequentially. Knowledge of when and which

LED has emitted a signal is used to triangulate the origin of the signal to determine the position of each marker. These systems have been typically limited to movements that do not involve a wide range of movement.

Traditionally, 16mm cinefilm was used because it offered a higher image resolution than video [58]. Due to developments in technology, digital cameras and computer based analysis software, the difference in resolution is somewhat reduced between cinefilm and video based systems. Commercially available automatic video based systems have an accuracy between 0.1 mm to 0.6 mm [51]. Automatic active marker systems offer a similar level of accuracy between 0.1 mm to 0.2 mm from CODA and OptoTrak, respectively, typically within a 3m field of view [51]. Automatic motion analysis systems offer increased acquisition rates in excess of the traditional 50 Hz but invariably depend on the number of markers being tracked. For example, CODA can achieve an acquisition rate of 800 Hz with only 6 markers but this decreases to 100 Hz as the number of markers increases to 56 [59]. The ProReflex system (Qualisys) offers the highest acquisition rate at 1000 Hz [60]. Although the automatic systems calculate information in real-time the latency can be from 3 ms to 5 ms for the active marker systems. Typically, optical motion analysis systems are inhibited by sunlight which causes shadowing, reflections and loss of contrast of the markers often restricting their use to a laboratory. Video based systems are not restricted by requiring markers or by a specified number of markers. Active markers are heavy and more expensive than passive markers since they require battery packs to be placed somewhere on the subject with wires connected to the markers. The systems that stipulate that markers are required are precluded for use in sports competition. All optical motion capture systems require a line of sight for maximum accuracy [32, 48, 50-52]. Passive marker systems also suffer from marker blurring caused by markers getting to within to 2mm of each other [51], crossing paths or becoming non visible. This may require a large amount of post processing since points have to be manually estimated. Automatic acquisition with passive markers may interpolate the blurred or occluded markers to alleviate this limitation. Active markers have the advantage that they are intrinsically identified by virtue of their position and in a time multiplexed sequence but still require a line of sight for maximum accuracy. However, they only track markers rather than the image.

Both types of markers when attached to the skin may experience movement between the skin and the underlying bone [61]. Placement of the markers requires a level of experience and knowledge of anatomical body landmarks. In all cases the subjects are required to wear clothing to allow the points of interest to be visible for capture or for positioning markers. Most camera based systems are typically laborious to set up as they require multiple cameras to be positioned appropriately, calibrated and synchronised. Whereas, scanner systems typically take less time to set up since they are factory calibrated, and only one scanner unit is required for three dimensional movements. Both systems offer wireless tracking of motion. A single scanner system typically has a range between 2 m and 6 m in front of the measurement unit and a width and height of 1.5 times. The measurement volume may be extended by adding additional measurement units. Camera based systems typically have a bigger range up to 70 m. However, the field of view can be reduced by zooming in and thus is likely to increase the accuracy of the system. All optical systems find linear and angular displacements directly but the process of differentiation to yield acceleration can introduce a large amount of noise [57]. All optical systems are expensive in comparison with the other available techniques mentioned. For example, the ProReflex system (Quailsys) starts at £20,000 for a basic two camera system, Vicon offers a range of products from £48,000 to £90,000 depending on the frequency of movements and resolution required and Motion analysis corporation systems such as the Falcon costs around £18,000 and the Eagle or Hawk from around £70,000. For active optical capture systems the Optotrak costs £32,000 to £38,000 for only one sensor and 24 markers, respectively, and a basic CODAmotion system starts at around £40,000, with the added costs of expensive markers.

1.3.6 Inertial Sensor Systems

Inertial sensors have been used since the 1920s for guidance, navigation and control purposes on ships, submarines and aeroplanes. Inertial navigation is the process whereby the measurements provided by inertial sensors, accelerometers and gyroscopes are used to define the rotational and translational motion of the vehicle or object within the inertial reference frame. Although advancing technologies have improved the performance and reliability of the sensors over the years, they are still

bulky and heavy. The driving force to achieve equivalent performance at lower cost caused the advent of MEMS inertial sensors [17]. The principle of inertial navigation can be applied to measuring human movements. Their small and compact size is light and means they are more suitable as a wearable device to a variety of applications such as biomechanical analysis.

The MEMS inertial sensors are available in chip form which means the typical size of an inertial measurement unit (IMU) can be quite small and light. The sensors are completely self-containing so do not require any external sources (other than power), and therefore have minimal range restrictions and no line of sight requirements. They respond to both frequency and intensity of movements, without being sensitive to external interference such as light and ferromagnetic objects. The latency of the system potentially depends only on the computational demands of the data processing and filtering algorithms required since there is no dependency on a source. The system, therefore, displays the potential to provide real-time information at relatively high sample rates. The system has the potential to transmit data by wireless means from the subject to the host computer. The sensors typically cost less than £5 and £30 each for the accelerometers and gyroscopes, respectively [62, 63]. The cost advantage over the other technologies due to the small size, mass production and low power requirements is huge.

However, the inertial sensors have some disadvantages. The outputs of the sensors may contain errors and could be caused by noise, inherent drift of the stationary output, nonlinearity of the output or temperature effects. Also, the absolute orientation is difficult to measure because the accelerometers are sensitive to both gravitational acceleration (static) and linear acceleration (dynamic) which are difficult to separate. The gyroscopes offer a solution by integration of the measured angular rate output, but due to the errors in the output, the resultant orientation is only reliable for short periods. These errors are largely due to the instability of the output of the gyroscope whilst stationary [56]. Integration is also required to derive positional information from the measured accelerations. The integration procedure requires the knowledge of initial conditions and to be implemented over a short duration to limit the propagation of errors. The movements of interest do not always offer periods of inactivity to determine accurate initial conditions.

Commercially available inertial systems available are Angularis VR-360 (Angularis Inertial Technologies) [64], InertiaCube3 (Intersense)[65], MT9 (Xsens) [66], MotionPak (BEI Systron Donner) [67] and Triax100 (Dynastream and Nike) [68]. Commercially available systems such as the InertialCube3 and the MT9 offer an accuracy to the nearest degree and a resolution of 0.03 to 0.05°. The sample rates are typically 180 Hz and 512 Hz respectively with a latency of less than 6 ms. The measurement ranges are $\pm$ 900°s^{-1} to 1200°s^{-1} and $\pm$ 20 g. The InertialCube can be wireless and works within a range of 30 m tracking a maximum of 4 sensors. Both systems are very small less than 5 cm^3, weigh less than 0.035 kg and cost around £1,500. They withstand shock up to 500 g when powered. They are powered by 5.5 V and typically draw 40 mA of current. Crossbow Technologies has developed the DMU-6X inertial measurement unit but is quite large at 76 cm^3 and is also expensive.

1.3.7 Summary

Each of the techniques described have their limitations. These limitations include the sensors or markers, the capture range, the environment, expense, the amount of equipment required and the time involved in setting it up. The sensors or markers required to be attached to the subject are often bulky, heavy and sometimes tethered. The non-expert positioning of the sensors or markers, unwanted movement and occlusion of the markers or sensors can cause accuracy errors. The capture range is limited by the field of view, strength of signals and tethering and limits the type of movements that can be analysed. The environmental interferences of light, wind and humidity and neighbouring magnetic objects often restrict the use of the systems to a dedicated laboratory space. Moreover, measurements of movements made in such restricted environments may not reflect the true functional ability of the subject. The systems reviewed can cost between £1,500 and up to and beyond £90,000. The numerous pieces of equipment required can be cumbersome to transport, time consuming to set up and require recalibration in comparison to an inertial sensor system. This often means the equipment remains set up in a dedicated laboratory. The MEMS inertial sensors offer the potential to avoid the majority of the limitations outlined for the other motion analysis techniques and are fast becoming a viable alternative. The sensors are small, light, inexpensive, self-contained, require low power and offer the potential to be portable. They can potentially measure parameters such as tilt, motion, vibration and shock which can be used further to describe human movements. However, it is uncertain how much the choice of inexpensive MEMS sensors will compromise the performance of the sensors.

1.4 Contribution of this Research

The focus of this thesis is outlined by the following aim:

To design and develop a three-dimensional motion capture system based only on MEMS sensors and to subsequently gain an understanding of the capabilities and potential of the system to measure useful kinematic parameters.

To achieve this aim the following objectives are to be met:

To design the system to meet a number of requirements such as providing a sufficient dynamic response and update rate, robust within the environment, not cumbersome, portable, and low cost.

To develop a procedure for calibrating the individual sensors.

To evaluate the performance of the sensors with regard to resolution, precision and drift.

To evaluate the potential of the system to provide reliable and accurate kinematic information, based on raw measurement data.

To tailor the design of the system to be used daily in the natural training environment for measuring the technical aspects of athletic events, in particular the short sprints.

1.5 Thesis Organisation

This thesis contains seven chapters. Chapter 2 explores the background information and surveys the relevant literature surrounding MEMS sensors. Chapter 3 outlines the specification for the inertial sensor system and a detailed description of the design of the inertial sensor system. Chapters 4 to 6 present the results of the research study. Chapter 4 presents the results from the experiments conducted to develop and verify the system. This involved the calibration routine, verification of the derived calibration parameters and axes arrangement of the sensors, and also the investigation into the variation of the gyroscope zero bias drift over time and temperature. Chapter 5 presents the results from the experiments conducted to gain an understanding of the potential of the system to identify temporal parameters. Chapter 6 presents the results from the experiments conducted to gain an understanding of the potential of the system to provide spatial parameters. Finally, Chapter 7 states the conclusions and recommends possible directions for future work.

Chapter 2 Review of the Literature

2.1 Introduction

This chapter reviews the literature to date that have used accelerometers, gyroscopes and magnetometers to measure human movements. Other body worn sensors used for the measurement of human body movements are inclinometers, pedometers, actometers, goniometers and foot switches. These sensors have been found to be associated with all or some of the following attributes and thus, have not been considered in this research study. These attributes are cumbersome, inaccurate, unreliable, slow response, require careful placement and frequent adjustments and not very robust. The first section of this chapter describes the types of devices used, the number of sensors required and their arrangement, the position of the sensors and the possible sensor calibration methods. The next section outlines the possible measurable parameters and how these were achieved. The third section outlines the variety of applications the sensors have been successfully implemented in. A description of the reported performances of the sensors in terms of the likely errors follows next. The fifth section collectively presents the processing procedures such as the decomposition of the acceleration signal, possible model assumptions and the types of orientation representations, reference frames and the rotation sequences available. Finally, the filtering algorithms implemented to optimise the sensor outputs and to provide the 'best' overall system estimates are described.

2.2 Inertial Sensors

2.2.1 Types of Sensor

The vast majority of investigations reviewed have used either piezoresistive accelerometers [20, 22, 54, 61, 69-88] or differential capacitance accelerometers [24, 89] and specifically those manufactured by Analog Devices [90-105]. Both of these types of accelerometer respond to gravitational acceleration as well as to acceleration due to movement. The most commonly used gyroscope has been the vibratory type [95, 102] and specifically the 'Gyrostar' sensor manufactured by Murata [54, 56, 74, 86, 87, 90, 92-94, 96, 97, 99, 100, 103-111]. There are several

types of electronic compasses currently available from fluxgate, magnetoresistive and magnetoinductive [112]. The investigations reviewed have used either fluxgate compass [89, 113, 114] or a magnetoresistive compass [115] and specifically those manufactured by Honeywell [92, 95, 103-105]. It is evident that the sensors described by Analog Devices, Murata and Honeywell have been extensively used for capturing human movements. This highlights the likely suitability of these sensors to potentially form the MEMS sensor system for this research study.

2.2.2 Number of Sensors and the Combinations

The first accelerometry investigations for capturing human movements began in the 1960s and 1970s. The sensors measured vertical and horizontal acceleration components as close as possible to the centre of gravity and used a pair of tandem sensors to measure the angular accelerations of the shank [116, 117]. Further to these studies, the theory behind multiple accelerometer systems to resolve full segmental kinematics of single segments was explored and represented a promising method to study limb motions and joint forces. The number of sensors used varied from six [21], to eight [118], nine [40, 69] and twelve [85, 101, 119]. The accelerations were measured from multiple accelerometers positioned appropriately on a rigid body (not necessarily at the centre of mass of the rigid body segment) and were required to solve the nonlinear acceleration equation reported by a number of authors [21, 69, 70]. From this equation the angular acceleration and velocity of the rigid body could be found directly [69]. Using these parameters it was possible to derive angular position and therefore the linear acceleration component can be extracted from the measured acceleration [70]. Padgaonkar et al. [69] reported that nine sensors were required to determine the angular acceleration and angular velocity vectors, arranged as three tri-axial units in three positions per rigid segment. Morris et al. [21] reduced the number to six or two tri-axial units since the nonlinear acceleration equations were treated as differential equations. On the contrary, Van den Bogert and Read [85] and Baseli [101] extended the number of sensors by three in order to avoid the singularities introduced by Padgaonkar et al. [69]. It is evident that accelerometers are perhaps a crucial element of any potential MEMS sensor system. An appropriate arrangement of a set of accelerometer can provide enough information to measure full segmental

kinematic parameters of human movement. However, the large number of sensors required per segment will involve a large number of attachment sites, potentially longer set up time, more signals to collect and digitise, plus the algorithms to extract the desired parameters are likely to be computationally demanding. Thus, many authors have sought solutions to reduce the number of sensors required.

Reductions in the number of sensors have been achieved by various methods. These methods include introducing model assumptions such that movements occur only in two dimensions [120] or interest in particular parameters causing some of the sensors to become redundant [22, 24, 73, 76, 78, 98, 121-123]. Other methods of reduction are implementing the process of integration [70, 124] or using known parameters [72] and operators [125]. Further reductions are to be expected [126, 127], Lotters et al. [126] introduced the theory behind the development of a tri-axial accelerometer using a single mass in a single housing unit which has been used experimentally [24], and more recently the commercial availability of Analog Devices tri-axial accelerometer following their press release in January 2005 [127]. The majority of these solutions come with limitations. Perhaps the most suitable solution not mentioned would be to introduce another type of sensor.

It wasn't until 1996 that miniature gyroscopes were first introduced for the direct measurement of angular velocity [128]. Traditionally, gyroscopes have been used extensively in navigation systems in planes and ships, but they are bulky, expensive and composed of components that have a short life time. Recently, manufactures have utilised the advantages of MEMS to produce miniature gyroscopes that offer similar advantages to its compatriots, the accelerometers. Miniature gyroscopes are attractive because they reduce the number of accelerometer sensors required since they measure angular velocity directly. They are also insensitive to gravitational acceleration and therefore can be positioned in an arbitrary orientation with respect to the gravitational vector. Tong and Granat [129] showed experimentally that two different positions anywhere along the same plane on the same segment of a rigid body gave an almost identical signal.

The gyroscope sensors have been documented in investigations as the only sensor [56, 106, 107, 109, 129] or in combination with accelerometers [54, 55, 74, 81, 86, 87,

93, 94, 97, 99, 130, 131]. Baten et al. [86] used one tangentially orientated accelerometer and one gyroscope for preliminary investigations into measuring back angle inclination. Veltink et al. [87] described a dynamometer which could in principle be positioned in different places to measure segment inclination and angular velocity from two accelerometers and one single gyroscope. Heyn et al. [130] implemented the configuration outlined by Willemsen et al. [120] of one gyroscope and four accelerometers per segment and used the formulas also outlined by Willemsen et al. [132] to obtain the moments about the knee joint. The same configuration and method was used later by Nene et al. [55] and then by Mayagoitia et al. [54]. Williamson and Andrews [93] and Sabatini et al. [97] only used a cluster consisting of one two-axis accelerometer and one gyroscope since the angular acceleration of each segment was not required to be measured directly. The smartsole invented by Kirtley et al. [131] used two gyroscopes and two bi-axial accelerometers.

The principles for measuring orientation and position of a moving body in three orthogonal directions using three gyroscopes and three accelerometers has been well established in the field of Inertial Navigation Systems (INS) [133-135]. Human body tracking is essentially a navigation problem with the aim of determining the orientation and position of the body segment of interest. This approach of a three accelerometer and three gyroscope arranged into one sensor unit was adopted by a number of authors [81, 90, 94, 99, 100, 136, 137]. Firstly, Luinge et al. [90] introduced just the theory for estimating orientation for the possibility of measurement of human kinematics. Baten et al. [86], Veltink et al. [99] and then Ohgi et al. [94] implemented this theory experimentally. Benbasat [100] proposed a multisensor design but with no immediate application. Vetlink et al. [137] reported the design of a tri-axial inertial sensor system combining a triaxial accelerometer and triaxial angular rate sensor into a single device. Presently there is no commercially available inertial device of this kind. Inertial sensors have also been combined with Global Navigation Satellite Systems (GNSS) (such as GPS, GLONASS) to provide a source of dead reckoning when the GPS signal was not available. Typically applications have been in avionics, marine, car navigation and more recently for pedestrian navigation [138, 139]. Terrier et al. [138] used a triaxial accelerometer and Ladetto [139] described an accelerometer and magnetometer system.

Although it has been shown that gyroscopes on their own can also provide useful information, the measurable parameters are limited in comparison to the accelerometer sensors. The sensor is best used in combination with accelerometers and together they provide a complementary mix of attributes. This combination in most cases reduces the number of sensors, only requires one attachment site per segment and the complexity of the processing algorithms is likely to be reduced.

The introduction of MEMS magnetic compasses or often named 'magnetoresistive sensors' in recent years have been documented in systems with only accelerometers [89, 115], with only gyroscopes [140], with gyroscopes and fluid inclinometers [113] and with gyroscopes and accelerometers [92, 95, 102, 105, 114, 136, 141]. Fontaine et al. [89] and Bonnet et al. [115] described a system consisting of three accelerometers and three magnetic compasses which did not require the use of external sources and integration. Careful weighting of the sensor data from the magnetic compass, with respect to the accelerometer data, handled situations with object acceleration and magnetic disturbances. Whereas Ladetto and Merminod [140] introduced a system to determine heading for localisation of a pedestrian when the GPS signal was not available. Since both gyroscopes and magnetic compasses have limitations, the rate of change from both of the sensors was compared to estimate the magnetic disturbance. In the absence of such disturbance, the continuous measurement of the heading provided information to enhance the output of the gyroscope. Foxlin et al. [113] described an inertial tracker, which incorporated three low cost solid state gyroscopes, two axis inclinometer and a two axis fluxgate compass. This work led to the commercial release of the IS-300, now formally known as Inertialcube3, a sourceless three degrees of freedom orientation tracker. The device uses gravimetric tilt-sensing to prevent any gyroscopic drift in pitch and roll, and geo-magnetic compassing to prevent any gyroscopic drift in the yaw angle [114]. Paradiso et al. [92] incorporated all three types of sensors alongside an array of other types of sensors for the design and implementation of expressive footwear. In 2002, Microstrain unveiled the 3DM-G Gyro enhanced orientation sensor composed of the three types of sensors. Bachmann et al. [95] reported that the sensor was bulky and the accuracy of the associated filtering algorithm was ± 5°. They suggested this was not acceptable for full body tracking applications. An alternative design was proposed that consisted of a

magnetic, angular rate, and gravity (MARG) sensors [95]. The system was composed of two dual axis accelerometers, three gyroscopes and one dual axis and one signal axis magnetometers arranged in three orthogonal sensing directions. Hutchings et al. [141] filed a patent using triaxial arrangements of the three types of sensors integrated with GPS signals to measure the kinematics of running. Saripalli et al. [105] developed a custom built low-cost inertial measurement unit (IMU) and magnetic compass named an embedded inertial measurement unit (EiMU) to aid the control of a model helicopter. The EiMU was comprised of three gyroscopes, two dual axis accelerometers and three uni-axial magnetometers. Luinge [136] initiated the commercialization of Xsens [66], a motion technology that offers a wireless sensor system of six inertial and three magnetic sensors with advanced signal analysis for the applications in sports, rehabilitation and entertainment markets. The addition of a magnetoresistive sensor in various combinations with other sensors is beneficial. However, the effect of the magnetic disturbance on the performance of the sensor is likely to limit its versatility somewhat. Although there are commercially available systems that utilise these sensors as part of their systems, the possible applications of these systems remain greatly unexplored.

Tri-axial accelerometer sensor units can be assembled from single or dual axis accelerometers or constructed using a single mass [126]. The theory for the construction of a three dimensional accelerometer based on only one mass with three translational degrees of freedom was presented by Lotters et al. [126]. Similar to the three dimensional accelerometer setup, a three dimensional gyroscope can be assembled using three single axis gyroscopes. A sensor unit, consisting of three uni-axial accelerometers and three uni-axial gyroscopes, approximately mounted at one point is called an inertial measurement unit (IMU). There have been a few studies which have used IMUs consisting of Analog Device accelerometers and Murata gyroscopes [100, 136].

2.2.3 The Location of the Sensors

The placement and positions of the sensors on the human body depends on the movement of interest and have been documented at the head [82, 83, 101, 113], upper body [75, 115, 136], sternum (chest) and thigh [20, 76], sternum, thigh, lower leg and

wrist [77, 80], wrist [94]. Several authors have used sensors in the lower back [24, 72, 73, 78, 82, 86, 115-117, 121, 123, 125, 142, 143], the lower limbs (thigh, shank and ankle) [21, 53, 70, 79, 84, 87, 91, 93, 106, 124, 129, 144], and on the foot [56, 73, 97, 99, 107, 145]. The lower back has been a frequently used position for placing sensors primarily because it approximately represents the centre of mass (CoM) of the body and so velocities and positions of the whole body can be derived.

The CoM is defined as the point around which every particle of a body's mass is equally distributed. In motion analysis, the CoM is typically estimated from a model based on a series of rigid, articulated body segments, which require estimates of both position and magnitude of each body segment. It is necessary to recalculate the position of the CoM using this method after each interval of time since the CoM continuously changes with time [146]. However, an alternative ad-hoc approach has been to choose a surface reference point in the proximity to where the CoM is believed to be, and estimate movements of the CoM relative to this point [78]. Any point moving parallel to the CoM will produce similar results as the CoM as far as position, velocity and acceleration are concerned. The error by choosing a surface reference point is therefore restricted to changes in the position of the reference point relative to the CoM. For gait analysis, this error can be minimised by selecting a convenient point in the lower part of the trunk. During quiet standing the whole body CoM has been located in the sacral section of the spinal cord, anterior to the segment s2, at 55-57% of body height [146]. It has been shown that the vertical acceleration component of a sensor mounted on the lower back has been proved to be the most important in the assessment of gait [77, 80, 147]. Accelerations measured at the lower back (sacrum) have allowed the identification of heel strike of each foot [72]. Although, this was contrary to Henty et al. [107] who suggested sensors positioned on the heel a more directly indicate foot contact. Overall, it is proposed that positioning the MEMS sensor system at a representative point of the CoM introduces several advantages. These advantages are minimal points of attachment, little cumbrance to the user and perhaps provides the most information from one point of attachment.

2.2.4 The Calibration Procedure

The purpose of the calibration procedure is to define the calibration parameters for each sensor in the system. These parameters are the zero bias or commonly named offset, and the scale factor. The zero bias is defined as the output of the sensors in a stationary position. In the case of the accelerometers the sensitive axis of the accelerometers is also required to be parallel to the earth's surface therefore measuring zero gravitational acceleration. The scale factor is the change in the sensor output at a rate of one measurement unit. The accelerometer sensor has been calibrated by rotation within the gravitational field [54, 72, 83, 86, 93, 95, 97, 102, 143] or by pendulum swings [81] using the static response of the sensor. The rotation within the gravitational field involved subjecting each sensitive axis to the gravitational force so that the sensors experience both ±1 g. The outputs were recorded in both positions and were used to determine the zero bias and the scale factor of the sensors.

The calibration of gyroscopes is not as well documented. The most commonly used method involved rotating the gyroscopes through known angles by hand and recording the time period to determine the sensors scale factor [54, 81, 86, 95, 97, 102], but the sensor has also been used without calibration [93]. The zero bias of the gyroscopes have been determined from periods of collected data when the sensors were stationary [86, 93, 95, 97, 102]. Tong and Granat [129] suggested using the average output over a period of 5 s, whereas Veltink [76] suggested 10 s was adequate to determine the zero bias of each gyroscope. Accelerometers have been used to help detect when the gyroscope was stationary by monitoring the low variance of the equivalent angle change of below 0.1° [93]. Williamson et al. [93] showed that finding a null prior to the experiment was more accurate than finding the null 24 hours before. The use of low-cost sensors often makes it necessary to perform the sensor calibration in-field immediately before use [102, 148]. Ferraris et al. [148] described a simultaneous calibration procedure for a sensor module containing three gyroscopes and accelerometers that could be executed anywhere. The procedure involved a simple dice roll manoeuvre and full rotations, utilising the local gravity component and known angles of rotation. The algorithm determined all scale factors and zero bias values plus the orientation of the three sensitive axes with respect to the housing. The

procedure took less than 20 minutes. This method was employed by Luinge [136]. Bachmann [102] outlined a similar procedure in his thesis. The method consisted of placing the sensor unit in a series of predetermined orientations and subjecting it to several rotations about single sensor axes. The accuracy of the calibration parameters resulting from the hand performed calibration procedure was verified by a precision Hass rotary table.

When the sensor module is placed in the desired position the sensor's reference frame nominally known as 'body' may not be aligned with the 'flat earth' reference frame (an explanation on reference frames follows in a later section) thus it is common to collect a period of data prior to an experiment to determine the relevant transformation matrix between the two coordinate systems [78, 115]. Alternatively, Smidt et al. [149] used an adjusting device for levelling the accelerometer while the subject was standing still.

It is evident that a calibration procedure is an essential routine that derives the respective calibration parameters. Without this routine the sensor outputs cannot be quantified. It is reasonable to assume the most suitable calibration procedure is the implementation of an initial accurate but perhaps laborious routine coupled with a frequently implemented, simpler, and in-situ calibration process.

2.3 Sensor Measurements

2.3.1 Accelerometer

The theoretical properties of the accelerometer signal were presented by Veltink and Boom [128]. Accelerometers measure acceleration which is made up of linear acceleration and gravitational acceleration [20, 53, 77, 128, 150, 151]. The linear acceleration can be extracted if the orientation of the sensor or module is known [132], thus eliminating the gravitational component. Then the single and double integration of the linear acceleration yields linear velocity and distance, respectively. The inertial component of the acceleration signal can be decomposed into three types of acceleration [53]. These are translation and rotational accelerations, and

accelerations due to non-rigidity (deformation) of the segment such as vibrations and muscular contractions. The gravitational component of the measured acceleration has been used to calculate inclination or tilt information [54, 128]. This property was true only under static conditions. The tilt was defined as the angles of the sensitive axes of the sensor with respect to the local vertical vector [53] and can be determined in two directions from the following equation 2-1 [78, 102, 152]:

$$\theta = \operatorname{asin}\left[\frac{a_X}{g}\right]$$

$$\phi = -\operatorname{asin}\left[\frac{a_Y}{g \cdot \cos\theta}\right]$$

2-1

Where, θ and ϕ are the tilt angles

a_x and a_y are the accelerations in two orthogonal directions parallel to the earth's surface or ground.

Alternatively, the arctangent was used in the following equation 2-2 [93]:

$$\theta = \operatorname{atan}\left[\frac{a_X}{a_Y}\right]$$

2-2

Williamson and Andrews [93] used this inverse tangent function in preference to the inverse sine function since it was less sensitive to noise and has an infinite range of inputs. The accelerometer measurements recorded prior to the commencement of the trial was averaged over 50 samples (at 100 Hz, t= 0.5 s) and then implemented in the equation above. Under dynamic conditions, if the measured acceleration was averaged for a sufficiently long period the object or subject's linear acceleration will eventually be zero (if a body was not continuously accelerating in one direction) [102], thus the resultant acceleration is equivalent to the gravitation acceleration and tilt can be determined following the equations above. The accelerometers cannot measure rotations around the vertical axis and therefore do not give a complete description of the orientation of the sensor module.

As described in the previous section, angular acceleration and velocity vectors have been determined from the direct measurement of a number of tri-axially arranged accelerometers per rigid segment without knowledge of the orientation of the leg [21, 40, 69, 70, 118, 119, 128]. More simply, assuming movements are in two dimensions, two accelerometers tangentially mounted on a rigid body at two points can determine the angular acceleration. This approach uses the property that gravity and the reference point are independent of the position along the rigid body, thus the difference in tangential acceleration experienced was related directly to the angular acceleration [54, 124]. A similar relationship, but with two radial accelerometers, measured accelerations at two points on one segment provided the square of the angular velocity [124]. Double integration of the angular acceleration from either method yields the angle of the segment avoiding the almost impossible task of separating the acceleration components [124, 128, 153]. It appeared more convenient to use the angular velocity for angle estimation, because it saves one integration step reducing the computational time and reducing subsequent propagation of error. However, the nonlinear square function prevented access to the sign of the estimated angles, which makes it unusable for angle estimation [124]. To determine the signs, an assumption concerning the sign of one of the angular velocity components must be imposed at the t=0 [70], which is always known.

Following on from the theory outlined by a number of authors [54, 120, 128], the three-dimensional acceleration signal vector can be expressed in any position on a rigid segment from the construction of a minimum of three independent linear accelerometer signal vectors at three points on the rigid body. Willemsen et al. [120] used this concept but for two dimensional analysis with the assumptions of rigid body conditions and a hinge joint to calculate knee joint. De Vries et al. [124] outlined the potential to use this concept to determine the shank, thigh and hip segment angles as well as the knee joint angles.

2.3.2 Gyroscopes

The theoretical aspects of the gyroscope signal were outlined by Pappas et al. [145]. Gyroscopes measure the angular rate about a fixed axis and yield the angular velocity of the attached rigid segment or object directly. The change in orientation can be estimated by integration of the angular velocity [154]. This orientation is expressed in the reference frame of the sensor module, nominally known as 'body' reference frame. Moreover, if an absolute orientation instead of a change in orientation is required, a reference orientation has to be obtained at least once during a recording. The accelerometers estimate of orientation under static conditions can be used as the initial conditions required for the gyroscope integration.

The orientation of the rigid body segment or the point of attachment is often estimated by combining the outputs from both accelerometers and gyroscope sensors. The accelerometers are likely to be subjected to dynamic accelerations for the majority of the time, preventing the reliable indication of orientation referred to as the 'slosh' effect [155]. Therefore, under these conditions the accelerometers only provide a long-term indication of orientation. Consequently, the gyroscope estimate of orientation is only reliable for a short period of time due to the build up of errors associated with the sensor and the integration process, an explanation follows in a later section. The combination of both sensors has been performed for mobile robots [156, 157] and the assessment of human movements [54, 81, 90, 95, 101]. In most applications, orientation is an essential quantity to be estimated. Moe-Nilssen et al. [158] reported a significant amount of change of inclination measured by accelerometers during walking. Therefore it was important to know the orientation of the sensor box with respect to gravity.

2.3.3 Inertial Measurement Unit (IMU)

Although single sensors have been shown to provide a lot of useful information [129], multiple sensor units or complete sensors, which sense in three orthogonal directions, are required for a three-dimensional representation of the attached rigid segment or object [89] and reliable analysis of movement [72, 73, 125]. In theory, a calibrated IMU measures three-dimensional angular velocity and acceleration orthogonally with

respect to the sensor module. Whenever a sensing axis deviates from the horizontal plane, the gravity component must be corrected for in order to estimate the linear acceleration. The acceleration vector expressed in the 'body' reference frame can be converted to 'flat earth' reference frame using the known instantaneous orientation of the body (see later section). Once the gravitational acceleration is eliminated from the measured acceleration, the velocity and position of the point of attachment with respect to the ground can be derived by single and double integration, respectively, with known initial conditions [21, 40, 69, 70, 113, 119, 149].

2.3.4 Magnetic Compass

Magnetic compasses detect the earth's magnetic field. The components of this field that are parallel to the earth's surface are used to determine the compass heading or azimuth. The magnetoresistive sensor is therefore required to be horizontal or level with respect to the earth's surface which is not often the case when attached to a rigid segment or object. Therefore reliable heading information (direction of movement) requires sensing in three orthogonal sensing axes and the tilt of the sensor to be known. The combination of accelerometers and magnetoresistive sensors under static conditions provides complete indication of the sensors module orientation. A more detailed explanation can be found in Caruso et al. [159].

2.3.5 Section Summary

In theory, all three types of sensor: accelerometers, gyroscopes and magnetometers provide valuable information about human movements. The accelerometers can be used to determine the direction of the local vertical vector, the orientation of the rigid segment, joint angles, and the linear velocity and position of the rigid segment. The gyroscope can be used to determine the absolute orientation of the segment or point of attachment provided initial conditions are known. The magnetometers can determine the heading or azimuth of the segment or point of attachment provided they are compensated for the tilt of the sensor module. It is reasonable to assume that potentially the best solution for measuring human movements during walking and

running and in particular analysing sprinting technique, is to use a combination of three accelerometers, three gyroscopes and three magnetometers.

2.4 Applications of the Sensors

A number of studies have been performed and documented which highlight the potential of MEMS sensors to capture the parameters that describe a variety of human movements. The validity of the MEMS sensor measurements can be compared to other motion capture system such as an optical system [54, 94, 115]. Further, the ability to identify events can be compared to foot switches (foot sensitive resistors (FSRs)) [53, 93, 97, 107, 129, 130, 145].

2.4.1 Physical Activity

Accelerometry can be used to provide an indirect method of assessing physical activity to enable the study of the effect of certain treatments. The gravitational acceleration is used to estimate metabolic energy expenditure during activity [22, 160] since the integral per unit time of this signal has been shown to have high correlation to energy expenditure. Accelerometers can also measure the functional use of body segments, the intensity of physical activity levels and/or the identification of tasks, during various actions. Examples of the measurable actions are sitting, lying and standing [150, 151], and activities associated with mobility such as walking, cycling and ascending and descending stairs [20, 76, 77, 80] and other daily functional activities [20, 161]. It is also possible to obtain results outside of a laboratory environment [80] or in a simulated semi-natural setting [20]. Such research has lead to commercially available systems such as the Caltrac and TriTrac-R3D (Professional Products Division of Reining International, Ltd), CSA (Computer Simulations and Applications Inc.), RT3 (Stayhealthy) [162], Dynaport [163] and BioTrainer-Pro (IM systems) [164].

2.4.2 Kinematics and Kinetic Parameters

The sensors can be used to measure the kinematics and kinetics of human movement. Kinematics is the study of motion without regard of the causes of motion. The complete kinematics of body segment requires the following parameters, all of which change with time. These are the position, velocity and acceleration of the segment centre of mass and the angle, angular velocity and angular acceleration of the segment in two or three planes [146]. All or some of these parameters can be derived experimentally [21, 54, 70, 81, 86, 87, 93, 98, 120, 124, 129, 130, 132, 136, 141]. Hayes et al. [70] outlined the theory to derive the angular position, velocity and acceleration of the lower leg and the acceleration of the mass centre at each time step during walking. Hutchings et al. [141] filed a patent for a system and method for measuring movements of objects. This system provides the following parameters such as speed, distance and height traversed by a person or object. The intended application is to measure movements of a person while walking and running although no commercial device has been released. Mayagoitia et al. [54] demonstrated the ability of inertial sensors to provide an array of kinematic parameters such as angular velocity and acceleration and knee linear acceleration as well as segment angles. The sensors used demonstrated the potential to estimate various kinematic parameters to within 7% at five different walking speeds compared to an optical motion analysis system. Out of the multiple accelerometry systems proposed [21, 40, 69], only Morris et al. [21] reported an experimental study that derived the kinematic parameters of the mid-shank origin during walking.

Segmental angles can be found by expressing the acceleration signal at a joint in two-dimensions [120, 132], integrating the angular acceleration [129, 130] or angular velocity [81, 87, 93], or using existing relations between acceleration and gravitational acceleration [87, 98] and anatomical constraints [136]. De Vries et al. [124] compared all of these methods for estimating leg segment angles and concluded that neither method was suitable on their own. Willemsen et al. [120] proposed the concept of directly describing the two-dimensional kinematics of the lower leg enabling the calculation of segment and joint angles. This method avoids using integration by utilising the property of expressing the accelerometer signals at the joints in the fixed body coordinate system. However, absolute segment angles can

only be determined if a reference body with known orientation is present. Willemsen et al. [132] extended this concept to calculate hip, knee and ankle angles with additional sensors. Once absolute segment angles are known it is possible to determine linear acceleration components at a particular point. Heyn et al. [130] presented the absolute angles of the shank and thigh obtained through an integration process. Vetlink et al. [87] outlined a hand held dynamometer comprised of inertial sensors and compared two methods of assessing shank angle during movements in a seated position. Baten et al. [81] presented a pilot study, which examined the accuracy and reproducibility of a practical implementation of an estimation method based on inertial sensors to derive three-dimensional body segment orientation. Tong and Granat [129] derived segment inclinations and knee angles from segment angular velocities registered at the thigh and shank from single uni-axial gyroscopes. Lee and Ha [98] developed a motion capture system based on a single sensor type, accelerometers. This study introduces the possibility of using more sensor modules to determine joint movements when the movement of interest is likely to have increase in degrees of freedom. Williamson and Andrews [93] derived knee joint angle and angular velocity of the thigh in real time during the actions of standing up and sitting down. The tilt of the thigh and shank segments can be calculated by combining the signals from accelerometers and gyroscopes and thus, the difference in the tilts yields the knee angle. The experiment is suitable to be conducted on able-bodied and a paraplegic person assisted by functional electrical stimulation (FES). Luinge [136] described a method for measuring the orientation of the forearm with respect to the upper arm utilising the third approach outlined by De Vries et al. [124].

Kinetics is the study of forces and moments that cause motion of a body or object. The resultant force and moments at particular joints during contact with the ground can be determined using inverse dynamic techniques and ground reaction forces [75]. However, resultant force and moments during the swing phase of locomotion when no external forces (other than gravity) are acting on the leg, can be deduced from inertial sensor derived parameters and applying the principles of linear and angular momentum [55, 70, 86, 119, 130, 136]. These parameters are orientation, angular velocity and acceleration of the segment. Kane et al. [119] determined and analysed the forces exerted on a tennis racket and the moments during impact and swing. Hayes et al. [70] proposed a theory for studying limb motions and joint kinetics, but no

actual application was developed. Van den Bogert et al. [75] estimated torque at the hip joint during walking and running using ground reaction forces. Heyn et al. [130] calculated the moment of the knee during the swing phase of gait. Nene et al. [55] developed the method presented by Heyn et al. [130] to investigate the relationship between muscular knee torque produced predominately by the rectus femoris (RF) at various walking speeds. Baten et al. [86] outlined a method for estimating load on the back in daily and work life and Lunige [136] carried out a study which estimated the load on the back while lifting empty beer crates. Accelerometers can also determine the levels of shock experienced at the tibia during impact [61, 88]. Investigations in this area provide valuable information for the development of adequate footwear and floor surfaces to help prevent injuries. LaFortune [61] found acceleration levels to be 2.7 g to 3.7 g and 10.6 g during walking at 1.5 ms^{-1} and running at 3.5 ms^{-1} and 4.7 ms^{-1}, respectively. Sterzing and Henning [88] found a lower peak level of 8.7 g during running at similar speeds between 3 ms^{-1} to 5 ms^{-1}.

2.4.3 Gait Analysis

Inertial sensors can be used to detect temporal and spatial parameters that describe human gait. In general, such parameters are identified by invariant signal features (i.e. sharp peaks) [56, 107] and events identified by rule based detection algorithms [56, 73, 79, 97]. The phases of a gait cycle are most commonly defined using four events. These are heel strike, foot flat, heel off and toe off [107, 129] or alternatively stance, toe-off, swing and heel strike [56, 79, 97, 144, 145]. Williamson and Andrews [93] extended the phases into five events defined as loading response, midstance, terminal stance, pre-swing and swing [97]. However, Dai et al. [165] and Willemsen [144] provided information of the transition between stance and swing phases. This information is considered the essential information of the gait cycle and can be used in artificial sensory feedback in the control of FES systems. The two most important investigated events are heel strike and toe-off [56, 97, 109]. The primary motivation for these investigations is to replace the use of FSRs. The problems associated with FSRs are, they prevent clear event prediction in some cases (for example, unloading of the foot can be seen as heel-off), typically have a short sensor life, require footwear to be worn, and have limited applications. Pappas et al. [56] identified heel strike by

using FSRs and toe off was identified by the change in sign of the measured angular velocity signal from the gyroscope sensor after heel off. A 100% detection rate was presented. Aminian et al. [109] used a similar sensor and found that toe-off was detected without any temporal change compared to the FSRs, this was verified in [129], but heel strike was affected by a small systematic delay of on average 10 ms. In contrast, Sabatini et al. [97] also used a similar sensor and found a delay for toe-off detection of on average 35 ms, whilst heel strike showed no delay.

The parameters such as step time, step length, duration of swing, cycle time, stride symmetry, inclination and speed during normal gait are also identifiable [72, 73, 79, 106, 109, 121, 125, 129, 143, 153]. Aminian et al. [73] used the acceleration pattern from three orthogonal directions at the trunk within each cycle time to estimate speed and inclination of walking using a Neural Network. Further, Aminian et al. [79] used the events of heel-strike and toe-off to derive the temporal parameters such as duration of swing and total or double stances of the gait cycle. Sekine et al. [121] demonstrated the ability to distinguish between walking on level ground and walking on a stairway. The low-frequency components of the accelerometer signal can identify posture changes, which in turn can distinguish between the two events. Tong and Grant [129] demonstrated that a single gyroscope could provide information on segment inclination, cadence, number of steps and estimation of stride length and walking speed. Aminian et al. [109] used the events of heel strike and toe-off to estimate stride length and stride velocity using a double segment gait model. Miyazaki [106] developed a simplified gait model and integrated the gyroscope measurements through an analogue integrator to give absolute thigh angle and thus estimated stride length, cycle time and also velocity during walking. The sensors can estimate the sagittal plane thigh velocity to within a ± 15% accuracy. Moe-Nilssen et al. [143] suggested a protocol for estimating the parameters such as cadence, step length, gait regularity and symmetry at various self administered walking speeds. DeVries et al. [153] consolidated that absolute angles were essential for the estimation of step length and would require a set of more than one accelerometer per segment.

2.4.4 Posture and Balance

Accelerometry can be used to assess balance and postural sway by measuring the position of the body relative to the surroundings and the ability of the body to generate forces to control movement. In particular, posture can be investigated for stability during standing [24], simulated stationary and rotational head movements [83], walking [78, 82, 115, 122, 142, 143] and in areas of occupational work [86]. Mayagoitia et al. [24] assessed the ability of male subjects to maintain balance while standing. Hansson et al. [83] reported a relatively small error even under dynamic accelerations of head inclinations and concluded that an accelerometer-based system was suitable for the objective assessment of posture during whole day recording in a work environment. Moe-Nilssen [158] investigated the assessment of the body's centre of mass to infer posture and balance during walking, eliminating the gravitational acceleration from the measured acceleration [78]. Menz et al. [82] studied acceleration patterns while subjects walked on level and an irregular surface, to develop an understanding of how a postural control system responded to challenging walking conditions. They implemented the harmonic ratio principle, which was initially described by Gage [116] and later modified by Smidt et al. [117], to highlight irregular acceleration patterns and provide a measure of stability. The maintenance of head stability is important for posture stability and can be largely facilitated by changing stepping patterns. Bonnet et al. [115] described an accelerometer and magneto-resistive device that estimated the trunk orientation in real time, which was sensitive in the anterior posterior and mediolateral sway directions. The assessment and quantification of balance function is possible with these sensors. Mayagoitia et al. [122] used an accelerometer system and developed a set of task tests to distinguish between stable and unstable subjects during standing. Waarsing et al. [142] introduced a performance parameter related to the power spectrum derived from the frequency of the irregular part of the acceleration signal. The measurement of this parameter in three orthogonal directions can provide an indication of stability.

2.4.5 Other Applications

There are various other applications of the sensors accelerometers, gyroscopes and magnetometers such as body segment tracking, virtual reality, robotics, underwater

vehicles, and others which have been less explored than the former mentioned ones. The sensors can be used to measure the forearm movements for gesture recognition [74, 100] and for analysing swimming technique [94]. Sakaguchi et al. [74] outlined a human arm tracking system for identifying gestures and segment positions for natural sign-languages. Other experiments involving the arm were carried out by Ohgi et al. [94] to discriminate the phases of freestyle and breaststroke swimming strokes. It is thought that inertial sensor-based motion analysers could enhance the training and coaching of swimmers. Full body motion capture systems are designed mainly for virtual reality applications [89, 95, 114]. Fontaine et al. [89] described a sourceless motion capture system which could be used for character animation. Foxlin et al. [114] described two commercially available motion capture systems, IS-300 and IS-600, for head mounted displays. Bachmann et al. [95] outlined a full body tracking system using 15 MARG sensors to track 15 limb segments [166]. The sensors have also been used in robots and vehicle navigation [156, 157]. Vaganay et al. [157] used the sensors to estimate attitude of the robot and Barshan and Durrant-Whyte [156] outlined a low cost inertial navigation system (INS) for mobile robots. Bachmann et al. [167] described a sensor based system for the autonomous underwater vehicle navigation. Other applications include expressive footwear [92], outdoor walking speed [168] and combined with GPS systems to aid navigation [138, 139]. Paradiso et al. [169] designed an expressive footwear system for dancers. One gyroscope can be used to directly measure the angular rate about the vertical, giving a clear response to spins and twist. A two axis accelerometer can measure tilt of the shoe with respect to gravity vector and respond to the moderate accelerations of foot swings. Impact shocks and kicks, at higher g levels can be measured in three axes by a triple piezoelectric accelerometer. Perrin [168] used a combination of accelerometry and altimetry to accurately measure outdoor walking speed. Bonnet et al. [115] and Ladetto et al. [140] combined the sensors with a GNSS positioning system (such as GPS, Galileo GLONASS). This approach reduces the problems associated with GPS signals such as latency, obstruction of the signal and degradation requiring a DGPS.

2.4.6 Section Summary

MEMS sensors can be used in numerous and diverse applications. However, it is apparent that their use in a sporting context remains largely unexplored. To the knowledge of the author, there have been no documented applications which have used MEMS inertial sensors as part of a motion analysis system to analyse the kinematic parameters that describe sprinting technique. The investigation conducted by Mayagoitia et al. [54] is perhaps the one of the more significant papers in relation to this research study. The investigation demonstrated the potential and accuracy of the sensors to determine several kinematic parameters such as linear acceleration of the knee. The sensor measurements were compared to an optical motion analysis system and reported an RMS error which was less than 7% at five different walking speeds. However, this theory is yet to be applied in a sporting context. Further, this concept could be translated to fixing the sensors to other body locations such as the body's CoM. The sensors also demonstrated their potential to detect the events of contact and non-contact [56, 97, 109]. This attribute is of great interest for the analysis of any locomotive movements. The time period between the points of contact can be used to determine stride frequency. Consequently, if the average velocity during the stride is known, then stride length can be calculated. It is clear from previous studies in other application areas that the sensors have the potential to measure a number of the required parameters to describe sprinting technique.

2.5 Sensor Errors

The main attributes that specify the performance of the inertial sensors are zero bias, scale factor, measurement range, temperature, environmental disturbances, non-linearity, noise and the attachment site and mounting. Each of these attributes could contain errors which influence the output of the sensors.

2.5.1 Zero Bias and Scale Factor

The zero bias and scale factor are determined through a calibration procedure (see section 2.2.4) prior to any experiments. These values are then used to convert the raw sensor outputs into their respective units. Therefore the stability of these parameters is

probably the most influential factor of the overall sensor performance since it affects the accuracy of the outputs. The zero bias (or offset) for the accelerometers and gyroscopes is the output of the sensors in a stationary position. For the accelerometers, this also means that the accelerometer's sensitive axis must be parallel with the earth's surface to experience zero gravitational acceleration. This is not the case for the magnetoresistive sensor as the zero bias is determined through a calibration procedure of rotations whilst on a level plane. The scale factor (or sensitivity) is the change in voltage at a rate of one measurement unit. The measurement units for the sensors are Vg^{-1}, $mVdeg^{-1}s^{-1}$, $mVV^{-1}g^{-1}$ for the accelerometer, gyroscope and magnetoresistive sensor, respectively. The unit g in the scale factor units for the magnetoresistive sensor represents Gauss, which is the measure of magnetic flux density. The earth's magnetic field intensity is about 0.5 to 0.6 gauss.

There is little quantified evidence in the literature about the stability of the zero bias and scale factor and thus the accuracy of the outputs. From the available literature, the bias stability of inexpensive, miniature gyroscopes is documented as being most concerning. This is largely due to the use of piezoelectric transducers which is the most frequently documented sensing element in the vibratory MEMS gyroscopes in the literature. The piezoelectric material is more susceptible to noise and temperature changes than the capacitive technique used in the accelerometers [170]. The zero bias is normally found prior to the commencement of each trial within an experiment. Using an average bias value, instead of calibrating the sensor for every trial, can deteriorate the accuracy of subsequent estimated parameters [86]. Typical bias stability of high quality gyroscope sensors such as ring laser gyro (RLG) and fibre optic gyro (FOG) is reported by several authors [17, 113, 114] to be on average $0.001°hr^{-1}$ and in the range of $0.1°hr^{-1}$ to $1°hr^{-1}$, respectively. However, the bias stability of commercially available sensors of these types are typically $0.0035°hr^{-1}$ [171] and $7.67°hr^{-1}$ [172], respectively. Foxlin et al. [113] reported that the stability of inexpensive MEMS gyroscopes can be as much as $0.1°s^{-1}$ to $1°s^{-1}$. This amount of drift can cause an angle error of 60° to 600° in only 10 minutes. Lunige [136] and Baerveldt and Klang [111] reported variations in the gyroscope output during stationary data collection to be $0.57°s^{-1}$ and $0.42°s^{-1}$, respectively. Barshan and

Durrant-Whyte [156] recorded a standard deviation of the output fluctuations over a 12 hour period of $0.16°s^{-1}$ and $0.24°s^{-1}$ for two types of gyroscope. It is therefore, reasonable to assume that the performance of the selected gyroscope sensor will require extensive investigation.

There is little reported information on the performance of the accelerometer sensors. Luinge [136] found a fluctuation of $0.1 ms^{-2}$ whilst the sensors were stationary. It was suggested that a zero bias error of $1 ms^{-2}$ (0.1 g) in a horizontal direction will cause an inclination error of nearly 6°.

2.5.2 Measurement Range

Choosing the correct sensor for adequate measurement range can prevent signal clipping, which will cause the collection of incorrect data values and saturation of the sensors [56] resulting potentially in permanent mechanical change. Different positions of the sensors on the human body exhibit different measurement ranges [97, 109, 173]. Sabatini et al. [97] found foot acceleration peaks during walking to be less than 5 g and peak angular velocities of $650°s^{-1}$ and $300°s^{-1}$ recorded at heel strike and mid swing, respectively. However, the measurement range of the gyroscope used was $\pm$ $300°s^{-1}$. Aminian et al. [109] and Wu and Ladin [173] found peak angular velocities to be $400°s^{-1}$ at mid swing for the shank. It is assumed that much lower rotational rates are likely to be experienced at the CoM. Pappas et al. [56] experienced saturation in the output of the gyroscope positioned on the heel because of large rotational velocities of the foot at high speeds of $13 kmh^{-1}$. It is evident that the sensors should be chosen well within the maximum likely recorded measurement.

It is known that the accelerometer output under stationary conditions can determine the local vertical vector, and therefore the tilt of an object, in two directions. Since the local vertical vector points down towards the earth, tilt and also rotations about this axis (known as azimuth) are not measurable by the accelerometers [90, 136, 174, 175]. This is seen as a fundamental limitation of the accelerometer device [83]. Ladetto et al. [174], Lunige [136] and Rehbinder and Hu [175] stated the main source of error in positions derived from inertial sensors was associated with the azimuth

determination. Luinge et al. [90] used only the integrated gyroscope signal to determine angular position about the azimuth and found the estimation became increasingly inaccurate over time.

For applications in which heading is important, additional sensors such as magnetometers or assumptions of the measured movement could be implemented [136, 174]. Ladetto et al. [174] introduced the combination of gyroscopes and a magnetic compass to provide complementary measures of the rotations about the azimuth axis. Lunige [136] conducted an experiment for measuring the orientation of the arm. The heading error between the forearm and the upper arm were minimised using knowledge that abduction and adduction of the elbow joint were constrained.

2.5.3 Temperature

Temperature variations of the surrounding environment [56, 93, 136, 156] and of the sensors themselves due to the mechanical nature [111, 156] can effect sensor performance [156] and in particular the stability of the zero bias. Again, the majority of the evidence surrounds the performance of the gyroscope zero bias stability, but in this case, with respect to temperature fluctuations. Pappas et al. [56] carried out $45°$ rotations at varying temperatures to show the effect of temperature on the gyroscope zero bias. A change in temperature between $18.7°C$ and $20.4°C$ can cause an angle error of about $10°$ and at higher temperatures of $50°C$ the angle errors can increase up to $70°$. Pappas et al. [56] also reported that the other calibration parameter, scale factor of the gyroscope varied within a range of $±$ 5%. It is thought that this result is a less important error than the bias stability. The ideal start-up output values of the gyroscope zero bias can be lower than expected and subsequently can vary within each trial of the experiment [156]. Further, after start-up, the output can increase with time in an exponential fashion. The time-variation of the zero bias can be attributed to thermal effects based on observations that the sensor units gradually heat up during operation. Barshan and Durrant-Whyte [156] reported an increase of 30 mV, equivalent to $1.35°s^{-1}$, in 10 minutes after switching on and thereafter a 10 mV change for the next 24 hours. An error model using the Levenberg-Marquardt iterative least squares fit method can compensate for the instability found in the zero biases [156].

Baerveldt and Klang [111] also attributed the rather high drift rate of $0.41°s^{-1}$ to the gyroscope heating up to reach a stable temperature after start up. Lunige [136] exposed gyroscopes to a change in temperature from 30°C to 20°C and the recorded zero bias varied at a rate of $2°s^{-1}°C^{-1}$. The investigations collectively highlight the desire to develop a temperature compensating circuitry, or to actively regulate the temperature of the gyroscope to a constant ambiance [56]. Otherwise considerable errors in any derived parameters such as orientation are likely to occur [136]. Again, it is reasonable to assume that the performance of any chosen gyroscope sensor requires investigation. In this instance, the performance with respect to the ambient temperature and also the internally produced temperature are of interest.

Two investigations have reported the performance of the accelerometer with respect to change in temperature [93, 136]. Williamson and Andrews [93] experienced a 6 mV (equivalent to an angle of 4°) variation in an accelerometer zero bias for a temperature variation between 20° and 21°. Lunige [136] exposed accelerometers to a change in temperature from 30°C to 20°C and the recorded variation in the zero bias was on average $0.2 \ ms^{-2}$, which corresponds to an angle error of 1.1°. Barshan and Durrant-Whyte [156] investigated the stability of the zero bias for a piezoresistive type accelerometer. Although the variation was not quantified, from the displayed results the variation was about $0.032 \ ms^{-2}$ (equivalent to 0.00326 g). The performance of the accelerometer with respect to temperature requires less attention since the magnitude of the likely errors are much less than the gyroscope sensor.

2.5.4 Environmental Disturbances

The only performance related disturbance due to environmental interferences mentioned in the literature, other than temperature effects, is ferromagnetic interference. This only affects the magnetoresistive sensor. When a magnetoresistive sensor is operating in an open area, the presence of any ferrous metals for example iron, nickel, steel or cobalt will distort, or bend the earth's field. This will in turn alter the compass heading [89]. Calibration of the magnetometer within the operating environment can reduce the measurement errors and increase the usability of the

device. However, this can be an obvious constraint to the versatility of the system and the idea of daily recording of human movements [159].

2.5.5 Non-Linearity

Non linearity of the sensors output is defined as the largest deviation in the accelerometer output curve over its specified input range, when the output is compared to a least squares best fit straight line. It is common practice to assume that the sensors operate on a linear response which has been supported by some investigations [89, 93, 95]. Williamson and Andrews [93] confirmed that the non-linearity of the sensors was less than 0.5%. Bachmann et al. [95] described a testing procedure using a precision rotary tilt table. Linear responses from the accelerometers were seen during 360° rotation at $1°s^{-1}$, and from the gyroscopes during 90° rotations at angular rates varying from $\pm 10°s^{-1}$ to $80°s^{-1}$. Fontaine et al. [89] also claimed that the accelerometers provided a linear response.

2.5.6 Noise

There are various causes of measurement noise. These are cable length and unshielded wires [56], environmental vibrations, electromagnetic interference (EMI), random, white noise with zero mean [56], or quantisation noise. Pappas et al. [56] defined that random noise increases with time with respect to the random walk law. Quantisation noise can be caused by the resolution limits of the A/D conversion process and also the sensor bandwidth and unwanted accelerations from skin and muscle movements. The typical noise floor is quoted in the data sheets of the sensors and is a contributing factor of the measured output of the sensors during stationary periods and in the absence of acceleration. It is possible to reduce the noise present on the sensor output by reducing the frequency response. However, this also has limitations.

2.5.7 Attachment Site and Mounting Arrangement

The placement of the sensors, specifically accelerometers, is an important design consideration of a MEMS sensor system since unwanted measurements of skin and

muscle movements can distort sensor output profiles [61]. LaFortune [61] presented evidence that skin mounted accelerometers caused distortions of acceleration profiles compared to bone mounted accelerometers. The most significant skin movements were observed during impacts and in running. Various solutions have been proposed to reduce the amount of distortion [21, 22, 130, 169]. Heyn et al. [130] used metal plates to eliminate skin and muscle movements, but these were found to be cumbersome [54] and unnecessary [129]. Tong and Granat [129] demonstrated that accurate information could be produced when the sensors were affixed by a more simple, practical and tolerable manner for daily use, such as a strap tied around a limb. Paradiso et al. [169] suggested that the introduction of mechanical stabilizers in the sensor housing would prevent unwanted measurements. Morris [21] chose a mounting site specifically to minimise the effects of soft tissue movements and used a high friction cast to heavily damp skin movements. It is thought that, with careful site selection, and appropriate form of fixation, non-invasive measurements could be made on the majority of the parts of the body without capturing unwanted signals. Alternatively, Bouten et al. [147] suggested filtering out the high frequency noise components resulting from 'jolting' of the sensor. This, as mentioned previously reduces the frequency response and can sometimes result in valuable information being eliminated.

Gyroscopes offer more flexibility surrounding mounting arrangements since they are insensitive to gravitational accelerations [129, 130]. Heyn et al. [130] concluded that gyroscopes could be placed anywhere along the same plane of the segment to give almost identical signals. Tong and Granat [129] utilised this conclusion and the site of attachment was chosen so as to avoid the potential areas of skin and muscle movements. Measurement results from a thigh mounted sensor showed a weaker correlation than a shank mounted sensor when both were compared to a motion analysis system. This is likely to be caused by the muscle movement in the thigh during walking.

2.6 Processing of the Outputs

Although inertial sensors have long been advocated for analysis of human movement their application has not gained widespread use because of methodological difficulties. The two major problems are accelerometer sensitivity to the local vertical vector (gravitational acceleration), which hinders the realisation of absolute linear accelerations, and unbounded drift arising through the integration of signals containing any number of sensor errors.

2.6.1 Decomposition of Accelerometer Signals

The composition of the acceleration signal and the desire to extract the various components (linear and gravitational acceleration) can introduce errors into the system. The linear acceleration component is extracted from the measured acceleration if the orientation of the sensors are known, thus eliminating the gravitational acceleration component. The gravitational acceleration can also be measured by the accelerometers themselves [153], but only when the object to which the sensors are attached is stationary or hardly moving (standing, swaying) i.e. under static accelerations [83, 90, 98, 128, 136]. The gravitational acceleration is of particular interest since it can be used to determine tilt in two directions. Hansson et al. [83] reported small errors of 1.3° when estimating the inclination under static conditions by accelerometry. However, these conditions are seldom the case in many of the applications mentioned previously and the presence of linear accelerations prevents the accelerometers providing a reliable indication of the object's tilt. This characteristic was referred to as 'slosh' [114]. Foxlin et al. [114] avoided the effect of 'slosh' by ignoring the accelerometer outputs during dynamic head motion and consulting them during natural pauses to provide a comparison to measurements from other sensors. This approach is only suitable to burst-like movements. Fontaine et al. [89] suggested it was possible to detect when the accelerometers measure anything else other than the gravitational field by calculating the normal of the acceleration by equation 2-3.

$$Normal = x^2 + y^2 + z^2 \qquad \textbf{2-3}$$

where x, y and z are accelerations in three orthogonal directions.

Any difference between the calculated normal and 1 identifies that dynamic acceleration is being experienced and the amount of difference gives the significance of the error. Moe-Nilssen [78] suggested that the approximation of tilt from the inverse sine of the anterior posterior and mediolateral accelerations could however be used as best estimates of tilt of the accelerometer, even when the subject tested was walking. This is unlikely to be the case for a wide number of applications. Lee and Ha [98] introduced the use of additional sensors under dynamic conditions to estimate the local vertical vector.

An alternative approach is to low-pass filter the accelerometer outputs [53, 76, 80, 103, 153], although this adds a lag to the computations. Bussmann et al. [53] demonstrated that the components of the measured acceleration differ in frequency and suggested they could be distinguished. DeVries et al. [153] and Foerster et al. [80] suggested that the gravitational component named the slow or DC component had a frequency content of under 0.5 Hz. Harada et al. [103] filtered the acceleration data, choosing a linear phase finite impulse response (FIR) filter so as not to distort the phase of the signal, using a cut off frequency of 1 Hz for measuring orientation of the point of attachment during daily life activities. Veltink et al. [76] described the design of a frequency detector to distinguish the static and dynamic nature of activities. The accelerometer signals were high pass filtered at a cut-off frequency of 0.5 Hz to eliminate the offset within the signal followed by rectification and low pass filtered at a cut-off frequency of 0.1 Hz to yield a measure of average signal deviation from the mean. The resultant was compared to a threshold level to discriminate either static or dynamic activities. Filtering the output of the sensors may isolate static and dynamic acceleration to some extent. However, it is important to acknowledge the frequency which divides the two categories of acceleration is likely to be unclear and this approach may only provide an approximation of the tilt of the sensor.

2.6.2 Integration

Various methods are available which obtain the orientation from the sensor outputs of rigid body segments or the point of attachment without integration [21, 70, 118, 120] and also with integration [81, 86, 93, 97, 99, 103, 113, 129, 130]. The integration of the gyroscope outputs can provide absolute orientation if initial conditions are known. Integration can be estimated by varying levels of numerical approximation algorithms such as the trapezium rule, Simpson's rule and increasing in complexity to the Gauss Quadrature [176]. Foxlin [113] integrated the gyroscope output following an approximation over a short time interval using the following Taylor series expansion in equation 2-4.

$$\theta(t + \Delta t) = \theta(t) + \dot{\theta}(t) \cdot \Delta t + \ddot{\theta}(t) \cdot \frac{\Delta t^2}{2} \qquad \textbf{2-4}$$

where θ is the angle

      $\dot{\theta}$ is the angular velocity   (the derivative of θ)

      $\ddot{\theta}$ is the angular acceleration   (the derivative of $\dot{\theta}$)

      t is the time

      Δt is the time step between samples

The number of terms retained depends on the sampling rate and an acceptable rate of error. For a first order integration algorithm, the error rate for an expected angular rate of $300°s^{-1}$ and a sampling rate of 1000Hz, is approximately $0.79°s^{-1}$ [113]. Sabatini et al. [97] and Williamson and Andrews [93] used the trapezium rule as an approximation to determine the tilt of the segment from the gyroscope outputs. The general method for this technique is expressed in equation 2-5 [176]:

$$\theta_t = \theta_{t-1} + \left(\frac{\dot{\theta}_{t-1} + \dot{\theta}_t}{2} \right) \Delta t \qquad \textbf{2-5}$$

Where, θ is the angle

      $\dot{\theta}$ is the angular velocity

      t is the time

This method is not very computationally demanding and provided the sampling rate is fairly high the likely errors can be minimised. An alternative analogue integration method using active and passive components was implemented by Miyazaki (1997). The disadvantages of analogue filtering compared to digital filtering are that additional circuitry is involved, it is less flexible, it is not easy to modify and it can be sensitive to temperature, supply change, interference and aging.

Integration can provide reliable results over a period of time with the use of high quality sensors and good initial conditions [175]. A well known problem when implementing integration is the appearance of unbounded drift in the integrated signal. This causes errors in the output signals of the low cost MEMS sensors. Bortz [154] presented a new concept for strapdown inertial navigation integration. The method isolated the non-commutativity rate vector (known to cause problems in integration to obtain transformation matrix) and treated it separately [40, 154]. The advantage of this method is that it generates an orthogonal transformation matrix, which needs to be evaluated only when it is required to transform a vector from body reference frame to an inertially-fixed frame such as 'flat earth'. The frequency at which the transformation matrix was updated is reduced and therefore the accumulating errors are also likely to be reduced. Mital and King [40] tested this concept against hypothetical data and concluded that integration using the above technique was relatively drift free for short periods. Baten et al. [86] also implemented this algorithm. It has been suggested that integration of the low cost MEMS sensors should be limited to short periods, for example 30 seconds [56, 81, 86, 103, 130]. Baten et al. [86] presented an error of $\pm$ 10% when estimating absolute back orientation through integrating the gyroscope signal. Heyn et al. [130] found comparable accuracy to an optical system when using integration to determine shank angle, although it was not quantified. Baten et al. [81] found integration drift errors of $0.02°s^{-1}$, $0.03°s^{-1}$ and $0.10°s^{-1}$ over a period of 180 s equivalent to 3°, 6° and 18° angle errors for no movement, single axis rotation and conic motion, respectively. Harada et al. [103] showed their three dimensional nine sensor device system can estimate absolute orientation with less than a 4° error. Pappas et al. [56] attributed the integration errors to the effects from temperature fluctuations. An error of 1.5° was

found when a gyroscope sensor was rotated 45° at a rate of 22°s^{-1}. This was equivalent to an error of 3.33%.

Improvement of the orientation estimate can be achieved by combining the attitude estimates from the accelerometer and the integrated gyroscope estimate of orientation [93, 95, 113, 157, 177]. The output of the accelerometer is used to determine inclination with the knowledge that it is reliable under static conditions and under dynamic acceleration only after a long period of time. This is because in the presence of dynamic acceleration, the acceleration signal deviates from the line of gravity and contains 'slosh' errors. Over a long enough period, the dynamic acceleration can be assumed to be zero. Thus, the average output over this period is equal to the gravitational acceleration component only. The output of the gyroscope for a short period under little temperature fluctuating conditions provides a reliable estimate of orientation [54, 81, 102]. Williamson and Andrews [93] concluded that a combined system was more accurate rather than using only an accelerometer to estimate inclination. This may be justified since combining the sensor types is likely to increase the bandwidth of the parameter.

The methods of overcoming the problem of integration drift are to periodically reset the integration algorithm [21, 70, 81], high pass filtering the gyroscope output [106, 129], or avoid the integration process altogether [120]. One method for resetting the integration algorithm and reducing the drift is to utilize the facts presented by Morris [21]. These are that the acceleration signals are cyclic and that the average value of the angular acceleration over a cycle must be zero. However, Willemsen et al. [120] suggested that this method would not be suitable in some applications that use feedback control systems such as FES. Also, implementation of this method is likely to add latency to the system reducing the potential of real time analysis. However, Baten et al. [81] implemented this approach, measuring the gyroscope bias and orientation under static conditions at the beginning and end of the movement and used linear interpolation to predict the effect of the drift. Alternatively, the foot flat phase of the gait cycle can provide an absolute estimate of orientation at every step (i.e. initial conditions) [56, 70, 93, 97, 99, 106, 129, 144, 165, 178]. During this event, the motion of the leg is assumed to be constrained and the accelerometers sensed only

gravitational acceleration since the velocity was assumed to be zero. For example, Tong and Granat [129] assumed that during midstance, the thigh and the shank were in a vertical position, and set the angles to zero at this point. The time period with which drift can accumulate by the integration process will be limited to one step per cycle. Using the measured acceleration during this phase, the estimated angles are absolute angles. However, DeVries et al. [124] showed that this method does not yield an adequate estimation of shank angle during stance phase, because contact between the foot and the floor constantly changes and the assumption of the joint as a simple hinge joint was not all encompassing. Pappas et al. [56] highlighted the difficulty of this method when applied to fast walking speeds. Since the stance phase of the cycle reduces as speed increases, the assumption of there being a period of zero velocity during this phase becomes less valid. At 13 kmh^{-1}, which is equivalent to a slow jogging pace, stance phase was recorded as 0.1 s.

An alterative method was to high pass filter the gyroscope output to eliminate the drifting zero bias. Various cut-off frequencies have been selected [106, 129]. Tong and Granat [129] and Miyazaki [106] used frequencies of 0.3 Hz and 0.5 Hz, respectively. The last alternative is to determine kinematic parameters without integration, typically from multiple accelerometer systems [120]. However, this approach is not without its problems. Willemsen et al. [120] experienced high frequency noise errors in their proposed approach to estimate joint angle and segment orientation.

Obtaining a change in position using a low cost IMU is even more problematic. The acceleration with respect to the 'flat earth' reference frame is integrated once to yield linear velocity and twice for positional information. The accuracy of the resultant velocity or position, not only depends on the quality of the accelerometer sensor, but also on the accuracy of the orientation estimate. Assuming the error in the accelerometer signal is fixed, the positional drift error will grow quadratically with time according to equation 2-6.

$$x = \frac{1}{2}a_b t^2 \qquad\qquad\qquad \textbf{2-6}$$

where, x is the position

       a_b is the acceleration in the 'body' reference frame

       t is the time

A good estimate of the orientation is required, because it is used in three algorithms to produce the linear accelerations with respect to the 'flat earth' reference frame [102]. These are the subtraction of gravitational acceleration component from the measured acceleration, transforming the gyroscope outputs into the appropriate angle representation, and rotating the absolute linear acceleration from the body fixed reference frame to the earth reference frame. The errors occurring when subtracting the gravitational accelerometer with an inaccurate orientation value is found by equation 2-7:

$$Error = g \sin(angle) \qquad\qquad\qquad \textbf{2-7}$$

where, g is the gravitational acceleration.

Since the gravitational component of acceleration can be significantly larger in most cases compared to the measured acceleration of many typical human movements [136], there is little scope to accommodate inaccurate orientation vectors. Miyazaki [106] concluded that the inherent zero bias drift in the gyroscope output prevented true determination of the absolute angle of the limb and also accurate calculation of the stride length was impossible.

The initial conditions for the integration can be determined at the beginning of the analysed movement. If the subject or object starts at rest then it is feasible to assume that the velocity and distance can be set to zero and the absolute orientation of the rigid body segment or point of attachment can be measured during this stationary period prior to the commencement of the experiment.

2.6.3 Model Assumptions

Numerous assumptions can be implemented which simplify the analysis of the human movement and reduce the number of sensors required. These assumptions are the number of dimensions of the analysed movement [54, 120], representation of the segment joints [54, 87, 132], definition of segments [54] and alignment of reference frames at the commencement of any experiments [81]. The most common assumption is that during walking and running the movement of the lower body (and projection of the centre of mass) occurs primarily in the sagittal plane. This assumption reduces the analysis of movement from three to two dimensions [54, 97, 120, 129, 130, 132]. However, this assumption typically only applies when it is assumed that movement in the third dimension can be ignored. Ideally, three dimensions will be measured in the proposed sensor system. In most experiments, although not widely documented, it is assumed that the sensors, particularly the accelerometers, are securely attached to a point or segment which acts as a rigid body [40, 69, 70, 76, 93, 120, 132, 144, 147]. A rigid body is defined as an idealisation of a body with volume and mass which has a shape that cannot change. Willemsen et al. [132] concluded that fixation of accelerometers was unlikely to fulfil the rigid-body condition. For this assumption to stand, careful selection of the site of attachment is required since any unwanted movements caused by the sensor and the point of attachment not acting as a rigid body is a possible source of error discussed in the error section. The assumption of the angular motion at a joint has helped to simplify the movement models. It is widely accepted that unloaded joint motion at the ankle and knee can be described using a one degree of freedom model such as the hinge joint, because there is a distinct movement path in these joints that offers minimal resistance. This assumption has been implemented for the knee joint [54, 55, 74, 87, 129, 132] and ankle joint [144]. Mayagoitia et al. [54] assumed that the shank and foot could be considered as a single segment. Baten et al. [81] assumed the initial conditions that the shank and thigh coordinate systems were in alignment to the 'flat earth' reference frame. This is not always the case and perhaps it is preferable to determine initial orientation and position of the sensor system.

2.6.4 Orientation Representation, Reference Frames and Rotation Sequences

In order to track the three-dimensional movements of humans either in a laboratory or in natural surroundings, it is conventional to express the movements within a set of reference frames to make some determination regarding the physical world. The most commonly used reference frame is the 'flat earth' or sometimes defined as the world reference frame [102, 179, 180]. This is a fixed frame defined as an arbitrarily selected origin on the surface of the earth (assuming it to be flat), for example at the starting position of the movement activity and with axes, X, Y and Z directed in the local north, east and down directions respectively. The velocity and positional information with respect to the earth reference frame of a rigid body reflects the velocity and actual distance travelled across the ground (earth's surface). Other reference frames exist, definitions of which can be found in Titterton and Weston [181]. Sensors affixed to objects or rigid body segments measure movements relative to what is known as a 'body' reference frame (where body refers to an object with mass) or local reference frame. The body reference frame is stationary or moving with uniform velocity relative to a fixed frame (i.e. 'flat earth' frame). It is defined as an orthogonal axis set which is aligned with the axes of the vehicle or object in or on which the sensor module is installed or affixed [181]. These two reference frames have been implemented by several authors [90, 94, 97, 99, 103, 115, 136, 175, 182] to describe the movements of the human body and it is thought that they are suitable for this research study.

The mathematical relationship of the orientation between two independent frames can be carried out by numerous models [183, 184]. The two most implemented in the literature are Euler angle [70, 103, 113, 156, 185] and quaternion [95, 103, 104, 179, 182, 185-187]. Euler angle representation is defined by a rotation matrix, which is rotated in succession about three independent axes by three independent Euler angles. There are twelve possible combinations to define rotations, each with potentially different results. This means that the order of these rotations is important. Quaternion representation is based on the axis-angle model, defined as a rotation following the right hand rule around an axis by some angle. A quaternion represents a three-

dimensional rotation as a four component row vector of unit length. A more in depth description of both models can be found in Kuipers [183]. The choice of model has depended largely on the required application and the objectives of the system since both have certain advantages. For example, the Euler angle model requires a three component vector representation compared with four for quaternions. The number of arithmetic operations in the Euler angle model is higher since quaternions are defined directly from the dynamic equations. Since Euler angles are easier to visualise they are often the preferred outputs and if it is necessary to compute angles at each orientation update, then quaternions are converted to Euler angles which adds more steps. Quarternions are then no longer the most computational efficient of the two. The most significant advantages of quaternions are that no singularity exists when the elevation angle passes through 90° (defined as nose up or down) and angles are only computed should a rate of change occur. Singularities is commonly defined as 'gimbal lock' [133, 135], since when elevation passes through 90° the other two axes became collinear and therefore the angles about these axes cannot be uniquely defined (due to divisions by zero). Both Hayes et al. [70] and Foxlin et al. [155] were aware of the limitations caused by singularities, but this was not found to produce any noticeable disturbances in practice.

Regardless of which orientation representation is chosen, a transformation between the two independent reference frames consisting of a transformation matrix and rotation sequence is required. The most commonly used rotation sequence in aircraft and aerospace applications is ZYX, and more importantly this sequence has been implemented by several authors [103, 140, 175, 184, 185]. Within this representation the body frame follows the right hand rule, and is defined, as positive x-axis of the aircraft points forwards along the longitudinal axis, the positive y-axis is directed along the right wing and the positive z-axis is normal to the x and y axes, pointing down. The 'flat earth' frame is defined as mentioned previously for X, Y and Z. The ZYX rotation relates the two frames by first a rotation about the z-axis by an angle that defines the heading. This is followed by a rotation about the new y-axis through an angle which defines the elevation of the aircraft. Finally, the last rotation was about the newest x-axis by an angle which defines the bank of the aircraft. It is thought that

this rotation sequence is suitable for this research study. A more in depth definition and description of other possible sequences can be found in Kuipers [183].

2.7 Filters

2.7.1 Introduction

It has been shown that the choice of small, light weight and low cost sensors for human tracking applications is limited by the output of the sensors being corrupted with noise. Thus various filtering algorithms have been implemented to make the most effective use of the sensor outputs and provide the optimal estimates of the parameters that describe the movements of interest. The purpose of a filter in the case of electronic signals is to separate signals of different frequencies yielding the desired frequency response. Further, a more sophisticated filter can perform the best separation of a signal from noise which are both noise-like in characteristic. "Best" separation is defined as the compromise of passing the signal and, at the same time, suppressing most of the noise in a linear manner by minimising mean-square error. These types of filters are based upon the spectral characteristics of the signals probability distributions known as probabilistic models and produce the optimal estimate of the signal. Two well known filter theories of this type are called Wiener and Kalman filters and a more simplistic type is the complementary filter.

2.7.2 Wiener and Kalman Filters

Wiener filters are not generally implemented into applications such as navigation and human body tracking and are therefore not discussed here. However it is worthy to point out that the Wiener theory minimises the mean square estimation error, subject to certain constraints and assumptions, which to some extent led to the birth of the Kalman filter. The Wiener filter depends on the known statistical functions of the signals and uses only this information in its optimal estimate. In many practical applications these functions may not be known. Although the filter can accommodate multiple inputs, only a single scalar output can be estimated. It is also not very computationally efficient since it reprocesses all previous data each time a new

estimate is required. Implementation of the filter on a computer requires that all previous measurement data be stored in memory and be available for recalculation. The theory is therefore not easily extended to complicated time-variable, multiple input and output problems. A description of this filter design can be found in either Brown and Hwang [188] or Grewel and Andrews [189]. The Kalman filter is an alternative method of formulating the linear minimum mean square error which utilizes state space methods. The two main features of this formulation are vector modelling of the random or known dynamic processes under consideration (as opposed to scalar) and recursive processing of the noisy input data. There are numerous possible dynamic models depending on the motion of interest and associated input and output state configurations. Also, it may be desirable to model parameters which can be difficult to measure, for example, the zero bias of the gyroscope. A detailed explanation and mathematical description of this filter is given in Brown and Hwang [188] or Grewel and Andrews [189]. The principal applications of Kalman filtering have been in control systems, and the tracking and navigation of a variety of vehicles. A key characteristic of the Kalman filter is its ability to combine the information from multiple types of systems with complementary characteristics to provide superior estimates to that of any of the systems alone. One example, which has been implemented extensively, was combining GPS and IMU for the field of navigation [190]. This principle has been applied to the outputs of the accelerometers and gyroscopes to produce the optimal estimate of orientation in stand alone IMU's [102, 113].

Due to the nonlinear characteristics of three-dimensional human movements, the traditional Kalman filter such as a discrete filter [185] was required to be linearized. This development has lead to various types of Kalman filters. These are linearized [175], extended [105, 156, 157, 182, 187], unscented [103] and sigma points [104]. The following review gives a few examples of the implementation of various types of Kalman filters using inertial sensor inputs. Emura and Tachi [185] designed a discrete Kalman filter to improve the performance of a magnetic motion sensing system by Polhemus, by using gyroscopes. The filter modelled the dynamic rotational motion of the head and the integration process. The magnetic motion capture system suffers from a low sampling rate and latency which is likely to cause difficulties when used for measuring rotational motion for head mounted display (HMD) in the field of

virtual reality. Gyroscopes offer complementary characteristics compared to magnetic motion capture system. It was shown that the performance of the system was enhanced when combining the gyroscope sensors. Rehbinder and Hu [175] used a modified linear Kalman filter to provide stable estimates of the attitude of a robot. The filter fused information from a three-axis gyroscope and a three-axis accelerometer and known natural conditions of the motion of interest. The filter was based on a switching architecture consisting of two modes, one when accelerations were low using a combination of the outputs from the two sensors, and one when accelerations were high relying solely on the gyroscope output due to the gravitational component in the measured acceleration.

Barshan and Durrant-Whyte [156] implemented an extended Kalman filter (EKF) to estimate position and orientation as part of a low-cost INS system. The filter incorporated error models of the performances of the accelerometers and gyroscopes over time. Testing of the algorithm found the orientation estimates were reliable over periods of 10 minutes and therefore successfully reduced the growth of the gyro drift error. However, the position estimates grew unbounded and were reliable only for 5 to 10 s. This was thought to be caused by large vibrations under unconstrained environmental conditions. The application of this system was for general use in mobile robot guidance problems. Vaganay et al. [157] designed a reduced order EKF to describe attitude of a mobile robot. The filter fused together roll and pitch estimations from accelerometers and odometry measurements and integrated gyroscopes outputs. The integration was implemented outside the filter. Thus, the process was not modelled within the filter. The filter estimated the drift of the orientation estimates to be $0.08°s^{-1}$. Marins et al. [187] proposed an alterative approach to a Kalman filter following on from the MARG system developed by Bachmann [102]. They found an EKF was computationally demanding making it unfeasible for real-time tracking. Instead, their approach utilized a Gauss-Newton iteration algorithm to find the optimal representation relating the measurements of linear acceleration and earth magnetic field from the body to the earth reference frame. In this approach, the input measurement and the process essentially become linearized and hence reduces the complexity and requires only a simple discrete Kalman filter. Testing of the filter by rotating the MARG through 90° about each axis

produced near zero angular rates apart from the appropriate change during the rotation and returned to near zero afterwards. Saripalli et al. [105] described an extended Kalman filter to merge information from an EiMU, differential GPS (DGPS) and external measures of height and velocity for the control of autonomous helicopters. Instead of the helicopter dynamics, the rigid body motion equations and the gyroscope drift were modelled in the filter using the acceleration and rotational velocities from the EiMU as inputs. The DGPS and stereo and vision-based measurements provided infrequent updates. The performance of the filter was not quantified. Santiago [182] designed an EKF to fuse together the linear and angular acceleration vector produced solely from 12 accelerometers and baro-altimeter measurements, and updates by GPS signals during periods of large acceleration. The navigation process was modelled within the filter generating a full state estimate instead of just the error.

Harada et al. [103] used an unscented Kalman filter (UKF) to estimate orientation for a portable device. The filter was based on a Gaussian distribution approximation and was composed of accelerometers, gyroscopes and magnetometers. It was reported that this type of filter was more suitable for the nonlinear systems then EKF. They suggested that an EKF was too complex for implementation and the method of linearization led to instability if time steps were not sufficiently small. Testing of the device showed an absolute orientation error of less than 4°. Harada et al. [104] developed their optimising algorithm further by introducing a sigma-points Kalman filter (SPKF). A SPKF uses a weighted statistical linear regression (WSLR) technique to calculate the optimal terms. Lee and Ha [98] described a geometric fusion algorithm which functions similarly to a form of the Kalman filter.

2.7.3 Complementary Filter

A complementary filter is a more straightforward and simplified version of the Wiener and Kalman filters. Its primary goal continues to be the minimisation of the square of the expected error and it has several advantages over the Wiener and Kalman filters. These advantages are that the theory of the filter is not based upon the assumption of having complete statistical data regarding the signals involved, less development time, lower computational time and processing, and the choice of any

appropriate parameter optimisation technique. A complementary filter combines multiple noisy measurements of the same parameter. The measurements must exhibit complementary spectral characteristics, and the transfer functions of the system are chosen in such a way to minimise the estimation error. Accelerometers and gyroscopes display complementary spectral characteristics. Accelerometer outputs utilised in attitude estimations become unreliable under dynamic acceleration conditions and therefore only provide reliable long term (low frequency) attitude estimates. The gyroscope outputs suffer from (low frequency) zero bias drift and therefore only provide reliable short term (high frequency) attitude estimates.

Although the performance is perhaps not as optimal, this type of filter has been implemented in numerous applications with remarkably accurate results [90, 102, 111, 113, 136, 177, 191]. Baerveldt and Klang [111] successfully fused the integrated signal of a rate gyroscope with the signal from an inclinometer to obtain optimal attitude estimations. The filter design was based on the known dynamics of the inclinometer. Roberts et al. [191] implemented a filter that calculated the error between the accelerometer and gyroscope attitude estimates. This error was then added to the angular rate error to be integrated again to yield a more optimal estimate. Lunige et al. [90] used the theory outlined in Brown and Hwang [188] and described a filter to estimate tilt of a three accelerometer three gyroscope sensor module unit. The gyroscope estimation of angle was split into tilt and rotation (method not stated). The tilt from both types of sensors was fused through a filter to provide a drift free estimate of tilt. The filter was essentially an error model which adjusts the sensor parameters like gain and offset and produces optimised estimates of output parameters. A more sophisticated complementary filter which had a separate bias was described by Foxlin [113]. The complementary filter fundamentals were extended into a reduced order linearized Kalman filter which modelled the errors of the gyroscopes such as high hysterises and nonlinearity and also the zero bias but as a separate error state. The system was implemented to track the motions of the head. An inclinometer described in this paper was replaced by accelerometers later on by Foxlin et al. [114].

Bachmann [102] implemented a type of complementary filter (named the quaternion filter) to estimate orientation. The basic design of the filter was outlined previously by Frey [152]. The orientation estimates combined from accelerometers and

magnetoresistive sensors were compared to those from the gyroscopes and the difference was added to the original angular rate output and integrated again. This method seemed theoretically robust and preliminary tests showed the accuracy of the filter to be within 1° during dynamic rotations. Luinge [136] and Luinge and Vetlink [177] described firstly a discrete-time complementary Kalman filter to estimate the acceleration, offset and gravity. The error model within the filter was based on a set of sensor assumptions. A further filter was then designed which fused the information of a tri-axial accelerometer system with a tri-axial gyroscopes system in order to measure orientation of a human body segment. The filter modelled the sensor signals, made assumptions about the sensors' behaviour and frequency, the magnitude of the outputs and incorporated assumptions about the movement being measured. The filter estimated the states of the model in a statistical most-likely sense, considered the measured signal and continuously adjusted the gyroscope zero bias.

2.8 Summary

The most commonly used body worn sensors for human movement analysis are differential capacitive accelerometers, piezoelectric vibrating gyroscope and magnetoresistive compasses. It is evident that for complete movement analysis of rigid bodies or point of attachment, a sensor module that measures parameters in three orthogonal directions is required for all three types of sensor. It is assumed that positioning of the sensor module at a point assumed to be representative to the CoM of the body provided a measure of overall body movements. A calibration procedure is essential to determine calibration parameters, zero bias and scale factor, to transform the sensor outputs into their respective units. The procedure can be easy to perform, repeatable and produce accurate calibration parameters.

All three types of sensor provide important information to help describe human movements. The accelerometers can be used to determine the direction of the local vertical vector, the orientation of the rigid body segment and joint angles. They can also be used to determine the linear velocity and position of the rigid body segment or point of attachment. However, the accelerometers do not measure rotation about the vertical axis and therefore cannot give a complete description of the orientation

vector. The gyroscopes can be used to determine the absolute orientation of the segment or point of attachment providing initial conditions were known. Initial conditions for the integration process can be found from accelerometer and magnetoresistive compass measurements under static conditions prior to the commencement of the experiment. The magnetoresistive compasses can be used to determine the heading or azimuth of the rigid body segment or point of attachment, provided the tilt of the sensor module is known. It is evident that the best solution for measuring human movements would be to use a combination of three accelerometers, three gyroscopes and three magnetometers. If the movement of interest can be assumed to be conducted with a near continuous heading then an inertial sensor module of three accelerometers and three gyroscopes can provide sufficient information. An example of such a movement would be the 100 m sprint.

The sensors can be positioned in various places largely depending on what was required to be measured. It is thought that a cluster of sensors positioned at a point assumed to represent the body's CoM would provide valuable information of overall body movements during walking and running, and in particular, sprinting. Subsequently, this approach results in one attachment site and a minimal number of sensors, reducing the likely size and cumbrousness of the system.

MEMS sensors can be used in numerous and diverse applications. In relation to designing a sensor system to be used as a training tool in the field of athletics, there are several important studies. Mayagoitia et al. [54] demonstrated the potential and accuracy of the sensors to determine several kinematic parameters such as linear acceleration of the knee. The sensor measurements were compared to an optical motion analysis system and reported an RMS error of less than 7% at five different walking speeds. The theory outlined in this paper was applied in a biomechanics study by Nene et al. [55]. This concept can be translated to other body segments or the body's CoM. Pappas et al. [56], Aminian et al. [109] and Sabatini et al. [97] demonstrated the potential of the sensors to detect the gait events of heel strike and toe-off. It is thought that the timings of these events can be used to estimate stride frequency. Consequently, if the average horizontal velocity is known for each stride then the stride length can be derived. A MEMS sensor system can also be used in sports situations [54, 141]. However, to the knowledge of the author there are no

applications where the sensors have been utilised as a training tool describing the kinematic parameters of human movements in the sporting context such as analysing sprinting motion.

The review highlighted that the most prominent error characteristics of the sensors are the noisy signals and the zero bias of the gyroscope drifting with respect to time and also temperature. These errors within the signal then cause accumulating drift when the gyroscope signals are integrated to produce the orientation vector. The amount of integration drift in the orientation vector is likely to cause further errors when the linear acceleration is separated from the measured acceleration, transformation of the angular rates to the respective representation and rotation of the accelerations to the earth reference frame. Therefore, the velocity and positional parameters derived through double integration of these linear accelerations can be difficult to estimate reliably and accurately for long periods of time. However, if the movement of interest is short in duration, for example, sprinting, and if there are periods when the system could be reset, then calculation of velocity and positional information may be feasible.

The preferred choice of angle representation from the literature is Euler angles, provided that the intended application is not concerned with the problem of singularities. The two reference frames commonly used in human movement analysis are the body and 'flat earth' frames. These frames are translated by the rotation sequence ZYX.

It is evident that some level of filtering is desirable to fuse together the outputs from the sensors to provide optimal parameter estimates. The complementary filter is perhaps not the most optimal of the filters discussed. However, it offers numerous advantages. These advantages are minimal development time, low levels of computational time and processing power, and the fact that statistical data about the signals is not required to be known.

Chapter 3 The System

3.1 Introduction

This chapter describes in detail the elements that comprise the proposed inertial sensor system. The first section presents the specification of the system in light of the facts outlined in the first two chapters. The second section describes the type of sensors chosen and how those sensors function. This is followed by a pictorial overview of the system. The fourth section presents the hardware of the system, this comprises schematic circuit designs, signal processing steps of the sensor outputs, how the data is acquired and details of the power supplied to the system. Next, the allocated arrangements of the sensitive axes of the sensors are defined. The sixth section outlines the processes required to convert the sensor outputs into usable, meaningful values. This is followed by details of the chosen enclosure and the method of attaching the system to the subject. Finally, the last section is a summary of the key elements.

3.2 The System Specification

The main aim of this thesis is outlined in chapter 1. Several features were considered imperative if this aim was to be met. Thus the system specification was outlined as follows:

> ➢ A kinematic analysis of an assumed representative point of body's CoM by direct measurement of accelerations and angular rates in three dimensions.

> ➢ Acceptable levels of accuracy, resolution and precision suitable for the intended application.

>> The accuracy of the system largely depended on the sensors themselves. The performance of the sensors is typically dictated by the factors of non-linearity, sensitive axis alignment error and in the case of a dual axis sensor the cross-axis sensitivity. Typical values of these

factors for the accelerometer were between 0.2% to 5% of the full scale (FS), to within 1° and ± 2%, respectively. The non-linearity term would increase or decrease the sensitivity of the sensors which would increase or decrease the accuracy, respectively. The alignment error would cause an increase of decrease to the respective signal equal to the sine of the alignment angle multiplied by the gravitational acceleration constant. The smaller the cross-axis sensitivity, the higher the accuracy of the acceleration signal in the non-sensing direction of a dual axes sensor.

The resolution of the system largely depended on the bandwidth and the noise performance of the sensor and also resolution of the A/D converter. A bandwidth of 50 Hz typically yielded a measurement noise of 0.0018 mg and $0.5°s^{-1}$. If a 12 bit A/D converter was used then the resolution of the sensors would be 1 mg and $0.14°s^{-1}$, respectively. The quantisation resolution was comparable to the noise performance which indicated that meaningful signals could be recorded.

The precision of the system largely depended on the stability and repeatability of the sensors with regard to random walk and temperature effects. Typical values are $0.5°s^{-1}$, and 2 $mg°C^{-1}$ and 10% of FS over temperature range, respectively.

➤ Capture both slow and fast human movements typically up to 50 Hz with an adequate measurement range.

The accelerations experienced at the assumed representative point of the CoM during walking have been found to be ± 1-1.5 g [79, 143] and up to 10 g to register impacts [61, 97]. Thus adequate measurement levels are ± 2 g and perhaps up to ± 10 g in the vertical direction. The angular rates experienced at the shank and thigh during walking have been found to be at maximum $400°s^{-1}$ and $230°s^{-1}$, respectively [54, 109, 192]. The angular movement at the assumed

representation point of the CoM during walking is likely to experience a lower angular rate, thus a range of $\pm 300°s^{-1}$ would be adequate.

➢ Provide low latency

The signals should be automatically processed and the desired parameters should be available within minutes after the data collection and in situ.

➢ Robust in all environments

The system should suffer no degradation in performance with regards to light, magnetic objects, signal reflections, transient noise and occlusions.

➢ Unrestricted capture range

➢ Not cumbersome to the user in terms of size, weight and as not to restrict movement.

The size of the system should be as small as physically possible which is largely dependent on the size of the actual sensors. Typically the sensors are less than 10 mm in any one dimension.

➢ Offer a suitable mounting arrangement

The system should be affixed quickly, repeatedly in the same position and offer low levels of unwanted movements between the affixing point and the body.

➢ Portable and self-contained (sourceless)

The system should be battery powered and offer the potential to support wireless transmissions.

➤ Quick and easy to set up

➤ Inexpensive

For example, the cost should be less than a few hundred pounds, thus making it viable for mass markets.

3.3 Sensors

The selected accelerometer and gyroscope sensors are presented and justified below. Following on from the review of the literature (see Chapter 2) it was assumed that the system would not require magnetoresistive sensors, and rely on the gyroscope sensor only to estimate the rotation about the z axis (azimuth). This assumption was supported by the fact that the system was designed to be limited to short data collection periods i.e. a few minutes, and to accommodate an interlude for resetting the accumulating errors between collection periods as a consequence of the intended application.

3.3.1 Accelerometers

An accelerometer is a device which senses both the dynamic and static accelerations about a defined axis. In the most general sense, the vast majority of accelerometers are typically modelled by a second order mass-damper-spring system. This system consists of a proof mass coupled to the sensor body by a spring like hinge or tether [8, 9, 76]. An applied acceleration and/or gravitational acceleration causes a displacement of the proof mass and deformation of the coupling occurring in a predetermined direction [178]. The amount of deformation or corresponding displacement is transduced by a sensing element and yields an electrical output proportional to the acceleration experienced. These electromechanical principles of the accelerometer have been formed in a MEMS device. There are numerous MEMS

accelerometers commercially available which can be predominantly categorised by the type of transduction method used. Within each category the sensors vary by mechanical design, fabrication technique, sensor material and the techniques of sensing electronics integration, and packaging of each specific sensor design.

The type of transduction methods implemented in accelerometer designs can be categorised, though not exclusively into: piezoelectric, piezoresistive and capacitive. Piezoelectric accelerometers like those by Measurement Specialties (formally AMP Inc.) [193] and used in [92] measure the change in electric charge of the piezoelectric material within the sensor. They require a dynamic input (time-varying) of some minimum frequency to generate a response and thus they have limited capabilities to measure low frequency inputs such as gravitational acceleration [194]. Piezoresistive accelerometers such as Entran EGAX [195] measure the change in resistance when strained or deflected and remain changed until the original position of the material is restored. Even though they sense low frequency inputs their operational temperature range is substantially limited [8, 9]. Capacitive micromachined accelerometers offer several benefits when compared to the piezoresistive and piezoelectric type accelerometers. These benefits are capable of low frequency response, low noise performance, high sensitivity, low drift and low temperature sensitivity [8, 17]. They measure the change in capacitance of the parallel plate typically formed by the mass separated by a narrow air gap from a fixed plate [8]. The displacement of the mass changes the air gap and thus the capacitance. Differential capacitance has increased performance over capacitive sensing due to the improved linearity response for small deflections. Also, the added advantage of this method is that the acceleration induced electrostatic force causing the deflection of the sensing elements means motion can be both induced and sensed allowing for the operation of a self test function. It was evident from the literature review that the most widely used accelerometer sensor for human movement analysis is the differential capacitive type and those specifically manufactured by Analog Devices [62].

Acar and Shkel (2003) evaluated four commercial available capacitive MEMS accelerometers. The sensors were manufactured by Endevco, Analog Devices, Silicon Designs and Motorola. The sensors were assessed in a number of tests to determine the characteristics such as sensitivity, resolution, linearity, frequency response,

transverse sensitivity (cross-axis), temperature effects, noise level and long term stability. In summary, although there was no clear preference of sensor, the Analog Devices' sensor demonstrated some significant performances. The sensor displayed the best sensitivity performance when subjected to a 100 Hz dynamic input, with no deviation over a 30 day period and less than 1% maximum deviation over the temperature range. The noise level and non-linearity responses of the sensor and the long term zero bias stability were recorded as 1.29 mg, 0.44% of full scale (FS) and 0.11% of FS, respectively, and were all ranked a close second behind the performance of the Endevco sensor. However, the cost and size of the Analog Devices sensor was considerably less at $8.50 a piece and 5 x 5 x 2 mm than the Endevco sensor. The lower cost and smaller size is a result of the manufacturing process. The Analog Devices and Endevco accelerometers are fabricated by using surface and bulk micromachining, respectively. Surface micromachining involves interfacing the sensing element and the signal conditioning circuitry onto the surface of a single substrate integrated circuit (IC) chip [8]. The substrate material can be for example silicon, glass or ceramic. This technique lends itself to batch fabrication and therefore the cost of the sensors can be low. Bulk micromachining involves etching the sensing element onto a silicon wafer and is not typically integrated with supporting conditioning circuitry resulting in a two chip device [8]. Therefore this fabrication technique produces a larger package size along with the increased expense restricts their applications [196]. The Analog Devices sensor offers a number of additional advantages. These are dual axis sensitivity, measurement ranges of ± 2g and ± 10g digital outputs which can be input straight into a microprocessor as well as analogue outputs, adjustable frequency response range up to 6 kHz, low operating voltage and low current consumption.

A summary of the characteristics of the device are shown in table 3-1 and visual description of the functionality of the sensor is displayed in figure 3-1. The figure displays two diagrams. The diagram on the left shows the accelerometer sensor at rest and with the sensitive axis parallel to the earth's surface therefore no dynamic and gravitational accelerations are experienced. The diagram on the right shows the response of the accelerometer sensor when an acceleration is applied. The proof mass is deflected and the differential capacitor becomes unbalanced. The accelerometer

provides an output with amplitude proportional to the acceleration applied. The full manufacturer's data sheet is found on the Analog Devices website [62].

Table 3-1 A summary of the characteristics of the Analog Devices capacitive accelerometer [62].

Parameter	Unit	Analog Devices
Type		ADXL202 (210)
Axes		2
Range	g	± 2 (± 10)
Sensitivity		
Analog	mVg^{-1}	312 (100)
Digital	$\% \, g^{-1}$	12.5 (4)
Supply Voltage	V	3 to 5.25
Current per axis	mA	0.6
Noise	$\mu g \sqrt{Hz}$	200
Frequency Response	kHz	6
Non- Linearity	% of FS	0.2
Size	mm	5x5x2
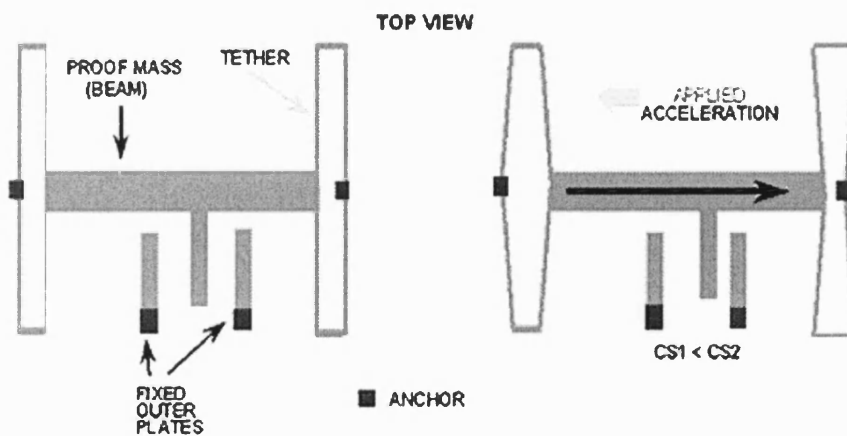
Figure 3-1 A diagram displaying the functionality of the Analog Devices differential capacitive accelerometer [62].

3.3.2 Gyroscopes

A gyroscope, commonly called the gyro, is a device which senses the rate of angular rotation about a defined axis. Almost all reported micromachined gyroscopes use vibrating mechanical elements to sense rotation. They have no rotating parts that require bearings, and hence they can be easily miniaturised into a MEMS device [196, 197]. Their operational principle is based on the Coriolis effect [190, 198]. Coriolis force, named after the French scientist and engineer G. G. de Coriolis (1792-1843), is an apparent force that arises whenever linear motion occurs in a rotating reference frame. In the case of vibrating gyroscopes the linear motion is typically produced by an oscillating element and controlled by an embedded circuit to oscillate at a constant amplitude. The Coriolis force experienced induces oscillations that have a direction perpendicular to both the axis of rotation and the axis of driven oscillation. These induced oscillations are detected by a sensing element and are proportional to the angular rate. A visual description of the effect is shown in figure 3-2. The figure displays a moving object which oscillates about the Y axis. A rotation about the z axis induces oscillations about the X axis which are proportional to the angular rate about the Z axis. The types of micromachined vibratory gyroscopes can be categorised, though not exclusively, into three groups [8, 196]. These are tuning forks such as those manufactured by Murata [63], Tokin [199] and Analog Devices [62], vibrating wheels such as those manufactured by Bosch [200] and wine glass resonators such as those manufactured by Silicon Sensing Systems [201]. A description of the more traditional gyroscope can be found in Barbour and Schmidt [17].
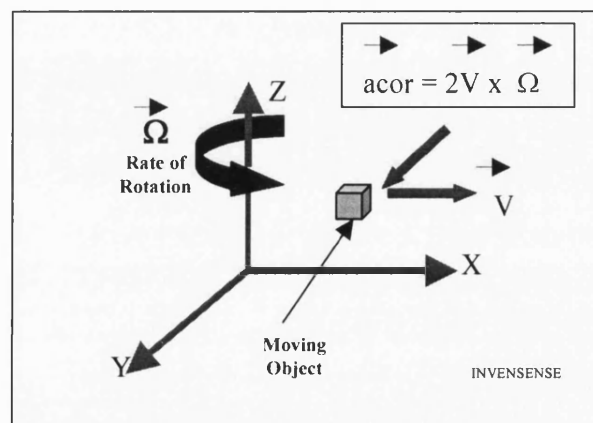
Figure 3-2 The Coriolis effect [197].

A tuning fork vibratory gyroscope typically contains a pair of masses that are driven to oscillate with equal amplitude but in opposite directions. When rotated, a Coriolis force is experienced and induces oscillations which are detected by a number of sensing elements such as capacitive [202] and piezoelectric [63, 199]. A vibrating wheel gyroscope has a wheel that is driven to vibrate about its axis of symmetry. A rotation results in the rocking or tilting of the wheel in a direction perpendicular to the driven movement. The change in air gap between the vibrating element and the substrate was typically detected with capacitive electrodes under the wheel. It is possible to sense two axes of rotation with a single vibrating wheel. A wine glass resonator is sometimes referred to as ring resonator [196]. The vibrating element is formed as a ring and is driven to oscillate. When rotated, a Coriolis force is experienced and causes the oscillation pattern to move around the resonator. The change in direction is sensed by electromagnetism. This design offers the advantages of being less sensitive to shock, vibration and linear acceleration [203].

Gyroscopes are much more challenging sensors than the accelerometers and this may be why the market is less mature. As a consequence, at the time when a gyroscope was selected for the inertial sensor system there was limited choice and certainly less documented reviews on the performances of commercially available MEMS gyroscope sensors [100, 178, 197]. Both Benbasat [100] and Verplaetse [178] compared the characteristics of several gyroscopes but of varying operating technologies. Whereas, Nasiri [197] presented the top four manufacturers of MEMS vibrating gyroscopes but only referring to their micromachining fabrication, driving and sensing elements and package type. Therefore, a summary of the performance parameters of these four manufactures specified in their data sheets is included and displayed in table 3-2.

Table 3-2 A summary of the characteristics of five vibratory MEMS gyroscopes.

Parameter	Units	Bosch	BEI	Analog Devices	Murata	Tokin
Part Number		SMG040	QRS11	ADXRS300	ENC-03J	CG-16D
Axes		2	1	1	1	1
Element material		Polysilicon	Quartz	Polysilicon	Ceramic Bimorph	Ceramic
Voltage Supply	V	4.8	± 5	4.75-5.25	2.7-5.25	5
Current Consumption	mA	<30	< 80	6	3.2	7
Range	$°s^{-1}$	± 250	± 50-1000	± 300	± 300	± 90
Linearity	% FS	± 1	0.05	0.1	± 5	n/g
Frequency Response	Hz	21-33	> 60	40	50	100
Noise	$°s^{-1}\sqrt{Hz}^{-1}$	0.2	0.01	0.1	0.05 [a]	n/s
Drift	$°s^{-1}$	n/s	0.2	n/s	0.5 [a]	n/s
Size	mm	17 x 18 x 5	38 x 38 x 16	7 x 7 x 4	7 x 12 x 3	8 x 20 x 8
Cost	£	n/s	$1400	$30	$80	n/s

[a]Not given on data sheet. Taken from [100]. However, this value originally claimed to be 7 $°s^{-1}$[204].

n/s refers to not specified on the data sheet or not found in the literature.

The Analog Devices gyroscope has some notable strengths when compared to the others. It requires only a single voltage supply unlike the BEI gyroscope, requiring less battery power. The sensor has a higher bandwidth and lower noise floor than the Bosch gyroscope. The sensor is also the smallest and the least expensive. However, the pins of the sensor are semi-spherical in shape, positioned on the underside of the sensor and configured with inner pins. This configuration proved to cause a number of associated difficulties. These difficulties were the limitations of the available equipment to design and make a printed circuit board (PCB) that gives connections to the inner pins and to solder the sensor onto the PCB. As an alternative, the Murata gyroscope offers the same operating range and voltage supply, lower current consumption and higher frequency response. The sensor is also only fractionally bigger and more expensive, but readily available to purchase from a UK distributor. The evidence presented in the literature review also supports the choice of this sensor. Murata offers two types of gyroscope, the ENC-03JA and ENC-03JB. The two types have different resonant frequencies and are typically used in combination if two sensors are mounted in close proximity. This reduces the interference effects caused by cross coupling and the sensing of unwanted signals [205].

3.3.3 Section Summary

The sensor system combined two two-axis accelerometers from Analog Devices and three single axis gyroscopes from Murata. Since the system contained only inertial sensors, it will from this point onwards be referred to as the inertial sensor system.

3.4 System Hardware

3.4.1 An Overview of the Inertial Sensor System

The figure 3-3 shows a pictorial overview of the whole inertial sensor system.
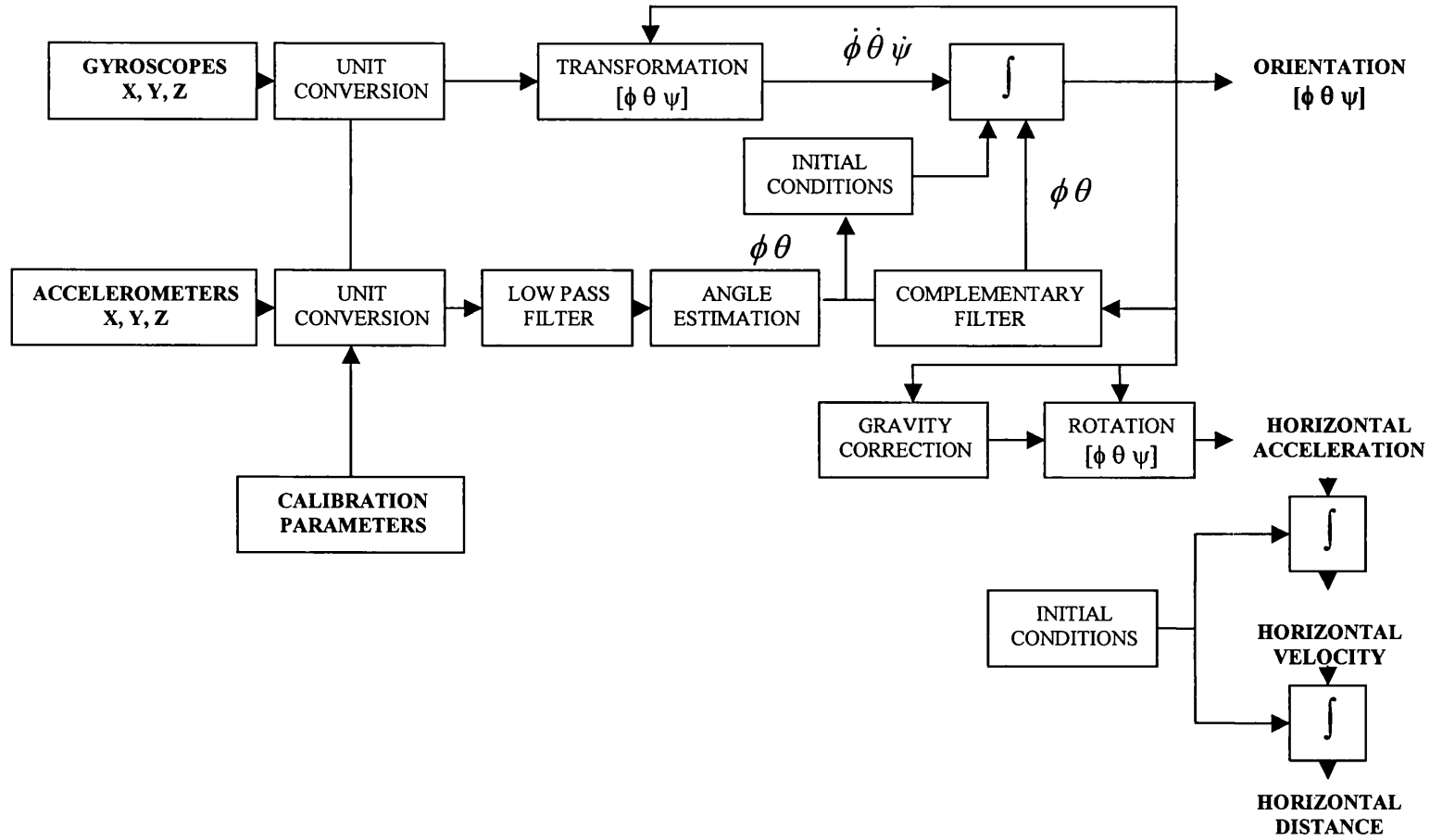
Figure 3-3 The overview of the inertial sensor system

3.4.2 Sensor Boards

3.4.2.1 Board 1: X and Y Axes

Board 1 is displayed in figure 3-4 and contains one dual axis accelerometer, IC1, two single axis gyroscopes, IC2 and IC3, a voltage regulator, IC4, and some passive components. All sensor outputs were fed directly to the connector which was coupled to the processing box. The accelerometer was operated on a fixed-output regulated +5 V supply which was decoupled from noise on the power supply by resistor, R1 and capacitor, C3. The accelerometer was band limited to 50 Hz by capacitors C1 and C2 connected across the analogue output pins and ground. Although the digital outputs were not being used, the duty cycle modulator was kept running at 8 ms repetition rate set by the value of resistor R2. The gyroscopes operate from an on-board fixed output regulated +3.3 V, 100 mA supply. Since the gyroscopes were mounted in close proximity their resonating frequencies needed to be different to minimise interference. Therefore, one gyroscope was an ENC-03JA, IC2, and the other was an ENC-03JB type, IC3. The components were arranged so that the rotation axis of each gyroscope was consistent with the sensitive axes of the accelerometer. The gyroscope, IC2, measured rotations about the accelerometer's x axis and IC3 measured rotations about the accelerometer's y axis.

3.4.2.2 Board 2: Z Axis

The second board in the box displayed in figure 3-5 was much smaller and contains only one dual axis accelerometer, IC6, and one single axis gyroscope, IC5, a voltage regulator, IC7, and some passive components. The circuitry was configured as detailed for board 1. The gyroscope was arranged so that the axis of rotation was consistent with the y sensitive axis of the accelerometer. This board was mounted orthogonally with respect to board 1 within the sensor box and hence the accelerometer's sensitive axes were such that x is sensitive in the same direction as the x axis from Board 1 and y is orthogonal to the x and y axes of board 1. The y axis on this board was renamed z axis and together the two boards sensed three

accelerations in orthogonal directions and three rotations about the three acceleration directions.

3.4.2.3 Connectors

Tables 3-3 and 3-4 outline the signal arrangements in the connectors for boards 1 and 2.

Table 3-3 Connector PL1 between sensor module and processing box.

Pin	Signal	Colour
1	+5V	Red
2	Spare Acceleration	Brown
3	Z Acceleration	Purple
4	Spare Acceleration	Brown
5	Z Acceleration	Purple
6	GND	Black
7	Z Gyroscope Vref	Grey
8	Z Gyroscope Vout	Grey
9	X Acceleration (Analogue)	Orange
10	Y Acceleration (Analogue)	Yellow
11	X Acceleration (Digital)	Orange
12	Y Acceleration (Digital)	Yellow
13	Y Gyroscope Vout	Blue
14	Y Gyroscope Vref	Blue
15	GND	
16	n/c	
17	n/c	
18	X Gyroscope Vref	Green
19	X Gyroscope Vout	Green
20	+5V	

Table 3-4 Connector PL2 between board 1 and board 2.

Pin	Signal	Colour
1	X Acceleration (Analogue)	Grey
2	Y Acceleration (Analogue)	Grey
3	X Acceleration (Digital)	Grey
4	Y Acceleration (Digital)	Grey
5	GND	Grey
6	Z Gyroscope Vref	Grey
7	Z Gyroscope Vout	Grey
8	+5V	Red
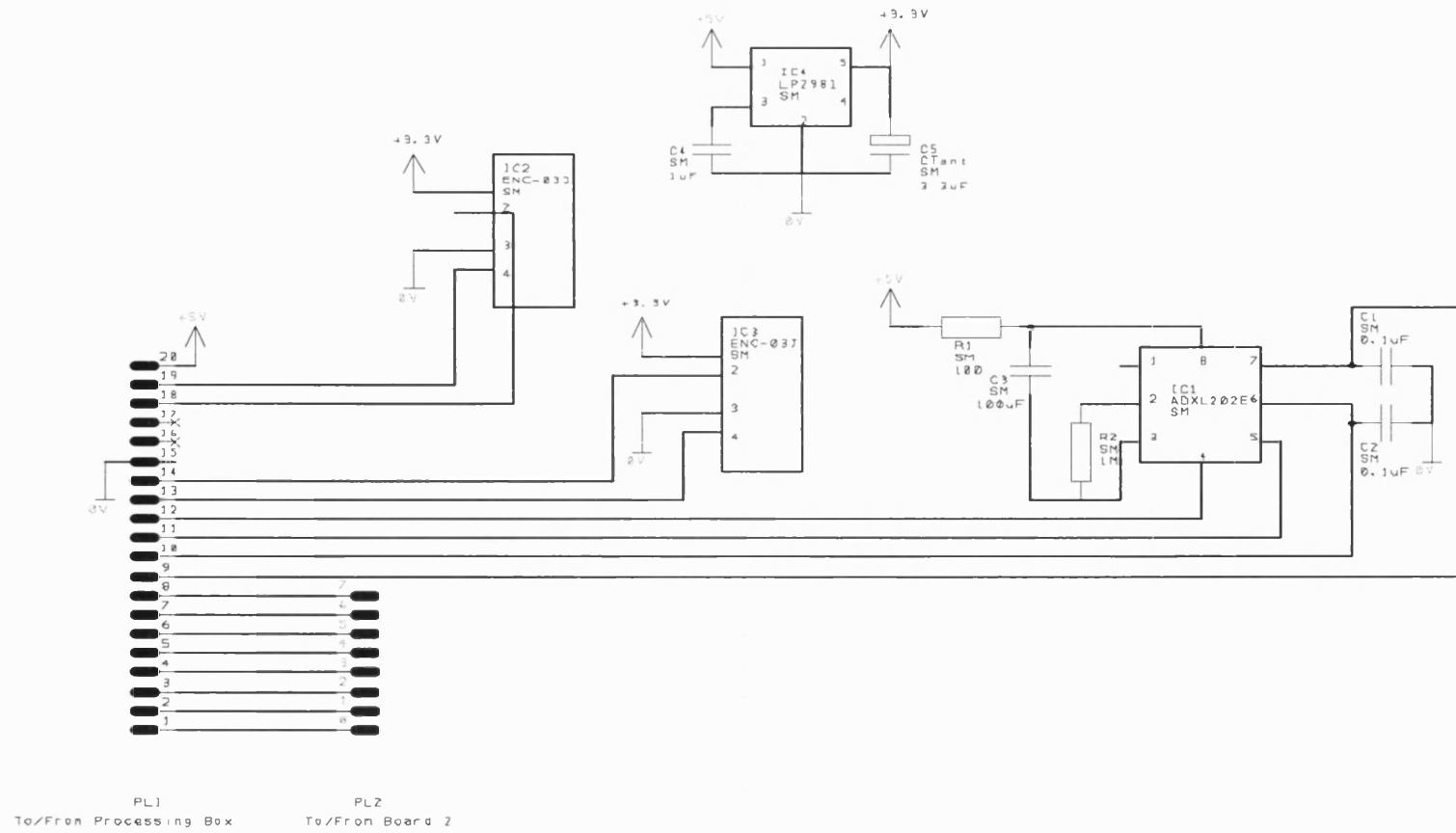
Figure 3-4 The schematic circuit for board 1 of the inertial sensor system.
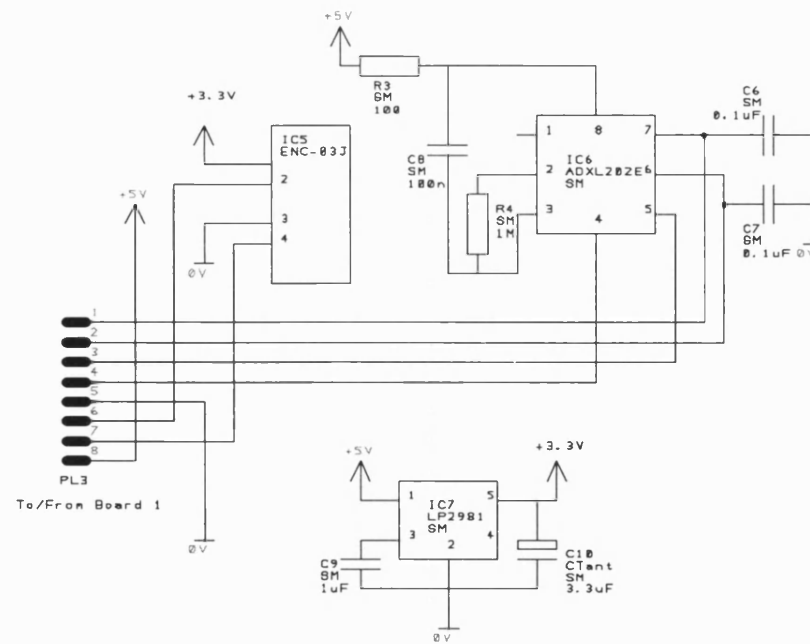
Figure 3-5 The schematic circuit for board 2 of the inertial sensor system.

3.4.3 Signal Processing

All of the sensor outputs required some signal processing before they were converted into a digital value. For the accelerometer sensors this meant amplification and a DC level shift to maximise the resolution. Whereas, the two outputs from each gyroscope, V_{out} and V_{ref}, were compared and the result was amplified and low pass filtered to increase resolution and to eliminate high frequency vibrations and transient noise, respectively.

3.4.3.1 Accelerometer Processing Board

The accelerometer processing board displayed in figure 3-6 consisted of one quad operational amplifier, IC12, two fixed voltage regulators, IC13 and IC14, and some passive components. The output of each accelerometer axis was fed into a high input impedance unity inverting buffer, IC12a. This buffer was required due to the relatively low output impedance, 32 kΩ, of the accelerometer analogue outputs. The buffered signal was then inverted and amplified, by operational amplifier, IC12b, at a gain determined by the resistor ratio of the sum of R22 + R30 + R23, to R23. Resistor R30 allowed the gain to be adjustable from 1.5 to 3.5 to make the full use of the input range of the A/D converter. The third amplifier in the circuit, IC12c, provided a DC voltage which was adjustable within a range from -10 V to +10 V. The two fixed output voltage regulators, IC13 and IC14, supply +5 V and -5 V, respectively, to each end of the multi-turn pot resistor R29. The input to IC12c varied in accordance to the resistance of R29, for example if the resistance is low then the input DC voltage level would be near 5 V. Subsequently, the DC voltage level into IC12c was amplified by a gain of 2 by the ratio of the resistors, R27 and R28. Therefore the range of -10 V to +10 V was achievable. The outputs of the operational amplifiers, IC12b and IC12c were fed into the fourth operation amplifier, IC12d which was configured as a current summing amplifier with unity gain. The operational principle of IC12d is to shift the DC level of the input from IC12b by the magnitude of the input from IC12c. The resistor R29, was adjusted so that when the raw output of the accelerometer read 2.5 V i.e. experiencing zero acceleration, the resultant output of IC12d was half of the specified input range of the A/D converter.

3.4.3.2 Gyroscope Processing Board

The gyroscope processing board, displayed in figure 3-7, performed a very simple operation involving amplification and low pass filtering of the change in the gyroscope output V_{out} compared to the other output V_{ref}. Each axis was configured identically. The amplification gain was set at 2.5 by the ratio of resistors R58 to R55. The cut off frequency of the lowpass filter was set at 106 Hz by the combination of resistor R58 and capacitor, C28. The signals into the processing board and out of the board via connectors PL5 and PL6 were defined in table 3-5 and 3-6, respectively.

Table 3-5 Connector PL5 raw gyroscope signals into the processing board.

Pin	Signal	Colour
1	X Gyroscope Vref	Grey
2	X Gyroscope Vout	Grey
3	Y Gyroscope Vout	Grey
4	Y Gyroscope Vref	Grey
5	Z Gyroscope Vout	Grey
6	Z Gyroscope Vref	Grey

Table 3-6 Connector PL6 processed gyroscope signals out of the processing board and sent to the A/D converter.

Pin	Signal	Colour
1	X Gyroscope	Orange
2	Y Gyroscope	Yellow
3	Z Gyroscope	Purple
4	n/c	
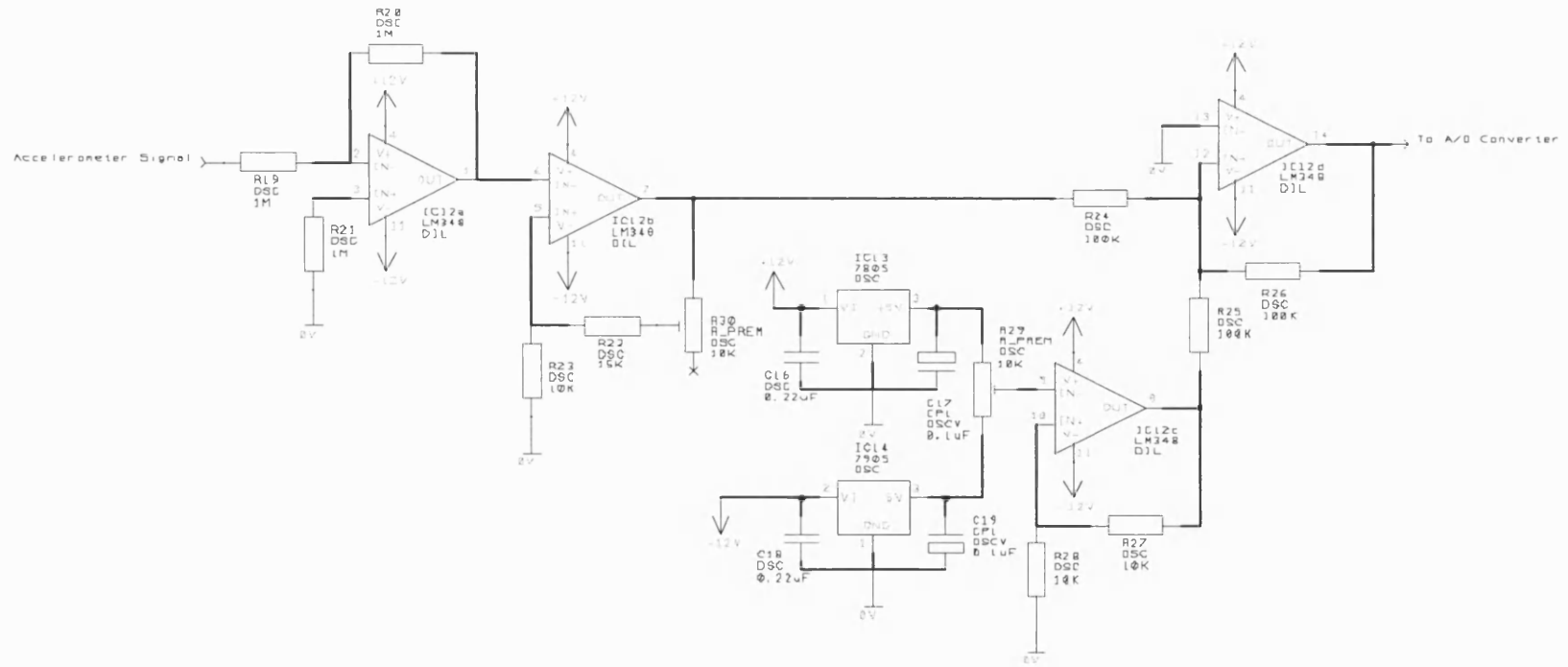
Figure 3-6 The schematic circuit for the processing of the accelerometer signal prior to digital conversion. (Only a single axis is shown here as this circuit is duplicated for the other two axes.)
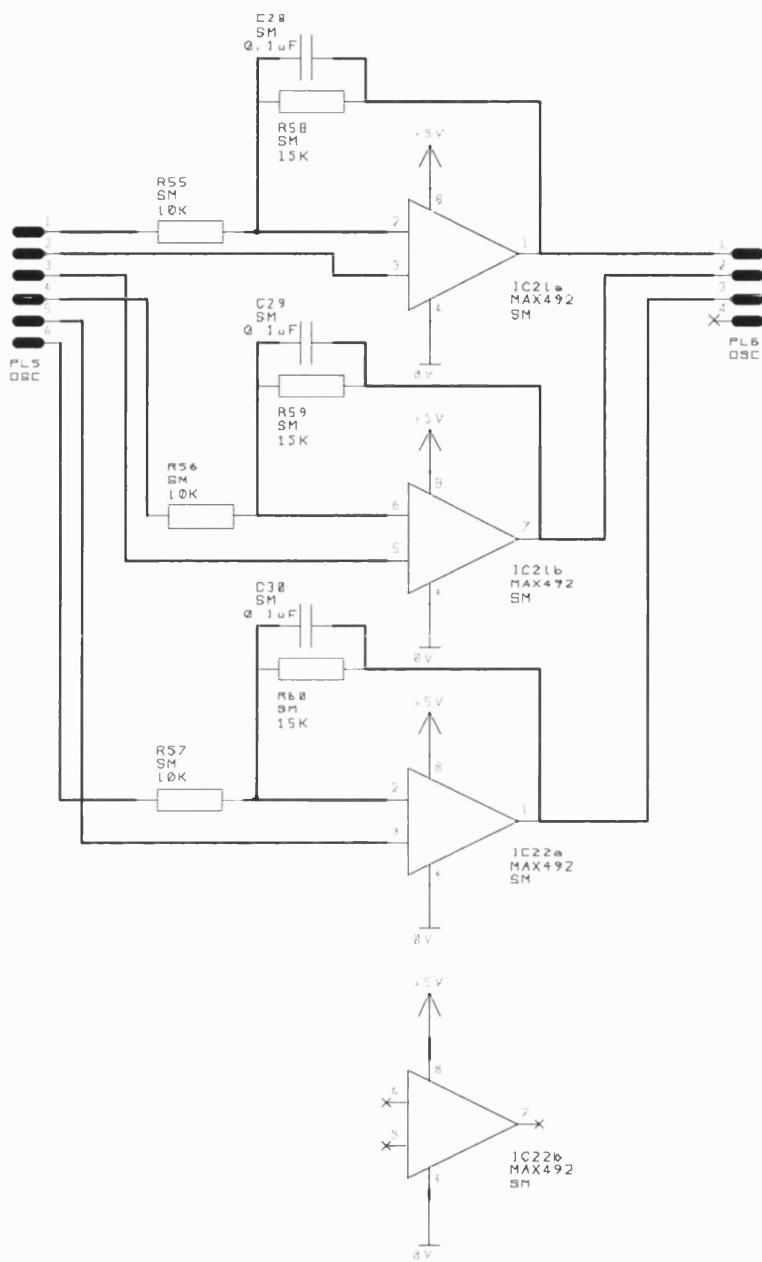
Figure 3-7 The schematic circuit of the gyroscope processing board prior to digital conversion.

3.4.4 Data Acquisition

It was thought that at this stage in the project, analysis of the sensor outputs carried a higher precedence than designing and implementing a data acquisition system. Therefore, an off-the-shelf data logging system from Pico Technology Ltd consisting of an A/D converter, parallel port interface and software controlled data recorder was selected. Once the sensor system outputs were shown to provide useful information then it would be straightforward to replace the data logger with a preferred data acquisition system tailored to the requirements of the sensor system. The ADC11/12 Pico data logger was chosen on the merits of the A/D converter. The converter offered the highest resolution for the largest number of channels. The converter offered 12 bit resolution and an input range of 2.5 V, thus, the smallest measurable change in voltage was 0.61 mV. This corresponds to 1 μg and $0.36°s^{-1}$ for the accelerometer and gyroscope sensors, respectively. The maximum number of channels available was 11 of which seven were subscribed by three accelerometer sensor signals, three gyroscope sensor signals and also one channel was assigned to be used for synchronisation to other data collection systems. The logger is capable of recording data at a rate of as little as once an hour to 1000Hz. It had the ability to display the data visually by a graph and/or on a spreadsheet in real time. However, because the data logger was controlled by software the parallel port interface was required to be connected at all times during recording. This may prove to be cumbersome during experiments but it was not a long term design feature of the overall marketable sensor system.

3.4.5 Power Supply

The whole system was supplied by four 9 V d-type batteries to provide +18 V, -18 V and mid rail (Ground). The battery supply was regulated to +12 V and -12 V, respectively to provide a dual supply to the operational amplifiers on the processing boards. Typically, a dual supply was required for the operation of the majority of operational amplifiers and it was also required for the chosen method to shift the DC level of the accelerometer signals. However, the disadvantages were the increased

number of components and batteries which increased the size, bulk and weight of the system. The +12V is regulated to +5V within the processing box to supply the sensor module via the connecting cabling and also the single supply to the operational amplifiers on the gyroscope board.

3.5 Sensor Arrangement and Module

It was evident from the literature review that the most commonly used reference system and method in which they were described for human movement applications was the aerodynamic model and Euler angle representation. A definition of this model can be found in Grewel et al. [190] and Kuipers [183]. The two reference systems that were used were body and 'flat earth' and are displayed in figure 3-8. The body reference frame denoted by B, had an origin based at the point of attachment and continuously moved with the body. The body coordinates within this frame were defined with the x axis "out of the nose" in the forward direction, the y axis, "out of the right side" and the z axis, "out of the belly". The 'flat' earth reference frame, denoted by E, was an inertial fixed frame with an arbitrarily selected origin, in this case on the ground at the starting position of the movement. The term 'flat earth' arises from the assumption that motion on or near the surface of the earth at speeds far below the orbital velocity has limited influence from the curvature of the earth [102]. The earth coordinates within this frame were defined following the convention of the X axis pointing North, Y axis pointing East and the Z axis point down known as NED [190].
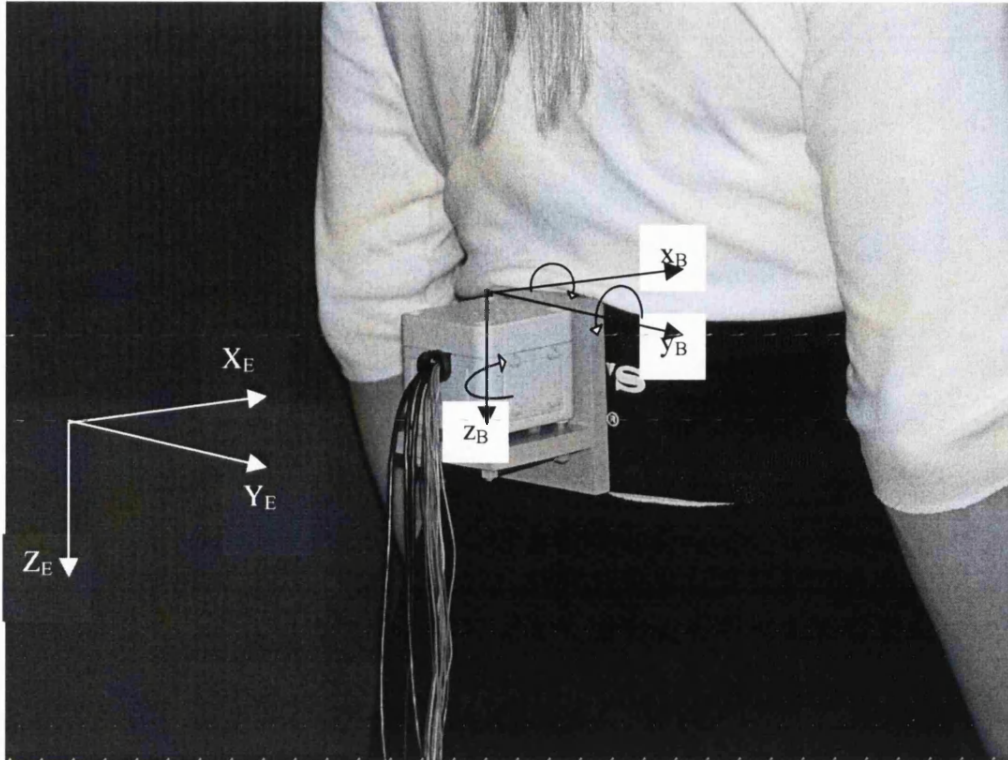
Figure 3-8 The 'flat earth' and 'body' reference frames and coordinate directions.

The orientation of the rigid body was represented by Euler angles. This representation approach was selected on its merits such as the preferred visual comprehension, less computational steps and also that the singularity limitation would never be broached. Euler angles specify a sequence of three angles defined as roll (bank) about the x axis by angle ϕ, pitch (elevation) about the y axis by angle θ, and yaw (azimuth) about the z axis by angle ψ. Positive rotations are to the right. A three dimensional sensor module of accelerometers and gyroscopes were arranged to provide three axes of acceleration and angular rate information in three directions to which the module was affixed. The three measurement directions are marked x, y and z and the gyroscope sensors are mounted with respect to the sensitive axes of the accelerometers. The arrows define the positive acceleration and rotation directions. The body coordinates can be expressed in the 'flat earth' reference frame by combinations of the rotation matrices about each axis denoted in the following equations 3-1 to 3-3.

$$\text{rot}(x, \phi) = \begin{bmatrix} 1 & 0 & 0 \\ 0 & \cos\phi & -\sin\phi \\ 0 & \sin\phi & \cos\phi \end{bmatrix} \qquad \textbf{3-1}$$

$$\text{rot}(y, \theta) = \begin{bmatrix} \cos\theta & 0 & \sin\theta \\ 0 & 1 & 0 \\ -\sin\theta & 0 & \cos\theta \end{bmatrix} \qquad \textbf{3-2}$$

$$\text{rot}(z, \psi) = \begin{bmatrix} \cos\psi & -\sin\psi & 0 \\ \sin\psi & \cos\psi & 0 \\ 0 & 0 & 1 \end{bmatrix} \qquad \textbf{3-3}$$

Where, ϕ is the roll angle about the x axis

θ is the pitch angle about the y axis

ψ is the yaw angle about the z axis

3.6 System Software

Once the sensor outputs have been recorded a certain amount of software processing was required to produce meaningful information. All of this processing was executed manually and off line. It is possible in collaboration with the Pico data logger to write a tailored software program which controls the A/D converter and executes the required processing to provide final outputs in real time. However, again at this stage the importance of analysing the data was prevalent over the need for real time answers. The processing steps fall into the following categorises: unit conversion, angular rate transformation, integration, accelerometer attitude estimation, complementary filtering, elimination of gravitational acceleration and rotation to the appropriate reference frame.

3.6.1 Unit Conversion

The first step of digital processing was to convert the sensor outputs from the measured unit of volts into the appropriate units of g and $°s^{-1}$ for accelerations and angular rates, respectively. All of the sensors underwent a calibration procedure from which the calibration parameters such as scale factor and zero bias were derived. These parameters are used in the equations 3-4 and 3-5 below.

$$\text{Acceleration}\,(g) = \frac{\text{Output (V)} - \text{Zero bias (V)}}{\text{Scale Factor (Vg}^{-1})} \qquad \textbf{3-4}$$

$$\text{Angular Rate}(°s^{-1}) = \frac{\text{Output (V)} - \text{Zero Bias (V)}}{\text{Scale Factor (mV}°^{-1}s^{-1})} \qquad \textbf{3-5}$$

3.6.2 Transformation Matrix: Angular Rates to Euler Rates

The aerodynamic model generates rotational velocities known as angular rates relative to the body coordinates within the body reference frame denoted as p, q and r about the body axes x, y and z. Unlike linear velocities which may be integrated to obtain position, the angular rates cannot be integrated to obtain Euler angles. Instead the angular rates were transformed following equation 3-6. To derive the transformation matrix, T, the angular rates must first be expressed about the body reference frame in terms of angular rates about the earth reference frame as displayed in equation 3-7. This process uses the transpose of the orientation matrices in equations 3-1 to 3-3. A more detailed derivation can be found in McGhee et al. [179].

$$\begin{bmatrix} \dot{\phi} \\ \dot{\theta} \\ \dot{\psi} \end{bmatrix}_E = T \begin{bmatrix} p \\ q \\ r \end{bmatrix}_B \qquad \textbf{3-6}$$

$$p = \dot{\phi} - \dot{\psi}\sin\theta$$

$$q = \dot{\theta}\cos\phi + \dot{\psi}\sin\phi\cos\theta \qquad \text{3-7}$$

$$r = -\dot{\theta}\sin\phi + \dot{\psi}\cos\phi\cos\theta$$

where, p, q and r   are the angular rates about the x, y and z axes

φ, θ and ψ   are the angles roll, pitch and yaw about the x, y and z axes

$\dot{\phi}, \dot{\theta}$ and $\dot{\psi}$ are the Euler rates about the x, y and z axes.

The equation 3-7 was rearranged to solve for the Euler rates and formed into the transformation matrix, T, displayed in equation 3-8.

$$\begin{bmatrix} \dot{\phi} \\ \dot{\theta} \\ \dot{\psi} \end{bmatrix}_E = \begin{bmatrix} 1 & \sin\phi\tan\theta & \cos\phi\tan\theta \\ 0 & \cos\phi & -\sin\phi \\ 0 & \sin\phi\sec\theta & \cos\phi\sec\theta \end{bmatrix} \times \begin{bmatrix} p \\ q \\ r \end{bmatrix}_B \qquad \text{3-8}$$

The resultant Euler rates were defined as roll rate, pitch rate and yaw rate, respectively. The orientation angles used in the matrix were the overall outputs from the system at the previous time step.

3.6.3 Integration: Euler Rates to Orientation Angles

The Euler rates were integrated by a numerical approximation, the trapezium rule, to yield the orientation angles. The trapezium rule is an approximation to the integral of a function and estimates the area under the curve of the function. This area is found by dividing the data collection period into a sequence of approximating trapezoids (conveniently using the sampling rate) and adding the areas of the trapezoids. A trapezoid is formed by replacing the function by a straight line between each sampling point and thus the area is found following equation 3-9.

$$\Delta A = \frac{1}{2}(f(t_i) + f(t_{i+1})) \cdot \Delta t \qquad\qquad \textbf{3-9}$$

where, ΔA is the area of the trapezoid

       f is the function

       t_i is the time at sampling interval i

       t_{i+1} is the time at sampling interval $i+1$.

       Δt is the sampling period

Therefore the integral can be expressed by equation 3-10 [206].

$$\int_a^b f(t)\, dt = \frac{\Delta t}{2}[f_a + f_b + 2\sum_{i=1}^{t_b-1} f(t_i)] \qquad\qquad \textbf{3-10}$$

where, a   is the starting point for the integration

       b   is the end point of the integration

       f_a is the function at the starting point a

       f_b is the function at the end point b

       t_b is the time at the end point b.

The round off errors introduced by the approximation can be minimised by the greater the number of sampling intervals, for example 1000 samples per second. This integration method was applied to the Euler rates to yield orientation angles and also to the linear accelerations with respect to the 'flat earth' coordinates to yield velocity and position.

3.6.4 Accelerometer Attitude Estimations

It was evident from the literature review that the accelerometer can be used to estimate the roll and pitch angles of the sensor module in the 'flat earth' reference frame with respect to the gravitational acceleration. The reliability of this estimation depended upon the amount of linear acceleration being experienced. The gravitational acceleration vector was derived by the multiplication of the gravity vector and the

rotation matrix R^T, as shown in equation 3-11. The matrix R^T was derived by the multiplication of the transpose of the rotation matrices found in equations 3-1 to 3-3.

$$\begin{bmatrix} X_g \\ Y_g \\ Z_g \end{bmatrix}_E = R^T \begin{bmatrix} 0 \\ 0 \\ g \end{bmatrix} \qquad \text{3-11}$$

where, g is the gravitational acceleration.

Therefore the resultant gravitation acceleration follows equation 3-12 to 3-14.

$$X_g = -g \sin \theta \qquad \text{3-12}$$

$$Y_g = g \sin \phi \cos \theta \qquad \text{3-13}$$

$$Z_g = g \cos \phi \cos \theta \qquad \text{3-14}$$

From these equations, the pitch angle was found easily by rearranging equation 3-12 into equation 3-15. The roll angle was found by dividing equation 3-13 by 3-14 and rearranging to yield equation 3-16

$$\theta = \arcsin \left[\frac{X_g}{-g} \right] \qquad \text{3-15}$$

$$\phi = \arctan \left[\frac{Y_g}{Z_g} \right] \qquad \text{3-16}$$

where, X_g, Y_g and Z_g are equal to a_x, a_y and a_z accelerations in the x, y and z directions, respectively (see section 2.3).

The accelerometer attitude estimates were executed through a Matlab program. Firstly, all of the accelerometer outputs were low-pass filtered by a 7th order Butterworth Matlab function filter at 0.5 Hz. The principle of the filter was to isolate

the static acceleration from as much of the dynamic acceleration as possible. The cut-off frequency was chosen following the experimental theory published on distinguishing between static and dynamic acceleration [76, 80, 151]. Then the attitude angles were estimated following the equations 3-15 to 3-16. The software code can be found on the supplied compact disc (CD).

3.6.5 Complementary Filtering

As previously discussed (see section 2.7.3), the complementary filter used in this system fused the high frequency (short term) characteristics of the gyroscopes with the low frequency (long term) characteristics of the accelerometers. Together the outputs generate the optimal estimation of the orientation of the inertial sensor system. The operation of the filter is presented as a flow diagram in figure 3-9 and was outlined in Brown and Hwang [188] and subsequently adapted by Bachmann [102]. A detailed theoretical derivation of the operation can be found in Bachmann [102].
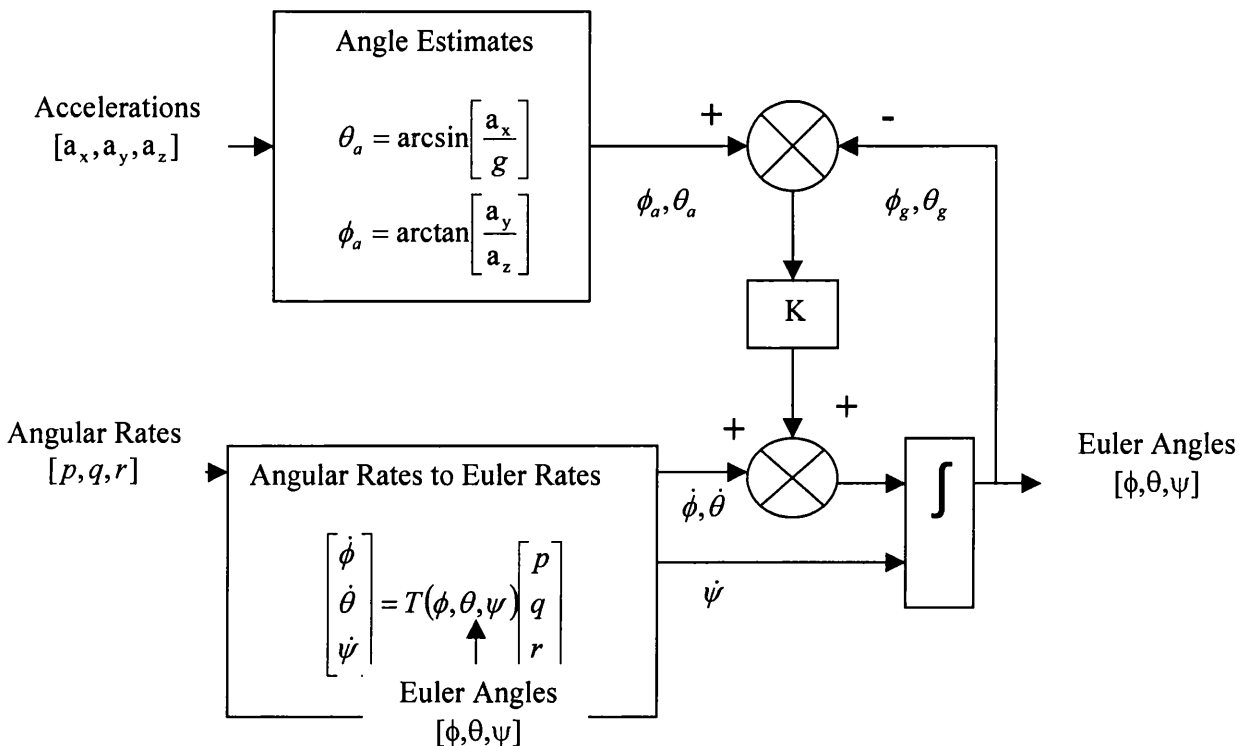
Figure 3-9 A flow diagram of the operation of the complementary filter.

The angular rate outputs of the gyroscope sensors (p,q,r) were transformed to Euler rates using the transformation matrix T (see section 3.6.2). The Euler rates were integrated to yield Euler angles. The pitch (about the X axis) and roll (about the Y axis) angles were compared to the attitude angles derived from the accelerometer outputs, the difference was multiplied by the factor, K, added to the Euler rate output and then integrated to yield and optimal estimate of the Euler angles. The Euler rate about the Z axis, azimuth, is simply integrated to yield an azimuth angle and not feed into the filter. The reasons for this were explained in section 2.3.1.

The key feature of the filter was the idea of a cross over frequency, f_c. This frequency represented the value below which the signals from the accelerometer sensors were given greater weighting and above which signals from the gyroscope sensors were favoured. The cross over frequency was adjusted by varying the filter gain, K by the equation 3-17.

$$K = 2\pi f_c$$
3-17

This frequency was chosen theoretically and fine adjustments were made experimentally. The filter was only implemented for two of the orientation angles, roll and pitch. There was no filter implemented for rotations about the z axis (yaw) due to no comparison available from the accelerometer or any other sensor. The accelerometers' outputs remained constant with respect to gravity during rotations about the z axis. It is possible to use the magnetoresistive sensor to provide a heading angle but this is beyond the scope of this project.

3.6.6 Gravitational Acceleration Compensation

Given that the orientation of the inertial sensor system was known, the linear acceleration was extracted from the measured acceleration by subtracting the gravitational acceleration. Using equations 3-12 to 3-14 the linear acceleration denoted by l is expressed in matrix form by equation 3-18.

$$\begin{bmatrix} 1_x \\ 1_y \\ 1_z \end{bmatrix}_B = \begin{bmatrix} a_x \\ a_y \\ a_z \end{bmatrix}_B + \begin{bmatrix} -g\sin\theta \\ g\sin\phi\cos\theta \\ g\cos\phi\cos\theta \end{bmatrix} \qquad \textbf{3-18}$$

3.6.7 Rotation Matrix: Body to Earth Coordinate Transform

The aerodynamic model typically represented the transformation between the body and 'flat earth' coordinates with the direction cosines matrix. The rotation sequence used was the ZYX convention and is described following the right hand rule as the first rotation about the z axis by the yaw angle, ψ, then about the new y axis by the pitch angle, θ, and finally about the new x axis by the roll angle, ϕ. The rotation matrices from equations 3-1 to 3-3 were multiplied to yield the rotation matrix R as displayed in equation 3-19.

$$R = R_\psi^Z R_\theta^Y R_\phi^X = \begin{bmatrix} \cos\theta\cos\psi & \sin\phi\sin\theta\cos\psi - \cos\phi\sin\psi & \cos\phi\sin\theta\cos\psi + \sin\phi\sin\psi \\ \cos\theta\sin\psi & \sin\phi\sin\theta\sin\psi + \cos\phi\cos\psi & \cos\phi\sin\theta\sin\psi - \sin\phi\cos\psi \\ -\sin\theta & \sin\phi\cos\theta & \cos\phi\cos\theta \end{bmatrix} \qquad \textbf{3-19}$$

This matrix was used to transform the linear accelerations about the x, y and z axes in body coordinates to the linear accelerations about the X, Y and Z in 'flat earth' co-ordinates by equation 3-20.

$$\begin{bmatrix} A_x \\ A_y \\ A_z \end{bmatrix}_E = R[\phi,\theta,\psi] \begin{bmatrix} 1_x \\ 1_y \\ 1_z \end{bmatrix}_B \qquad \textbf{3-20}$$

3.7 Casing and Method of Attachment

The two sensor boards were mounted inside an enclosed polycarbonate box with dimensions 65 x 65 x 57 mm (L x W x H). The orthogonality of the box was

measured using a workshop milling machine. The machine needle can move in two axes and provides a position to the nearest 0.0125 mm. Following the result of an experiment that confirmed the sides and base of the box could be assumed to be orthogonal, it seemed viable to mount board 1 and board 2 onto the base and one of the sides, respectively. It was assumed that the boards containing the sensors were positioned inside the casing such that the x, y and z axes were parallel with the width, length and height of the casing, respectively. A hole was cut at the back of the box to provide an access for the connecting cabling and a grommet was placed around the cabling to prevent any shearing of the wires. The box was fixed onto the leg of an off-centred T-shaped plastic structure measuring 75 x 75 x 100 mm (W x D x H) and then the head of the T was attached to a substantial belt designed for lumbar support during weight lifting training. A picture of the method of attachment can be found in Appendix B. Following the evidence from the literature review the belt was secured to the subject by a velcro strap and was positioned onto the lower back at the assumed representative point of the body's CoM during quiet standing.

3.8 Summary

The inertial sensor system was comprised of two dual axis accelerometers manufactured by Analog Devices and three single axis gyroscopes manufactured by Murata. They were mounted and arranged into a small box which was subsequently designed to be attached to the subject at the point assumed to be representative of the body's CoM. The two reference frames were taken from the aerodynamics model and were defined as body and 'flat earth'. The measurement directions with respect to the body coordinates were defined as x axis "out of the nose", y axis as "out of the right" and the z axis as "out of the belly". The sensors sensitive axes were aligned with this convention. The angular rates denoted as p, q and r were transformed to Euler rates and then integrated by the trapezium rule to yield an estimation of the Euler angles, and thus orientation. Simultaneously, the accelerometer outputs were low-pass filtered and then implemented into the attitude estimation equations to yield an estimation of the roll and pitch angles. The estimations from both sensors were then fused by a complementary filter with gain K to provide the most optimal estimation of the orientation angles, roll and pitch. The yaw angle depended solely on the gyroscope

output sensitive about the z axis. Using the known orientation, the measured acceleration could be separated into its components of gravitational and linear acceleration. Following on from this, the linear accelerations were rotated into the 'flat earth' reference frame denoted by the NED axes arrangement using the rotation sequence ZYX.

Chapter 4 Results 1: Development and Validation

4.1 Introduction

The first imperative step towards developing the sensor system was to apply a suitable and repeatable calibration procedure to deliver the set of calibration parameters required to convert the sensor outputs into the respective units. Subsequently, these calibration parameters along with the proposed processing steps necessary to produce usable acceleration data in three orthogonal directions with respect to the earth coordinate system were verified following a series of relevant experiments. Lastly, specific attention was applied to the response of the zero bias gyroscope output over time and temperature, and validating the use of this output as an integral part of the system. The zero bias drift has been frequently highlighted as a limitation to the accuracy of the orientation estimates derived from the gyroscope outputs.

4.2 Calibration

4.2.1 Introduction

Practical use of the sensor system depends heavily on an accurate and easily repeatable calibration procedure. The purpose of the procedure was to identify the zero bias and scale factor for each sensor. These parameters are imperative for describing the sensor outputs in their respective units. The accuracy of these parameters influences the three orthogonal acceleration estimates produced by the system with respect to the earth coordinates. A simple experiment that incorporates the calibration of both types of sensors is outlined below. The results presented were then used in subsequent experiments.

The calibration procedure for all sensors was carried out in a simultaneous manner as both types of sensor required rotations about each sensitive axis. The accelerometers utilised the earth's gravitational acceleration. This has a vector of magnitude 1g pointing towards the centre of the earth, or more commonly denoted as downwards. Each sensitive axis of each accelerometer sensed the gravitational acceleration positively when the sensitive axis was downwards, and negatively when the sensitive axis was upwards. However, the gyroscopes were each rotated about their sensitive

axis of rotation for a period of time. The known rate of rotation was utilised to evaluate the change in voltage induced at the sensor output. For example, when the sensor system was rotated about its y axis, the gyroscope sensitive about the y axis demonstrated a change in output voltage. Correspondingly, the x and z accelerometer outputs varied in a sinusoidal fashion sensing both positive and negative magnitudes of gravitational acceleration.

4.2.2 Rotating Arm Mechanism

The mechanism which is displayed in figure 4-1 consisted of a shaft which rotated through a set of bearings. At one end of the shaft there was an arm which rotated perpendicular to it, and at the other end there was, either a direct current (DC) motor or handle. The sensor system was easily and quickly secured to the arm by two screws fixings in any of the three orthogonal orientations. The DC motor was attached securely by a two-way grub screw cuff and was used for rotations of constant speed. Alternatively, the arm was rotated by using a handle to turn it through the required angle. An additional function of the mechanism was an adjustable friction system to provide little or maximum resistance to the rotating shaft. This was important when angle movements were performed as the position of the arm needed to be maintained without an operator.
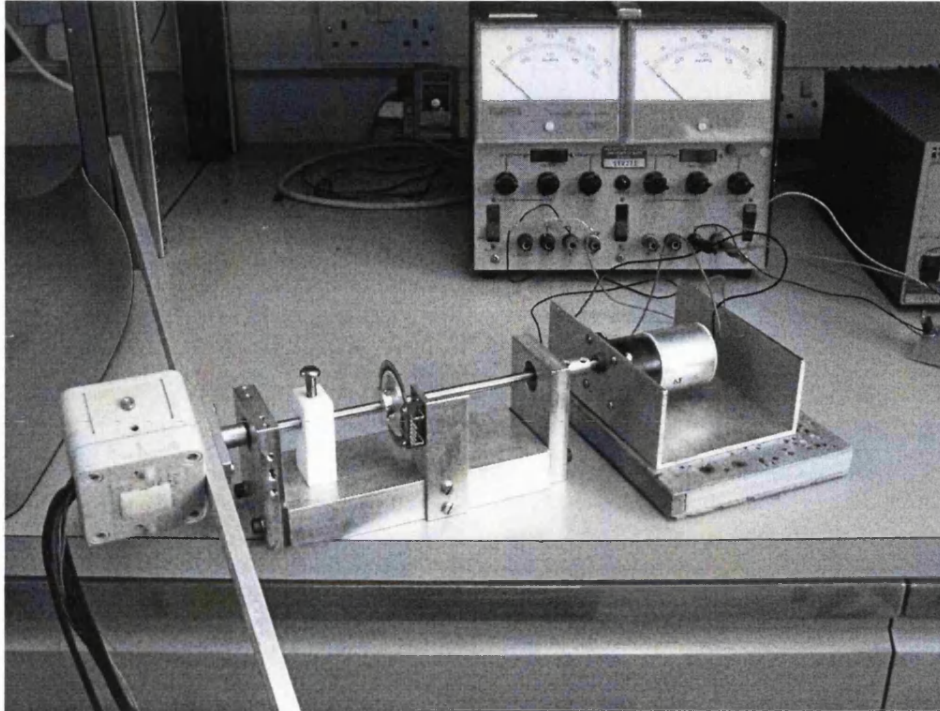
Figure 4-1 The rotating arm mechanism.

The power supply and the direction of rotation of the dc motor were controlled by a PIC microprocessor, PIC16F84 and H bridge mosfet driver circuit (see appendix A). The PIC was programmed to provide two signals to the H bridge mosfet driver (TC4426A). One of the signals was a pulse width modulated (PWM) signal that determined the rotation speed of the motor by the ratio of the on to off period of the pulses. The second signal defined the direction of rotation. A logic low signal denoted forward direction and a logic high denoted reverse direction. A H bridge circuit was essentially four transistors arranged in a H configuration. The transistors functioned in pairs, for example pair A and pair B. Switching on pair A only (that is to say applying a voltage to the base of the transistor resulting in a collector-emitter current) specified the direction of the current through the H bridge and thus the direction of rotation of the motor. The programming code for the PIC can be found on the CD. The diodes are for protecting the chip from over and under voltage supplies. The pull-up resistors prevent jerking of the motor when powered up or down.

4.2.3 Method

There were two sets of equipment required for this experiment. One for initiating and collecting sensor data which consisted of the sensor system mounted on the rotating arm mechanism, a dc motor with its own power supply and a control circuit for moving the arm, the processing box and Pico A/D, and a computer for recording the data. The second set of equipment provided an independent measure of angular displacement and thus angular rate. It consisted of a CODA motion analysis system, CODA markers and a CODA acquisition computer. A trigger signal from the CODA acquisition system rose from 0 to 5 V (which was subsequently potential divided down to 1.5 V) when acquisition had begun. This was recorded on a channel of the Pico A/D converter. The trigger pulse enabled the two data acquisition systems to be manually synchronised and then a comparison of the two sets of data was made.

The rotating arm mechanism with the sensor system attached was mounted securely onto a table which was resting on a known level surface. The three dimensional coordinate system was calibrated using three markers on this levelled table. CODA markers 1 and 2 on the table defined the x axis and CODA markers 1 and 3 defined the y axis. Marker 1 was the origin and the movements of the two markers on the rotating arm were quantified in terms of three dimensional coordinates (x, y, z) relative to this origin. The sensor system was secured to the rotating arm in the first of three orientations. The DC motor was attached to the other end of the shaft the mechanism was positioned on the table so that the rotating arm was parallel with the calibrated x axis. The processing circuits, power supplies and PC were situated on a nearby table. The movement of the rotating arm within the xz plane was validated by a preliminary collection of marker data and adjustments were made accordingly by manipulating the position of the mechanism to minimise movement registered in the y direction. Since the inertial sensor system was mounted onto the rotating arm which forms a rigid body then it was assumed that since: *'all points on a rigid body undergoing rotation about a fixed axis necessarily have the same angular displacement, speed and acceleration'* [207], the markers on either end of the arm would experience the same rotational kinematics as the gyroscope sensors.
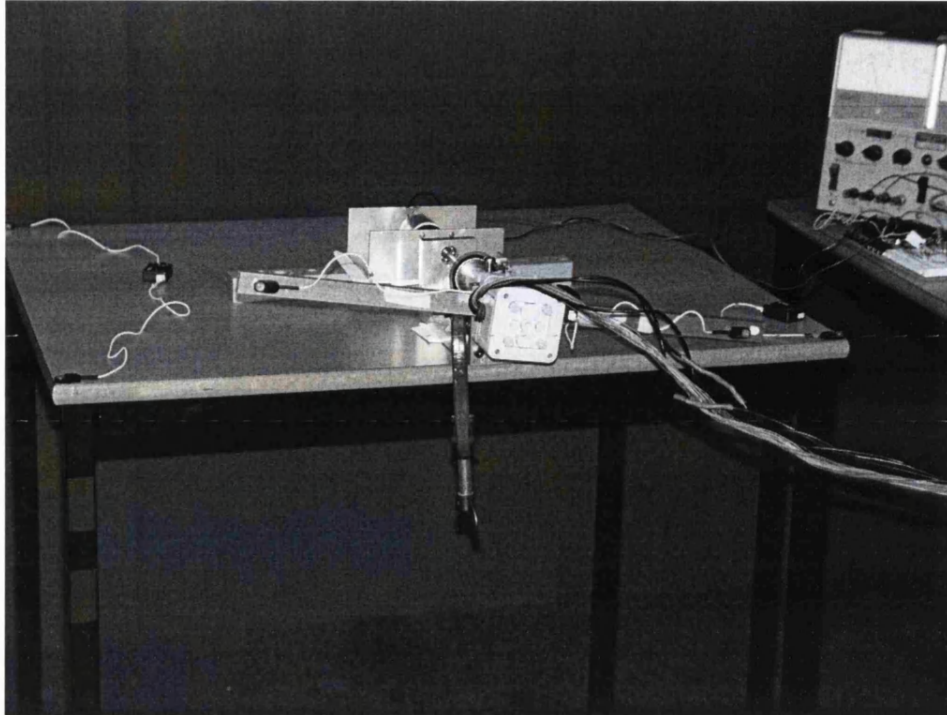
Figure 4-2 The positions of the CODA markers during the calibration.

Sensor and marker data was collected at a sampling rate of 200Hz for 50 and 60 s by the CODA and Pico data acquisition systems, respectively. The Pico data acquisition system was initiated first allowing for a collection period of a few seconds whilst the sensors were stationary. Next, the motor was activated followed shortly by the CODA acquisition system. Each orthogonal position was subjected to two rotations in a clockwise direction and two in an anticlockwise direction.

Although the inertial sensor module is rotated at a constant velocity, the distance between the centre of rotation and the accelerometer sensors is very small. Therefore the centrifugal acceleration acting on the accelerometers is insignificant. During one rotation the accelerometer will experience the gravitational acceleration as ± 1 g. For each accelerometer axis averages of the minimum and maximum acceleration outputs experienced during each trial and over all of the trials were calculated and were used in equation 4-1 to produce the desired calibration parameters.

$$\text{Zero Bias (V)} = \frac{\text{Max Acceleration (V)} + \text{Min Acceleration (V)}}{2}$$

4-1

$$\text{Scale Factor (mVg}^{-1}) = \frac{\text{Max Acceleration (mV)} - \text{Min Acceleration (mV)}}{2g}$$

For each of the three single axis gyroscopes the zero bias value was found by averaging the sensor outputs during the stationary collection period at the beginning of each trial. These zero bias values for each sensor are likely to change so it is a requirement that these values need to be identified prior to each subsequent experiment. The other calibration parameter was the scale factor and this was derived by rearranging equation 3-5 into equation 4-2.

$$\text{Scale Factor (mV}^{\circ -1}\text{s}^{-1}) = \frac{\text{Output (mV)} - \text{Zero Bias (mV)}}{\text{Angular Rate (}^{\circ}\text{s}^{-1})}$$

4-2

The angular rate of the sensor at each time sample was found by evaluating the known angular positions of the two CODA markers on either end of the mechanical arm. A rigid straight line was defined between these two markers in the CODA acquisition system. It was assumed that the point of rotation lies on this stick. The instantaneous angle of the stick with respect to the x axis was found by using right-angled geometry through the equation 4-3.

$$\text{angle (}^{\circ}) = a\tan\frac{\text{Z difference (mm)}}{\text{X difference (mm)}}$$

4-3
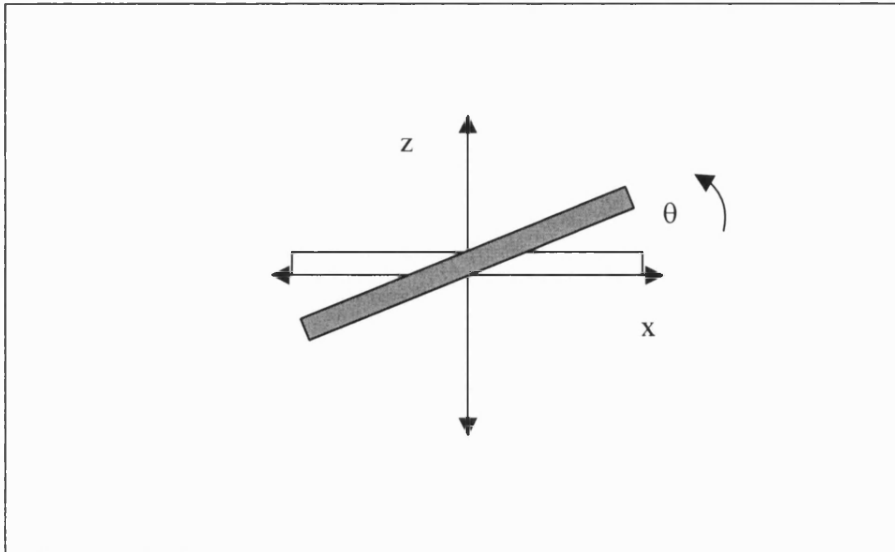
Figure 4-3 Pictorial description of the derivation of the angle of the arm.

The difference between two consecutive instantaneous angles multiplied by the sampling frequency gave the instantaneous angular rate at each time sample. The delay of the trigger pulse from the CODA acquisition was less than two sampling periods. The two data sets were aligned one sample period after the trigger was identified on the Pico acquisition system. The scale factor at each time step was derived following equation 4-2. An average scale factor for each experiment was found and further an average scale factor for each of the two experiments for each rotation direction was found.

4.2.4 Results

The stages of analysis of the accelerometers and gyroscopes responses are detailed below. All of the data was taken from the experiment: Anticlockwise Rotation about y axis trial 1. Firstly, the movement of the mechanical arm was assessed for its planar motion and hence its accuracy in providing calibration parameters. An indication of planar motion can be shown by circular movements of the rotating arm as opposed to spherical. Also, there was minimal movement of the arm in the y axis which was assumed to be insignificant. The two CODA markers positioned on the mechanical arm, marker 5 and marker 6 each traced a circle in the xz plane when rotated as displayed in figure 4-4.
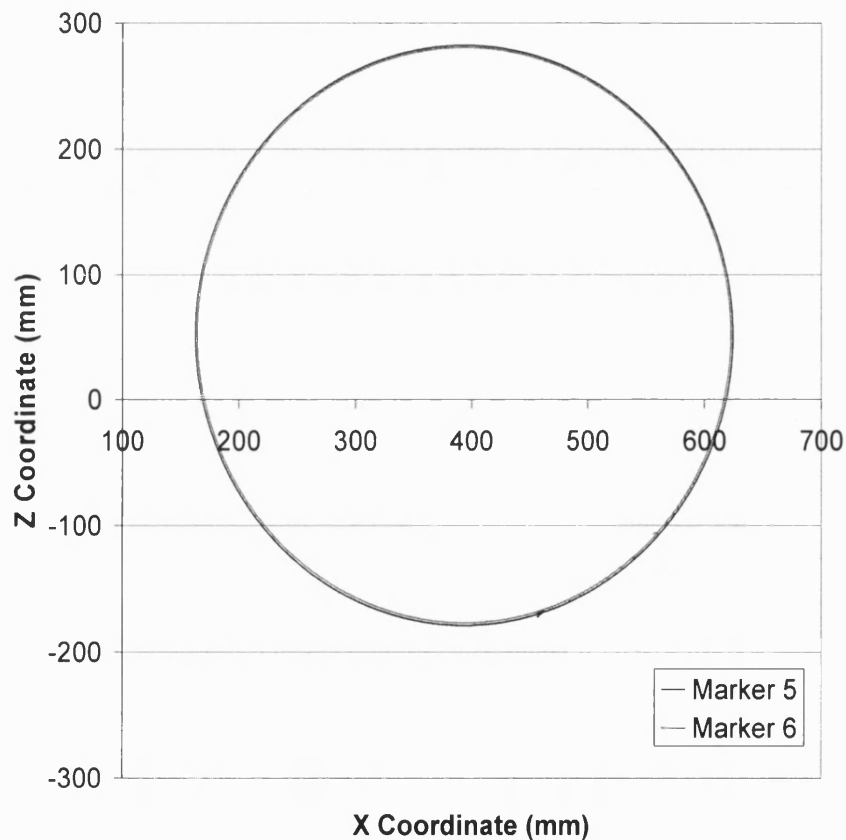
Figure 4-4 The positions of markers 5 and 6 within the xz plane during a typical rotation of the mechanical arm.

Next, the analysis of the accelerometer response is presented. An example of the response of the accelerometers during one rotation trial is shown in figure 4-5. In this case the rotation was about the y axis therefore sinusoidal variation in the x and z axes outputs and minimal variation in the y axis output was seen.
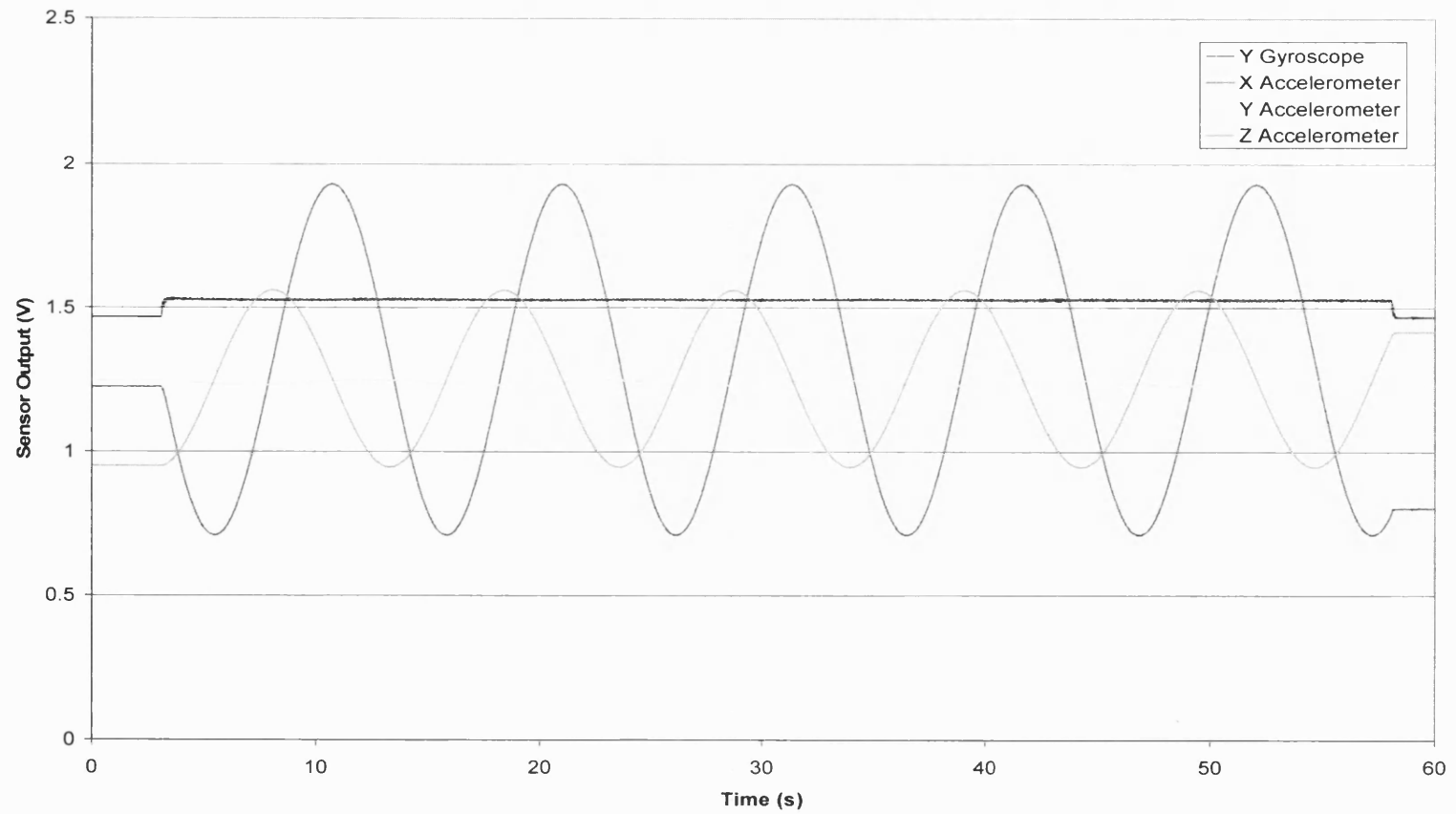
Figure 4-5 An example of the response from all accelerometers and y gyroscope during a rotation about the y axis.

Finally, analysis of the gyroscope response is presented. The visual shape of the response from the gyroscope and the derived angular rate from CODA were compared and are displayed in figure 4-6. By comparison, the two signals displayed similar shaped responses, suggesting the angular rate output derived by CODA was likely to deduce a suitable scale factor at each time step.
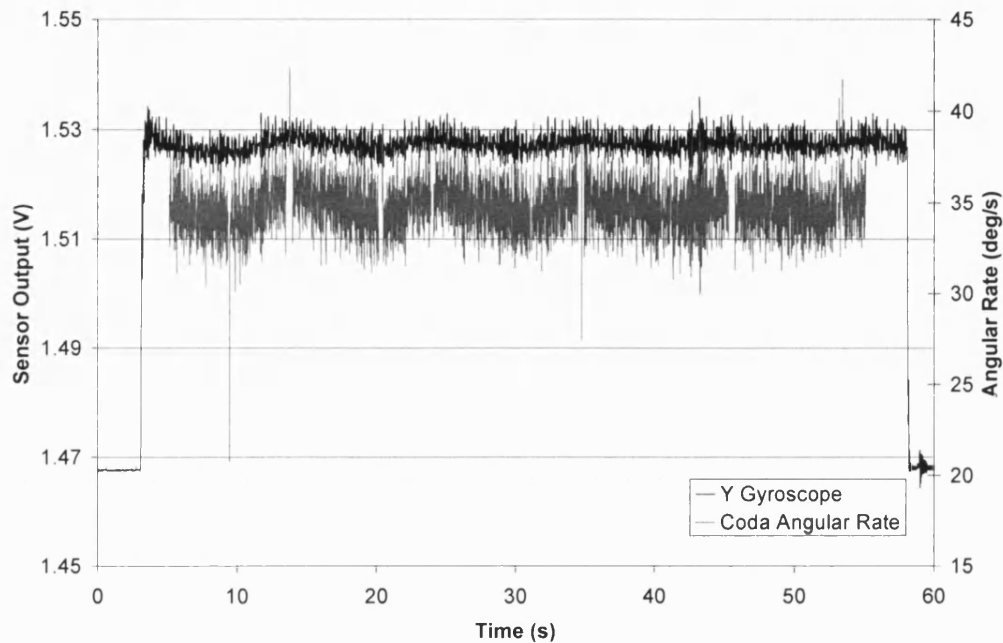
Figure 4-6 A comparison of the y gyroscope sensor output in volts and the derived angular rate output from the CODA acquisition system.

The angular rate difference that occurred between the angular rate output from the gyroscope sensor using the average scale factor and the angular rate output derived from the CODA acquisition system is displayed in figure 4-7. This difference was within $\pm\ 2°s^{-1}$ in 92.2% of samples.
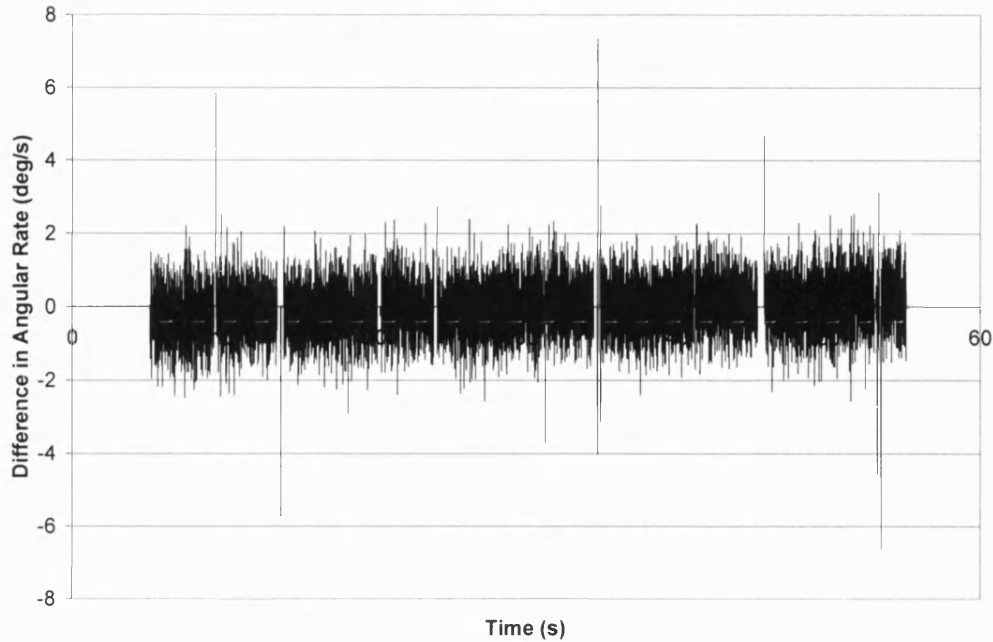
Figure 4-7 The difference between the gyroscope sensor and the CODA angular rate outputs.

Average scale factors, standard deviations and confidence intervals of the data from all three gyroscopes for each trial were displayed in table 4-1. Confidence intervals for the data sets from each trial are calculated to provide a measure of the spread of the data about the mean with a 95% probability that the population mean lay within this range [208]. The results in table 4-1 showed a significant difference in scale factors between the two rotation directions for all axes. However, repetitions of rotations about each axis showed similar scale factor magnitudes. The confidence interval values demonstrated that 95% of the data lay within 2 μV across all trials.

Table 4-1 Statistical analysis on the average scale factors derived from each trial.

	Rotation Direction	Average Scale Factor	Standard Deviation	95% CI $\bar{x}+1.96\dfrac{\sigma}{\sqrt{n}}$	95% CI $\bar{x}-1.96\dfrac{\sigma}{\sqrt{n}}$
		mV		mV	mV
X Axis	Anticlockwise	1.7651	0.0462	1.7660	1.7642
	Clockwise	1.7762	0.0402	1.7769	1.7758
Y Axis	Anticlockwise1	1.6956	0.0459	1.6945	1.6947
	Anticlockwise2	1.6974	0.0479	1.6984	1.6965
	Clockwise1	1.7209	0.0372	1.7216	1.7202
	Clockwise2	1.7220	0.0422	1.7228	1.7211
Z Axis	Anticlockwise1	1.7148	0.0413	1.7156	1.7140
	Anticlockwise2	1.7193	0.0502	1.7204	1.7189
	Clockwise1	1.7232	0.0526	1.7242	1.7221
	Clockwise2	1.7233	0.0415	1.7241	1.7224

The resultant calibration parameters for the accelerometers and gyroscopes are shown in tables 4-2 and 4-3, respectively. The accelerometer signals were processed prior to digital conversion to satisfy the constraints of the A/D converter and to provide maximum resolution. Reversing the process deduced the raw zero bias and scale factor parameters. The zero bias parameters were found to be 2.26 V, 2.48 V and 2.42 V and the scale factors were 305 mVg^{-1}, 292 mVg^{-1} and 97 mVg^{-1}. All of these values were within 9% and 7% of the stipulated zero bias of 2.5 V and scale factor of 312 mVg^{-1} or 100 mVg^{-1}, respectively. The gyroscope signals were processed prior to digital conversion to eliminate high frequency noise and increase the resolution. The raw scale factor values were deduced by dividing by the multiplication factor yielding 0.7106 $mV^{o-1}s^{-1}$, 0.6836 $mV^{o-1}s^{-1}$ and 0.6881 $mV^{o-1}s^{-1}$. These values were within 6% of the stipulated scale factor denoted in the data sheet of 0.67 $mV^{o-1}s^{-1}$. The average scale factor from both rotations would be used so that the direction of rotation was not required to be known before the signals were converted into the appropriate units. However, this could potentially introduce errors into the unit converted signal.

Table 4-2 A summary of the accelerometer calibration parameters.

Parameter		Accelerometers X	Y	Z
Zero Bias	V	1.3257	1.2368	1.7171
Scale Factor	Vg^{-1}	0.6100	0.5840	0.3073

Table 4-3 A summary of the gyroscope scale factor parameters.

Rotation	Gyroscopes ($mV^{\circ-1}s^{-1}$) X	Y	Z
Anticlockwise	1.7651	1.6965	1.7171
Clockwise	1.7762	1.7214	1.7232
Average	**1.7766**	**1.7090**	**1.7202**

4.2.5 Discussion

The results from verifying the motion of the mechanical arm suggested near planar motion since the CODA markers measured near circular movements and the maximum registered movement in the Y coordinate was only 4 mm. It was therefore assumed that the experimental setup provided an adequate means for deducing calibration parameters. For the accelerometers, the raw zero bias values were 2.26 V, 2.48 V and 2.42 V and the scale factors values were 305 mVg^{-1}, 292 mVg^{-1} and 97 mVg^{-1}. All of these values were within 9% and 7% of the stipulated zero bias and scale factor parameters denoted from the sensor data sheet. The difference in scale factors was due to the fact that the z accelerometer measures a greater range of $\pm$ 10 g. For the gyroscopes, the zero bias values were found immediately prior to any experiments. The reason for this statement is detailed in the later section of this chapter. For the gyroscopes, the raw scale factors were 0.7106 mV$^{\circ-1}$s^{-1}, 0.6836 mV$^{\circ-1}$s^{-1} and 0.6881 mV$^{\circ-1}$s^{-1}. These values were within 6% of the stipulated scale factor parameter denoted from the sensor data sheet. A good comparison was seen between the angular rate derived from CODA and the angular rate calculated by using the average scale factor yielding a difference within $\pm$ 2°s^{-1}.

4.3 Verification

4.3.1 Introduction

The overall purpose of all the verification experiments outlined below was to validate the functioning of the overall sensor system. The experiments are categorised as follows:

1) Definition of positive linear acceleration and positive rotation axes.

2) Validation of gyroscope calibration parameters.

3) Validation of angle estimates by executing the following:

   a. Implementation of the chosen integration process.

   b. Implementation of the accelerometer attitude estimation process which also incorporates the validation of the accelerometer calibration parameters.

4) Validation of the functioning of the overall system and in particular the implementation of the rotation matrix

Firstly, the three positive acceleration directions and three positive rotation directions about those acceleration directions were defined. This involved the sensor system being subjected to a series of linear accelerations along a flat surface and rotations about each axis by hand. Next, the gyroscope scale factors derived from the previous section were verified by subjecting the sensor system to five different but constant rotational rates in both positive and negative directions. The five rates of rotation were selected by defining a series of fixed voltage levels which supplied a dc motor, thus controlling the rate of rotation of arm. An independent measure of the rate of rotation was determined by capturing an average output pulse from a high resolution encoder on an oscilloscope. The output pulse period was used to derive the angular rate of the rotating arm. The next verification experiment involved controlled rotations of the sensor system through a series of 90° rotations about each axis. The digitised outputs of the gyroscopes were integrated by the trapezium rule to provide an angle estimate. The digitised outputs of the accelerometer were low pass filtered and then substituted into the attitude angle estimation equations, 3-15 and 3-16, to also provide an angle

estimate. These processing steps were outlined in chapter 3. The derived angles from the gyroscopes and the accelerometers were compared to an independent high resolution angle measurement from an optical encoder. Finally, the last verification experiment consisted of controlled rotations of the sensor system through a series of known angle rotations from 15° to 90° about the y (pitch) axis. All six sensor outputs were utilised and each processing step outlined in the previous chapter was implemented to provide three orthogonal linear accelerations with respect to earth coordinates and three Euler angles. Correct functioning of the rotation matrix was judged by all three accelerations remaining at zero and that only the Euler angle of interest registering the applied angle movement.

4.3.2 Optical Encoder and PIC Pulse Counter

A high resolution incremental optical encoder made by Agilent Technology was chosen as an independent angle measurement system used as a comparison to that produced by the sensor system. The technology utilised an optical codewheel and an encoder module housing a light source and two pairs of photoelectric sensors which sensed both direction and size of the motion. The film codewheel, HEDS-6120-T06, was mounted on the shaft of the rotating arm mechanism. The codewheel material was chosen to be film as the wheel was not required to endure high temperatures or rugged experiments which required metal wheels and was cheaper than glass offering the same high resolution. The encoder, HEDS-9000, was mounted on an upright support so that gap dimension between the wheel and the detector were within the tolerances specified in the datasheet. Since the code wheel is a one-track disk, the two pairs of sensors are arranged in such a way that one is displaced from the other by one and one-half slot widths. The encoder provided a pulse train at a resolution of 2000 pulses per revolution from each of the two pairs of photoelectric sensors. These pulses were interpreted to obtain rotational position and direction. Since the direction of rotation was known then only one of the two pulse trains was feed into a PIC microprocessor (PIC16F84A). An interrupt run software program on the PIC chip counted the number of pulses and displayed a running total value on a miniature liquid crystal display (LCD) screen. The PIC software code can be found on the enclosed CD. As an alternative a typical output of the pulse train for a constant

rotational speed was captured on an oscilloscope and used to manually calculate the rotational speed. From the number of pulses collected over a period or the average pulse period, the number of pulses per second and thus the rotational velocity in degrees per second was derived. Equation 4-4 was used to find the rotation rate:

$$\text{Rate of rotation } (°s^{-1}) = \frac{\text{pulses per second}}{2000} \times 360 \qquad \textbf{4-4}$$

4.3.3 Method

The first experiment only required the use of a flat surface and a ruler fixed to the surface acting as a guide for the path of the sensor system. The positive linear acceleration axes were evaluated first. The sensor system was manually pushed 600 mm in a smooth manner along the guide three times. The sensor system was orientated so that in turn each positive axis was pointing in the direction of travel. Next the positive rotation directions were defined. The sensor system was placed in a stationary position on the flat surface and rotated manually about each of the three axes in turn by approximately 90° in both directions. The sensor outputs for all of the above experiments were recorded for 40 s at 100 Hz. An increase in output would signify a positive acceleration or rotation experienced. The arrangement of the sensors sensitive axes and the chosen rotation sequence are detailed in the previous chapter. The rotation sequence chosen was a NED convention which follows the right hand rule. Positive accelerations should be seen when the sensor system was accelerated in the north (forward), east (right) and down directions. Positive rotations should be seen when rotated in a clockwise direction (right bank) about the x axis (roll), anticlockwise (climb) about the y axis (pitch) and clockwise (right turn) about the z axis (yaw). The results are displayed on pages 119 and 120.

The other three verification experiments all required the use of the sensor system attached to the rotating arm. For the first of the three remaining verification experiments, five clearly different rotation rates were chosen by selecting the operating voltages: 4, 6, 8, 10 and 12 V respectively. The voltage supply to the motor

was measured by a fluke multi-meter to ensure that the same voltages were supplied to the experiments of all three axes. The polarity of the power supply was alternated to change the motor rotation direction and was switched on and off manually at specified intervals. The gyroscope output for each axis was collected for 60 s at 200 Hz with a stationary period at the beginning and end of the collection period. The gyroscope output during this stationary period was averaged to provide the zero bias calibration parameter. This parameter along with the derived scale factors of the gyroscope outputs were converted into a rotation rate with units, $°s^{-1}$. The rate of rotation of the rotary shaft was measured by capturing an average pulse period from the optical encoder on an oscilloscope. Comparisons were made between the five gyroscope angular rates and the rates of rotation found from the optical encoder. The results are displayed on pages 121 to 124.

The next verification experiment involved rotated the arm manually through an angle of approximately 90° ten times in each rotation direction and about each axis. The number of degrees rotated was determined by the number of pulses counted by the PIC pulse counter circuit and this was displayed on the LCD screen. A 90° rotation is equivalent to 500 pulses. The sensor outputs were collected for 10 s at 200 Hz, again with a stationary period at the beginning and end. The PIC pulse counter circuit was reset after each rotation. Once the data was collected, both the accelerometers and gyroscope outputs were converted into their respective units using the previously derived calibration parameters. The accelerometer sensor which is sensitive about the axis of rotation should remain at a constant output during the rotation since its orientation with respect to gravity is not changing. The other two accelerometer sensors with perpendicular sensitive axes, experienced the gravitational acceleration as they were rotated simultaneously. The outputs were utilised in equation 3-16 to yield an instantaneous angle at each time sample. The gyroscope angular rate output about the axis of rotation was integrated using the trapezium approximation method to yield an instantaneous angle estimate at each time sample. For both the sensors the angle estimates were summed to yield accumulative angles which were compared to the angle derived from the number of pulses counted from the optical encoder. The start of the rotation was defined by a trigger pulse sent from the PIC pulse counter circuit into Channel 11 of the A/D converter. The point at which rotation ended was

harder to identify as there was no trigger pulse and was performed by visual inspection of the gyroscope graph. In hindsight, it would have been preferable to re-use the trigger pulse returning the signal to 0 V once 500 pulses had been counted to indicate 90° of rotation. The results are displayed on pages 125 to 128.

The final experiment involved moving the rotating arm manually through a series of angles (approximately 15, 30, 45, 60, 75, and 90°) about the Y axis (Pitch). The encoder pulses were counted by the PIC pulse counter circuit (83, 167, 250, 333, 417 and 500 pulses respectively). The sensor outputs were collected following the previous verification experiment and were processed by the steps outlined in chapter 3. These steps included conversion into appropriate units using the derived calibration parameters, transformation of angular rates to Euler rates, integration of the Euler rates to yield Euler angles, subtraction of gravitational component of the measured acceleration and finally, rotation of the linear acceleration components from body to earth reference frames. The initial attitude of the inertial sensor module was derived from the accelerometer sensor outputs during the stationary period at the beginning of each trial. The initial yaw angle was assumed to be zero degrees. The results are displayed on pages 129 to 131.

4.3.4 Results

The results from the first verification experiment which defined the positive acceleration and rotation directions of the sensor system are displayed in figures 4-8 and 4-9.
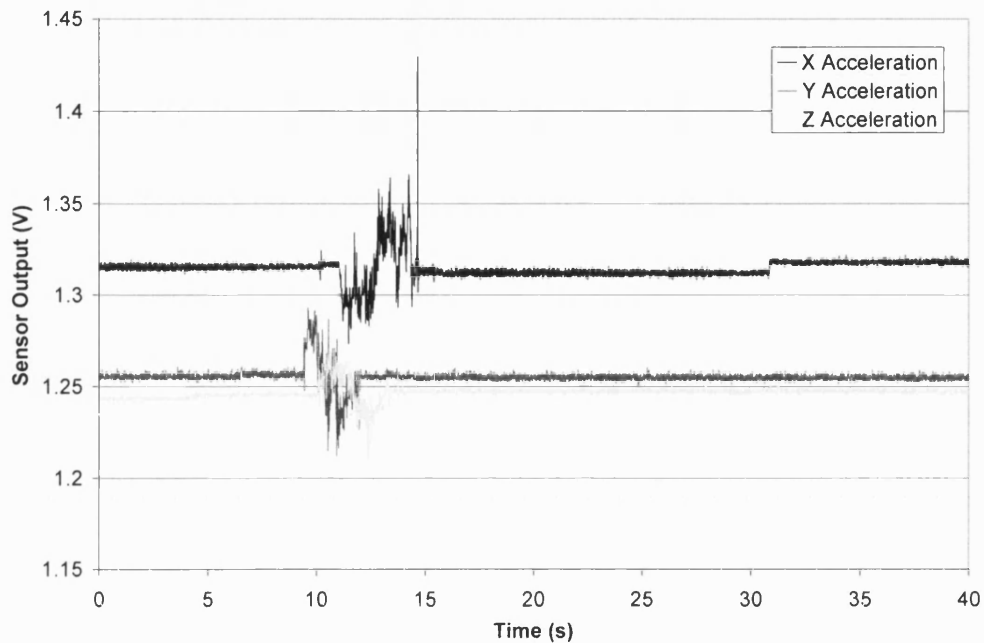
Figure 4-8 Accelerometer outputs when accelerated in a north, east or down direction (NED).

The acceleration results showed a partial contradiction to what was expected. Accelerations in the east and downward directions were positive accelerations and acceleration in the northerly direction was a negative acceleration.
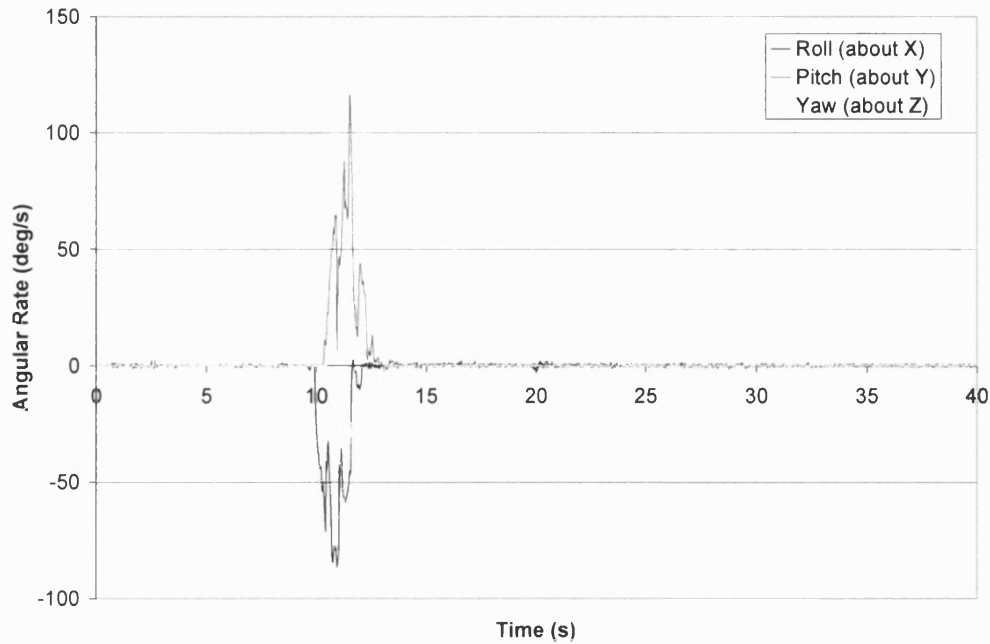
Figure 4-9 Gyroscope outputs when rotated clockwise about x and z axes and counter-clockwise about y axis.

The gyroscope output results showed negative rotations about the x and z axes and a positive rotation about y axis. The orientation arrangement of the gyroscopes was a critical design error and in retrospect they should have been arranged to comply with the chosen rotation sequence. However, since the conversion of the sensor outputs into the respective units normalises the outputs about zero, it was easy to modify the particular accelerometer and gyroscope outputs to respond in the opposite way by multiplying by -1. Thus the NED arrangement was still achieved.

The second verification experiment showed five clear changes in output from each of the gyroscope sensors when the supply voltage and thus the speed of the motor was increased, see tables 4-4 and 4-5. The voltage differences translated to five distinctive angular rates. Figure 4-10 shows an example from the counter clockwise experiment about the x axis.
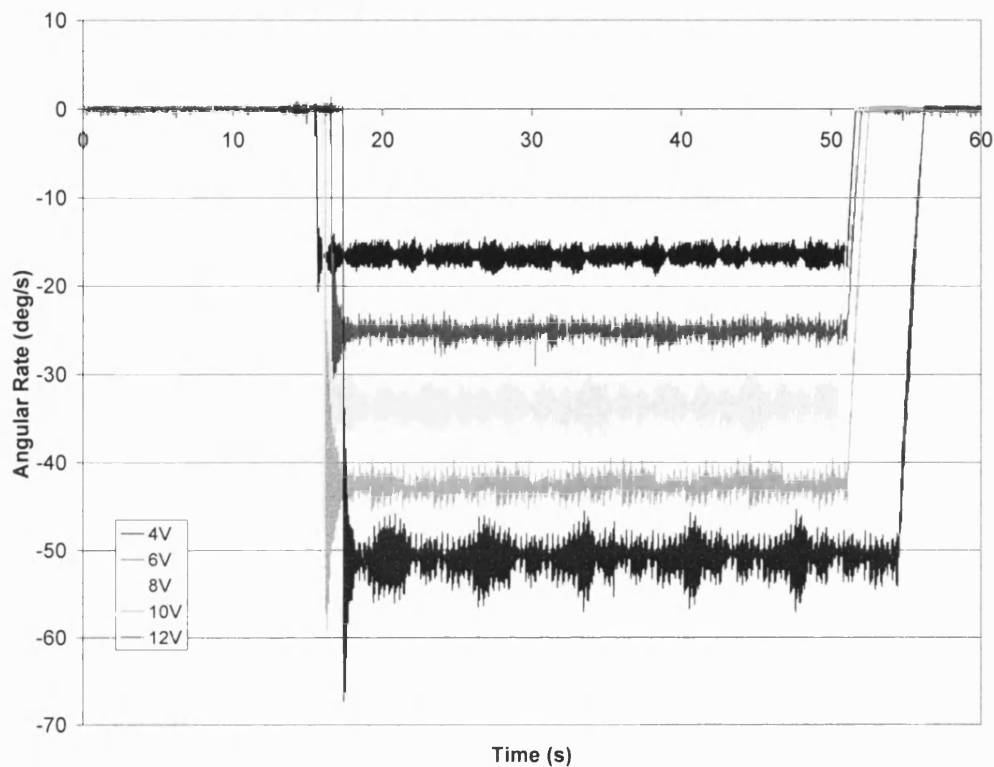
Figure 4-10 The increasing angular rate derived from the gyroscope output due to the increasing supply voltage to the motor during a counter-clockwise rotation about the X axis.

Typical average pulse periods from the optical encoder at each speed for each axis experiment were captured on an oscilloscope and the data downloaded into an excel file. An example of a typical pulse from the encoder is displayed in figure 4-11. The time period for one pulse was utilised in equation 4-4 to determine the angular rate of the rotating arm and thus the sensor system. There were very strong comparisons between the two sets of angular rate values (tables 4-4 and 4-5) which suggested that the scale factor was sufficiently accurate.

Table 4-4 Counter-clockwise rotation results for all three axes

Motor Supply		Gyroscope		Encoder		Difference
		Change in Voltage	Angular Rate	Pulse Period	Angular Rate	Angular Rate
V		V	°s^{-1}	s	°s^{-1}	°s^{-1}
X Axis	4	0.029	16.55	0.0113	15.92	0.62
	6	0.044	25.10	0.0073	24.73	0.37
	8	0.059	33.59	0.0054	33.34	0.26
	10	0.075	42.61	0.0043	41.76	0.84
	12	0.088	49.73	0.0036	49.72	0.01

Motor Supply		Change in Voltage	Angular Rate	Pulse Period	Angular Rate	Angular Rate
V		V	°s^{-1}	s	°s^{-1}	°s^{-1}
Y Axis	4	0.028	16.23	0.0110	16.37	0.14
	6	0.043	25.18	0.0072	25.14	0.04
	8	0.057	33.82	0.0054	33.27	0.55
	10	0.072	42.64	0.0042	42.75	0.11
	12	0.087	51.18	0.0035	51.58	0.40

Motor Supply		Change in Voltage	Angular Rate	Pulse Period	Angular Rate	Angular Rate
V		V	°s^{-1}	s	°s^{-1}	°s^{-1}
Z Axis	4	0.028	16.31	0.0106	16.96	0.64
	6	0.043	25.10	0.0073	24.79	0.31
	8	0.058	33.81	0.0051	35.02	1.20
	10	0.073	42.55	0.0042	43.17	0.62
	12	0.086	50.34	0.0035	50.99	0.65

Table 4-5 Clockwise rotation results for all three axes.

Motor Supply		Gyroscope		Encoder		Difference
		Change in Voltage	Angular Rate	Pulse Period	Angular Rate	Angular Rate
V		V	$°s^{-1}$	s	$°s^{-1}$	$°s^{-1}$
X Axis	4	0.029	16.33	0.0112	16.07	0.26
	6	0.044	24.78	0.0074	24.33	0.46
	8	0.059	33.48	0.0054	33.27	0.21
	10	0.075	42.07	0.0043	41.96	0.11
	12	0.090	50.90	0.0036	50.26	0.64

Motor Supply		Change in Voltage	Angular Rate	Pulse Period	Angular Rate	Angular Rate
V		V	$°s^{-1}$	s	$°s^{-1}$	$°s^{-1}$
Y Axis	4	0.028	16.43	0.0111	16.25	0.18
	6	0.043	24.70	0.0073	24.66	0.04
	8	0.057	33.37	0.0054	33.39	0.02
	10	0.072	42.01	0.0044	41.10	0.90
	12	0.086	50.19	0.0035	51.27	1.08

Motor Supply		Change in Voltage	Angular Rate	Pulse Period	Angular Rate	Angular Rate
V		V	$°s^{-1}$	s	$°s^{-1}$	$°s^{-1}$
Z Axis	4	0.028	16.17	0.0102	15.87	0.30
	6	0.043	25.02	0.0072	25.07	0.05
	8	0.058	33.71	0.0050	32.26	1.45
	10	0.073	42.24	0.0043	41.48	0.77
	12	0.087	50.24	0.0036	50.70	0.46
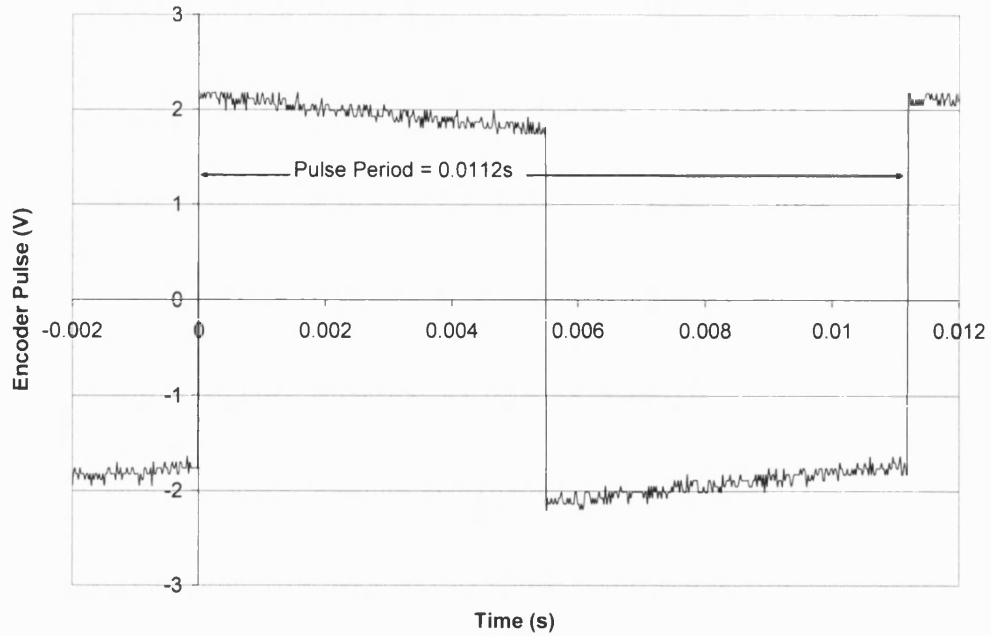
Figure 4-11 A typical output pulse from the optical encoder at a motor supply of 4 V captured on an oscilloscope.

The results from the third verification experiment demonstrated the ability of each type of sensor to define the orientation of the sensor system. An example of the sensors response to a rotation of 90°, in this case counter clockwise is displayed in figure 4-12. It was clear from the figure that the trigger pulse was an accurate method of identifying the beginning of rotation as this corresponded to the changes in output from the sensors. The end of rotation was determined visually by when the gyroscope output returned to its initial value.
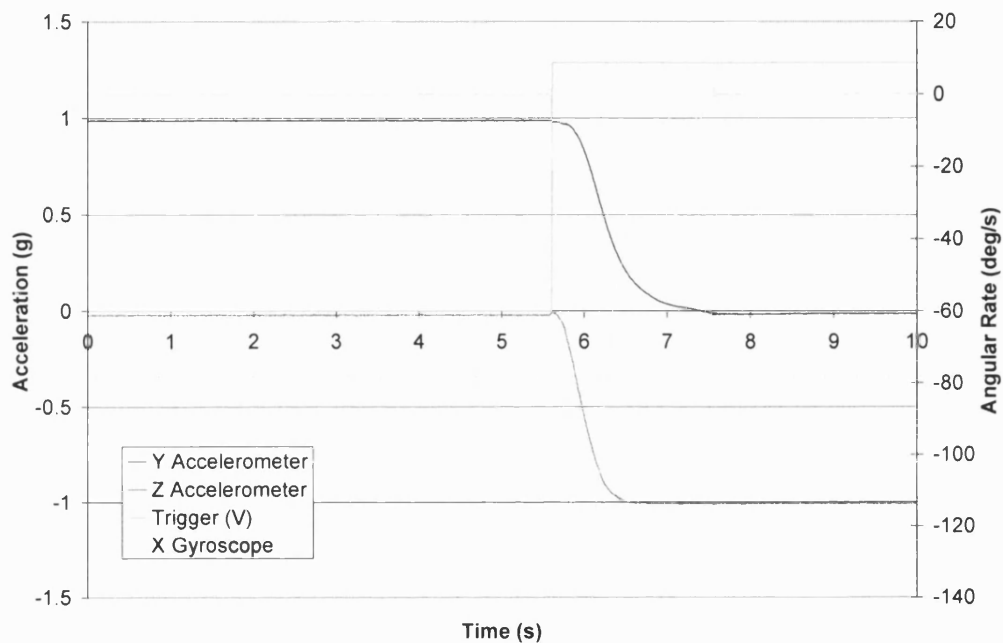
Figure 4-12 The response of the sensors during a 90° rotation in the counter-clockwise direction.

A typically example of the instantaneous angle estimates through the period of rotation is displayed in figure 4-13.
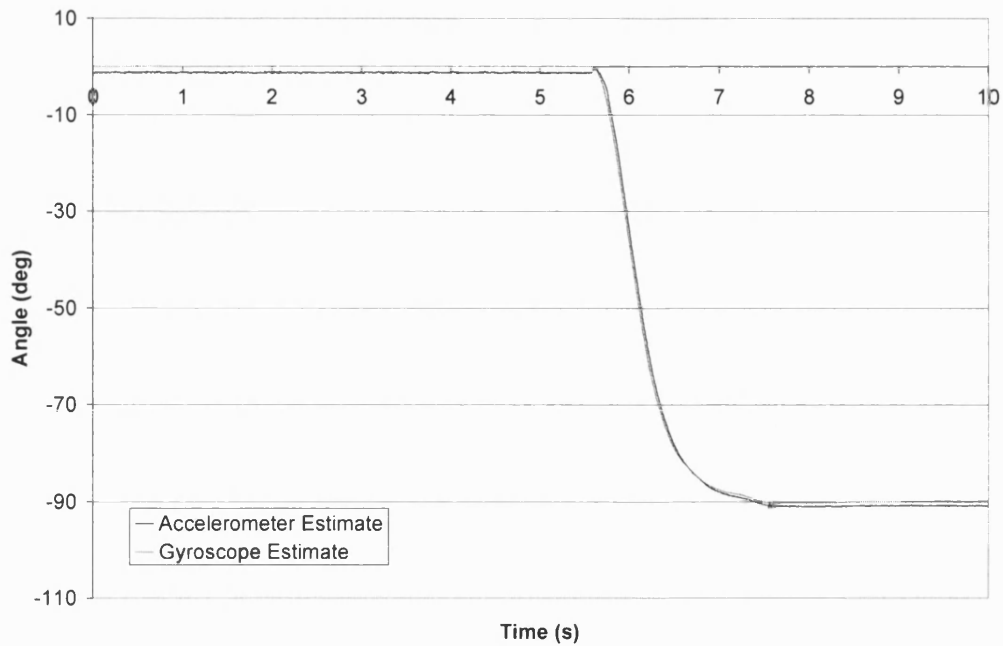
Figure 4-13 A typical example of the derived angle estimates from both the accelerometer and gyroscope sensor outputs.

All of the results for the ten trials in each rotation direction are displayed in tables 4-6 and 4-7. The majority of the estimates were within a ± 2° difference to the measured angles. The majority of the average values for the respective ten trials for each axis were within ± 1° and the standard deviations of the estimates showed good consistency within each set of the ten trials. The slight difference in angle was likely to be a combination of scale factor errors and the errors introduced by the estimation processes (integration and attitude estimation) used. At this point in the project this error was accepted and therefore validated the use of the scale factors.

Table 4-6 The results of the angle estimates from the inertial sensor system and deduced optical encoder angles during ten rotations in the clockwise direction.

		Pulses	Encoder Angle	Accelerometer Angle	Gyroscope Angle	
					Using Rotation SF	Using Average SF
			deg	deg	deg	deg
X Axis	1	505	90.90	89.97	89.67	89.95
	2	504	90.72	89.94	89.61	89.89
	3	505	90.90	89.54	89.57	89.84
	4	504	90.72	89.47	89.69	89.97
	5	504	90.72	89.77	89.45	89.73
	6	504	90.72	89.66	88.34	88.61
	7	504	90.72	89.85	89.41	89.69
	8	504	90.72	89.78	89.22	89.50
	9	504	90.72	89.67	89.31	89.59
	10	504	90.72	89.46	89.35	89.63
Average		504.2	90.76	89.71	89.36	89.64
Std		0.4	0.08	0.18	0.39	0.39
Y Axis	1	502	90.36	89.57	89.11	89.76
	2	502	90.36	89.55	89.03	89.68
	3	501	90.18	89.21	88.93	89.58
	4	502	90.36	89.24	88.96	89.61
	5	502	90.36	89.35	89.01	89.66
	6	502	90.36	89.37	88.93	89.57
	7	502	90.36	89.12	88.92	89.57
	8	502	90.36	89.18	89.04	89.69
	9	502	90.36	89.18	88.96	89.61
	10	502	90.36	89.32	89.13	89.78
Average		501.9	90.34	89.31	89.00	89.65
Std		0.3	0.06	0.15	0.08	0.08
Z Axis	1	503	90.54	90.91	90.44	90.60
	2	503	90.54	90.88	90.80	90.96
	3	504	90.72	91.70	90.58	90.74
	4	504	90.72	90.78	90.59	90.76
	5	504	90.72	91.94	90.58	90.74
	6	504	90.72	91.13	90.57	90.73
	7	504	90.72	91.68	90.59	90.75
	8	504	90.72	91.68	90.61	90.78
	9	503	90.54	90.27	90.51	90.67
	10	504	90.72	91.47	90.57	90.73
Average		503.7	90.67	91.24	90.58	90.75
Std		0.5	0.09	0.53	0.09	0.09

Table 4-7 The results of the angle estimates from the sensor system and deduced optical encoder angles during ten rotations in the counter clockwise direction.

		Pulses	Encoder Angle	Accelerometer Angle	Gyroscope Angle	
					Using Rotation SF	Using Average SF
			deg	deg	deg	deg
X Axis	1	503	-90.54	-90.09	-90.08	-89.77
	2	503	-90.54	-90.22	-90.15	-89.87
	3	503	-90.54	-90.07	-89.96	-89.67
	4	503	-90.54	-89.41	-90.23	-89.95
	5	503	-90.54	-89.63	-90.13	-89.85
	6	503	-90.54	-89.38	-90.01	-89.73
	7	503	-90.54	-89.75	-89.92	-89.64
	8	503	-90.54	-90.04	-89.79	-89.51
	9	503	-90.54	-89.69	-89.35	-89.63
	10	503	-90.54	-93.47	-93.94	-93.65
Average		503	-90.54	-90.18	-90.36	-90.13
Std		0.00	0.00	1.19	1.29	1.25
Y Axis	1	505	-90.90	-89.58	-90.81	-90.15
	2	505	-90.90	-89.43	-90.82	-90.16
	3	505	-90.90	-90.01	-90.79	-90.13
	4	505	-90.90	-90.26	-90.68	-90.02
	5	505	-90.90	-90.88	-90.78	-90.11
	6	504	-90.72	-90.72	-90.84	-90.18
	7	504	-90.72	-89.73	-90.83	-90.17
	8	504	-90.72	-90.01	-90.71	-90.05
	9	504	-90.72	-90.44	-90.75	-90.09
	10	504	-90.72	-89.75	-90.67	-90.01
Average		504.5	-90.81	-90.08	-90.77	-90.11
Std		0.5	0.09	0.49	0.06	0.06
Z Axis	1	505	-90.90	-91.53	-90.96	-90.80
	2	504	-90.72	-91.73	-91.01	-90.84
	3	505	-90.90	-91.63	-90.91	-90.75
	4	505	-90.90	-91.70	-90.93	-90.77
	5	505	-90.90	-91.85	-91.09	-90.93
	6	505	-90.90	-91.97	-90.76	-90.60
	7	505	-90.90	-91.41	-90.95	-90.79
	8	505	-90.90	-91.79	-91.08	-90.92
	9	505	-90.90	-91.73	-91.02	-90.86
	10	504	-90.72	-91.85	-90.96	-90.80
Average		504.8	-90.86	-91.72	-90.97	-90.81
Std		0.4	0.08	0.16	0.09	0.09

The last verification experiment successfully demonstrated the correct functionality of the processing steps. Figure 4-14 displays an example of one of the six angles, approximately 30°, which the y axis was rotated through. This provided evidence that the transformation matrix was functioning correctly. It is clear from the figure that the only angle to increase is the pitch angle. The other angles demonstrated very minimal fluctuations about zero degrees.
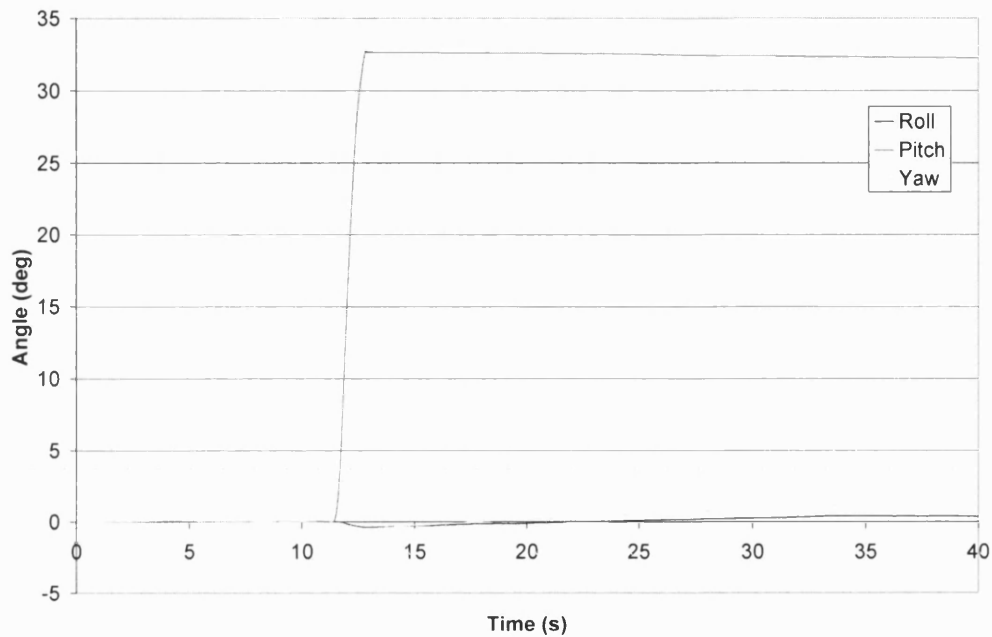
Figure 4-14 The resultant Euler angles from a 30° rotation about the y axis (pitch).

Since, the accelerometers measured both gravitational and dynamic accelerations the outputs of the accelerometers registered some movement during the rotations as displayed in figure 4-15.
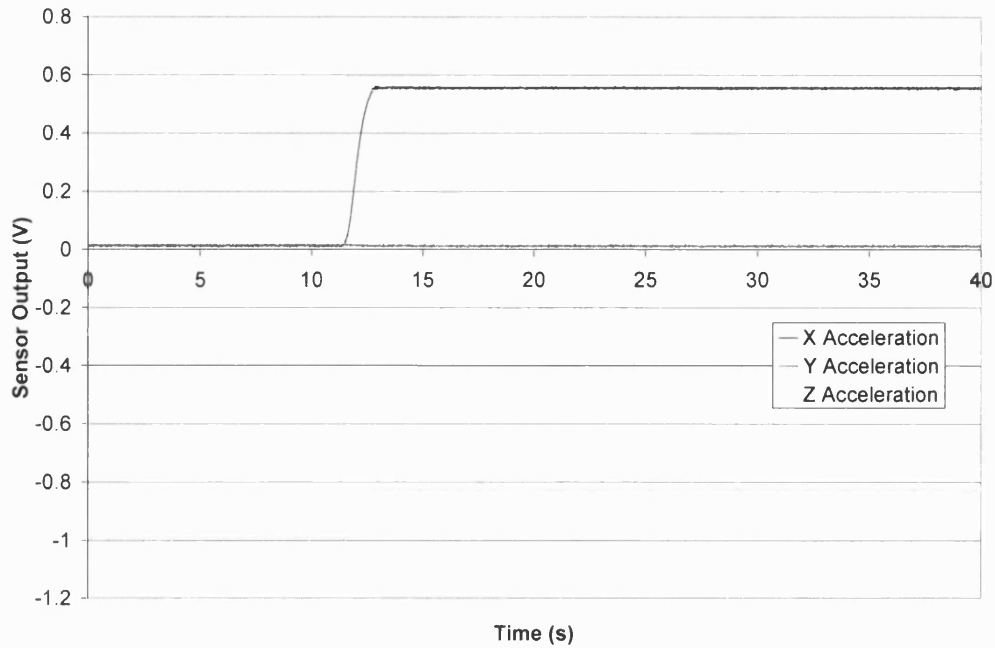
Figure 4-15 The acceleration outputs captured during a 30° rotation about the y axis (pitch).

The next two steps performed were subtracting the gravitational component from the measured acceleration and translating the accelerations measured from the body to the earth reference frames by applying the rotation matrix. Since, the gravitational acceleration components were derived from the rotation matrix, testing the overall output of the system would therefore verify both steps at once. Since the sensor system was only rotated, it was assumed that the accelerometers experienced an insignificant magnitude of linear acceleration in any direction. Implementation of the rotation matrix resulted in the acceleration values denoted in figure 4-15 being reduced to zero accelerations as displayed in figure 4-16.
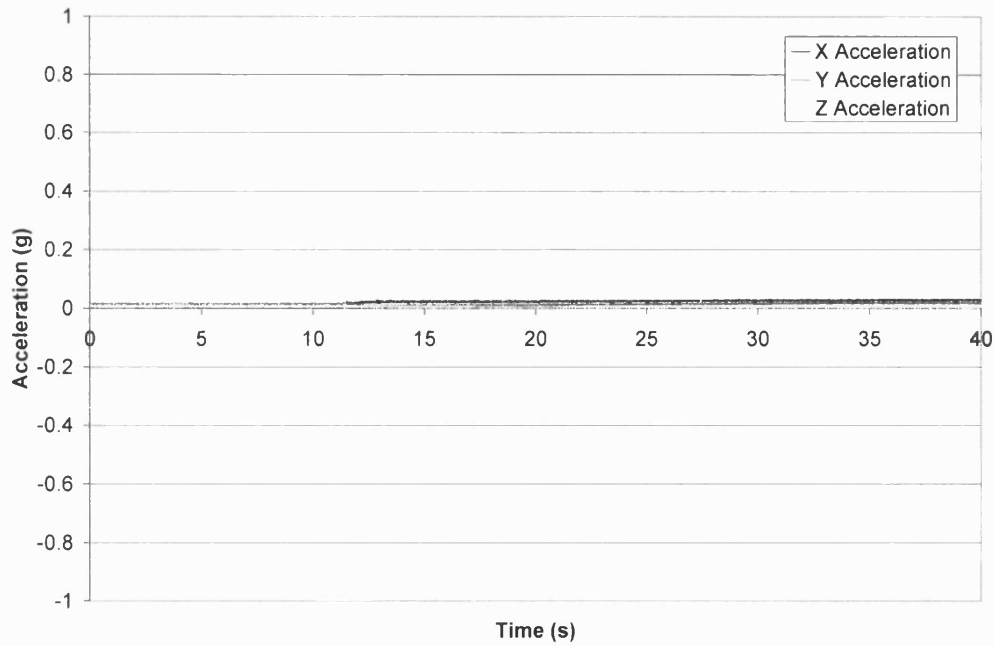
Figure 4-16 The acceleration outputs with respect to the 'flat earth' reference frame captured during a 30° rotation about the y axis (pitch).

The results for five of the six selected angles, 15, 30, 45, 60 and 75° were consistent to the example show above. However, when the sensor system was rotated 90° about the y axis (pitch) errors occurred in the other angles due to 'gimbal lock'. Gimbal lock occurred when the pitch angle neared 90° and therefore the angle became undefined in the equations used to calculate the other Euler angles (see section 2.6.4). An example of the resultant response of the Euler angles under such a condition is displayed in figure 4-17.
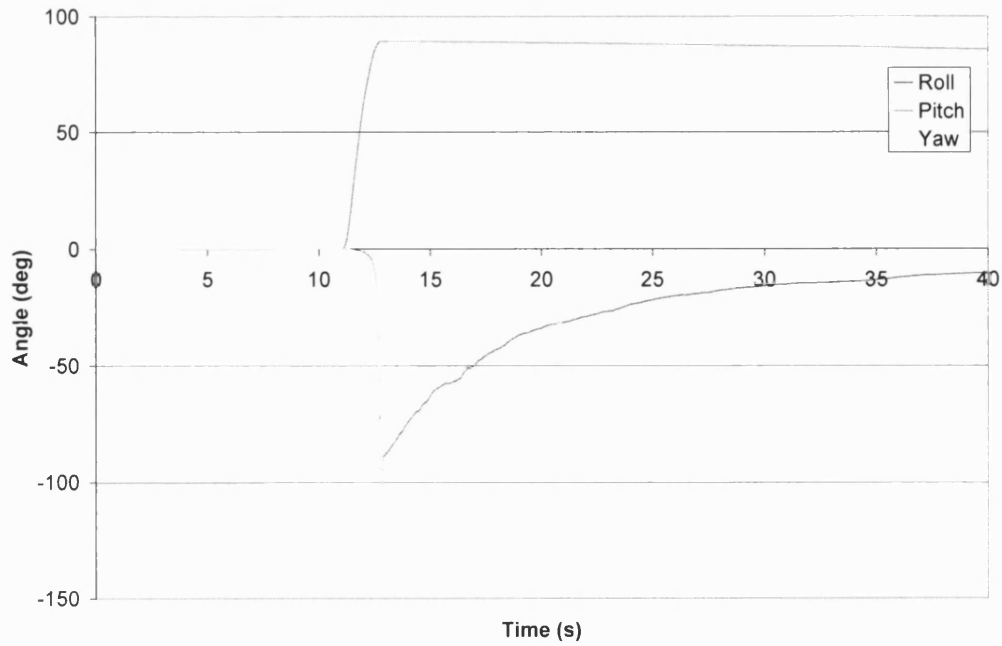
Figure 4-17 The resultant Euler angles during a 90° rotation about the y axis (pitch). This condition is named 'Gimbal lock'.

It was assumed that this condition would not occur for the intended application and thus no further problems were anticipated.

4.3.5 Discussion

The first verification experiment produced surprising results. The accelerometer sensors were arranged on the sensor system circuit boards following the sensitive axis illustration in the manufactures datasheet. The results from this first experiment demonstrated that a positive acceleration was in fact in the opposite direction to information interpreted on the sensor's data sheets. Definition of the positive rotation directions showed that two out of the three gyroscopes were orientated incorrectly. These gyroscope sensors should have been orientated on the sensor system circuit boards with consideration to the prospective body to earth coordinates transformation process to be applied. The accelerometer and gyroscope outputs once calibrated i.e. distributed about the horizontal axis, could be inverted by simply multiplying by a factor of minus one. The following axes needed conversion to facilitate a NED arrangement: x accelerometer, y and z gyroscopes.

The gyroscope scale factors implemented to deduce angular rates showed encouraging results by identifying five clearly defined angular rates. Each of the five angular rates showed good agreement to those determined by the optical encoder. The angular displacement experiments also demonstrated surprisingly consistent results. The accelerometer and gyroscope angle estimates were within ± 1° compared to the optical encoder angles. The accelerometer angle estimates proved to be slightly superior to the gyroscope estimates in terms of magnitude. This experiment also validated the accelerometer calibration parameters. Finally, the overall sensor system outputs compared favourably to the hypothesised results. These results suggested the implementation of the rotation matrix was of correct functionality.

4.4 Gyroscope Drift Experiments

4.4.1 Introduction

The purpose of the following experiments was to characterise the performance of each gyroscope output when in a stationary position and to deduce a method for predicting this output. The output of the gyroscope in a stationary position was denoted as the zero bias value and this value was captured by invoking a stationary data collection period prior to any experiments. It had been shown that the zero bias value varies considerably each time the sensor was powered-up [156]. Further drifting of this value was then seen. The uncompensated drifting from an initial zero bias value would introduce errors in the newly converted angular rate output. These errors were more prominent due to the small magnitude of the scale factor, 0.67 $mV^{o-1}s^{-1}$. These errors were likely to be magnified even further during the integration process and then carried forward into subsequent equations.

One of the main causes of the zero bias variation has been shown to be thermal effects [56, 93, 111, 136, 156]. The gyroscope sensor is a mechanical device and when it was powered up its elements began oscillating at a constant frequency even when the gyroscope was stationary. This mechanical work created heat which caused the ambient temperature within the sensor itself to increase initially and then stabilised after a period of time. Secondly, transient effects which caused thermal expansion of the elements and its housing also affected the stability of the zero bias value. The manufacturers recommended use of the sensor was to apply a high pass filter directly across the output of the sensor at a cut of frequency of 0.3 Hz to eliminate any dc component of the signal thus reducing the effects of the temperature. As denoted in the introduction this human movement measurement system was required to measure slow rotations of less than 1 Hz and so a method for compensation of the zero bias drift was investigated.

4.4.2 Temperature Sensors

Several preliminary experiments were conducted to find the most feasible method of measuring the temperature that could be used as part of a compensation method for eliminating the drift. Firstly, the ambient temperature in close proximity to the sensor system was measured using a PT100 probe. The probe in conjunction with a Pico PT104 16-bit resolution data logger provided an accurate measure of temperature to 0.01°C. This ambient temperature measurement did not provide a repeatable response with respect to the gyroscope sensor output. This was due to the probe measuring the temperature environment around the sensor system as opposed to the temperature of the sensor. Further, this set up was conducted inside a medium-sized temperature regulated room which added little improvement to the relationship from the previous experiment. Subsequently, the sensor system was placed in a rectangular box of dimensions, 28 x 15 x 10 mm with a fan mounted on the inside of one of the lengths and small holes on the opposite length to help circulate the flow of air around the box. The fan and the enclosed box produced a smaller regulated environment around the sensor system hoping to provide an actual temperature measurement in close proximity to the gyroscopes. Although the temperature and gyroscope zero bias output response displayed an increased linear relationship, the practicalities of applying such principles on a smaller scale to produce a wearable, fan cooled temperature regulated environment for the sensors was unrealistic. This experiment highlighted the need for a temperature regulated space and for the temperature measurement to be taken as close as possible to the gyroscopes. A more practical implementation of the last experiment was to mount three temperature sensors each within close proximity to its respective gyroscope. Since the box is small in size, the ambient temperature should be to some extent self-regulated.

The temperature sensors used were analog devices AD592. This device is a two terminal monolithical integrated circuit transducer which provides a current output proportional to absolute temperature. The sensor benefits from high accuracy, minimal nonlinearity errors and a low price compared to older technology sensors such as thermistors, resistance temperature detectors (RTDs) and thermocouples. The sensors were utilised in accordance with the manufacturer's reference design, found

on the Analog Devices' website [62]. This circuit was chosen over the simpler circuit design found in figure 4 (on the datasheet) due to the greater amplification of the temperature output by a scale factor of 100 $mV°C^{-1}$. The trimming function (adjustment of R1) was not utilised. This is because an absolute temperature value was not desired. The change in temperature output over a collection period was the important factor to allow a comparison with the gyroscope output. The DC level output of the circuit was shifted using a current summing amplifier as described previously. The range of the analogue output was 25°C and was centred about the laboratory temperature of 20°C. The 12-bit A/D converter gave a resolution of 0.01°C.

For each temperature sensor, the two legs of the sensor were mounted on solder pins affixed to the circuit board within 1 mm of each gyroscope. Orientation of the temperature sensor was such that the flat face was resting slightly above the top surface of the gyroscope. Three separate screened wires from underneath the boards carried the induced currents to three identical processing circuits housed in the 'processing' box and from there to the respective A/D channels.

4.4.3 Method

Two types of temperature experiments were conducted. Firstly, an experiment to investigate the response and repeatability of the gyroscope output from power-up over a period of 30 minutes in a laboratory environment regulated at approximately 20°C. The sensor system was placed on a level surface, powered up and remained stationary for the 30 minute data collection period. A PT100 probe was placed near to the sensor box measuring the ambient temperature outside of the box. After the collection period the power supply to the sensor system was disconnected for another 30 minute period. This process was repeated eight times each day for two consecutive days. All outputs were recorded at 1 Hz yielding a total of 1800 samples per experiment. The results are displayed on pages 138 to 149.

Secondly, an investigation was performed into the changes in response due to different ambient temperatures outside the sensor box. An incubator (used in the

biological department for developing cells in controlled environments) was used to provide two temperature environments, 12° and 30°. These values represent the lower and upper ends of the measurable temperature range through the A/D converter and typically the extremes of the likely environment the sensor system will be used in. The sensor system was placed on a shelf inside the incubator alongside a PT100 probe to record the ambient temperature outside the sensor box. The door of the incubator remained closed for the duration of the experiments, with the wires protruding though a gap in the seal. The incubator was brought to the required temperature prior to commencing the experiments. Results from the first set of experiments showed that a shorter collection period of 15 minutes after power up at a sampling rate of 1 Hz was sufficient to capture the desired gyroscope output response. Several consecutive experiments were conducted over consecutive days. The results are displayed on pages 150 to 153.

4.4.4 Results

The response of each gyroscope was investigated and typical outputs were seen in figures 4-15 to 4-17. All three gyroscopes outputs increased over time whilst in a stationary position. These typical output responses from the gyroscopes raised the question of what was a suitable zero bias value. If the initial output was used, an angular rate error in the region of 5 to 9°s^{-1} over a 30 minute period was produced. On these grounds, a method of predicting the gyroscope output using a temperature measurement was sought.
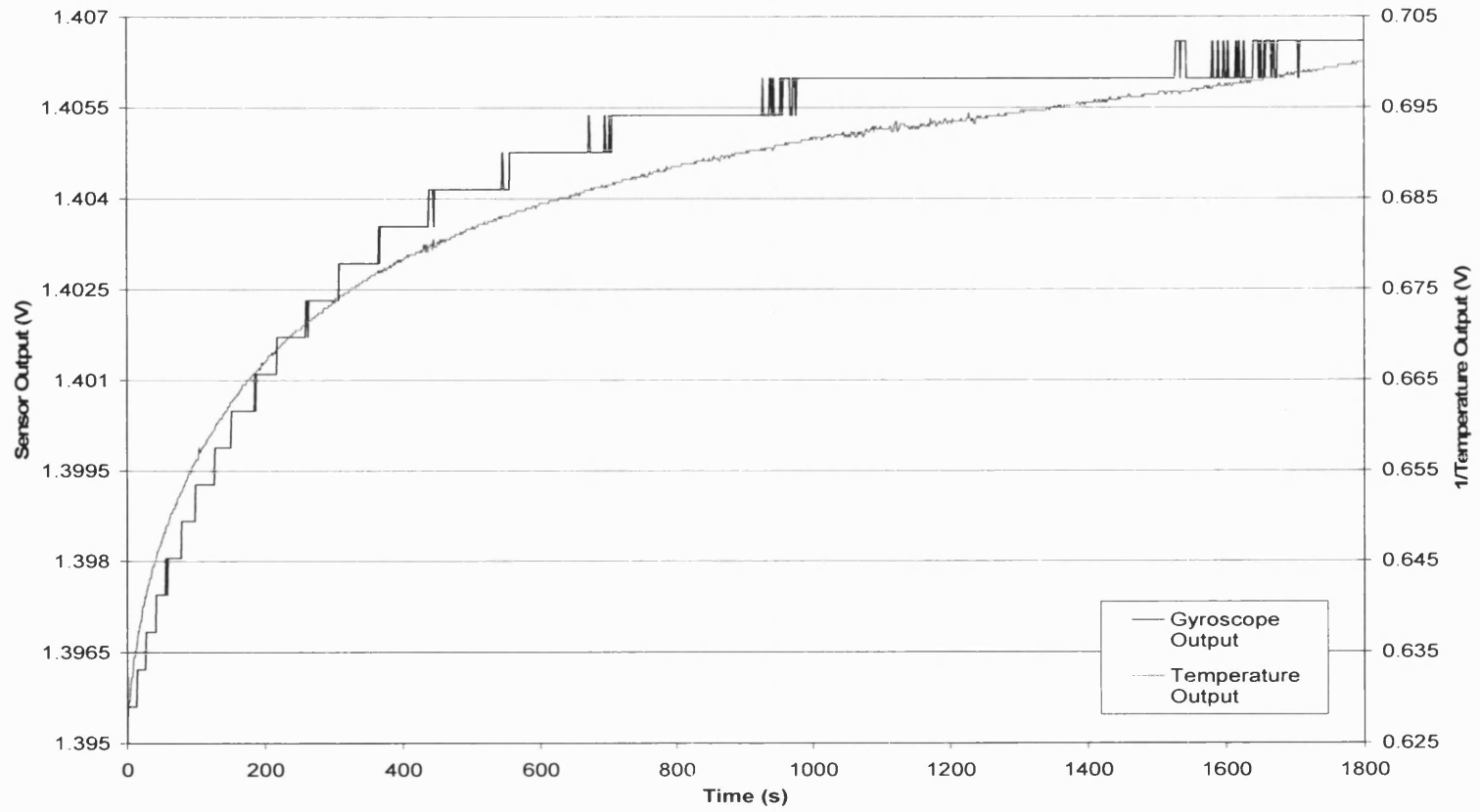
Figure 4-18 The response of the x axis gyroscope and the respective temperature sensor output from day 1, trial 1.
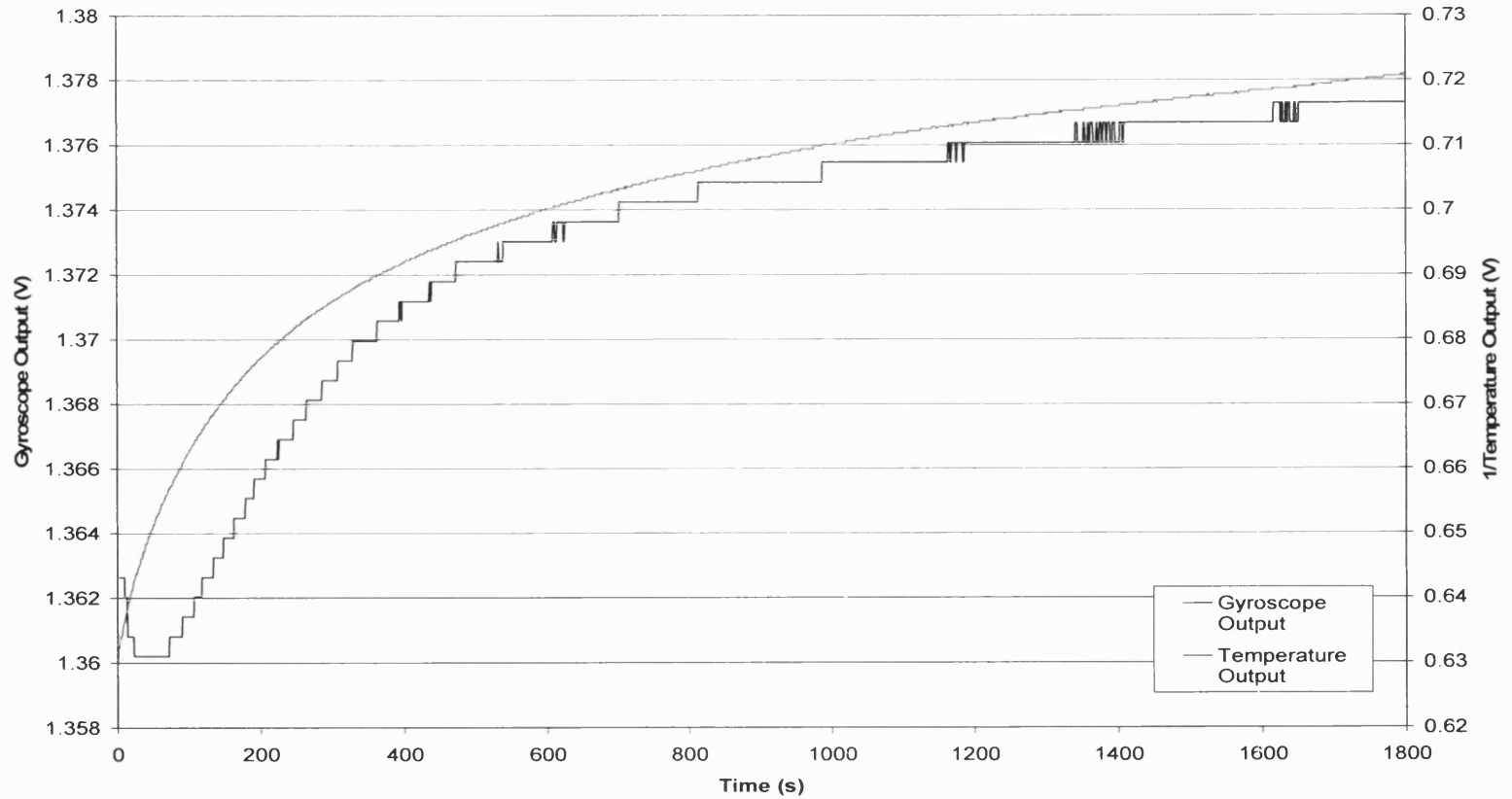
Figure 4-19 The response of the y axis gyroscope and the respective temperature sensor output from day 1, trial 1.
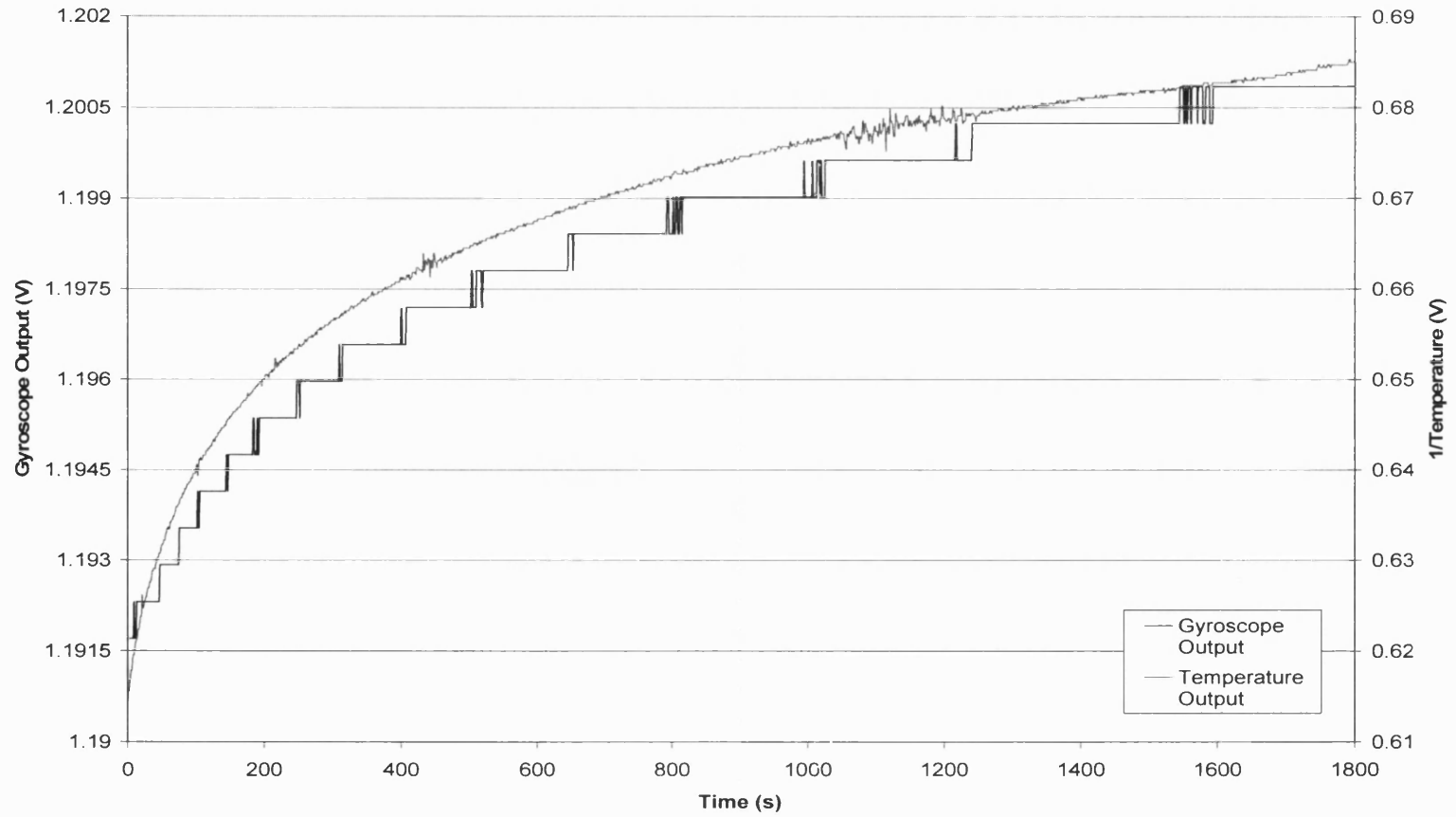
Figure 4-20 The response of the z axis gyroscope and the respective temperature sensor output from day 1, trial 1.

The temperature measurements recorded within millimetres of each of the gyroscopes produced similar shaped responses to that of the gyroscope output as seen in the previous three figures. All trials were reviewed to decipher the possibility of a linear relationship existing between the two variables. A linear approximation was chosen because it is simple and far less complex than other approximations that would be beyond the scope of this thesis. First order linear approximations in the form of equations 4-5 and 4-6 were utilised to ascertain the linearity between the two variables.

$$S_{xy} = \sum (x - \bar{x}) \times (y - \bar{y})$$
$$S_{xx} = \sum (x - \bar{x})^2 \qquad \qquad \textbf{4-5}$$
$$S_{yy} = \sum (y - \bar{y})^2$$

$$m = \frac{S_{xy}}{S_{xx}} \qquad \qquad \textbf{4-6}$$
$$b = \bar{y} - (m \times \bar{x})$$

where, x and y   are the temperature and gyroscope outputs

m   is the gradient

b   is the intersect.

The gradient, intersect and temperature output were implemented in the standard equation for a straight line to predict the drifting zero bias value. A comparison of the actual output against the predicted for each sensor cluster is displayed in figures 4-18 to 4-20.
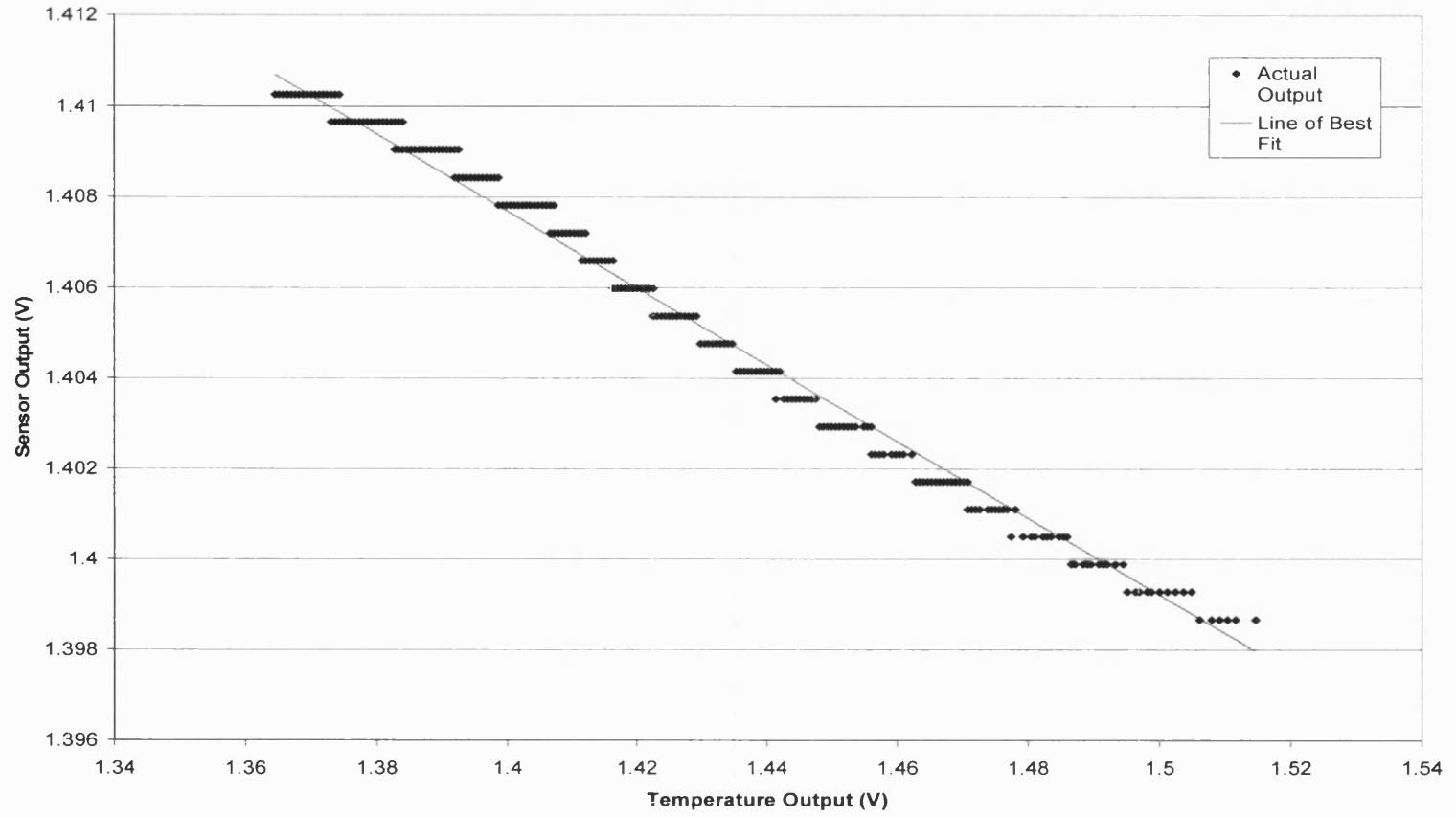
Figure 4-21 Actual sensor output and a line of best fit from day 1, trial 2 about the x axis
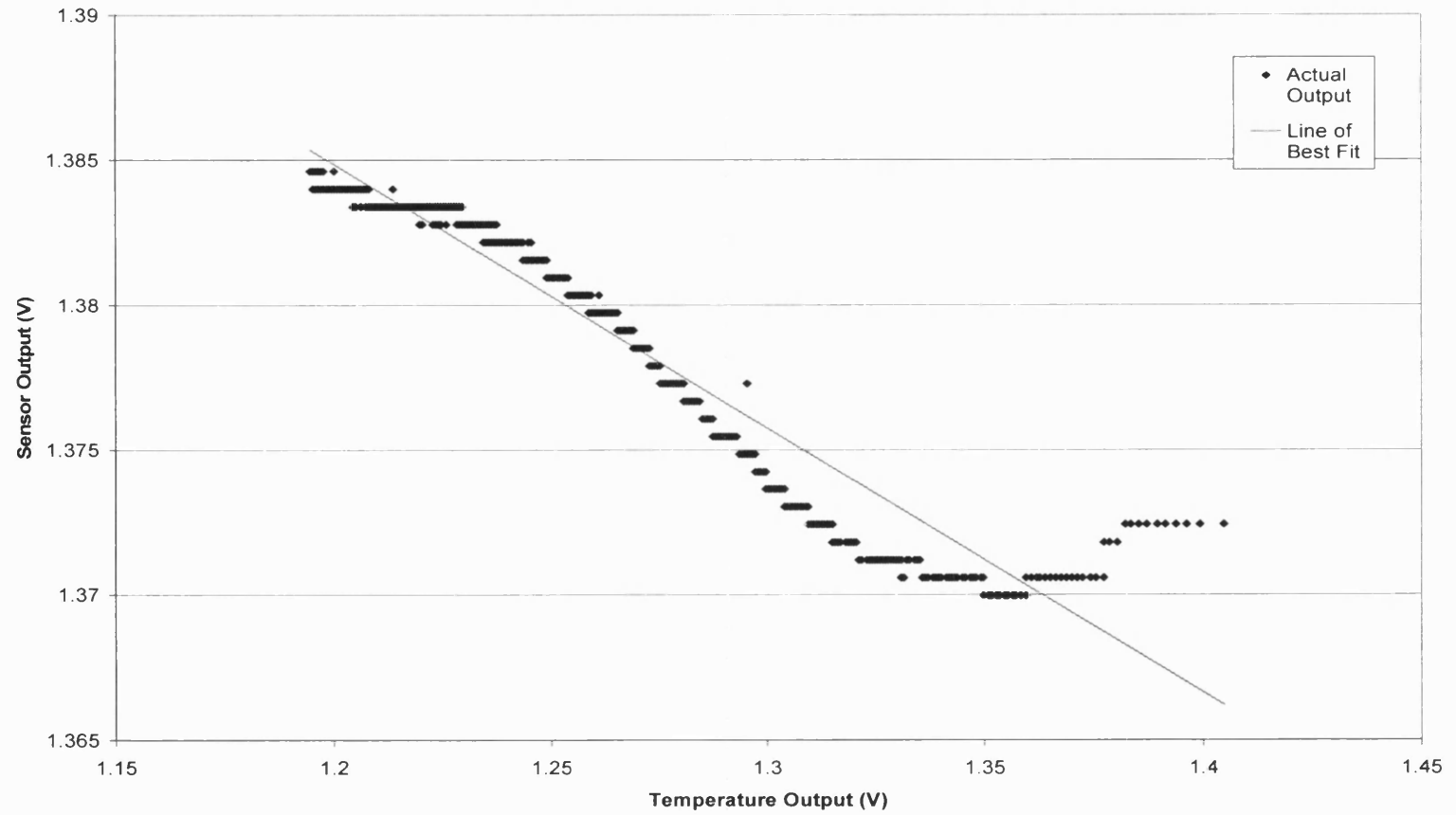
Figure 4-22 Actual sensor output and a line of best fit (for a straight line approximation) from day 2, trial 4 about the y axis
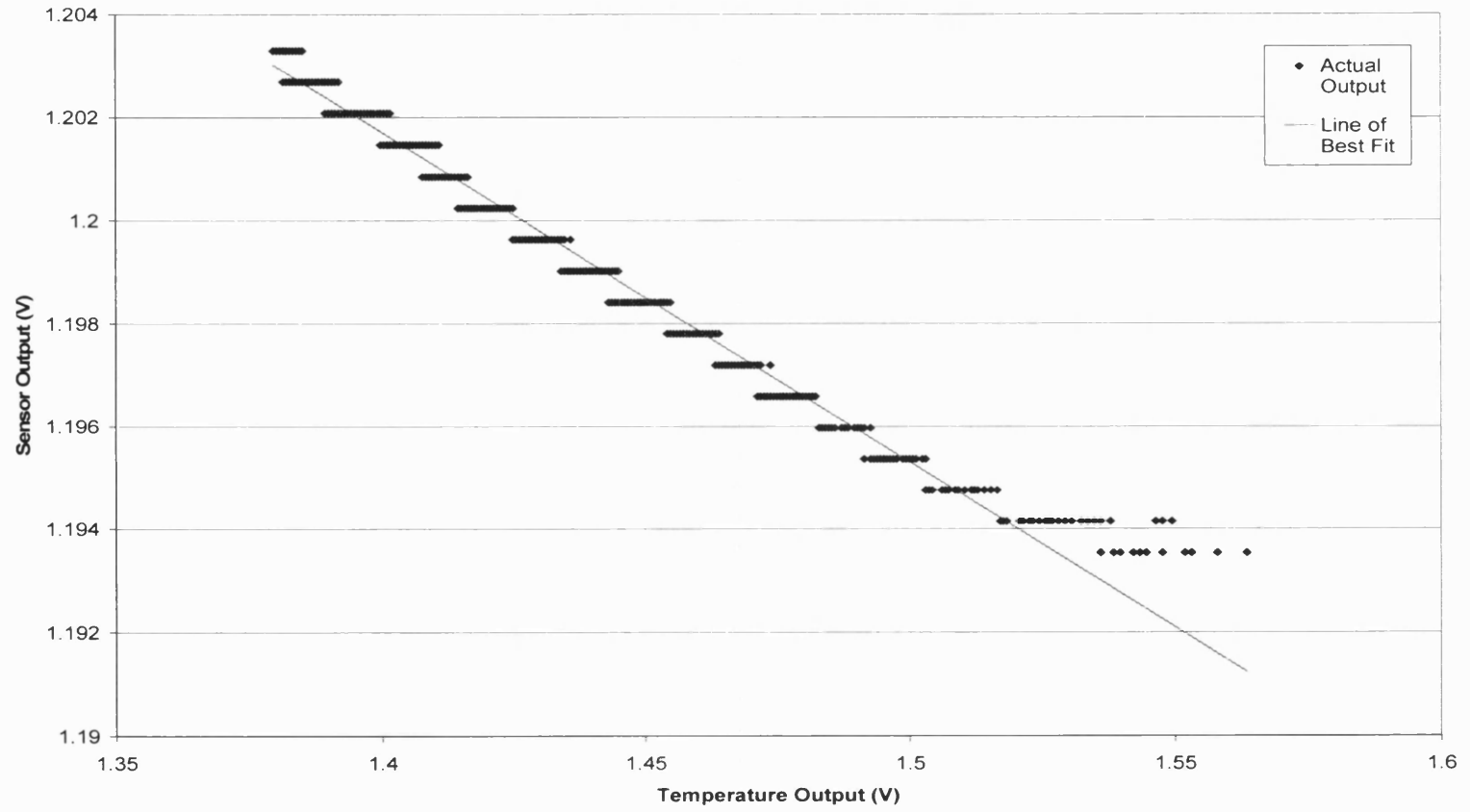
Figure 4-23 Actual sensor output and a line of best fit from day 2, trial 2 about the z axis.

The x and z axes gyroscopes and the respective temperature sensors demonstrated a moderately linear relationship. However, it was evident that a linear approximation was perhaps not the most suitable line of best fit for the y axis gyroscope , figure 4-19. Coincidently, this gyroscope is the ENC-03JB type which is different from the x and z axes sensors being of the A type. The angular rate error was calculated by dividing the difference between the actual and the predicted outputs, by the respective scale factors for each axis. The RMS error for the y axis was $0.58°s^{-1}$ with a maximum of $3.62°s^{-1}$ and a minimum of $-1.55°s^{-1}$. Although a linear approximation may not seem the best approach, these errors were a significant reduction in angular rate error. This is compared to an angular rate error of $7°s^{-1}$, without applying any compensation. An example of the typical angular rate error is displayed in figure 4-21.
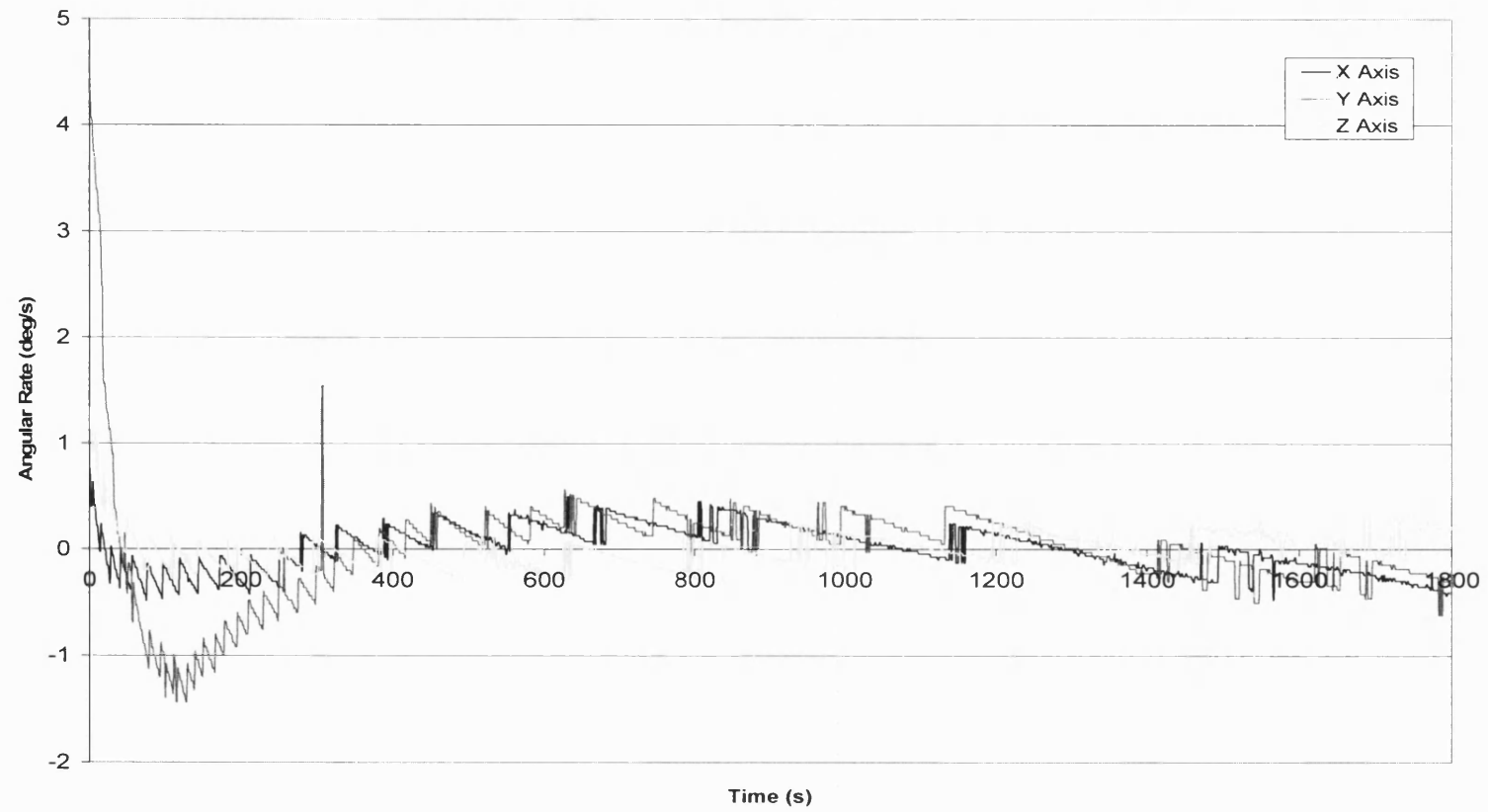
Figure 4-24 Angular rate errors for all axes from day 2 trial 2.

The following parameters for all axes and for both days are displayed in tables 4-8 to 4-10: the start up output of the gyroscopes, the gradients and intersects of the linear lines of best fit and the angular rate errors without and with predicting the angular rate output. The start values exhibit small variations which can be seen in the low magnitude of the standard deviation. However, the scale factors are smaller in magnitude which would result in initial large angular rates. This highlights the need to use derived zero bias parameters immediately prior to each trial. Using the temperature output to prediction the zero bias reduced the angular rate error to $1°s^{-1}$ and $1.3°s^{-1}$ for the x and z axes, respectively, and $4.5°s^{-1}$ for the y axis. This was compared to using the initial output as the zero bias.

Table 4-8 Gradient scale factors and angular rate error ranges for the x axis.

x Axis		Sensor Start Value		Gradient	Intersect	Angular Rate Error without Correction		Angular Rate Error with Correction	
		Gyro	Temp			Min	Max	Min	Max
		V	V	V	V	deg/s	deg/s	deg/s	deg/s
Day 1	1	1.3956	1.5965	-0.0790	1.5198	0.00	6.19	-0.44	1.07
	2	1.3987	1.5147	-0.0848	1.5264	0.00	6.53	-0.38	0.41
	3	1.3993	1.5031	-0.0821	1.5216	0.00	7.90	-0.52	0.81
	4	1.4029	1.4316	-0.0911	1.5319	0.00	7.56	-0.43	0.83
	5	1.4954	1.3981	-0.0950	1.5364	0.00	6.53	-0.40	1.04
	6	1.4035	1.4298	-0.0987	1.5421	0.00	6.53	-0.43	1.45
Average		1.4159	1.4789	-0.0885	1.5297	0.00	6.87	-0.43	0.94
Std		0.0390	0.0733	0.0077	0.0087	0.00	0.69	0.05	0.35
Day 2	1	1.3932	1.6722	-0.0705	1.5092	0.00	7.56	-0.44	1.01
	2	1.4096	1.3942	-0.0806	1.5219	0.00	7.13	-0.48	0.82
	3	1.4023	1.4768	-0.0834	1.5236	0.00	6.87	-0.52	1.06
	4	1.4054	1.4115	-0.0885	1.5282	0.00	8.25	-0.47	1.17
	5	1.4097	1.3468	-0.0941	1.5347	0.00	6.87	-0.41	0.93
	6	1.4127	1.3132	-0.0878	1.5269	0.00	7.90	-0.44	0.61
Average		1.4055	1.4358	-0.0841	1.5241	0.00	7.43	-0.46	0.94
Std		0.0070	0.1287	0.0081	0.0085	0.00	0.57	0.04	0.20

Table 4-9 Gradient scale factors and angular rate error ranges for the y axis.

Y Axis		Sensor Start Value		Gradient	Intersect	Angular Rate Error without Correction		Angular Rate Error with Correction	
		Gyro	Temp			Min	Max	Min	Max
		V	V	V	V	deg/s	deg/s	deg/s	deg/s
Day 1	1	1.3626	1.5891	-0.1158	1.5382	-1.43	8.57	-1.33	4.97
	2	1.3663	1.5031	-0.1133	1.5307	-1.07	8.57	-1.16	3.46
	3	1.3700	1.4884	-0.1055	1.5193	-1.78	7.50	-1.49	4.56
	4	1.3718	1.4322	-0.1049	1.5154	-1.43	7.51	-1.34	3.92
	5	1.3736	1.3974	-0.1164	1.5282	-1.43	7.50	-1.46	4.74
	6	1.3736	1.4188	-0.1143	1.5275	-1.08	6.79	-1.63	4.82
Average		1.3697	1.4715	-0.1117	1.5265	-1.37	7.74	-1.40	4.41
Std		0.0044	0.0706	0.0051	0.0082	0.27	0.70	0.16	0.59
Day 2	1	1.3559	1.6648	-0.0931	1.5045	-1.78	8.93	-1.66	3.80
	2	1.3620	1.5360	-0.1108	1.5243	-1.43	8.93	-1.44	4.62
	3	1.3681	1.4695	-0.1149	1.5280	-1.78	8.22	-1.52	5.23
	4	1.3724	1.4048	-0.0911	1.4943	-1.43	7.14	-1.55	3.63
	5	1.3736	1.3425	-0.1216	1.5276	-1.79	7.14	-1.31	5.43
	6	1.3724	1.3120	-0.1043	1.5017	-1.43	7.86	-1.29	4.42
Average		1.3674	1.4549	-0.1060	1.5134	-1.61	8.04	-1.46	4.52
Std		0.0071	0.1315	0.0121	0.0149	0.19	0.81	0.15	0.73

Table 4-10 Gradient scale factors and angular rate error ranges for the z axis.

Z Axis		Sensor Start Value		Gradient	Intersect	Angular Rate Error without Correction		Angular Rate Error with Correction	
		Gyro	Temp			Min	Max	Min	Max
		V	V	V	V	deg/s	deg/s	deg/s	deg/s
Day 1	1	1.1917	1.6294	-0.0672	1.2987	0.00	5.32	-0.38	1.41
	2	1.1960	1.5434	-0.0659	1.2965	0.00	5.68	-0.33	0.66
	3	1.1990	1.5299	-0.0630	1.2930	0.00	4.97	-0.35	1.37
	4	1.2015	1.4640	-0.0653	1.2951	0.00	5.32	-0.28	1.09
	5	1.2033	1.4286	-0.0731	1.3055	0.00	5.32	-0.34	1.33
	6	1.2033	1.4579	-0.0702	1.3033	0.00	4.61	-0.46	1.40
Average		1.1991	1.5089	-0.0674	1.2987	0.00	5.20	-0.36	1.21
Std		0.0046	0.0738	0.0037	0.0048	0.00	0.37	0.06	0.29
Day 2	1	1.1868	1.6886	-0.0573	1.2818	0.00	6.03	-0.33	1.19
	2	1.1935	1.5635	-0.0641	1.2915	0.00	5.68	-0.33	1.33
	3	1.1978	1.5031	-0.0722	1.3030	0.00	5.33	-0.52	1.89
	4	1.2027	1.4359	-0.0567	1.2827	0.00	5.32	-0.49	0.78
	5	1.2051	1.3687	-0.0724	1.3017	0.00	4.61	-0.44	1.45
	6	1.2057	1.3339	-0.0626	1.2874	0.00	5.68	-0.40	1.06
Average		1.1986	1.4823	-0.0642	1.2914	0.00	5.44	-0.42	1.28
Std		0.0074	0.1316	0.0069	0.0092	0.00	0.49	0.08	0.38

The second experiment in this section was to investigate the response of the sensors whilst in different but controlled temperature environments. The chosen temperatures were 12.85°C, 22.97°C and 30.20°C. The results of six out of the eight trials performed under each temperature condition are displayed in tables 4-11 to 4-13. The first trial was discarded since it was likely to contain variations due to the initial trial, after this the first six trials were selected therefore discarding the last trial also.

During all trials it was noted that the x and z axes gyroscopes drifted up and the y gyroscope drifted down with respect to time regardless of the temperature environment. The y gyroscope sensor used in this experiment was a different sensor than used in the previous section. The sensor change was required due to the lid of the sensor becoming unstuck. It was found that the response of several gyroscope sensors of the same manufacturing part displayed both increasing and decreasing drifting outputs. The point demonstrated in this experiment was not dependent on whether the drifting output increases or decreases. The initial output value of each gyroscope varied with respect to the ambient temperature. The x and z axes outputs increased as the ambient temperature increased, while the y axis output decreased as the ambient temperature increased. Within the series of six trials for each temperature condition there was also a variation in the initial gyroscope outputs. For example, the variation was greatest in the y axis gyroscope, 10.37 mV compared to 3.05 mV and 4.27 mV for x and z, respectively. If the initial gyroscope output was recorded and assigned to be the zero bias then the accumulated angular rate error was as large as $8.6°s^{-1}$, $17.5°s^{-1}$ and $4.3°s^{-1}$ for x, y and z axes gyroscopes respectively. The average angular rate errors for each temperature condition increased as the ambient temperature increased. The average gradients for each axis changed with respect to the ambient temperature. The x and z axis gyroscopes average gradient value decreased as the ambient temperature increased, while the y axis value increased. When the straight line approximation was applied to the data sets to predict the zero bias values the range of angular rate error was somewhat reduced.

Table 4-11 Gradient scale factors and angular rate errors for the x axis under varying temperature environments.

X Axis		Temperature	Sensor Start Value Gyro	Temp	Gradient	Intersect	Error without Correction Min	Max	Error with Correction Min	Max
		°C	V	V	V	V	deg/s	deg/s	deg/s	deg/s
Low Temperature	1	12.61	1.3034	2.4939	-0.0747	1.4864	0.00	4.81	-0.85	1.88
	2	13.05	1.3046	2.4542	-0.0837	1.5057	-0.34	5.16	-0.73	2.42
	3	12.97	1.3065	2.4444	-0.0766	1.4899	-0.34	4.13	-0.81	2.13
	4	12.91	1.3059	2.4438	-0.0774	1.4920	-0.34	4.47	-0.72	1.75
	5	12.83	1.3053	2.4640	-0.0748	1.4860	-0.34	4.47	-0.71	1.95
	6	12.75	1.3053	2.4725	-0.0731	1.4823	-0.34	4.13	-0.66	2.08
Average		12.85	1.3051	2.4621	-0.0767	1.4904	-0.29	4.53	-0.74	2.04
Std		0.16	0.0011	0.0191	0.0037	0.0082				
Room Temperature	1	22.97	1.3669	1.3645	-0.1060	1.5112	0.00	5.50	-0.65	0.69
	2	22.99	1.3663	1.3950	-0.1075	1.5123	-0.34	8.59	-0.75	3.54
	3	22.97	1.3651	1.4023	-0.1100	1.5152	-0.34	8.59	-0.78	3.40
	4	22.98	1.3657	1.4243	-0.1086	1.5130	-0.34	5.84	-0.75	2.26
	5	22.96	1.3651	1.3919	-0.1128	1.5185	-0.34	6.19	-0.68	2.00
	6	22.97	1.3669	1.3462	-0.1207	1.5284	0.00	5.16	-0.49	0.63
Average		22.97	1.3660	1.3874	-0.1109	1.5164	-0.23	6.64	-0.68	2.09
Std		0.01	0.0008	0.0279	0.0053	0.0064				
High Temperature	1	30.21	1.4176	0.6728	-0.1195	1.4947	-0.34	8.25	-0.96	1.85
	2	30.19	1.4182	0.6667	-0.1204	1.4946	0.00	7.56	-0.91	2.21
	3	30.21	1.4170	0.6630	-0.1213	1.4945	0.00	8.25	-0.73	1.65
	4	30.21	1.4176	0.6569	-0.1241	1.4954	0.00	7.56	-1.04	2.04
	5	30.18	1.4182	0.6477	-0.1241	1.4956	-0.34	6.87	-1.03	1.67
	6	30.18	1.4164	0.6661	-0.1232	1.4950	0.00	7.90	-0.86	1.93
Average		30.20	1.4175	0.6622	-0.1221	1.4950	-0.11	7.73	-0.92	1.89
Std		0.02	0.0007	0.0088	0.0020	0.0005				

Table 4-12 Gradient scale factors and angular rate errors for the y axis under varying temperature environments.

Y Axis		Temperature	Sensor Start Value Gyro	Temp	Gradient	Intersect	Error without Correction Min	Max	Error with Correction Min	Max
		°C	V	V	V	V	deg/s	deg/s	deg/s	deg/s
Low Temperature	1	12.61	2.2485	2.4762	0.1841	1.7950	-16.07	0.00	-1.34	0.74
	2	13.05	2.2405	2.4347	0.1722	1.8231	-16.79	0.00	-1.37	3.82
	3	12.97	2.2393	2.4225	0.1249	1.9371	-12.15	0.00	-2.18	3.09
	4	12.91	2.2399	2.4231	0.1402	1.9025	-11.43	0.00	-2.47	2.87
	5	12.83	2.2418	2.4438	0.1394	1.9223	-11.43	0.00	-2.65	2.80
	6	12.75	2.2442	2.4524	0.1360	1.9126	-12.50	0.00	-2.29	3.01
Average		12.85	2.2424	2.4421	0.1495	1.8821	-13.40	0.00	-2.05	2.72
Std		0.16	0.0035	0.0204	0.0232	0.0584				
Room Temperature	1	22.97	2.0763	1.3651	0.2097	1.7896	-14.29	0.00	-0.64	0.60
	2	22.99	2.0806	1.3981	0.2090	1.7924	-16.44	0.00	-0.57	0.74
	3	22.97	2.0843	1.4066	0.2132	1.7881	-17.51	0.00	-0.72	0.65
	4	22.98	2.0763	1.4005	0.2145	1.7872	-16.79	0.36	-0.68	0.76
	5	22.96	2.0830	1.3938	0.2160	1.7854	-16.07	0.36	-1.97	0.63
	6	22.97	2.0763	1.3431	0.2077	1.7975	-12.14	0.00	-0.80	0.64
Average		22.97	2.0795	1.3845	0.2117	1.7900	-15.54	0.12	-0.89	0.67
Std		0.01	0.0037	0.0249	0.0033	0.0044				
High Temperature	1	30.21	1.9457	0.6917	0.1871	1.8250	-17.50	0.00	-0.73	0.69
	2	30.19	1.9469	0.6807	0.1866	1.8270	-16.79	0.00	-0.88	0.89
	3	30.21	1.9481	0.6764	0.1915	1.8264	-16.79	0.00	-0.86	0.81
	4	30.21	1.9475	0.6752	0.2002	1.8215	-17.15	0.00	-0.77	0.88
	5	30.18	1.9518	0.6630	0.1931	1.8255	-15.00	0.00	-0.81	0.77
	6	30.18	1.9560	0.6807	0.1955	1.8244	-16.79	0.00	-0.83	0.85
Average		30.20	1.9493	0.6780	0.1923	1.8249	-16.67	0.00	-0.81	0.82
Std		0.02	0.0039	0.0094	0.0052	0.0019				

Table 4-13 Gradient scale factors and angular rate errors for the z axis under varying temperature environments.

Z Axis		Temperature	Sensor Start Value		Gradient	Intersect	Error without Correction		Error with Correction	
			Gyro	Temp			Min	Max	Min	Max
		°C	V	V	V	V	deg/s	deg/s	deg/s	deg/s
Low Temperature	1	12.61	1.1935	2.4841	-0.0290	1.2663	0.00	3.19	-0.78	0.46
	2	13.05	1.1948	2.3932	-0.0226	1.2502	0.00	3.19	-0.90	0.64
	3	12.97	1.1954	2.3852	-0.0218	1.2487	0.00	3.19	-0.85	0.66
	4	12.91	1.1954	2.3846	-0.0215	1.2481	0.00	3.19	-0.88	0.60
	5	12.83	1.1954	2.4011	-0.0175	1.2391	0.00	3.19	-1.12	0.59
	6	12.75	1.1954	2.2161	-0.0144	1.2288	0.00	3.19	-0.97	0.62
Average		12.85	1.1950	2.3774	-0.0211	1.2468	0.00	3.19	-0.92	0.59
Std		0.16	0.0007	0.0876	0.0050	0.0125				
Room Temperature	1	22.97	1.2314	1.3877	-0.0453	1.2942	0.00	3.20	-0.33	0.53
	2	22.99	1.2320	1.4182	-0.0403	1.2888	0.00	3.20	-0.33	0.31
	3	22.97	1.2320	1.4206	-0.0395	1.2884	0.00	3.55	-0.44	0.38
	4	22.98	1.2332	1.4243	-0.0374	1.2862	0.00	3.20	-0.40	0.38
	5	22.96	1.2338	1.4097	-0.0359	1.2846	0.00	2.84	-0.33	0.30
	6	22.97	1.2357	1.3614	-0.0364	1.2853	0.00	4.26	-0.35	2.45
Average		22.97	1.2330	1.4036	-0.0391	1.2879	0.00	3.37	-0.36	0.72
Std		0.01	0.0016	0.0245	0.0035	0.0035				
High Temperature	1	30.21	1.2534	0.7149	-0.0448	1.2851	0.00	4.26	-0.55	0.54
	2	30.19	1.2552	0.7076	-0.0430	1.2849	0.00	3.55	-0.49	0.56
	3	30.21	1.2558	0.6990	-0.0411	1.2845	0.00	3.54	-0.53	0.51
	4	30.21	1.2570	0.6978	-0.0392	1.2837	-0.35	3.20	-0.61	0.56
	5	30.18	1.2576	0.6874	-0.0407	1.2851	0.00	3.19	-0.59	0.48
	6	30.18	1.2570	0.7027	-0.0410	1.2856	0.00	3.55	-0.57	0.73
Average		30.20	1.2560	0.7016	-0.0417	1.2848	-0.06	3.55	-0.56	0.56
Std		0.02	0.0016	0.0093	0.0020	0.0007				

4.4.5 Discussion

If the initial gyroscope output was assigned to the zero bias value the accumulated angular rate error range was between 5 to 8 $°s^{-1}$ for all axes. Although the relationship between the two variables was only moderately linear, the implementation of a rather simplistic first order linear approximation predicted a zero bias output at each time step that reduced the angular rate error significantly. Similar experiments conducted under various temperature conditions suggested that the same relationship holds yet there was a visible variation in gradient with respect to the change in temperature and a less obvious explanation of the variation in the intersects. This variation in gradient and intercept would introduce errors if an average set of parameters were implemented regardless of the ambient temperature. The least linearity section of all axes for all trials was from as little as a few seconds to 60 s. This suggested a further reduction in the angular rate errors was possible by stipulating a maximum boot up time period of 60 s.

4.5 Summary

An accurate, practical and repeatable calibration method was achieved. Calibration parameters were verified along with the processing steps required to produce the desired outputs. The three positive accelerations and rotation directions were defined along with the modifications needed to comply with the NED axes arrangement. The gyroscopes and accelerometer calibration parameters were verified along with the methodology and both types of sensor provided accurate orientation angles. The last two processing steps: gravitational compensation and rotation of the accelerations from body to earth coordinates were valid. Finally the implemented approximation technique to predict the drifting zero bias value for each gyroscope proved successful in minimising the angular rate error.

Chapter 5 Results 2: Timing Experiments

5.1 Introduction

The main purpose of this chapter was to evaluate the performance of the inertial sensor system with respect to a number of factors. Firstly, the potential of the inertial system to identify certain characteristic events that occurred within the experiments was demonstrated. Subsequently, the ability of the inertial sensor system to measure a periodic movement and finally, the ability to describe both rapid and slow changes in acceleration was established. However, in order to draw a comparison between the inertial sensor system and the performance of another measurement system such as the force plate the outputs from both systems needed to be synchronised. The first section of this chapter describes the synchronisation method utilised. This is then followed by the outline of the experiments conducted to evaluate the performance of the inertial sensor system.

5.2 Drop Tests

5.2.1 Introduction

The purpose of the drop test experiment was to identify the time delay, if any, between the force plate and inertial sensor acquisition systems. This was achieved by selecting a specific event which was easily identified on both systems. The event chosen was a sharp single vertical impact of a light, rigid object such as a metal rod, onto the force plate. The events were recorded on both systems and the calculated time difference averaged over all trials was used to synchronise the systems in subsequent experiments. Once the systems were synchronised comparisons of the output responses could be made.

5.2.2 Apparatus

The apparatus for the drop test experiment included the force plate and inertial sensor acquisition systems, the inertial sensor module, a metal rod and adhesive tape. The

force plate used was a Kistler 9287BA. The plate measured force in three orthogonal axes and was controlled remotely by a PC through the software package, Bioware version 3.2. The metal rod was light, rigid and hollow with a square cross section. The inertial sensor module was attached securely to one flat side of metal rod by adhesive tape.

5.2.3 Method

The inertial sensor module was attached to the metal rod so that the Z axis was parallel with the edge of the rod and the sensitive axis pointing upwards. The inertial sensor system was set up exactly as detailed in the experiments in chapter 4. The force plate system was permanently set up in a walkway in a biomechanics laboratory and connected to a PC. The rod was dropped from waist height, where the bottom of the rod was approximately 400 mm above the force plate. The rod made five clearly defined contacts with the force plate within in each trial. It was assumed that the rod would impact the force plate in a vertical orientation. Each strike of the force plate was a sharp, clean single contact. Data was collected for ten and twelve seconds at a sampling rate of 1000 Hz by the force plate and inertial sensor acquisition systems respectively. The inertial sensor system was started fractionally before the force plate system. The two systems were activated by manual instruction. A trigger pulse sent from the force plate system was recorded on a channel of the data logger within the inertial sensor system. The trigger pulse indicated the start of the data acquisition of the force plate system by increasing to 1.6 V from the nominal 0 V value. The trial was repeated ten times.

It was proposed that each contact with the force plate made by the rod would be easily identified in both data acquisition systems. The force plate indicated a point of contact by a rapid change in measured force in the vertical direction. The inertial sensor system utilized the vertical acceleration component, z, to indicate the point of contact. When the rod was held in a stationary position the magnitude of the measured acceleration would be equal to the gravitational acceleration. Once the rod was dropped, the accelerometer would experience free fall as it accelerated towards the

ground. Then upon contact with the force plate, a change in acceleration due to the reaction force of the impact should be seen.

5.2.4 Results

A typical response of a single contact from both systems is displayed in figure 5-1. In this experiment it was assumed that the inertial sensor system remained in a vertical position and so the true vertical acceleration was measured at all times. The figure demonstrated the ease of identifying the point of contact in both systems. At the beginning of each drop the rod was held at arms length over the force plate. In this stationary position the vertical accelerometer experienced zero acceleration. Once the rod was dropped the vertical accelerometer was instantly in free-fall and therefore the acceleration experienced decreased towards -1 g. When the rod made contact with the force plate, the force plate system recorded a large reaction force in the upward direction (positive) and the inertial sensor system also recorded a large positive vertical acceleration. The rod was caught and resumed a stationary position shortly after one impact. Therefore the vertical acceleration returned to experiencing zero acceleration.
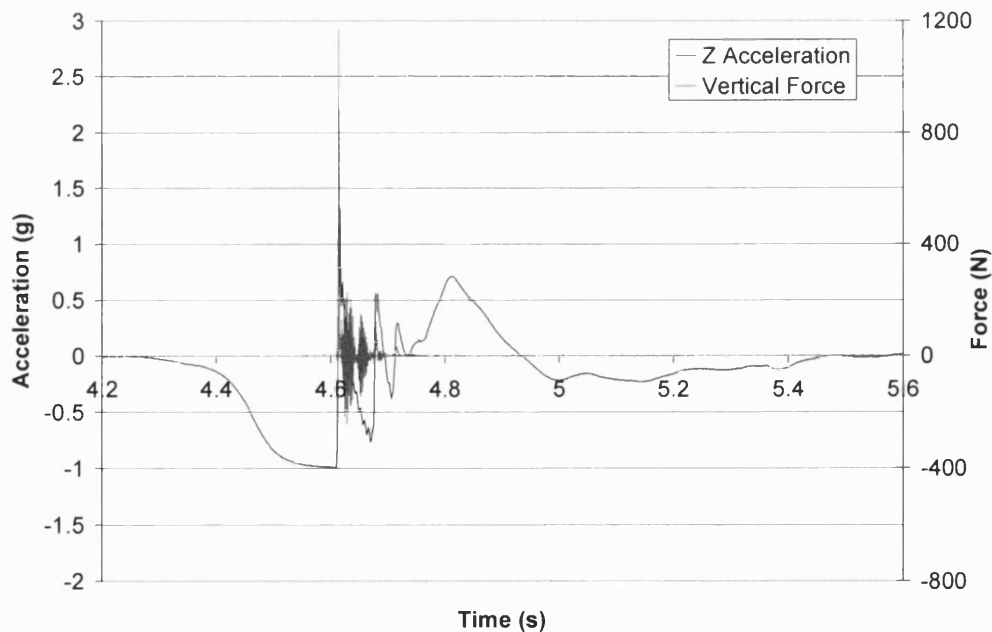
Figure 5-1 A snap shot of one contact by the rod on the force plate.

The timings of the points of contact identified in the vertical acceleration component were recorded. The time point at which the trigger pulse was sent from the force plate indicating the start of its data collection was subtracted from these timings. The resultant timings were then compared to the timings of the points of contact identified in the force plate system. The average time differences for all contacts within each trial and for all trials were calculated. The overall averaged time delay between the systems was found to be 15 ms with a standard deviation of 1 ms. The results from all ten trials are displayed in table 5-1.

Table 5-1 The drop test experimental results from all ten trials.

		Trigger Pulse	Accelerometer Impact (recorded)	Accelerometer Impact (recorded-trigger)	Force Plate Impact	Delay
		s	s	s	s	ms
Trial 1	1	3.404	4.611	1.208[1]	1.192	16
	2	3.404	6.532	3.129	3.114	15
	3	3.404	8.305	4.902	4.887	15
	4	3.404	10.122	6.718	6.703	15
	5	3.404	11.816	8.413	8.397	16
					Average	15
					Std	0
Trial 2	1	1.698	3.214	1.516	1.503	13
	2	1.698	4.835	3.137	3.123	14
	3	1.698	6.587	4.889	4.876	13
	4	1.698	8.463	6.765	6.751	14
	5	1.698	10.176	8.477	8.464	13
					Average	13
					Std	1
Trial 3	1	1.659	2.811	1.153	1.138	15
	2	1.659	4.253	2.595	2.579	16
	3	1.659	5.808	4.150	4.136	14
	4	1.659	7.431	5.772	5.758	14
	5	1.659	8.961	7.302	7.287	15
					Average	15
					Std	1
Trial 4	1	1.434	2.561	1.127	1.112	15
	2	1.434	4.095	2.661	2.645	16
	3	1.434	5.554	4.120	4.106	14
	4	1.434	7.130	5.696	5.680	16
	5	1.434	8.652	7.218	7.202	16
					Average	15
					Std	1
Trial 5	1	1.519	2.578	1.059	1.044	15
	2	1.519	4.145	2.625	2.610	15
	3	1.519	5.723	4.192	4.176	16
	4	1.519	7.163	5.644	5.629	15
	5	1.519	8.842	7.322	7.306	16
					Average	15
					Std	1

Table 5-1 continued.

		Trigger Pulse	Accelerometer Impact (recorded)	Accelerometer Impact (recorded-trigger)	Force Plate Impact	Delay
		s	s	s	s	ms
Trial 6	1	1.380	2.465	1.086[1]	1.069	17
	2	1.380	3.937	2.558	2.541	17
	3	1.380	5.551	4.171	4.157	14
	4	1.380	7.443	6.064	6.048	16
	5	1.380	9.087	7.708	7.692	16
					Average	16
					Std	1
Trial 7	1	1.427	2.566	1.140	1.127	13
	2	1.427	4.293	2.867	2.852	15
	3	1.427	5.997	4.571	4.556	15
	4	1.427	7.625	6.198	6.183	15
	5	1.427	9.277	7.850	7.834	16
					Average	15
					Std	1
Trial 8	1	1.441	2.563	1.122	1.108	14
	2	1.441	4.128	2.687	2.671	16
	3	1.441	5.793	4.352	4.335	17
	4	1.441	7.490	6.049	6.033	16
	5	1.441	9.120	7.679	7.663	16
					Average	16
					Std	1
Trial 9	1	1.608	2.816	1.208	1.192	16
	2	1.608	4.458	2.850	2.834	16
	3	1.608	6.225	4.617	4.602	15
	4	1.608	7.984	6.375	6.360	15
	5	1.608	9.737	8.129	8.114	15
					Average	15
					Std	0
Trial 10	1	1.408	2.560	1.152	1.136	16
	2	1.408	4.374	2.966	2.951	15
	3	1.408	6.135	4.727	4.713	14
	4	1.408	8.046	6.638	6.623	15
	5	1.408	9.655	8.247	8.231	16
					Average	15
					Std	1
					Overall Average	15
					Overall Std	1

[1]There appears to be a calculation error. This is not the case. The calculation is done in Excel and uses more significant figures than are shown.

5.2.5 Discussion

All impacts on the force plate were very visible and easily identified to the nearest time sample on both systems. The averaged time delay between the systems was found to be 15 ms with a standard deviation of 1 ms for 50 samples.

5.3 Vertical Bounce and Counter Move Jump Trials

5.3.1 Introduction

This experiment was divided into two parts. The first part involved subjecting the inertial sensor module to a series of vertical bounce trials conducted on a force plate. At the point of contact of each bounce the subject landed with straight legs and a fast flapping action of the feet before take off. These actions produced rapid acceleration changes which should help to clearly identify points of contact and take off. The timings of these events identified by both the force plate and inertial sensor systems were compared. The second part of the experiment comprised of a series of counter-movement jumps [209]. These jumps were performed with a squat prior to take off and also as part of the landing. This type of movement produced slow acceleration changes and a more complex output pattern than the vertical bounce jumps. The response from the inertial sensor system was compared to vertical ground reaction force (GRF) and the similarity between them was quantified.

5.3.2 Method

The inertial sensor module was attached to a weightlifting belt as described in chapter 3. This belt was secured around the lumbar region of the subject. The inertial sensor module was therefore positioned in the closest possible way to the subject's centre of mass whilst in a standing position. The inertial sensor system was set up as detailed in the chapter 4. The force plate system was set up and activated as detailed in the previous experiment of this chapter. The inertial sensor system was activated first, by manual instruction, to allow the trigger pulse to be recorded. The results from the drop test experiment showed that an average discrepancy of 15 ms (to the nearest ms) existed between the two systems. This value and the point at which the trigger pulse increased from the nominal 0 V was used to synchronise the two data sets from the two systems. The subject executed eight trials with ten jumps in each trial for both types of jump. A period of approximately five minutes was given to the subject in

between trials to allow recovery. The vertical bounce jumps were conducted in a way which induced rapid changes in acceleration at the point of contact. The counter movement jumps were performed in a way which induced slower changes in accelerations about this point and a more descriptive response during the contact phase. All jumps were repeated in the same manner and to the subject's best ability. The data was recorded on both acquisition systems at 1000 Hz for 15 and 20 s for the force plate and inertial sensor systems, respectively. The inertial sensor system outputs were processed offline following the steps outlined in chapter 4. The output of interest for this experiment was the vertical acceleration component, z. The acceleration in this direction was limited to a range of ± 3 g. From the ten jumps in each trial, eight were selected for analysis discarding the first and last jumps. The first and last jumps were discarded to eliminate any features introduced into the responses from starting and finishing each trial.

For the vertical bounce jump experiments, the vertical GRF produced by the force plate was analysed to determine the timings of the points of contact and take-off. The events were indicated by a change in force above or below the average force output during the non contact periods plus two standard deviations. It was assumed that these points would provide accurate timing information that would be used as a reference. The vertical acceleration component was analysed about these reference points for any repeating characteristic features such as local minimum or maximum points, similar gradients or axis crossing points. The method used to identify either a local maximum or minimum point was a simple subtraction sum. The previous acceleration value was subtracted from the current value at each time sample. This subtraction sum was applied to the whole acceleration data set. The analysis of the resultant from the subtraction sum began at the first positive acceleration peak of the contact phase (point B in figure 5-3) and worked backwards or forwards for the points of contact and take off, respectively. All of the changes in polarity were recorded. Comparisons of the timings of the events of contact and take off for the vertical acceleration component and the vertical GRF were made. Also, the frequency of the contact points (i.e. the time period from contact to contact) for both systems were deduced and compared.

For the counter movement jumps, the response of the vertical GRF was compared to the response of the vertical acceleration component during periods of contact. In order to quantify the likeness of the two responses the vertical GRF was converted into an acceleration. This was achieved by dividing it by the subject's mass. The subject's mass was measured by taking the average of the vertical GRF output over all the data in each trial. The overall mass was an average of the masses from each trial. This method provides the best estimate since the subject began and ended the experiment at rest resulting in a net impulse over each trial equal to zero. The overall average weight from the eight vertical bounce trials was 807.72 N and the equivalent mass was 82.34 kg. Analogue filtering was implemented at the output of the accelerometer prior to digitization to increase the noise performance of the sensor. As a consequence the filtering limited the transient performance resulting in the 'ringing' of the output when presented with a step change at the input. To reduce this effect a running average filter was implemented of a capture length of 100 samples. The filter length was determined empirically as the best compromise between noise and transient performance. The filter reduced the maximum signal bandwidth from 500 to 5 Hz. The similarity of the responses was quantified by calculating the average root mean squared (RMS) error only during the periods of contact for each trial. This error was also computed as a percentage of the measured acceleration range. The measured acceleration range was found by finding the maximum and minimum recorded acceleration within each trial.

It was hypothesised that the vertical GRF response for both types of jump could be categorised into several distinctive parts. These parts were a period of non-contact (i.e. approximately 0 N) when the subject is in the air, followed by a contact phase and finally the force measurement decreases until the level required to indicate the non-contact period (~0 N). The response of the vertical GRF during the contact phase would be different for the two types of jump. The contact phase for a vertical bounce jump was assumed to consist of a steep positive gradient forming a peak at the initial point of contact and then a positive increase in force prior to take off. The contact phase for a counter movement jump was assumed to produce lower force peaks due to the softer landing occurring by executing the squatting action. It was hypothesised that the response of inertial sensor system would ideally mirror that of the force plate for both types of jump since acceleration is proportional to force. Thus, it was

assumed that the acceleration component would consistently produce prominent features at certain timing points around the points of contact and take off and would be capable of describing both slow and rapid accelerations.

5.3.3 Results

The first section of the experiment involved a series of vertical bounce jumps. The response of the vertical acceleration component showed a periodic output which compared favourably to the response from the force plate for all trials. An example of the responses from both systems during this experiment is displayed in figure 5-2 and an expanded version shown in figure 5-3. The vertical acceleration component clearly showed periods of contact and non contact. The period of contact was illustrated with a positive peak limited to 3 g by the capture range of the sensor. The period of non-contact was illustrated initially by a ringing effect i.e. damped response but this settled at around -1 g (gravitational acceleration) after a short period.
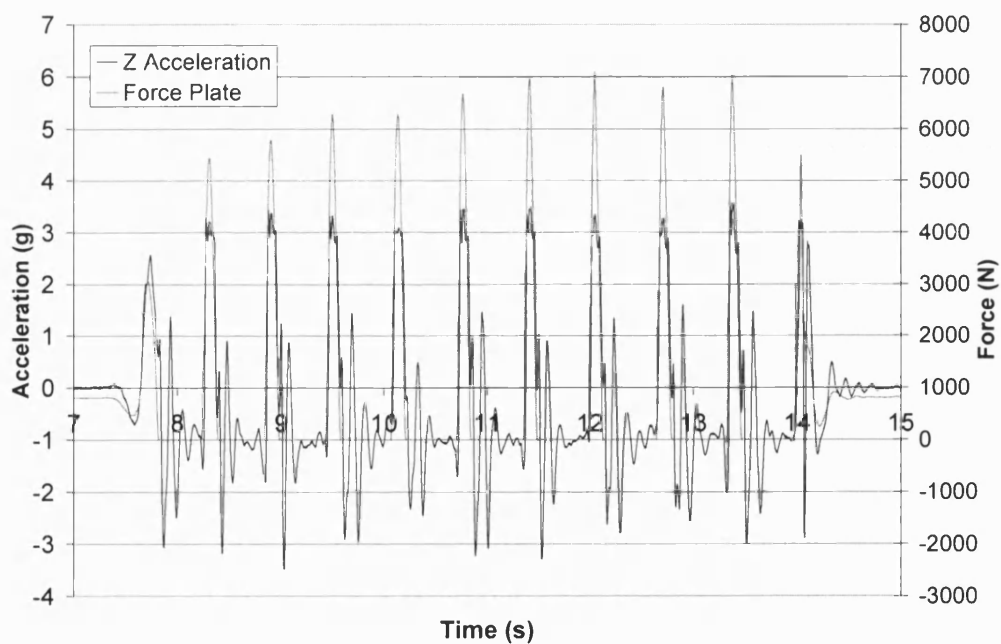
Figure 5-2 The responses from both systems during vertical bounce trial 1.
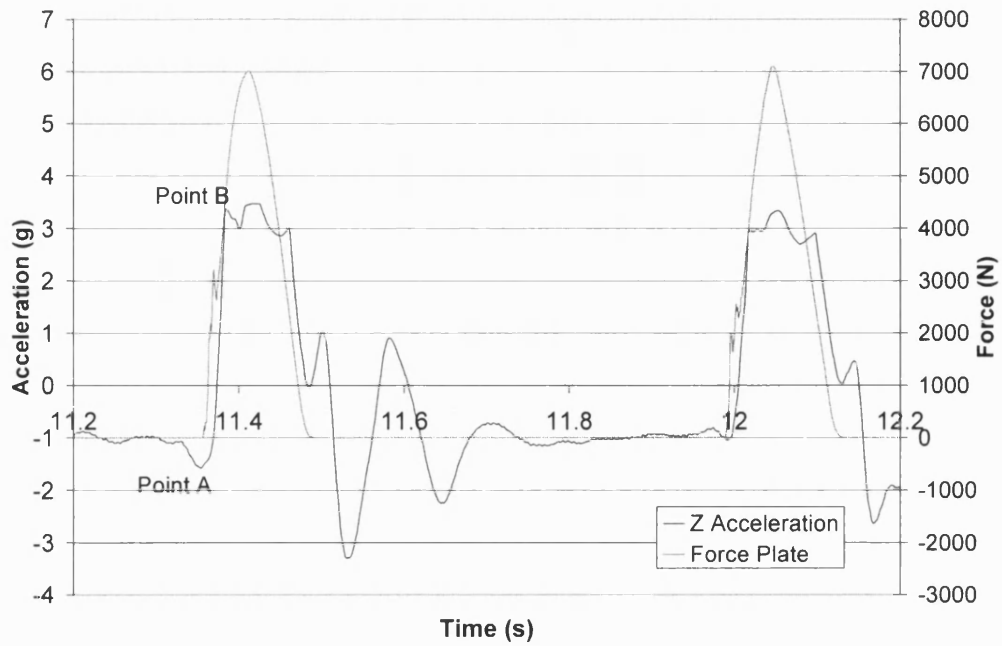
**Figure 5-3 The expanded responses from both systems during vertical bounce
    trial 1.**

The vertical GRF clearly identified the timings of the points of contact and take off.
An example of the vertical GRF response identifying these points is displayed in
figure 5-4 and the timings for all jumps and all trials are displayed in table 5-2.
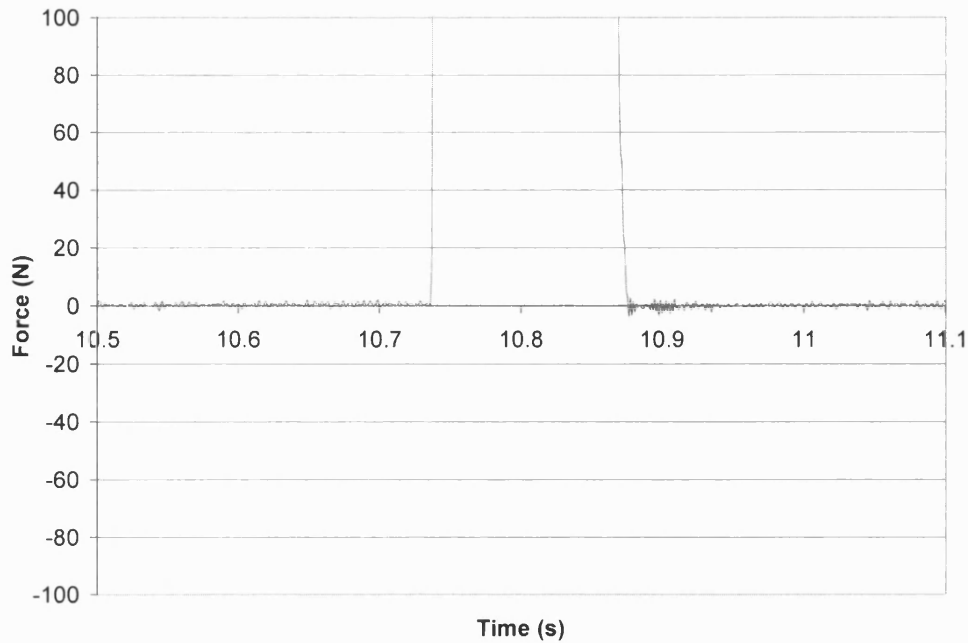
Figure 5-4 An example of the vertical GRF response showing how clearly the points of contact and take off were identified.

The evaluation of the vertical acceleration component about the actual points of contact showed a minimum point as the most prominent feature (point A in figure 5-3). This was followed by a steep increase in acceleration to value of more than 3 g. This minimum point occurred consistently after the actual point of contact at an average 8 ms across all trials. The evaluation of the vertical acceleration component about the actual points of take-off showed several prominent features. These were a steep negative gradient, followed by a minimum peak and then an oscillating output which eventually settled near to -1 g. However, not one of these listed features demonstrated the potential to provide a means of identifying the point of take off clearly, accurately and repeatedly. The frequencies deduced from both systems, when compared, showed extremely similar and consistent values with an average difference of 2 mHz across all trials. The timings for the points of contact and the frequencies deduced from both systems for all jumps are displayed in table 5-2.

Table 5-2 Timings of the contact points and contact frequencies deduced from the vertical acceleration component and the vertical GRF for the ten trials.

|		Z Accel	Contact Point Force Plate	Difference	Contact to Contact Frequencies Accelerometer		Force Plate		Difference
		Time	Time	Time	Time	Freq	Time	Freq	Freq
		s	s	ms	s	Hz	s	Hz	mHz
Trial 1	2	8.854	8.843	11					
	3	9.447	9.436	11	0.593	1.686	0.593	1.686	0
	4	10.077	10.068	9	0.630	1.587	0.632	1.582	5
	5	10.714	10.705	9	0.637	1.570	0.637	1.570	1
	6	11.355	11.354	1	0.641	1.560	0.649	1.541	19
	7	11.996	11.985	11	0.641	1.560	0.631	1.584	-25
	8	12.649	12.643	6	0.653	1.531	0.658	1.520	11
	9	13.327	13.320	7	0.678	1.475	0.677	1.477	-2
			Average	8	0.639	1.567	0.640	1.566	1
			Std	3	0.026	0.064	0.026	0.065	14
Trial 2	2	10.171	10.158	13					
	3	10.779	10.767	12	0.608	1.644	0.609	1.641	3
	4	11.401	11.390	11	0.622	1.608	0.623	1.605	3
	5	12.026	12.020	7	0.625	1.600	0.629	1.590	10
	6	12.611	12.629	-18	0.585	1.710	0.609	1.641	69
	7	13.281	13.270	11	0.669	1.494	0.641	1.560	-67
	8	13.905	13.895	10	0.624	1.602	0.625	1.600	3
	9	14.535	14.524	11	0.630	1.587	0.629	1.589	-2
			Average	7	0.623	1.606	0.624	1.604	3
			Std	10	0.025	0.065	0.011	0.029	39
Trial 3	2	9.398	9.373	26					
	3	10.638	10.627	11	1.240	0.807	1.254	0.797	9
	4	11.268	11.253	15	0.630	1.587	0.626	1.597	-10
	5	11.897	11.887	10	0.629	1.591	0.634	1.578	12
	6	12.548	12.537	11	0.651	1.535	0.650	1.538	-2
	7	13.168	13.153	15	0.620	1.613	0.616	1.623	-10
	8	13.807	13.812	-5	0.639	1.566	0.658	1.519	47
	9	14.468	14.460	8	0.661	1.513	0.648	1.543	-30
			Average	11	0.724	1.459	0.727	1.456	2
			Std	8	0.228	0.290	0.233	0.293	24
Trial 4	2	9.471	9.461	11					
	3	10.094	10.083	11	0.623	1.605	0.623	1.606	0
	4	10.715	10.705	11	0.621	1.610	0.621	1.610	0
	5	11.340	11.335	5	0.625	1.600	0.631	1.585	15
	6	11.975	11.973	2	0.635	1.576	0.638	1.568	7
	7	12.618	12.614	4	0.643	1.556	0.641	1.560	-5
	8	13.255	13.257	-2	0.637	1.570	0.643	1.556	14
	9	13.912	13.901	11	0.657	1.521	0.644	1.552	-30
			Average	7	0.634	1.577	0.634	1.577	0
			Std	5	0.013	0.032	0.009	0.024	15

Table 5-2 continued.

		Contact Point Force Plate	Difference	Contact to Contact Frequencies				Difference
	Z Accel			Accelerometer		Force Plate		
	Time	Time	Time	Time	Freq	Time	Freq	Freq
	s	s	ms	s	Hz	s	Hz	mHz
Trial 5 2	9.154	9.145	9					
3	9.772	9.763	9	0.618	1.618	0.618	1.618	0
4	10.381	10.375	6	0.609	1.642	0.612	1.634	8
5	10.995	10.986	9	0.614	1.629	0.611	1.637	-8
6	11.615	11.606	9	0.620	1.613	0.620	1.612	0
7	12.236	12.229	7	0.621	1.610	0.623	1.605	5
8	12.849	12.842	7	0.613	1.631	0.613	1.631	0
9	13.500	13.491	9	0.651	1.537	0.649	1.541	-5
		Average	8	0.621	1.611	0.621	1.611	0
		Std	1	0.014	0.035	0.013	0.033	5
Trial 6 2	8.773	8.764	9					
3	9.356	9.343	13	0.583	1.714	0.580	1.726	-12
4	9.949	9.939	11	0.593	1.686	0.595	1.680	6
5	10.556	10.548	8	0.606	1.649	0.609	1.641	8
6	11.164	11.161	3	0.608	1.645	0.613	1.631	13
7	12.417	12.415	2	1.253	0.798	1.254	0.797	1
8	13.059	13.050	9	0.642	1.558	0.635	1.575	-17
9	13.682	13.681	1	0.623	1.606	0.631	1.586	20
		Average	7	0.701	1.522	0.702	1.520	3
		Std	4	0.244	0.323	0.244	0.323	13
Trial 7 2	8.387	8.375	12					
3	9.006	8.995	11	0.619	1.615	0.620	1.612	3
4	9.631	9.621	10	0.625	1.599	0.626	1.597	3
5	10.266	10.251	15	0.635	1.575	0.630	1.587	-12
6	10.880	10.875	5	0.614	1.628	0.624	1.603	26
7	11.522	11.509	14	0.642	1.557	0.633	1.579	-22
8	12.133	12.128	5	0.610	1.638	0.619	1.615	23
9	12.769	12.757	13	0.637	1.570	0.629	1.590	-20
		Average	10	0.626	1.598	0.626	1.598	0
		Std	4	0.012	0.031	0.005	0.013	19
Trial 8 2	9.380	9.368	12					
3	9.948	9.940	8	0.568	1.760	0.572	1.748	12
4	10.562	10.556	6	0.614	1.628	0.616	1.623	5
5	11.176	11.166	11	0.614	1.628	0.609	1.642	-13
6	11.775	11.764	11	0.599	1.670	0.599	1.670	0
7	12.381	12.372	10	0.606	1.649	0.607	1.647	3
8	12.990	12.989	1	0.608	1.644	0.617	1.621	24
9	13.620	13.617	3	0.630	1.587	0.628	1.592	-5
		Average	8	0.606	1.653	0.607	1.649	4
		Std	4	0.019	0.054	0.018	0.050	12
		Overall Average	8	0.647	1.574	0.648	1.572	2
		Overall Std	6	0.118	0.159	0.119	0.158	19

The second section of the experiment involved a series of counter movement jumps. An example of a typical response form both systems is displayed in figure 5-5. The figure clearly highlighted the close likeness of the output responses.
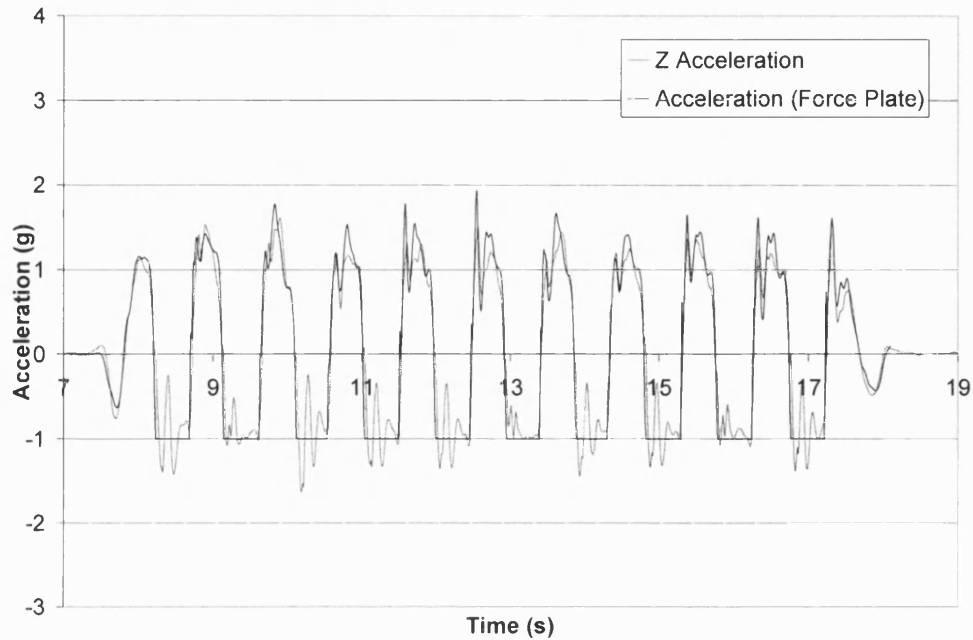
Figure 5-5 An example of the responses from both systems during counter movement jump trial 1.

The RMS errors, relative to the force plate, were extremely consistent at an average of 0.305 g. This average error was computed as a percentage of the acceleration range measured in this direction of the inertial sensor system and was found to be 10.10%. The RMS errors, recorded acceleration ranges and error percentages for all trials are displayed   in table 5-3.

Table 5-3 Results from the analysis of the likeness of the responses from the force plate and the inertial sensor system.

Trial	RMS error (g)	Vertical Acceleration range (g)	% error
1	0.295	3.241	9.12
2	0.334	3.129	10.68
3	0.359	3.086	11.65
4	0.294	3.043	9.66
5	0.300	2.861	10.50
6	0.288	3.020	9.53
7	0.267	2.820	9.46
8	0.305	2.999	10.18
Average	0.305	3.025	10.10
Std	0.029	0.137	0.83

5.3.4 Discussion

The point of contact in the vertical acceleration component of the vertical bounce jumps was identified by finding the minimum peak prior to the steep positive gradient caused by the impact. The average time difference found between the minimum peak and the force plate point of contact was found to be 8 ms. This result was lower than a delay of 10ms reported by Aminian et al. [109], and 65 ms reported by Heiden and Burnett [84], for walking and running, respectively. The point of take-off was much harder to identify and required further investigation to explore more complex methods of feature detection. The frequency of the contact points deduced from the vertical acceleration response compared well to those from the force plate. This result demonstrated the ability of the inertial sensor system to measure periodic movements and provide timing information between identified events. This information in the context of this thesis could be used to calculate the parameter stride frequency. The counter movement jump experiments demonstrated the ability of the inertial sensor system to produce a more descriptive acceleration response. The accuracy and reliability of the force measurements depend on the criterion specification of the force platform [146]. The specification of the force plate is outlined on the Kistler website [210] and have been regarded suitable for the use in sports biomechanics [146]. Bartlett [146] stated that Kistler was regarded as 'generally very accurate'. Therefore the force measurement is generally accepted as the true measurement and has been used by many authors as a source for comparison [211]. The comparison of the acceleration output to that of the force plate produced a match with a 10.10% error over the measured acceleration range. Bobbert et al. [211] used positional data to estimate the magnitude of the vertical force during running with errors of 10%. This result was stated as an acceptable error to provide mechanical analysis of the landing phase in running.

5.4 Summary

The time discrepancy that existed between the two data acquisition systems was 15 ms. This time delay was used to synchronise the two systems and to enable comparison. The response of the vertical acceleration component, z, was shown to have the potential to be used to identify the points of contact. The periodicity of these contact points could be used to illustrate movement frequency such as stride frequency. However, the identification of the points of contact in subsequent experiments involving more complex movements is subject to further investigation. The response of the acceleration component showed the potential to offer the sensitivity to describe both rapid and slow acceleration changes and detailed movements. However, it was shown that the acceleration response could not identify the point of take-off in the scope of this thesis.

Chapter 6 Results 3: Horizontal Velocity Experiments

6.1 Introduction

This chapter comprises of two experiments. The purpose of the first experiment was to examine the response of the estimated horizontal velocity derived from the inertial sensor system and to investigate the ability of the vertical acceleration component to identify the point of contact from a running movement. The purpose of the second experiment was to investigate the sources of errors discovered in the horizontal velocity results from the first experiment and to demonstrate how these errors could be reduced. Further the experiment was designed to demonstrate the potential of the inertial sensor system to distinguish between different distances travelled and to consolidate that the periodicity of the acceleration signals could be used to determine step frequency.

6.2 Running Trials over a Force Plate

6.2.1 Introduction

The primary purpose of the first experiment was to investigate the ability of the inertial sensor system to quantitatively describe the movement of the subject whilst running over a force plate in a forward direction. The derived change in horizontal velocity component between the points of contact and take off was compared to the change in velocity deduced from the force plate system. The vertical ground reaction force was used as a reference to identify the single point of contact in each trial. Following the results of the previous experiment, the response of the acceleration component was analysed for local minimum points prior to a positive acceleration of a steep gradient. The periodic response of the vertical acceleration component from the inertial sensor system was examined for its ability to identify all of the individual steps taken.

6.2.2 Method

The inertial sensor module was attached to a weightlifting belt and was secured around the lumbar region of the subject as described in chapter 3. It was assumed that the inertial sensor system's x axis (i.e. forward acceleration) was pointing directly in the direction of movement. The inertial sensor and force plate systems were set up, initiated and synchronised as detailed in chapter 4 and 5, respectively. Since the inertial sensor module was tethered, the sensor acquisition system equipment was arranged on a trolley so that it could be wheeled in the same direction as the subject. The trolley was pushed a few metres to prevent the tether becoming taut and cumbersome to the subject. The subject ran a short distance making sure that the third step made contact with the force plate. Data was collected for ten and twelve seconds at a sampling rate of 1000 Hz for the force plate and inertial sensor acquisition system, respectively.

Linear momentum is a quantity associated with how a mass moves along a straight path.

$$\text{Linear Momentum} = \text{mass} \times \text{velocity} \qquad \textbf{6-1}$$

A change in momentum of an object is equal to the impulse exerted on it and known as the momentum-impulse theorem. Impulse is defined as a force changing with time.

$$\text{Impulse} = \int_{t_1}^{t_2} F_x(t)\,dt \qquad \textbf{6-2}$$

where:

t_1	=	first contact with the force plate
t_2	=	last contact with the force plate
F_x	=	force in the anterior-posterior (forward) direction

A force can change the linear momentum of a mass [49]. When the subject made contact with the ground, the reaction force resulting from the contact was acting on

the subject causing the linear momentum of the subject to change. Since the subject's mass remained constant the subject must therefore have experienced a change in velocity.

$$\text{mass} \times \text{velocity}_{\text{final}} - \text{mass} \times \text{velocity}_{\text{initial}} = \int_{t_1}^{t_2} F_x(t)dt \qquad \textbf{6-3}$$

The points of contact and take off were identified from the response of the vertical GRF. The anterior-posterior force measured between these points was integrated with time to yield impulse in the forward direction. The integration method applied was the trapezium rule. The induced error from the approximation was assumed to be insignificant due to the large number of samples available per second. The impulse was set to zero at the point of contact. At the point of take off the accumulated sum was recorded as the net impulse during contact with the force plate. This impulse was then divided by the subject's mass to yield the change in velocity. It was assumed that the weight of the subject deduced from the force data collected during the vertical bounce jump experiment could be used with the data collected from the running experiments. This was because the experiments were conducted consecutively and with the same subject. The subject's weight was measured by taking the average over the whole vertical force data for each trial. The overall average weight over the eight vertical bounce trials was 807.72 N and the equivalent mass was 82.34 Kg.

The inertial sensor system raw outputs were processed off-line following the steps outlined in chapter 3. The calibration parameter, zero bias, for each of the three gyroscopes was computed by taking the average output over the first six seconds of the collection period when the subject was known to be stationary. The horizontal acceleration component was converted into units of ms^{-2} by multiplying by 9.81 ms^{-2}, (since 1g equals 9.81 ms^{-2}) and then integrated to yield an estimated horizontal velocity. The integration process applied was the same method as detailed above and commenced at time, t=0. Any non-zero horizontal acceleration discrepancies present during the stationary periods would introduce errors into the estimated velocity. These errors would accumulate over time and the estimated velocity would drift either up or down. With this in mind, the relative velocity values were computed as the actual increase in velocity from the defined start of movement to the actual points of contact

and take off. The start of movement was defined by visual inspection of the graph of the horizontal acceleration component. This acceleration component was chosen since it clearly defined the starting point. The relative velocity at the points of contact and take off (defined by the force plate system) were recorded and the difference yielded the change in velocity. The change in velocity found from the force plate acquisition system was compared to the value found from the inertial sensor system.

The response of the vertical acceleration component of the inertial sensor system was analysed to determine its ability to identify the point of contact. There was only one contact with the force plate per trial to analyse, totalling eight contacts. The point of contact identified from the vertical GRF from the force plate system was used as a reference to identify a minimum point in the acceleration component. The method previously used for the vertical bounce jump experiments was implemented. The timings of any other minimum points within each of the trials were also identified and were used to define the other steps taken in each trial.

6.2.3 Results

The anterior-posterior GRF, F_x, from all trials showed similar characteristic responses. The responses displayed sinusoidal shaped waveforms with amplitudes of approximately 25% of the subjects body weight (BW). The shape of the response corresponds to the examples displayed in Nigg [49]. The majority of the first half of the horizontal component of the ground reaction force was negative and the second half was positive. The derived net impulse results varied from -5.68 to 9.87 Ns. The anterior-posterior GRF responses from the three trials that represent the range of the net impulses are displayed in figure 6-1.
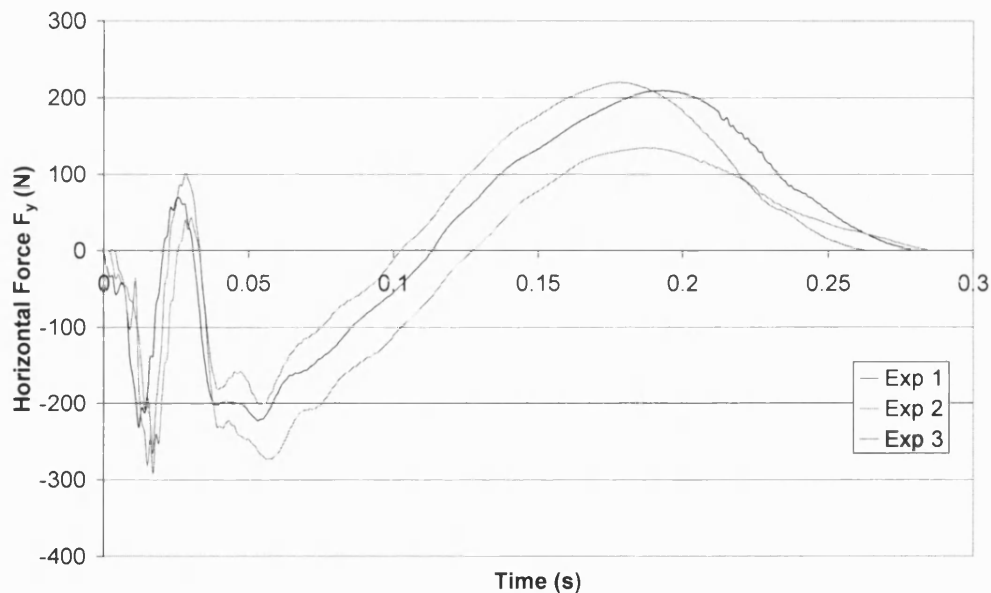
Figure 6-1 The anterior-posterior GRF responses from the three selected trials.

The horizontal acceleration component from all trials showed similar periodic responses. The individual steps within the acceleration component for each trial were outlined using the vertical acceleration component (see figure 6-7). An example of the response of the acceleration component with the individual steps outlined by vertical grid lines is shown in figure 6-2. For the first few steps, the net horizontal acceleration was shown to be positive within each step. The last steps showed the opposite.
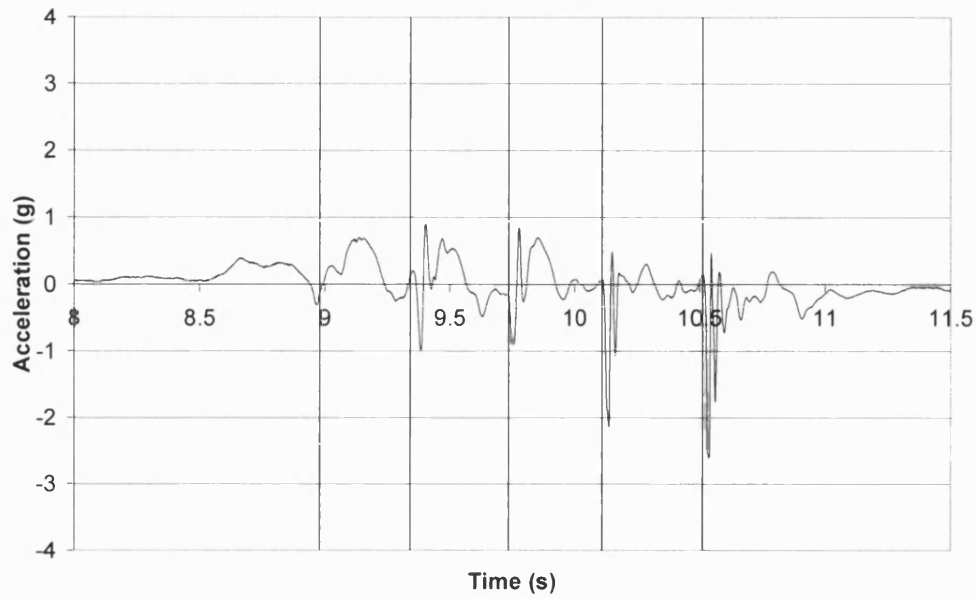
Figure 6-2 An example of the response of the horizontal acceleration component with the individual steps outlined.

This pattern of acceleration was reflected in the estimated horizontal velocity. The estimated velocity during the movement was similarly shaped in the form of a parabola for all trials. An example of the estimated velocity is shown in figure 6-3.
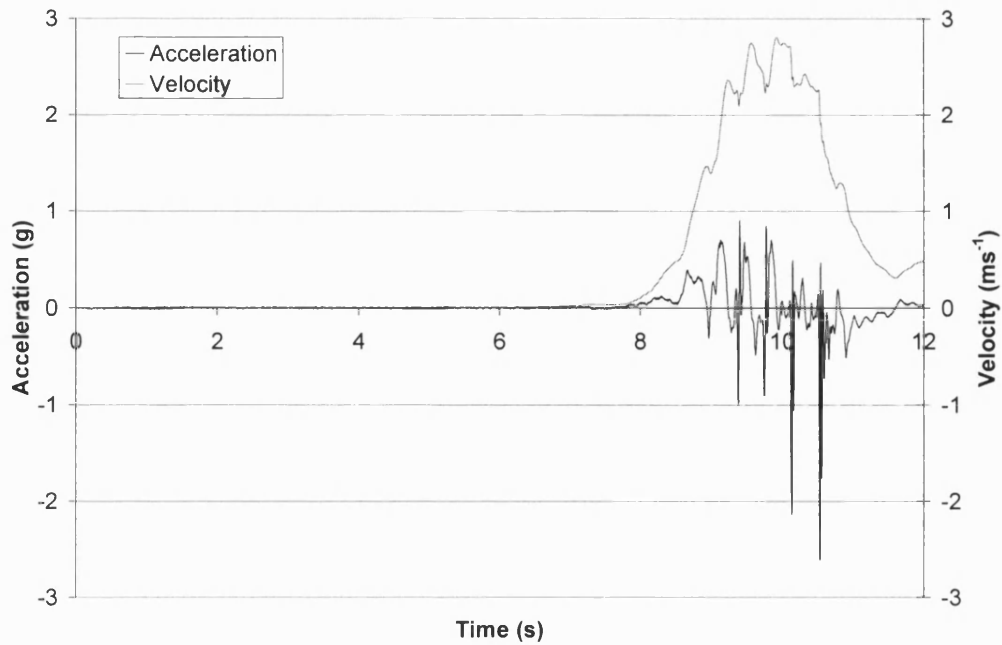
Figure 6-3 An example of the response of the horizontal acceleration component and the respective estimated horizontal velocity.

Within the parabola shaped response the velocity repeatedly oscillated. These oscillations coincided with the outlined steps. The estimated velocity was compared to the single step on the force plate from each trial as displayed in figure 6-4. Following the point of contact (defined by the vertical GRF) the estimated velocity reached a minimum point and then a maximum point shortly before take off.
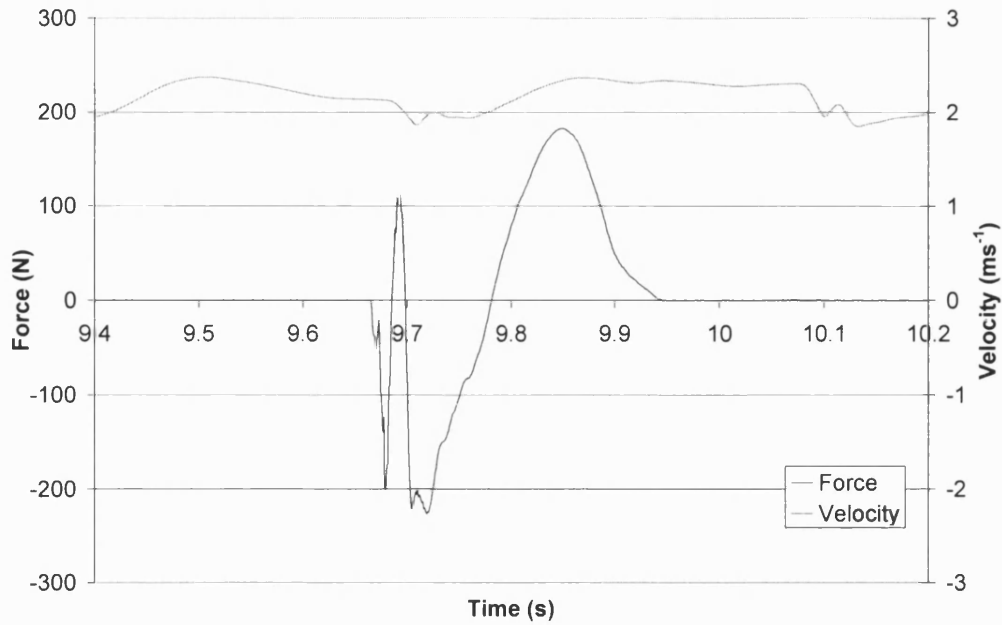
Figure 6-4 An example of the estimated horizontal velocity compared to the horizontal GRF.

The estimated velocity clearly displayed an element of drift in all trials. Across all trials, some showed positive drifting and others showed negative drifting. The amount of drift within the signal during the trial as a whole, and the likely causes, require further investigation. Although there was an element of drift present, the shape of the velocity response seemed to visually emerge from the signal. An example of the worst case of drift occurring over all trials is shown in figure 6-5.
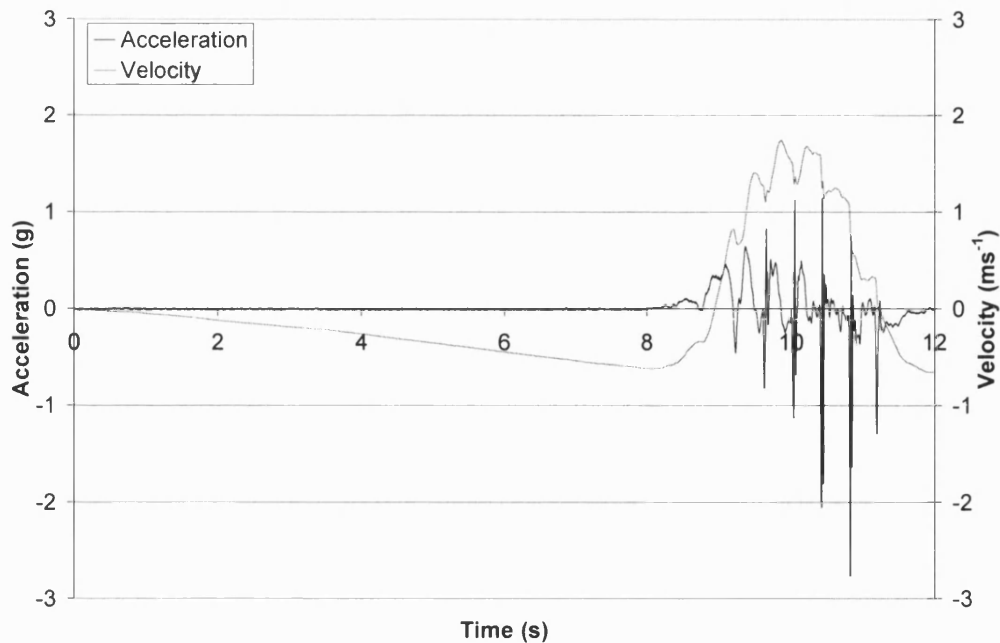
Figure 6-5 An example of the worst case of drift out of all the trials.

The derived impulses and their respective change in velocities from the anterior-posterior GRF are shown in table 6-1 for all trials. The relative velocity values at the points of contact and take-off and the computed change in velocities from the inertial sensor system are also shown in table 6-1. The change in velocity derived form the force measurements were proportional to the derived impulses. The average velocities at the points of contact and take off (determined by the force plate) were 2.41 ms^{-1} and 2.60 ms^{-1}, respectively. Although the speed of the trials was not dictated the relative velocity values of both events were fairly consistent, with standard deviations of 0.13 ms^{-1} and 0.18 ms^{-1}, respectively. The change in velocity values across all trials derived from the inertial sensor system varied considerably from 0.08 to 0.27 ms^{-1}. A comparison of the change in velocities deduced from both systems presented no relationship. The average change in velocity value deduced from the inertial sensor system was seven times the magnitude of the average change in velocity from the force plate system.

Table 6-1 The change in velocity results deduced from both acquisition systems.

| Experiment | Event | Force Plate | | Accelerometer | | Difference |
		Impulse$_x$ Ns	ΔV_x ms^{-1}	V_x ms^{-1}	ΔV_x ms^{-1}	ΔV_x ms^{-1}
1	Contact			2.47		
	Take-off	7.01	0.09	2.68	0.21	0.13
2	Contact			2.35		
	Take-off	6.29	0.08	2.57	0.22	0.14
3	Contact			2.60		
	Take-off	4.72	0.06	2.85	0.24	0.19
4	Contact			2.42		
	Take-off	-5.68	-0.07	2.52	0.11	0.17
5	Contact			2.15		
	Take-off	0.19	0.00	2.23	0.08	0.08
6	Contact			2.36		
	Take-off	3.88	0.05	2.56	0.20	0.15
7	Contact			2.50		
	Take-off	0.06	0.00	2.70	0.20	0.20
8	Contact			2.41		
	Take-off	9.87	0.12	2.68	0.27	0.15
		Average	**0.04**		**0.19**	**0.15**
		Std	**0.06**		**0.06**	**0.04**

The vertical GRF displayed two positive peaks during contact with the force plate. The second peak was of greater magnitude than the first. The response of the vertical acceleration component also showed two positive peaks but exhibited a 'ringing effect' shortly after the actual point of contact. An explanation of this effect was given in chapter 5, section 5.3.2. As the subject's velocity increased the 'ringing effect' increased occurring in the same place each time. An increase in the ringing effect was denoted as an increase in the magnitude of the peaks in the oscillations. There was little visual association between the patterns of the force and acceleration responses, an example is shown in figure 6-6. In particular, the second of the positive peaks in the response of the acceleration component was in most cases of lower magnitude than the first.
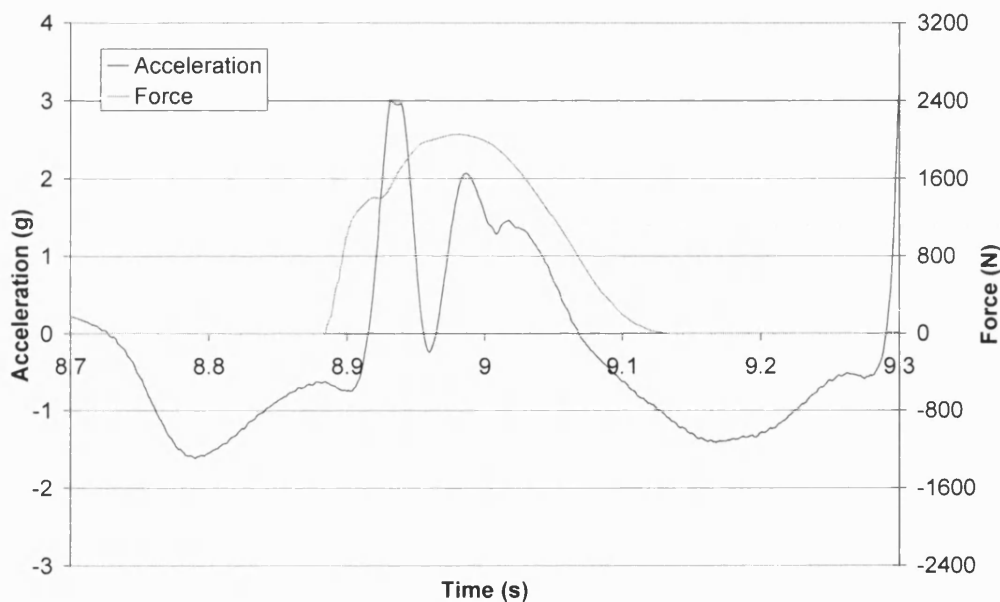
Figure 6-6 An example of the comparison between the vertical GRF and acceleration responses.

Only one single contact on the force plate was available for analysis within each trial. A local minimum point in the vertical acceleration signal was identified as the prominent feature at an average 15 ms after to the actual point of contact. The timing results are shown in table 6-2.

Table 6-2 Identification of the points of contact in the responses from both acquisition systems and for all trials.

Experiment	Force Plate Time(s)	Accelerometer Time(s)	Difference Time (ms)
1	10.061	10.070	9
2	8.883	8.902	19
3	8.980	8.991	11
4	8.955	8.971	16
5	9.998	10.013	16
6	9.665	9.679	14
7	9.705	9.720	16
8	9.718	9.735	17
		Average	15
		Std	3

Using the same feature, the additional contacts that occurred before and after the contact with the force plate were identified in the vertical acceleration component. An example of the response of the vertical acceleration component and the local minimum points defined as possible points of contact is shown in figure 6-7. There was no alternative measurement of the contacts to provide a comparison to the periodicity of the acceleration component.
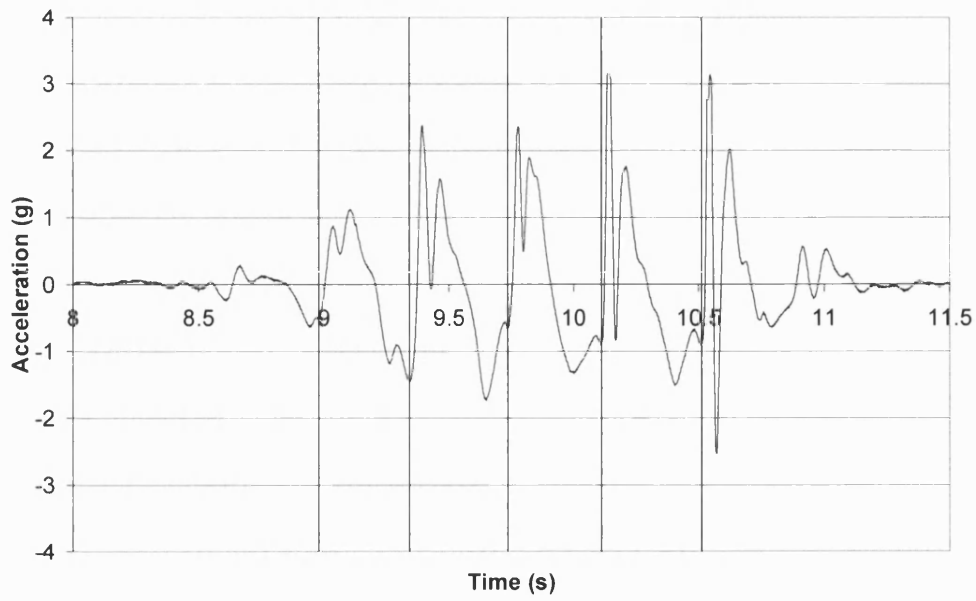
Figure 6-7 An example of the response of the vertical acceleration component with the vertical grid lines stipulating all possible points of contact within the trial.

6.2.4 Discussion

The anterior-posterior GRF displayed a sinusoidal shaped response with the majority of the first half a negative force and the second half a positive force. The negative and positive forces were associated with the reaction force pushing backwards on the subject i.e. braking and forwards on the subject i.e. propulsion, respectively. The magnitude of the anterior-posterior GRF was shown to be approximately 25% of the subjects BW which was consistent with the literature [212]. The derived net impulse values varied from -5.68 to 9.87 Ns. The polarity of the net impulse indicated the subject experienced either a slowing down or a speeding up. To travel at a constant speed the net impulse for a complete step will always be zero (if air resistance is ignored). The horizontal acceleration component showed the first few steps to have a positive net acceleration and the last steps showed the opposite. The positive net acceleration within a step was associated with the acceleration required for the subject to change from a stationary position to move in the forward direction. Whereas the negative net acceleration within a step was associated with the de-acceleration required for the subject to change from moving in a forward direction to stopping. An element of drift was shown in the estimated velocity results. An obvious cause of the drift was the non-zero discrepancies in the order of < 0.01 g in the horizontal acceleration in the first and last sections of each trial. During these sections the subject was known to be stationary, therefore all accelerations should have been zero. The non-zero discrepancies were either positive or negative. Through the integration process this error accumulated over time. The effects of the drift and the likely causes required further investigation. The parabola shaped estimated velocity during movement was expected since the subject started at rest and returned to rest. The relative velocities at the points of interest seemed to be of reasonable magnitude. In comparing the change in velocities from both systems for each trial, the inertial sensor system values were an average seven times larger than the force plate information. A comparison of the change in velocity results from both systems presented no relationship.

The vertical GRF displayed two positive peaks during the contact phase. These peaks were associated with the impact to the ground and the propulsion of the subject,

respectively. The lack of visual association between the vertical GRF and the vertical acceleration component could be attributed to the 'ringing effect' identified in Chapter 5. It was likely that a similar ringing effect could contribute to the greater magnitude of the first acceleration peak seen at the point of contact. The response of the vertical acceleration component identified the point of contact by a minimum point similar to the feature used in the vertical bounce jump experiments. The average time discrepancy was 15 ms after the actual point of contact. This time delay was 7 ms more than the point of contact found in the vertical bounce jump experiments. This may be attributed to the manner in which the contacts were performed in the two experiments. The vertical bounce jumps were conducted in a way which induced rapid changes in acceleration at the points of contacts. Whereas the running trials displayed much slower changes in acceleration at the points of contacts. The minimum points within each trial successfully identified four steps. Unfortunately, there was no alternative measurement of the contacts to compare the contact periodicity of the acceleration component.

6.3 Walking Trials on an Athletics Track

6.3.1 Introduction

The main purpose of this experiment was to investigate the core factors influencing the drifting of the horizontal acceleration component which was highlighted in the pervious experiment. The two factors chosen for investigation were the Y gyroscope zero bias value and the pitch angle. These were chosen on the theoretical basis that they had the most influence on the horizontal acceleration component and hence the horizontal velocity component. The two factors were in turn manipulated to rectify the horizontal velocity component so that the velocity was equal to zero at the end of the movement. The secondary purpose of this experiment was to demonstrate the ability of the inertial sensor system to clearly distinguish between the three different distances covered within the trials. The average velocities and the estimated distances were compared within each corresponding group to the actual distances travelled. The third purpose of this experiment was to illustrate the periodicity of the vertical acceleration component and its ability to define the number of steps counted during each trial.

6.3.2 Method

The inertial sensor module was attached to a weightlifting belt and was secured around the lumbar region of the subject as described in chapter 3. Again, it was assumed that the inertial sensor module's x axis was pointing directly in the direction of movement. The inertial sensor system was the only acquisition system used and was set up as described in Chapter 4. The system's equipment consisted of a Laptop as the PC since the system was required to be portable and battery powered. The equipment was installed on a three-wheeled children's buggy and was pushed along side the subject during the trials to prevent the tether becoming taut and cumbersome. This type of buggy was easy to control along a straight line.

A subject walked three different distances in a straight line along an indoor athletics track. The distances were 10 m, 17 m and 24 m to three designated pink marks painted on the track. The distances to each mark were measured using a tape measure. Five trials at each distance were executed consecutively totalling fifteen trials. Data was collected for 30 s at a sampling rate of 100 Hz for all trials. The data collection period began with the subject remaining stationary for a period of approximately three seconds. The subject resumed a stationary position once the stipulated distance had been reached and remained stationary until the end of the data collection period. The raw sensor outputs from the inertial sensor system were processed off-line following the steps previously described in Chapter 3. The zero bias of the gyroscope was computed by taking the average output of each gyroscope over the stationary periods of the collected data for all trials. The inertial sensor module was powered for more than 30 minutes prior to commencement of the experiment. It was assumed that there would be minimal drifting of the gyroscope zero bias since the experiments were short in duration, the inertial sensor module was allowed a period to 'warm up' and the zero bias was measured during the stationary periods of each trial. The horizontal acceleration component (about the earth coordinates) was integrated once to yield an estimated velocity. The integration method implemented was the same as described in the previous experiment of this chapter. The timings of the start and stop of the movement were identified from the horizontal acceleration component. The number of steps executed by the subject was counted.

An ideal horizontal acceleration component should be zero during the stationary periods and produce a periodic output corresponding to the number of steps executed during the movement. The acceleration component was analysed for any corrupting, drifting or fluctuating outputs within the stationary period. The stationary period when the output was known to be zero was the easiest place to try to understand which components were introducing errors into the response. The contributing factors which constitute the response of the acceleration component were outlined. The analysis began at the end result, the acceleration about the earth coordinates and stepped backwards through the processing steps (see chapter 3) to the raw inertial sensor outputs. The horizontal acceleration components about the earth and body coordinates were compared. This comparison illustrated any differences resulting from the implementation of the rotation matrix shown in equation 3-19. The linear acceleration

in the x axis about the body reference frame was computed following equation 3-18 and for the x axis only is shown in equation 6-4.

$$x_l = x_m - g\sin(\theta)$$ **6-4**

where, x_l is the linear acceleration in the x axis in the units of g

x_m is the measured acceleration in the x axis in the units of g

θ is the pitch angle

g   is the gravitational acceleration.

The pitch angle was integrated using the numerical approximation outlined in equation 3.10 and specifically in equation 6-5.

$$\theta(t) = \dot{\theta}\Delta t + \theta(t-1)$$ **6-5**

where, $\dot{\theta}$ is the pitch rate

Δt is the sampling period

t   is the current time point

t-1   is the previous time point

The pitch rate, $\dot{\theta}$, was computed by the implementation of the transformation matrix to the angular rate output about the y axis. The pitch rate and the angular rate output about the y axis were compared. Further, the angular rate output was a result of converting the raw y gyroscope output from the units of V to $°s^{-1}$ by using the pre-determined calibration parameter scale factor and the zero bias found during or immediately prior to the experiment.

In summary, the contributing factors which constitute the horizontal acceleration component are:

1) Rotation matrix
2) The pitch angle
3) Integration process
4) Transformation matrix

5) The pre-determined calibration parameters for the Y gyroscope

6) The raw gyroscope output about the Y axis

7) The pre-determined calibration parameters for the X accelerometer

8) The raw acceleration output along the X axis

There are several components within the rotation and transformation matrices that have not been mentioned here. It was assumed that the implementation of these matrices introduced insignificant changes to the respective signals. This was based on the type of movement executed, walking, involving insignificant changes to the orientation of the inertial sensor module. This assumption was only valid if the inertial sensor module's x axis was parallel with the ground when secured to the subject at the commencement of the experiment i.e. the two coordinate systems were in alignment. As explained previously, although the integration process is a crude approximation, since there were a large number of samples, the induced error was likely to be insignificant. It was shown following the validation experiments in Chapter 5 that the pre-determined calibration parameters for both types of sensors and the stability of the accelerometer's output whilst stationary were verified. The gyroscope zero bias was not a constant pre-determined value and was determined within the data collected for each experiment. Therefore, the components chosen for investigation within this experiment were the Y gyroscope calibration parameter, zero bias, and the pitch angle.

The effect of manipulating the gyroscope zero bias value and the pitch angle on the horizontal velocity was investigated. The response of the estimated horizontal velocity was set to zero at the start of movement. It was assumed that at the end of the movement the velocity should return to zero. The zero bias value of the gyroscope was varied until such a condition was satisfied for each trial. The new zero bias values and the differences between these and the average zero bias values deduced from the collected data and were recorded. The amount of change experienced across all trials was analysed. The average velocity value between the start and end of the movement was computed and multiplied by the corresponding time difference to yield an estimated distance travelled for each trial. These distances were compared within each group of trials. Conversely, the pitch angle was improved in order to satisfy the horizontal velocity assumption stated above. The average output of the y gyroscope

computed from the stationary periods within the collected data was used as the zero bias value. The simple complementary filter described in chapter 3 was implemented for the pitch angle only. The theory behind the complementary filter suggests that a constant K factor value should be chosen on the basis of the reliability and accuracy of the output of each type of sensor during the movements executed in the experiment. It had been shown that this factor was determined experimentally [102]. It was assumed for this section of the experiment that there were no other errors in the signal other than ones caused by the pitch angle. The K factor of the filter was iteratively selected for each trial individually which satisfied the velocity assumption. It was interesting to discover if the K values remained constant or varied across the trials. The K factor values were recorded and analysed within each group and across all trials. Again, the average velocity value between the start and end of the movement was computed and multiplied by the corresponding time difference to yield an estimated distance travelled for each trial.

6.3.3 Results

An example of the drift of the horizontal acceleration component similar to the results from the previous experiment in this chapter is displayed in figure 6-8. The figure showed the presence of non-zero discrepancies during the stationary period and also illustrated an element of drifting over the whole period. Although the drifting was present the acceleration component still demonstrated periodicity.
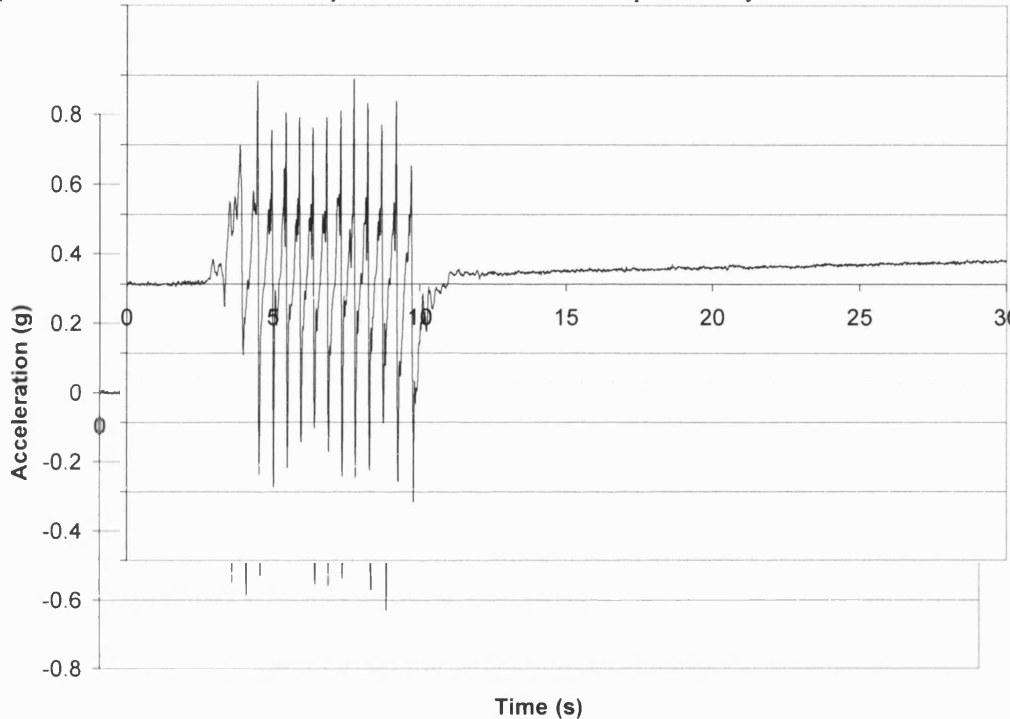
Figure 6-8 The horizontal acceleration component from trial 1.

The assumptions made about the influence of the rotation and transformation matrices were successfully validated. The difference between the earth and body horizontal accelerations during the stationary periods was proved to be fairly insignificant at an average of 0.00083 g across all trials. The transformation between the angular rate about the y axis and the pitch rate during the stationary periods proved to be the more significant process with an average difference of $0.01°s^{-1}$ across all trials.

The zero bias values of the gyroscope about the y axis across all trials was an average difference of 0.29 mV equivalent to $0.17°s^{-1}$ alone. The range of the differences varied from as little as 0.01 mV to 1 mV. The variations in the average zero bias required to

correct the horizontal velocity component so that at the end of the movement the velocity returned to zero, was an average of 0.13 mV. The majority of the trials (79%) required the zero bias voltage level to decrease. Whereas the remaining trials, which happened to be one from each group required the zero bias voltage level to increase. When these new zero bias values were utilised over the whole collection period the stationary periods exhibited non-zero accelerations. An example of the corrected velocity component is displayed in figure 6-9 and the zero bias values for all trials are displayed in table 6-3.
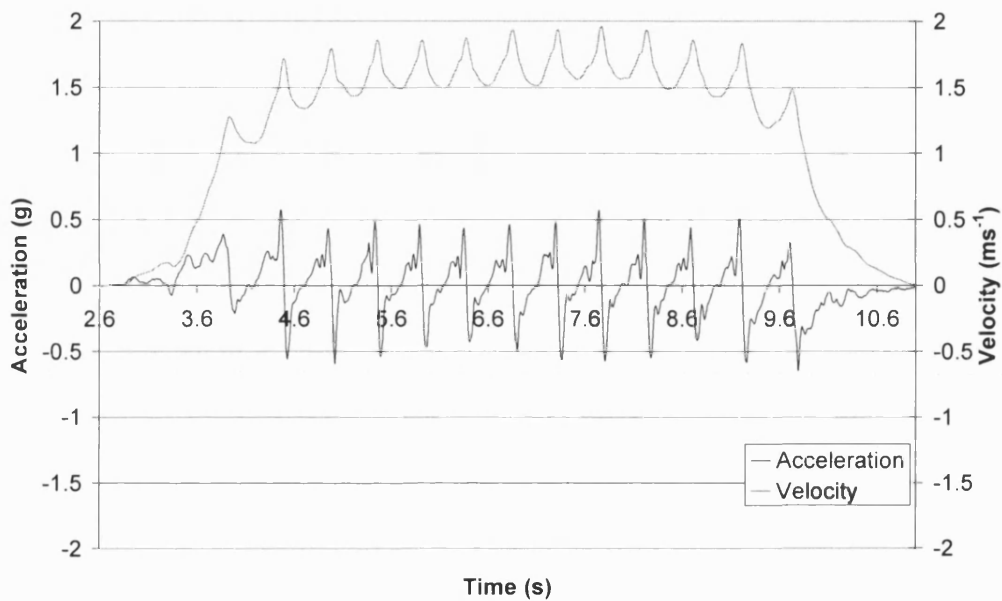
Figure 6-9 The horizontal acceleration and velocity components from trial 3 with the zero bias value set to satisfy the velocity assumption.

Table 6-3 The gyroscope zero bias values.

Trial	Average Bias Prior V	Average Bias After V	Difference mV	Difference $°s^{-1}$	Average Bias V	New Bias V	Difference mV	Difference $°s^{-1}$
1	1.41271	1.41238	0.34	0.20	1.41255	1.41227	0.27	0.16
2	1.41200	1.41251	0.52	0.30	1.41226	1.41236	0.11	0.06
3	1.41308	1.41253	0.55	0.32	1.41281	1.41263	0.18	0.11
4	1.41259	1.41286	0.27	0.16	1.41273	1.41270	0.03	0.02
5	1.41341	1.41295	0.46	0.27	1.41318	1.41278	0.40	0.23
6	1.41330	1.41337	0.06	0.04	1.41334	1.41322	0.11	0.07
7	1.41355	1.41333	0.22	0.13	1.41344	1.41341	0.03	0.02
8	1.41352	1.41387	0.35	0.21	1.41369	1.41361	0.08	0.05
9	1.41426	1.41405	0.20	0.12	1.41415	1.41393	0.22	0.13
10	1.41384	1.41454	0.70	0.41	1.41419	1.41423	0.04	0.02
11	1.41432	1.41467	0.35	0.20	1.41449	1.41443	0.06	0.04
12	1.41452	1.41454	0.02	0.01	1.41453	1.41465	0.12	0.07
13	(1.41491)	(1.41391)	(1.00)	(0.59)	Corrupted data			
14	1.41491	1.41492	0.01	0.01	1.41491	1.41484	0.07	0.04
15	1.41493	1.41489	0.04	0.02	1.41491	1.41488	0.03	0.02
Average	1.41364	1.41367	0.29	0.17	1.41366	1.41357	0.13	0.07

The velocity and distance results are displayed in table 6-4. Using the corrected horizontal velocity component the average velocities for the three groups were 1.15 ms^{-1}, 1.33 ms^{-1} and 1.48 ms^{-1}. The estimated distances maintained clear distinctions between the groups of trials and were within an average 0.37 m, 0.74 m and 0.56 m of the actual distances walked.

Table 6-4 The velocity and distance results for all trials.

Trial	Start Time	Stop Time	Walking Time	Average Velocity	Distance	Distance Error
	s	s	s	ms^{-1}	m	m
1	3.678	12.188	8.510	1.20	10.21	0.21
2	3.651	11.830	8.179	1.18	9.62	0.38
3	2.620	10.999	8.379	1.19	10.00	0.00
4	3.790	12.399	8.609	1.09	9.41	0.59
5	3.159	11.780	8.621	1.09	9.35	0.65
			Average	1.15	9.72	0.37
6	3.940	16.169	12.229	1.22	14.87	2.13
7	3.839	16.209	12.370	1.38	17.13	0.13
8	4.481	17.320	12.839	1.35	17.34	0.34
9	4.311	16.461	12.150	1.32	16.09	0.91
10	4.070	16.539	12.470	1.35	16.81	0.19
			Average	1.33	16.45	0.74
11	3.800	19.439	15.639	1.48	23.20	0.80
12	4.451	20.450	16.000	1.47	23.49	0.51
13	(4.800)	(21.010)	(16.210)	Corrupted Data		
14	4.460	21.330	16.870	1.43	24.16	0.16
15	3.370	19.720	16.349	1.52	24.85	0.85
			Average	1.48	23.93	0.58

The comparison between the pitch angles deduced from the gyroscope and the accelerometer based attitude equations is displayed in figure 6-10. The figure showed several differences. These were the lagging of the accelerometer based attitude estimate (due to the low pass filtering), the difference in the DC levels of the estimates and the significant difference in the magnitude of the angle at the end of movement. The implementation of the filter is also shown in figure 6-10.
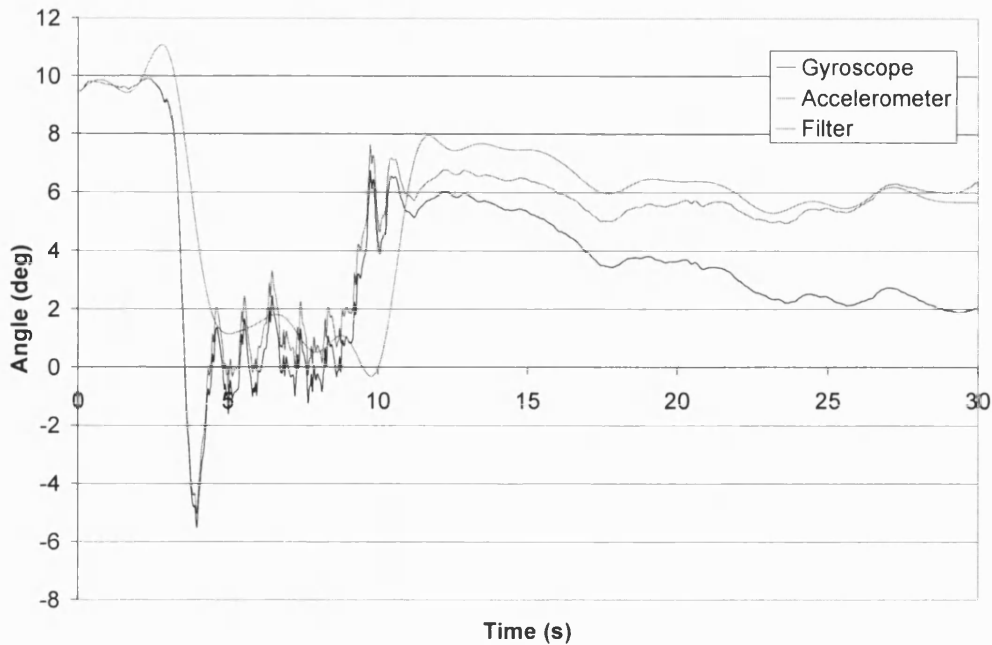
Figure 6-10 The pitch angles from both types of sensor and the combined angle from the complementary filter.

The operation of the filter successfully combined the low frequency of the accelerometer angle estimation with the sensitive response (high frequency) from the gyroscope angle estimation. The results of the K factor are displayed in table 6-5. The variations to the K factor of the complementary filter required to correct the horizontal velocity component so that at the end of the movement the velocity returned to zero, were found to be an average of 0.08, 0.04 and 0.03 for the three groups of trials, respectively. The average velocity values and deduced distances using the filtered pitch angle were again found to fall into three distinctive groups. The magnitudes of the distances were on average 0.42 m, 0.85 m and 0.92 m of the actual distances walked. These distance errors were found to be higher compared to those from changing the gyroscope zero bias. An example of the corrected velocity component is displayed in figure 6-11.
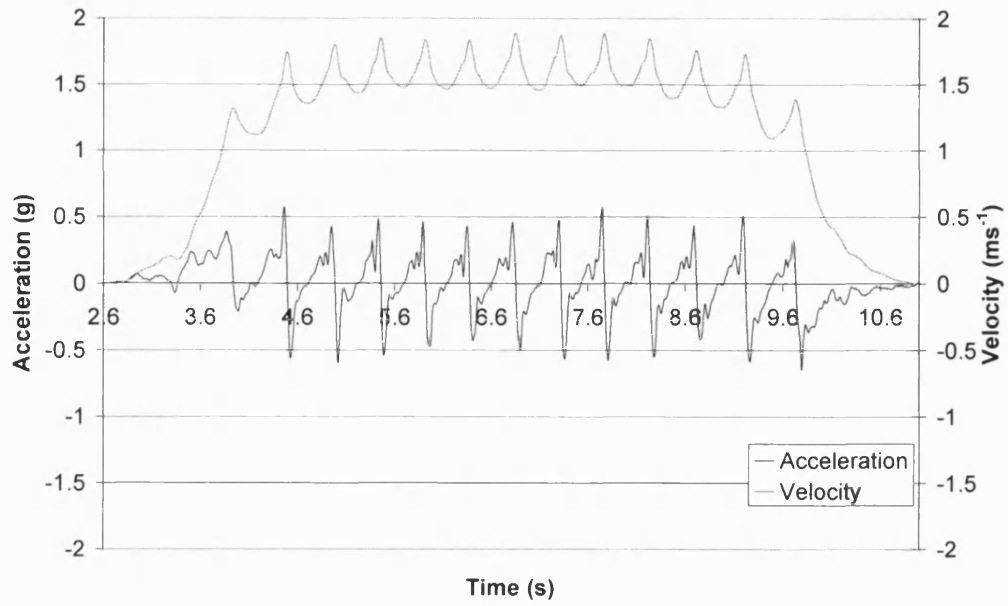
Figure 6-11 The horizontal acceleration and velocity components using the complementary filtered pitch angle with a K factor of 0.0714 for trial 3.

Table 6-5 The K values of the complementary filter and the average velocity and estimated distances.

Trial	Walking Time	Average Bias	Filter value K	Average Velocity	Distance	Distance Error
	s	V		ms^{-1}	m	m
1	8.510	1.41255	0.105	1.12	9.56	0.44
2	8.179	1.41226	0.090	1.23	10.10	0.10
3	8.379	1.41281	0.071	1.16	9.73	0.27
4	8.609	1.41273	0.025	1.07	9.22	0.78
5	8.621	1.41318	0.132	1.10	9.47	0.53
			Average	**1.14**	**9.62**	**0.42**
6	12.229	1.41334	0.067	1.18	14.40	2.60
7	12.370	1.41344	0.016	1.37	16.93	0.07
8	12.839	1.41369	0.039	1.33	17.10	0.10
9	12.150	1.41415	0.090	1.31	15.93	1.07
10	12.470	1.41419	0.032	1.40	17.40	0.40
			Average	**1.32**	**16.35**	**0.85**
11	15.639	1.41449	0.034	1.42	22.22	1.78
12	16.000	1.41453	0.030	1.46	23.42	0.58
13	(16.210)		Corrupted Data			
14	16.870	1.41491	0.036	1.36	22.97	1.03
15	16.349	1.41491	0.020	1.45	23.73	0.27
			Average	**1.42**	**23.08**	**0.92**

The number of steps counted and deduced from the vertical acceleration component corresponded exactly. The step frequencies were found to be an average of 1.57 steps·s^{-1}, 1.77 steps·s^{-1} and 1.89 steps·s^{-1} for each of the groups. An example of the vertical acceleration component clearly displaying the number of steps is displayed in figure 6-12 and the results of the number of steps deduced and the corresponding frequencies are displayed in table 6-6.
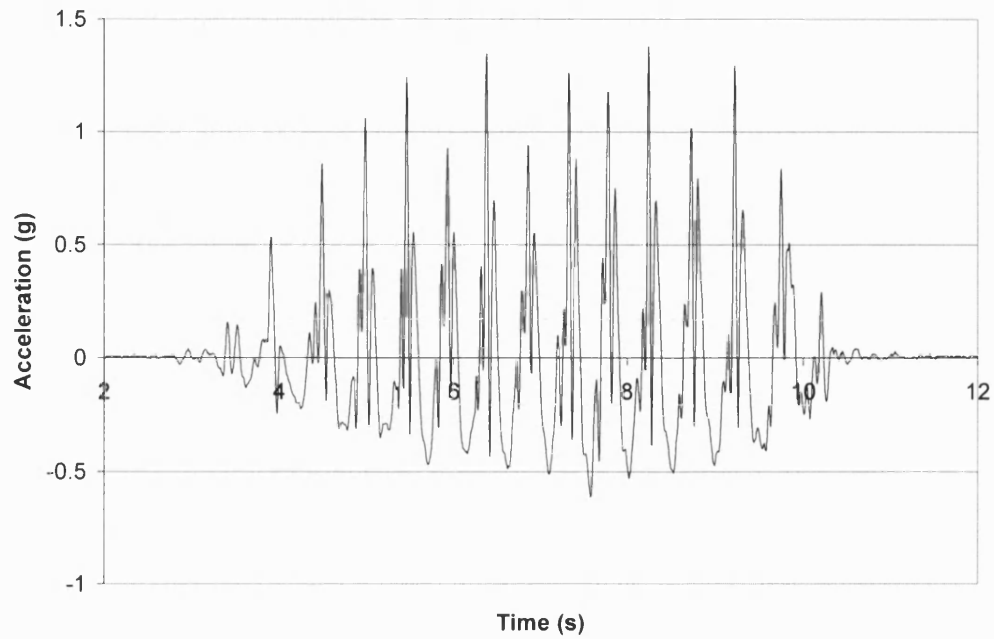
Figure 6-12 The vertical acceleration component displaying 13 steps from Trial 3.

Table 6-6 The number of steps counted during the trials and deduced from the vertical acceleration component.

Trial	Actual Steps	Time	Step Frequency	Deduced Steps
		s	steps·s^{-1}	
1	14	8.510	1.645	14
2	13	8.179	1.589	13
3	13	8.269	1.572	13
4	13	8.609	1.510	13
5	12	8.621	1.392	12
Average	**13**	**8.438**	**1.542**	**13**
6	22	12.229	1.799	22
7	23	12.370	1.859	23
8	22	12.839	1.713	22
9	22	12.150	1.811	22
10	22	12.470	1.764	22
Average	**22.2**	**12.412**	**1.789**	**22.2**
11	30	15.639	1.918	30
12	31	16.000	1.938	31
13	30	16.210	1.851	30
14	31	16.870	1.838	31
15	31	16.349	1.896	31
Average	**30.4**	**16.214**	**1.888**	**30.4**

6.3.4 Discussion

Although the horizontal acceleration component experienced drifting the response was found to be periodic. Within each step there were both negative and positive peaks of acceleration. The most positive and negative points of acceleration occurred just before and just after the positive vertical acceleration peak indicating contact. These points were attributed to the propulsion required to bring the limb through for a contact and the breaking occurring after contact, respectively.

The two factors investigated for their influence over the horizontal acceleration component showed significant results. For the zero bias investigation, the zero bias parameter deduced from the collected data showed a significant difference between the average zero bias found before and after the movement of 0.29 mV which was equivalent to $0.17°s^{-1}$. This result highlighted the unstable characteristics of the zero bias from this type of gyroscope. This raised the question whether this change was predictable or unpredictable and more importantly how to measure the zero bias when the gyroscope was subjected to movements. The small changes to the zero bias parameter to rectify the estimated velocity component were an average of 0.13 mV. Changes to the zero bias parameter resulted in the position of the horizontal acceleration about the x axis to change. Although this corrected the estimated velocity during the movement it was shown that the zero bias parameter used did not produce zero acceleration at the end of the movement whilst stationary. This result suggested that perhaps the zero bias levels of the gyroscope whilst stationary and moving should be different. For the pitch angle investigation, the pitch angle estimates deduced from the accelerometer and the gyroscope about the y axis showed some discrepancies. The DC level of the two pitch estimates were notably different. At the end of the movement, a variation in magnitude of the pitch angle between the two estimates was seen. The pitch angle estimate from the gyroscope then proceeded to drift. This was apparent for all trials. It was assumed that the accelerometer based attitude estimates were more accurate than the gyroscope estimates under static conditions i.e. during the stationary periods and under any conditions over a long period of time. Whereas the gyroscope deduced pitch angle comprised the high frequency components of the movement but was subject to drift over time. This trait could be the cause of the

difference in angle occurring at the end of the movement. Implementation of the filter showed improvement in the pitch angle as it became composed of a fusion of the low and high frequency components from the two estimates. The variations in the K factor to produce an appropriate pitch angle and thus the correct position of the acceleration component to produce a theoretically valid horizontal velocity were an average of 0.08, 0.04 and 0.03 for the three groups of trials. The difference in magnitude of the K factor between the groups could be associated with the speed of the movement. The average velocities and step frequencies of the three groups of trials were found to be 1.15, 1.33 and 1.48 ms^{-1} and 1.57, 1.77 and 1.89 $steps·s^{-1}$ respectively. The increases in velocities between the groups corresponded to the increases in walking speeds required to complete the increased distances within the same data collection period. The association of the K factor to the speed and frequency of the movement and the performance of the filter compared to an independent angle measurement required further investigation which was beyond the scope of this thesis.

The estimated distances deduced from both correcting methods were all within an average of 1 m of their respective distances for the zero bias and filter parameter investigations, respectively. The purpose of this experiment was not to assess the accuracy of the distance results, but to show that the inertial sensor system distinguished three groups of fairly significantly different distances. These results suggested that the inertial sensor system had the potential to describe the velocity and distance of movements if more investigation into reducing the errors is undergone. The number of steps outlined in the vertical acceleration component corresponded exactly to the steps counted for each trial. This result consolidated the ability of the inertial sensor system to identify each contact and to compute the step frequency.

6.4 Summary

The derived net impulse values derived from the anterior-posterior GRF varied from -5.68 to 9.87 Ns. The polarity indicated the subject experienced either a slowing down or a speeding up. The estimated velocity components exhibited elements of drift which was either up or down. Although the relative velocity results seemed to be of reasonable magnitude the change in velocity results deduced from the inertial sensor system varied between 0.08 to 0.27 ms^{-1} and were on average seven times greater in magnitude than the results from the force plate system. The change in velocity results between the force plate and the inertial sensor system presented no relationship. The response of the vertical acceleration component identified the point of contact by a minimum point at an average time discrepancy of 15 ms after the actual point of contact. All of the other minimum points within each trial successfully identified four of the individual steps.

The two factors investigated for their influence over the horizontal acceleration results required minimal changes in order to produce a valid estimated velocity. The small changes to the zero bias value to rectify the acceleration's position to produce a theoretically valid horizontal velocity component were an average of 0.13 mV. The average K factor values found for each group varied from 0.08, 0.04 and 0.03 for the three groups respectively. It was suggested that there may be a relationship existing between the K factor and the speed and frequency of the movements. The estimated distances were accurate to within 1m when adjusting the two factors. However, the inertial sensor system demonstrated the ability to distinguish between the groups of trials. The number of steps outlined in the vertical acceleration component corresponded exactly to the number of steps counted for each trial.

Chapter 7 Conclusions and Further Work

7.1 Introduction

The final chapter presents the conclusions of the research study following the results previously discussed. This research has laid some of the groundwork for the development of an MEMS inertial sensor system that measures human movements and provides useful kinematic parameters of technical sports. The success of the research study has been evaluated against the aim in terms of three purposes. These are:

> The design of inertial sensor system

> The development and verification of the system

> The understanding gained with respect to the potential of the system to measure temporal and spatial parameters.

Furthermore, a number of directions for further work are proposed.

7.2 Inertial Sensor System

The first purpose was to design a motion capture system based on MEMS sensors to meet the specified requirements. It was apparent that the inertial sensor system met a number of these requirements. The size of the sensor module was fairly small at 65 x 65 x 57 mm but was largely dictated by the physical size of the sensors in particular the gyroscope sensors. The sensor module was also light at 0.155 kg and together with the fixings and belt weighed a total of 0.625 kg. The selected position of the sensor module and method of attachment did not restrict movement and was not cumbersome to the user. Only inertial sensors were used which meant that the system was self-contained, required no external sources and that the only environmental interference was temperature. The inertial sensor system measured accelerations and angular rates in three dimensions. The frequency response was 50 Hz with acceleration measurement range of $\pm$ 2 g in the anterior-posterior and medial-lateral directions and $\pm$ 3 g for the vertical direction. The angular rate measurement range

was $\pm$ 300°s^{-1} about each axis. The inertial sensor system was inexpensive at an estimated £350 and took less than 10 minutes to set up and initiate.

At this stage in the project the inertial sensor system did not offer the desired levels of latency or portability. The outputs of the system were tethered to a processing box which pre-processed the outputs and converted them into digital signals. The outputs were then processed further to provide useful kinematic parameters through algorithms implemented on a PC.

7.3 Development and Verification

The second purpose aimed to develop and verify the functionality of the system. This specifically involved the implementation of a calibration procedure, and the verification of the calibration parameters, the axes arrangement, and the processing algorithms. Further, an investigation was implemented to gain an understanding of the performance of the zero bias output of the gyroscope with respect to time and temperature.

The proposed calibration routine which used the opto-electronic motion capture system, CODA, was found to calibrate the inertial sensor system successfully. This procedure was thought to be the principal method for determining calibration parameters but was not suitable to be executed frequently. Therefore, in conjunction with this procedure, a calibration method that was simpler, frequently implementable and involved an in-situ course of movements executed by hand was specified. This procedure was similar to those outlined by Bachmann [102] and Ferraris et al. [148]. It was evident that the zero bias of the gyroscope sensors was required to be found during a stationary period, immediately prior to the commencement of any experiments.

The resultant calibration parameters were successfully verified through two simple experiments involving constant rotations at five pre-selected rates and repeated rotations through a known angle. The angular rates and angles derived by the inertial sensor system demonstrated highly comparable results with respect to the optical

encoder system. It was apparent that there was little difference in the derived angular rates when using either the respective scale factor for the direction of rotation or the average scale factor. Thus, the average scale factor was used for further experiments and meant that the direction of rotation was not required to be known prior to the unit conversion processing step. The accelerometer and gyroscope sensors individually showed their potential to determine the absolute orientation of the inertial sensor system. The accelerometers performed well under static conditions but were not tested for angle estimation during dynamic conditions. Angle estimations through the integration of the gyroscope outputs (no transformation was applied since it was assumed that the two reference frames were aligned) indicated the usability of the gyroscope sensors to determine orientation of the inertial sensors system for short periods of time.

An understanding of the sensor axes sensitivity arrangement was gained experimentally and was subsequently configured to follow the NED arrangement.

The proposed algorithms of the processing steps applied to derive kinematic parameters with respect to the earth reference frame were successfully verified by more experiments. These experiments involved pure rotations thorough a series of known angles. It was assumed that the algorithms were correct since the results indicated the correct orientation for each rotation and that the linear accelerations with respect to the earth reference frame in all three axes showed no acceleration.

The investigation into the performance of the zero bias of the gyroscopes with respect to time and temperature introduced some important issues which were considered with regard to the functioning of the system. It was evident that the zero bias output of the gyroscope in temperature regulated conditions varied considerably with respect to time. It was thought that this variation occurring immediately after power up was attributed to the sensor self-heating. This parameter was therefore required to be either predicted during the first 30 minutes or alternatively measured after the inertial sensor system had been powered for 30 minutes prior to the commencement of the experiment. It was shown that prediction of the zero bias output could be achieved by applying a linear approximation using temperature measurements taken in very close proximity to each gyroscope. However, the proposed prediction method was not

implemented within the scope of this thesis. The alternative method of conducting the experiments once the inertial sensor system was powered for 30 minutes was implemented. After this period the zero bias was known to become somewhat more stable and since the period of data collection was likely to be limited to short durations, for example less than 30 seconds, it was hoped that the zero bias performed adequately. The importance of the stability of the zero bias was highlighted since it was used not only in the conversion of the output signal to an angular rate but subsequently in further algorithms. These algorithms were: integration to yield angles, the transformation to Euler rates, the elimination of the gravitation acceleration and also the rotation matrix to rotate the acceleration into the earth reference frame.

7.4 Measurement of Temporal Parameters

The third purpose aimed to obtain an understanding of the capabilities and potential of the inertial sensor system to provide useful kinematic parameters. There were two sections for this purpose. The first of these was to gain an understanding of the potential of the system to measure temporal parameters. This involved the experiments of the synchronisation of the inertial sensor system to the force plate system, and the identification of the points of contact and non-contact during vertical bouncing and running.

The force plate and the inertial sensor systems were synchronised in order to compare the responsiveness and capabilities of the system to determine certain events. The results showed there to be an average delay of 15 ms between the inertial sensor system and the force plate recording the point of contact. Therefore in subsequent experiments the recorded data sets were offset by this time delay. The results from the vertical bouncing and running experiments showed that the inertial system was capable of identifying the point at which the subject contacted the ground. In both cases this event was identified by a local minimum point within the vertical acceleration output immediately prior to the large positive acceleration peak induced by the impact. It has been shown that similar characteristic patterns in the sensor signals have been used to signify certain events [97]. This characteristic feature was found to be 8 ms and 15 ms, respectively after the force plate indicated the point of

contact. These times were preferable compared to previously documented delays of 10 ms and 65 ms, respectively [84, 109]. It was evident that this time lag was constant since the frequency of the contacts described by the inertial sensor system compared almost exactly to force plate system. This repetitive pattern produced by the inertial sensor system was used to identify the correct number of steps taken during the walking trials executed on an indoor running track. However, the point at which the subject left the ground was harder to identify and was beyond the scope of this thesis.

7.5 Measurements of Spatial Parameters

The third purpose aimed to obtain an understanding of the capabilities and potential of the inertial sensor system to provide useful kinematic parameters. The second part to this purpose was to obtain an understanding of the potential of the inertial sensor system to provide spatial parameters. This involved the experiments of comparing the change in velocity during stance phase whilst running over the force plate, and the identification of three different distances travelled whilst walking on an indoor running track.

The inertial sensor system showed considerably less potential to provide usable spatial parameters such as velocity and distance, than its ability to provide temporal parameters. The change in velocity results derived from the inertial sensor system during the contact phase of running trial over the force plate bore no relationship to the change in velocity results deduced from the impulse indirectly measured by the force plate system. Further, the derived velocity parameter from the walking trials on an indoor track drifted unpredictably which highlighted the instability of the horizontal acceleration output of the inertial sensor system. The likely causes of this instability were deemed to be either or a combination of, the pitch angle and the zero bias of the gyroscope sensitive about the y axis. Investigations into the effects of these two factors introduced some stimulating results. The two factors were manipulated to satisfy the assumption that the velocity having started at zero at the commencement of the movement returned to zero at the termination of the movement. It was shown that by changing the zero bias value fractionally the derived velocity parameter satisfied the assumption, thus, improving the usability of the velocity parameter. Further, it was

shown that a preliminary investigation which implemented a simple complementary filter to provide an optimal estimate of the pitch angle, also helped to improve the usability of the velocity parameter. The filter provided the 'best' estimate of the orientation of the inertial sensor system by fusing the available orientation estimates from the accelerometer and gyroscope sensors.

7.6 Future Research Directions

The inertial sensor system designed, developed and evaluated in this research study is far from an ideal motion capture system for measuring human movements. Thus the system would benefit from a number of future research directions. These are improved performance of the gyroscope sensors, reductions in size of the inertial sensor module, improved latency and portability, further investigation into temperature compensation of the gyroscope sensors, and further investigation into the implementation of the complementary filter and determination of the value of K factor. Lastly, an investigation into the suitability and potential of the system to measure the essential kinematic parameters of the technical aspects of athletic events, in particular the short sprint events is required. Measurements of these parameters have been shown to describe and analyse technique and are utilised to enhance performance.

The first area that requires attention if further work was to be conducted would be to change the selected gyroscope sensor. At the time when the sensor was selected there was a somewhat limited choice. The chosen gyroscope sensor was found to have two main disadvantages. These were its physical size and the instability of the zero bias with respect to time and temperature. There is now a wider selection of sensors due to the advancements of functionality and packaging of the more complex and robust gyroscope sensor technology which has reduced their physical size, making them more suitable as body worn sensors. For example, the KGF01 by Kionix [213], the recent CRS07-11 by Silicon Sensing [214], and IDG-1000c or IDG-300i by InvenSense [215]. These sensors are considerably more expensive, difficult to mount and/or still larger in size. Any of these characteristics may be required to be

accommodated at the gain of a better performance. In turn the overall performance of the inertial sensor system is likely to be improved.

With further advances in MEMS sensors looming there is likely to be a smaller gyroscope with adequate performance ratings available in the near future. The physical size of the gyroscope largely dictates the overall size of the inertial sensor system. The connectors, PCB boards and cabling can all be readily reduced in size. Without a reduction in size of this sensor the reduction to the overall sensor module is somewhat limited. Further, if a three-axis gyroscope became available together with the now available three-axis accelerometer from Analog Devices [127] this would eliminate the need for two boards mounted orthogonally thus reducing the height dimension of the sensor module. There is evidence to suggest that further into the future there is likely to be a three-axis accelerometer and three-axis angular rate sensor combined into one sensor which uses a single mass, potentially offering the most reduction in size. The pre-processing boards could be changed to contain single supply amplifiers, if the amplification can be accommodated, and condensed onto surface mount boards. Further, these boards could be housed within the sensor module together with a microprocessor which facilitates an A/D converter function with enough input channels to replace the Pico Technology data logger. The data would be either stored or transmitted.

The latency of the system can be improved by utilising the microprocessor housed in the inertial sensor module mentioned in the above section. The microprocessor could be used to implement all of the processing steps involving the algorithms such as, integration, transforming to Euler angles, gravity compensating and filtering as well as A/D conversion. The system could offer the potential to calculate kinematic parameters in near to real time depending on the time to process the algorithms. The information could then be displayed in real time, stored and/or transmitted. The portability of the system can be improved by reducing the power requirement and subsequently reducing the size of the batteries. For example, rechargeable, slim, lithium batteries similar to those used in mobile phones or by Varta PoLiFlex [216]. Further portability could be achieved in either two ways. Firstly, the calculated kinematic parameters could be stored on board, for example on a PCMCIA data

acquisition card, and downloaded later after the experiment. Alternatively, the digital data could be transmitted wirelessly to a receiver and stored on a PC [217].

Even if a more preferable gyroscope sensor is chosen, it is likely that the performance of the sensor may still be affected by the external and/or internal temperature. In the case of the some sensors, the device provides an internal temperature measurements output onto one of the pins of the IC [213]. This could eliminate the need for additional temperature sensors. The simple linear approximation that was implemented in this thesis could be explored further to provide a more preferable prediction of the output of the gyroscope using the temperature measurements recorded within close proximity of the gyroscope sensors. For example, the Levenberg-Marquardt iterative least squares fit method implemented by Barshan and Durrant-Whyte [156]. A description of this method can be found in Borse [206] and Press [176].

Preliminary investigations involving the implementation of a complementary filter were conducted. In light of the results further investigations are required in order to determine the most suitable value for the K factor and the suitability of the complexity of the complementary filter. Although the value of the K factor can be found theoretically, an experimental approach found a variation in value that could be linked to the speed of the movement. This assumption required further investigation. It is also unclear if such a simplistic filter provides adequate estimations of orientation. From the literature review, other investigations that have initially used a simpler approach, have then modified their system to incorporate a more complex filter. A more complex filter typically models some of the processes as well as predicting the zero bias output of the gyroscope [102, 113]. Again, further investigations are required to gain an understanding of the level of performance provided by the complementary filter.

The performance of the inertial sensor system needs to be improved before the capability and potential of the system to measure kinematic parameters of the technical aspects of athletic events such as the sprinting events can be realised. There are several variables that influence sprint running one of which is technique [218]. The most investigated parameters that constitute technique in sprinting are horizontal

velocity [219-221], stride length and stride frequency [219, 222-224], and contact time [222]. Theoretically, an inertial sensor system should have the ability to measure all of these parameters. There are two variables of the horizontal velocity that are of great interest, maximum horizontal velocity and average velocity at every 10m sections. The maximum horizontal velocity that an individual can achieve is of interest since it is a precondition of a potentially excellent performance [220, 225]. The time at which the maximum horizontal velocity occurred can be found by searching for the highest instantaneous velocity recording within the collected data. The knowledge of the average horizontal velocity every 10 m can be used to provide velocity curves which can be compared between runs and to other athletes. The velocity curve identifies the different sections that constitute a sprint run such as the acceleration period, the section which recorded the maximum horizontal velocity and the ability to sustain maximum velocity towards the end [221]. The average velocity every 10 m can be calculated by averaging the instantaneous velocities at each sampling point. Stride length and stride frequency and particularly the relationship between these parameters have been shown to influence sprinting performance [219, 222-224]. Kunz and Kaufmann [223] suggested that too long a stride length may decrease stride frequency and too fast a stride frequency may shorten stride length, both of these conditions can decrease performance. It has also been shown that these parameters increase with increases in speeds. However, at high speeds, above 7 ms^{-1}, there is smaller increment in stride length and a greater increment in stride rate for a given increase in speed [224, 226]. It has been shown that the inertial sensor system can identify the point of contact during certain movements. If it is possible to determine the point of contact during sprinting then the stride frequency can be deduced from the time period between contacts. Also, if the average velocity between two contact points is known then the stride length can also be deduced. The duration of contact is another important parameter which influences sprinting performance. In short, the less time that is spent in contact with the ground the higher the stride rate [222]. An increase in performance through shortening contact time is based on the assumption that stride length is not compromised, that touch down distance is minimal and that the athlete has the required leg strength. It is likely to be harder for the inertial sensor system to determine the duration of contact since it has been shown that the point of take off is difficult to identify repeatedly. It is evident that measurements of any or all of these parameters mentioned above, provide valuable

insight into technique of sprint running and with regular monitoring are likely to aid the training of athletes to help achieve enhanced performance.

Clearly, there is a need for a low-cost, self-contained and portable motion capture system based on MEMS inertial sensors that is not cumbersome to the user, is quick to set up and provides kinematic parameters to describe the technical aspects of sports in real time. The work that has been demonstrated in this research study has shown that inertial sensors have the potential to measure temporal parameters, such as the point of contact and stride frequency. This information can now be used and built upon to provide an improved inertial sensor system for the use of measuring human movements.

References

[1]   R. S. Payne, "MEMS commercialization: ingredients for success," *Proceedings of the 13th Annual International Conference on Micro Electro Mechanical Systems (MEMS)*, 2000.

[2]   C. Trimble and L. Lang, "ADI: Micro-electro-mechanical systems (MEMS)," The Centre for Global Leadership, Tuck School of Business at Dartmouth, Hanover, New Hampshire 2-0018, 2002.

[3]   C.-H. Han, "MEMS accelerometers for air bag deployment for automobile," University of Hawaii, www.-ee.eng.hawaii.edu/~cheol/ee626/accelerometer.html, (cited June 2005), 1998.

[4]   Hewlett Packard: www.hp.com, cited July, 2005.

[5]   G. Yuandong, A. Baldi, B. Ziale, and R. A. Siegel, "Modulation of drug delivery by hydrogel-incorporating MEMS devices," *Proceedings of the Microtechnologies in Medicine and Biology 2nd Annual International IEEE-EMB Special Topic Conference*, 2002.

[6]   P. F. Van Kessel, L. J. Hornbeck, R. E. Meier, and M. R. Douglass, "A MEMS-based projection display," *Proceedings of the IEEE*, vol. 86, pp. 1687-1704, 1998.

[7]   Sercalo: www.sercalo.com, cited July, 2005.

[8]   N. Yazdi, F. Ayazi, and K. Najafi, "Micromachined inertial sensors," *Proceeding of the IEEE*, vol. 86, pp. 1640-1659, 1998.

[9]   C. Acar and A. M. Shkel, "Experimental evaluation and comparative analysis of commercial variable-capacitance MEMS accelerometers," *Micromechanics and Microengineering*, vol. 13, pp. 634-645, 2003.

[10]   J. Israelsohn, "Newton's chips: low-g accelerometer IC's," EDN Europe Magazine,2004.pp. 37-42

[11]   A. Beliveau, G. T. Spencer, K. A. Thonas, and S. L. Roberson, "Evaluation of MEMS capacitive accelerometers," IEEE Design and Test of Computers,1999.pp. 48-56

[12]   M. A. Clifford, "Accelerometer jump into the consumer goods market," Sensors Magazine,2004,

[13]   H. Weinberg, "MEMS sensors," Sensors Magazine,2002,

[14]   J. Lee, G.-J. Nam, J. Chae, H. Kim, and A. J. Drake, "Two-dimensional position detection systems with MEMS Accelerometer for MOUSE applications," *Proceedings of the IEEE Design Automation Conference*, 2001.

[15]   A. Chu, "Accelerometer selection based on applications," Endevco TP 291, cited June 2005.

[16]   BEI Technologies, Inc: www.bei-tech.com/markets/markets.htm, cited July, 2005.

[17]   N. Barbour and G. Schmidt, "Inertial sensor technology trends," *IEEE Sensors*, vol. 1, pp. 332-339, 2001.

[18]   N. Yazdi and K. Najafi, "An all-silicon single-wafer micro-g accelerometer with a combined surface and bulk micromachining process," *Journal of Microelectromechanical Systems*, vol. 9, pp. 554-550, 2000.

[19]   E. Haeuber, M. Shaughnessy, L. W. Forrester, K. L. Coleman, and R. F. Macko, "Accelerometer monitoring of home- and community-based

ambulatory activity after stroke," *Archives of Physical Medicine and Rehabilitation*, vol. 85, pp. 1997-2001, 2004.

[20] H. B. J. Bussmann, P. J. Reuvekamp, P. H. Veltink, W. L. J. Martens, and H. J. Stam, "Validity and reliability of measurements obtained with an "activity monitor" in people with and without a transtibial amputation," *Physical Therapy*, vol. 78, pp. 989-998, 1998.

[21] J. R. W. Morris, "Accelerometry - A technique for the measurement of human body movements," *Journal of Biomechanics*, vol. 6, pp. 729-736, 1973.

[22] C. V. C. Bouten, K. T. M. Koekkoek, M. Verduin, R. Kodde, and J. D. Janssen, "A triaxial accelerometer and portable data processing unit for the assessment of daily physical activity," *IEEE Transactions on Biomedical Engineering*, vol. 44, pp. 136-147, 1997.

[23] B. S. Troy, E. E. Sabelman, D. E. Kenney, and S. Dunn-Gabrielli, "Accelerometric motion analysis of balance-impaired elderly subjects," *Proceedings of the Proceedings of the Rehabilitation Engineering and Assistive Technology Society of North America (RESNA) Annual Conference*, Salt Lake City, Utah, 1996.

[24] R. E. Mayagoitia, J. C. Lotters, P. H. Veltink, and H. Hermens, "Standing balance evaluation using a triaxial accelerometer," *Gait and Posture*, vol. 16, pp. 55-59, 2002.

[25] T.-C. Soong, "Biomechanics (analyses and applications) of shotput and discus and javelin throws," in *Human body dynamics: impact, occupational, and athletic aspects*, D. N. Ghista, Ed.: Clarendon Press, 1981.

[26] K. R. Williams, "The dynamics of running," in *Biomechanics in Sport: Performance enhancement and injury prevention*, V. M. Zatsiorsky, Ed.: Blackweel Sciences Ltd., 2000, pp. 161-183.

[27] B. Elliott, T. Marsh, and B. Blanksby, "A three-dimensional cinematographic analysis of the tennis serve," *International Journal of Sport Biomechanics*, vol. 2, pp. 260-271, 1986.

[28] T. Bober, "Comments on speed and technique interrelation in sprinting," *Hungarian Review of Sports Medicine*, vol. 38, pp. 181-187, 1987.

[29] A. Salo, P. Grimshaw, and J. Viitasalo, "The use of motion analysis as a coaching aid to improve the individual technique in sprint hurdles," *Proceedings of the International Society of Biomechanics in Sports (ISBS)*, Stuttgart, 1999.

[30] Acoustic Positioning Research (APR) Inc.: www.positioning-research.com, April, 2005.

[31] VR Depot: www.vrdepot.com, April, 2005.

[32] G. Welch and E. Foxlin, "Motion tracking: no silver bullet, but a respectable arsenal," *IEEE Computer Graphics and Applications*, vol. 22, pp. 24-38, 2002.

[33] D. A. Bohn, "Environmental effects on the speed of sound," *Journal of Audio Engineering Society*, vol. 36, 1988.

[34] Polhemus: www.polhemus.com/LIBERTY.htm, cited April, 2005.

[35] Ascension Technology Corporation: www.ascension-tech.com/products/motionstar.php, cited April, 2005.

[36] K. Meyer, H. L. Applewhite, and F. A. Biocca, "A Survey of Position Trackers," *Presence: Teleoperators and Virtual Environments*, pp. 173-200, 1992.

[37] puppetworks.com: www.puppetworks.com/products_bodytracker.shtml, cited April, 2005.

[38]   noDNA: www.nodna.com, cited April, 2005.

[39]   M. J. Lake and P. R. Cavanagh, "Six weeks of training does not change running mechanics or improve running economy," *Medicine and Science in Sports and Exercise*, vol. 28, pp. 860-869, 1996.

[40]   N. K. Mital and A. I. King, "Computation of rigid-body rotation in three-dimensional space from body-fixed linear acceleration measurements," *Journal of Applied Mechanics*, vol. 46, pp. 925-930, 1979.

[41]   A. Salo, P. N. Grimshaw, and L. Marar, "Three-dimensional biomechanical analysis of sprint hurdles at different competitive levels," *Medicine and Science in Sports and Exercise*, vol. 29, pp. 231-237, 1997.

[42]   M. Coh, B. Jost, and S. Stuhec, "Kinematic and dynamic structure of the sprinting stride of top female sprinters," *Biology of Sport*, vol. 15, pp. 237-243, 1998.

[43]   J. P. Hunter, R. N. Marshall, and P. McNair, "Reliability of biomechanical variables of sprint running," *Medicine and Science in Sports and Exercise*, vol. 36, pp. 850-861, 2004.

[44]   A. M. Chaudhari, R. W. Bragg, E. J. Alexander, and T. P. Andriacchi, "A video-based, markerless motion tracking system for biomechanical analysis in an arbitrary environment," *Proceedings of the Proceedings of the ASME Bioengineering Conference*, Utah, US, 2001.

[45]   E. J. Alexander and T. P. Andriacchi, "Improving the analysis of human movement using markless motion capture," *Proceedings of the Proceedings of the ASME Bioengineering conference*, Florida, US, 2003.

[46]   Y. I. Abdel-Aziz and H. M. Karara, "Direct linear transformation from comparator coordinates into object space coordinates in close-range photo-grammetry," *Proceedings of the Proceedings of the Symposium on Close-Range Photogrammetry*, Falls Church, VA: American Society of Photogrammetry, 1971.

[47]   N. R. Miller, R. Shapiro, and T. M. McLaughlin, "A technique for obtaining spatial kinematic parameters of segments of biomechanical systems from cinematographic data," *Journal of Biomechanics*, vol. 13, pp. 535-547, 1980.

[48]   A. Gruen, "Fundamentals of videogrammetry - A review," *Human Movement Science*, vol. 16, pp. 155-187, 1997.

[49]   B. M. Nigg, *Biomechanics of the Musculo-Skeletal System*, 2nd ed: John Wiley & Sons Ltd, 1999.

[50]   Y. Ehara, H. Fujimoto, S. Miyazaki, M. Mochimaru, S. Tanaka, and S. Yamamoto, "Comparison of the performance of 3D camera systems II," *Gait and Posture*, vol. 5, pp. 251-255, 1997.

[51]   J. G. Richards, "The measurement of human motion: A comparison of commercially available systems," *Human Movement Science*, vol. 18, pp. 589-602, 1999.

[52]   M. R. Yeadon and J. H. Challis, "The future of performance related sports biomechanics research," *Journal of Sports Sciences*, vol. 12, pp. 3-32, 1994.

[53]   J. B. J. Bussmann, L. Damen, and H. J. Stam, "Analysis and decomposition of signals obtained by thigh-fixed uni-axial accelerometry during normal walking," *Medical and Biological Engineering and Computing*, vol. 38, pp. 632-638, 2000.

[54]   R. E. Mayagoitia, A. V. Nene, and P. H. Veltink, "Accelerometer and rate gyroscope measurement of kinematics: an inexpensive alternative to optical

motion analysis systems," *Journal of Biomechanics*, vol. 35, pp. 537-542, 2002.

[55]   A. Nene, R. Mayagoitia, and P. Veltink, "Assessment of rectus femoris function during initial swing phase," *Gait and Posture*, vol. 9, pp. 1-9, 1999.

[56]   I. P. I. Pappas, M. R. Popovic, T. Keller, V. Dietz, and M. Morari, "A reliable gait phase detection system," *IEEE Transactions on Neural Systems and Rehabilitation Engineering*, vol. 9, pp. 113-125, 2001.

[57]   Z. Ladin, W. C. Flowers, and W. Messner, "A quantitative comparison of a position measurement system and accelerometry," *Journal of Biomechanics*, vol. 22, pp. 295-7, 1989.

[58]   R. M. Angulo and J. Dapena, "Comparison of film and video techniques for estimating three-dimensional coordinates within a large field," *International Journal of Sport Biomechanics*, vol. 8, pp. 145-151, 1992.

[59]   Codamotion: www.charndyn.com, cited April, 2005.

[60]   Qualisys: www.qualisys.se/index.html, cited April, 2005.

[61]   M. A. Lafortune, "Three-dimensional acceleration of the tibia during walking and running," *Journal of Biomechanics*, vol. 24, pp. 877-886, 1991.

[62]   Analog Devices: www.analog.com/en/, cited June, 2005.

[63]   Murata: www.murata-europe.com/, cited June, 2005.

[64]   G. A. Henault, "A computer simulation study and component evaluation for a quarternion filter for sourceless tracking of human limb segment motion," master's thesis in *Department of Computer Science,* Naval Postgraduate School: Monterey, California, 1997.pp. 107

[65]   InterSense: www.intersense.com, cited April, 2005.

[66]   Xsens: www.xsens.com/download/MT9_brochure.pdf, cited April, 2005.

[67]   BEI Systron Donner Inertial Division: www.systron.com/pro_MotPk.asp, cited July, 2005.

[68]   Dynastream Innovations: www.dynastream.com, cited April, 2005.

[69]   A. J. Padgaonkar, K. W. Krieger, and A. I. King, "Measurement of angular acceleration of a rigid body using linear accelerometers," *Journal of Applied Mechanics*, vol. 42, pp. 552-556, 1975.

[70]   W. C. Hayes, J. D. Gran, M. L. Nagurka, J. M. Feldman, and C. Oatis, "Leg motion analysis during gait by multiaxial accelerometry - theoretical foundations and preliminary validations," *Journal of Biomechanical Engineering*, vol. 105, pp. 283-289, 1983.

[71]   Z. Ladin and W. Ge, "Combining position and acceleration measurements for joint force estimation," *Journal of Biomechanics*, vol. 24, pp. 1173-1187, 1991.

[72]   A. L. Evans, G. Duncan, and W. Gilchrist, "Recording accelerations in body movements," *Medical and Biological Engineering and Computing*, vol. 29, pp. 102-104, 1991.

[73]   K. Aminian, P. Robert, E. Jequier, and Y. Schutz, "Incline, speed, and distance assessment during unconstrained walking," *Medicine and Science in Sports and Exercise*, vol. 27, pp. 226-234, 1995.

[74]   T. Sakaguchi, T. Kanamori, H. Katayose, K. Sato, and S. Inokuchi, "Human motion capture by integrating gyroscopes and accelerometers," *Proceedings of the IEEE International Conference on Multisensor Fusion and Integration for Intelligent Systems SCIE/RSJ*, 1996.

[75]   A. J. van den Bogert, L. Read, and B. M. Nigg, "A method for inverse dynamic analysis using accelerometry," *Journal of Biomechanics*, vol. 29, pp. 949-954, 1996.

[76]   P. H. Veltink, H. B. J. Bussmann, W. de Vries, W. L. J. Martens, and R. C. van Lummel, "Detection of static and dynamic activities using uniaxial accelerometers," *IEEE Transactions on Rehabilitation Engineering*, vol. 4, pp. 375-385, 1996.

[77]   J. Fahrenberg, F. Foerster, M. Smeja, and W. Muller, "Assessment of posture and motion by multichannel piezoresistive accelerometer recordings," *Psychophysiology*, vol. 34, pp. 607-612, 1997.

[78]   R. Moe-Nilssen, "A new method for evaluating motor control in gait under real- life environmental conditions. Part 1: The instrument," *Clinical Biomechanics*, vol. 13, pp. 320-327, 1998.

[79]   K. Aminian, K. Rezakhanlou, E. De Andres, C. Fritsch, P. F. Leyvraz, and P. Robert, "Temporal feature estimation during walking using miniature accelerometers: an analysis of gait improvement after hip arthroplasty," *Medical and Biological Engineering and Computing*, vol. 37, pp. 686-691, 1999.

[80]   F. Foerster, M. Smeja, and J. Fahrenberg, "Detection of posture and motion by accelerometry: a validation study in ambulatory monitoring," *Computers in Human Behavior*, vol. 15, pp. 571-583, 1999.

[81]   C. T. M. Baten, H. J. Luinge, and H. Van Moerkerk, "Estimating body segment orientation applying inertial sensing," *Proceedings of the 6th International Symposium on the 3-D Analysis of Human Movements*, Cape Town, South Africa, 2000.

[82]   H. B. Menz, S. R. Lord, and R. C. Fitzpatrick, "Acceleration patterns of the head and pelvis when walking on level and irregular surfaces," *Gait and Posture*, vol. 18, pp. 35-46, 2003.

[83]   G. A. Hansson, P. Asterland, N. G. Holmer, and S. Skerfving, "Validity and reliability of triaxial accelerometers for inclinometry in posture analysis," *Medical & Biological Engineering & Computing*, vol. 39, pp. 405-413, 2001.

[84]   T. Heiden and A. Burnett, "Determination of heel strike and toe-off in the running stride using an accelerometer: application to field-based gait studies," *Proceedings of the 22nd International Symposium of Biomechanics in Sports*, University of Ottawa, Canada, 2004.

[85]   A. J. van den Bogert and L. Read, "A method for inverse dynamics analysis using accelerometry," *Proceedings of the Second World Congress of Biomechanics: Dynamic Analysis using Body Fixed Sensors*, Amsterdam, 1994.

[86]   C. T. M. Baten, P. Oosterhoff, I. Kingma, P. H. Veltink, and H. Hermens, "Inertial sensing in ambulatory back load estimation," *Proceedings of the 18th Annual IEEE International Conference of the Engineering in Medicine and Biology Society (EMBS)*, Amsterdam, 1996.

[87]   P. H. Veltink, D. M. Nieuwland, J. Harlaar, and C. T. M. Baten, "Inertial sensing in a hand held dynometer," *Proceedings of the 18th Annual IEEE International Conference of the Engineering in Medicine and Biology Society (EMBS)*, Amsterdam, 1996.

[88]   T. F. Sterzing and E. M. Henning, "Measurement of plantar pressures, rearfoot motion, and tibial shock during running 10km on a 400m track," *Proceedings of the 4th Symposium on Footwear Biomechanics*, Canmore, Canada, 1999.

[89] D. Fontaine, D. David, and Y. Caritu, "Sourceless human body motion capture," *Proceedings of the Smart Objects Conference*, Grenoble, France, 2003.

[90] H. J. Luinge, P. H. Veltink, and C. T. M. Baten, "Estimating orientation with gyroscopes and accelerometers," *Technology and Health Care*, vol. 7, pp. 455-459, 1999.

[91] R. Williamson and B. J. Andrews, "Gait event detection for FES using accelerometers and supervised machine learning," *IEEE Transactions on Rehabilitation Engineering*, vol. 8, pp. 312-319, 2000.

[92] J. A. Paradiso, K. Hsiao, A. Y. Benbasat, and Z. Teegarden, "Design and implementation of expressive footwear," *IBM Systems Journal*, vol. 39, pp. 511-529, 2000.

[93] R. Williamson and B. J. Andrews, "Detecting absolute human knee angle and angular velocity using accelerometers and rate gyroscopes," *Medical and Biological Engineering and Computing*, vol. 39, pp. 294-302, 2001.

[94] Y. Ohgi, "Microcomputer-based acceleration sensor device for sports biomechanics," *Proceedings of the IEEE Sensors*, 2002.

[95] E. R. Bachmann, X. Yun, R. B. McGhee, and M. J. Zyda, "Design and implementation of MARG sensors for three-degrees of freedom (DOF) orientation measurement of rigid bodies," *Proceedings of the IEEE International Conference on Robotics and Automation*, Taipei, Taiwan, 2003.

[96] H. Y. Lau and K. Y. Tong, "Portable gait detection system for FES in difference walking environments," *Proceedings of the World Congress on Medical Physics and Biomedical Engineering*, Sydney, 2003.

[97] A. M. Sabatini, C. Martelloni, S. Scapellato, and F. Cavallo, "Assessment of walking features from foot inertial sensing," *IEEE Transactions on Biomedical Engineering*, vol. 52, pp. 486-494, 2005.

[98] J. Lee and I. Ha, "Sensor fusion and calibration for motion captures using accelerometers," *Proceedings of the IEEE International Conference on Robotics and Automotion*, Detroit, USA, 1999.

[99] P. H. Veltink, P. Slycke, E. Morsink, J. Hemssems, G. Bultstra, and H. Hermens, "Towards automatic optimization of gait supported by a two-channel implantable drop foot simulator," *Proceedings of the 7th Vienna International Workshop on Functional Electrical Stimulation. Session: Dropped Foot Stimulators*, 2001.

[100] A. Y. Benbasat, "An inertial measurement unit for user interfaces," master of science in *Media Arts and Sciences,* Massachusetts Institute of Technology, 2000

[101] G. Baseli, G. Legnani, F. Franco, F. Brognoli, A. Marras, F. Quaranta, and B. Zappa, "Assessment of inertial and gravitational inputs to the vestibular system," *Journal of Biomechanics*, vol. 34, pp. 821-826, 2001.

[102] E. R. Bachmann, "Inertial and magnetic tracking of limb segment orientation for inserting into synthetic environments," Ph.D. in *Department of Computer Science,* Naval postgraduate school: Monterey, California, 2000

[103] T. Harada, H. Uchino, T. Mori, and K. Sato, "Portable orientation estimation device based on accelerometers, magnetometers and gyroscope sensors for sensor network," *Proceedings of the IEEE Conference on Multisensor fusion and integration for intelligent systems*, 2003.

[104] T. Harada, H. Uchino, T. Mori, and T. Sato, "Portable absolute orientation estimation device with wireless network under accelerated situation,"

Proceedings of the IEEE International Conference on Robotics and Automation (ICRA), New Orleans, Louisiana, 2004.

[105] S. Saripalli, J. M. Roberts, P. I. Corke, and G. Buskey, "A tale of two helicopters," *Proceedings of the IEEE International Conference on Intelligent Robots and Systems (IROS)*, 2003.

[106] S. Miyazaki, "Long-term unrestrained measurement of stride length and walking velocity utilizing a piezoelectric gyroscope," *IEEE Transactions on Biomedical Engineering*, vol. 44, pp. 753-759, 1997.

[107] J. R. Henty, D. E. Wood, and D. J. Ewins, "Detection of gait events using vibratory gyroscope," *Proceedings of the 4th Annual Conference of the International Functional Electrical Stimulation Society (IFESS)*, Sendai, Japan, 1999.

[108] K. Y. Tong and M. H. Granat, "A practical gait analysis system using gyroscopes," *Medical Engineering & Physics*, vol. 21, pp. 87-94, 1999.

[109] K. Aminian, B. Najafi, C. Bula, P. F. Leyvraz, and P. Robert, "Spatio-temporal parameters of gait measured by an ambulatory system using miniature gyroscopes," *Journal of Biomechanics*, vol. 35, pp. 689-699, 2002.

[110] C. Kirtley and K. Tong, "Insole gyro system for gait analysis," *Proceedings of the Annual Conference of Rehabilitation Engineering and Assistive Technology Society of North America (RESNA)*, 2000.

[111] A.-J. Baerveldt and R. Klang, "A low-cost and low-weight attitude estimation for an autonomous helicopter," *Proceedings of the IEEE International Conference on Intelligent Engineering Systems (INES)*, 1997.

[112] M. J. Caruso, "A new perspective on magnetic field sensing," Sensors magazine,1998,

[113] E. Foxlin, "Inertial head-tracker sensor fusion by a complementary separate-bias kalman filter," *Proceedings of the IEEE Virtual Reality Annual International Symposium (VRAIS)*, Santa Clara, California, 1996.

[114] E. Foxlin, M. Harrington, and Y. Alshuler, "Miniature six-degrees of freedom (DOF) inertial system for tracking HMDs," *Proceedings of the International Society for Optical Engineering (SPIE), AeroSense, Helmet and Head-Mounted Displays III*, Orlando, Florida, 1998.

[115] S. Bonnet, P. Couturier, F. Favre-Reguillon, and R. Guillemaud, "Evaluation of postural stability by means of a single inertial sensor," *Proceedings of the 26th Annual IEEE International Conference of the Engineering in Medicine and Biology and Society (EMBS)*, San Francisco, USA, 2004.

[116] H. Gage, "Accelerographic analysis of human gait," *American Society for Mechanical Engineers*, vol. 64-WA/HUF, pp. 137-152, 1964.

[117] G. L. Smidt, J. Arora, and R. C. Johnston, "Accelerographic analysis of several types of walking," *Americal Journal of Physical Medicine*, vol. 50, pp. 285-300, 1971.

[118] J. A. Gilbert, G. Maxwell Maret, J. H. McElhaney, and F. W. Clippinger, "A System to measure the forces and moments at the knee and hip during level walking," *Journal of Orthopaedic Research*, vol. 2, pp. 281-288, 1984.

[119] T. R. Kane, W. C. Hayes, and J. D. Priest, "Experimental determination of forces exerted in tennis play," *In Biomechanics*, vol. IV, pp. 284-290, 1974.

[120] A. T. M. Willemsen, J. A. Vanalste, and H. B. K. Boom, "Real-time gait assessment utilizing a new way of accelerometry," *Journal of Biomechanics*, vol. 23, pp. 859-863, 1990.

[121] M. Sekine, T. Tamura, M. Ogawa, T. Togawa, and Y. Fukui, "Classification of acceleration waveform in a continuous walking record," *Proceedings of the 20th Annual IEEE International Conference of the Engineering in Medicine and Biology Society (EMBS)*, 1998.

[122] R. E. Mayagoitia, J. C. Lotters, and P. H. Veltink, "Standing stability evaluation using a triaxial accelerometer," *Proceedings of the 18th Annual IEEE International Conference of the Engineering in Medicine and Biology Society (EMBS)*, Amsterdam, 1996.

[123] G. A. L. Meijer, K. R. Westerterp, F. M. H. Verhoeven, H. B. M. Koper, and F. Tenhoor, "Methods to assess physical-activity with special reference to motion sensors and accelerometers," *IEEE Transactions on Biomedical Engineering*, vol. 38, pp. 221-229, 1991.

[124] W. deVries, P. H. Veltink, M. P. Koper, and B. F. J. M. Koopman, "Calculation of segment and joint angles of the lower extremities during gait using accelerometers," *Proceedings of the 2nd World Congress of Biomechanics: Dynamic Analysis using Body Fixed Sensors*, Amsterdam, 1994.

[125] G. Currie, D. Rafferty, G. Duncan, F. Bell, and A. L. Evans, "Measurement of gait by accelerometer and walkway - a comparison study," *Medical and Biological Engineering and Computing*, vol. 30, pp. 669-670, 1992.

[126] J. C. Lotters, J. G. Bomer, A. J. Verloop, E. A. Droog, W. Olthuis, P. H. Veltink, and P. Bergveld, "Design, fabrication and characterization of a highly symmetrical capacitive triaxial accelerometer," *Sensors and Actuators A Physical*, vol. 66, pp. 205-212, 1998.

[127] Analog Devices: www.analog.com/en/press/, "Analog devices expands low-g portfolio with 3-axis accelerometer technology for portable applications," January 31st, 2005.

[128] P. H. Veltink and H. B. K. Boom, "Three-dimensional movement analysis using acceleometry theoretical concepts," in *Neuroprosthetics: From Basic Research to Clinical Application*, A. Pedotti, M. Ferrarin, J. Quintern, and R. Riener, Eds.: Springer-Verlag Telos, 1996, pp. 317-325.

[129] K. Y. Tong and M. H. Granat, "A practical gait analysis system using gyroscopes," *Medical Engineering and Physics*, vol. 21, pp. 87-94, 1999.

[130] A. Heyn, R. E. Mayagoitia, A. V. Nene, and P. H. Veltink, "The kinematics of the swing phase obtained from accelerometer and gyroscope measurements," in *18th Annual IEEE International Conference of the Engineering in Medicine and Biology Society (EMBS)*, vol. 18. New York: IEEE, 1997, pp. 463-464.

[131] C. Kirtley, "Instrumented Insole," Patent US2003009308, US, 2003.

[132] A. T. M. Willemsen, C. Frigo, and H. B. K. Boom, "Lower-extremity angle measurement with accelerometers - error and sensitivity analysis," *IEEE Transactions on Biomedical Engineering*, vol. 38, pp. 1186-1193, 1991.

[133] C. Broxmeyer, *Inertial Navigation Systems*: McGraw-Hill Book Company, 1964.

[134] G. E. Beck, *Navigation Systems*. London: Van Nostrand Reinhold, 1971.

[135] C. F. O'Donnell, *Inertial Navigation: Analysis and Design*: McGraw-Hill Book Company, 1964.

[136] H. J. Luinge, "Inertial sensing of human movement," PhD in *Computer Science,* University of Twente: Enschede, 2002

[137] P. H. Veltink, H. J. Luinge, B. J. Kooi, C. T. M. Baten, P. Slycke, W. Olthuis, and P. Bergveld, "The artificial vestibular system - design of a tri-axial inertial

sensor system and its application in the study of human movement," *Proceedings of the Symposium of the International Society for Postural and Gait Research (ISPG). Session: Perturbations of Gait and Posture*, 2001.

[138]   P. Terrier, Q. Ladetto, B. Merminod, and Y. Schutz, "High-precision satellite positioning system as a new tool to study the biomechanics of human locomotion," *Journal of Biomechanics*, vol. 33, pp. 1717-1722, 2000.

[139]   Q. Ladetto, V. Gabaglio, and J. Van Seeters, "Pedestrian navigation method and apparatus operative in a dead reckoning mode," Patent 6826477, US, Ecole Polytechnique Federale de Lausanne (EPFL), 2004.

[140]   Q. Ladetto and B. Merminod, "Digital magnetic compass and gyroscope integration for pedestrian navigation," *Proceedings of the 9th St. Petersburg International Conference on Integrated Navigation Systems*, Russia, 2002.

[141]   L. J. Hutchings, R. Gross, and S. Jarpe, "System and method for measuring movement of objects," Patent 6122960, US, Acceleron Technologies, LLC., 2000.

[142]   J. H. Waarsing, R. E. Mayagoitia, and P. H. Veltink, "Quantifying the stability of walking using accelerometers," *Proceedings of the 18th Annual IEEE International Conference of the Engineering in Medicine and Biology Society (EMBS)*, Amsterdam, 1996.

[143]   R. Moe-Nilssen, "Test-retest reliability of trunk accelerometry during standing and walking," *Archives of Physical Medicine and Rehabilitation*, vol. 79, pp. 1377-1385, 1998.

[144]   A. T. M. Willemsen, F. Bloemhof, and H. B. K. Boom, "Automatic stance-swing phase detection from accelerometer data for peroneal nerve-stimulation," *IEEE Transactions on Biomedical Engineering*, vol. 37, pp. 1201-1208, 1990.

[145]   I. P. I. Pappas, T. Keller, and M. R. Popovic, "Experimental evaluation of the gyroscope sensor used in new gait phase detection system," *Proceedings of the 4th Annual Conference of the International Functional Electrical Stimulation Society (IFESS)*, Sendai, Japan, 1999.

[146]   R. Bartlett, *Introduction to sports biomechanics*: E & FN Spon, 1997.

[147]   C. V. C. Bouten, A. Sauren, M. Verduin, and J. D. Janssen, "Effects of placement and orientation of body-fixed accelerometers on the assessment of energy expenditure during walking," *Medical and Biological Engineering and Computing*, vol. 35, pp. 50-56, 1997.

[148]   F. Ferraris, U. Grimaldi, and M. Parvis, "Procedure for effortless in-field calibration of three-axis gyros and accelerometers," *Sensors and Materials*, vol. 7, pp. 311-330, 1995.

[149]   G. L. Smidt, R. H. Deusinger, J. Arora, and J. P. Albright, "An automated accelerometry system for gait analysis," *Journal of Biomechanics*, vol. 10, pp. 367-375, 1977.

[150]   H. J. Busser, "Using piezoresistive accelerometers in posture and motion monitoring," *Proceedings of the 2nd World Congress of Biomechanics: Dynamic Analysis using Body Fixed Sensors*, Amsterdam, 1994.

[151]   W. L. J. Martens, "Exploring the information content and some applications of body-mounted piezo-resistive accelerometers," *Proceedings of the 2nd World Congress of Biomechanics: Dynamic Analysis using Body Fixed Sensors*, Amsterdam, 1994.

[152] W. Frey, "Application of inertial sensors and flux-gate magnetometer to real-time human body motion capture," master of science in *Computer Science*, Naval Postgraduate School, 1996

[153] W. deVries, M. P. Koper, P. H. Veltink, and B. F. J. M. Koopman, "Decomposition of accelerometer signals at the lower extremities into gravity and acceleration components during gait," *Proceedings of the 2nd World Congress of Biomechanics: Dynamic Analysis using Body Fixed Sensors*, Amsterdam, 1994.

[154] J. E. Bortz, "A new mathematical formulation for strapdown inertial navigation," *IEEE Transactions on Aerospace and Electronic Systems*, vol. 7, pp. 61-66, 1971.

[155] E. Foxlin, "An inertial head orientation tracker with automatic drift compensation to use with HMD's," *Proceedings of the Virtual Reality Software and Technology (VRST)*, Singapore, 1994.

[156] B. Barshan and H. F. Durrant-Whyte, "Inertial navigation systems for mobile robots," *IEEE Transactions on Robotics and Automation*, vol. 11, pp. 328-342, 1995.

[157] J. Vaganay, M. J. Aldon, and A. Fournier, "Mobile robot attitude estimation by fusion of inertial data," *Proceedings of the IEEE International Conference on Robotics and Automation*, 1993.

[158] R. Moe-Nilssen, "A new method for evaluating motor control in gait under real- life environmental conditions. Part 2: Gait analysis," *Clinical Biomechanics*, vol. 13, pp. 328-335, 1998.

[159] M. J. Caruso, T. Bratland, C. H. Smith, and R. Schneider, "Anisotropic magnetoresistive sensors theory and applications," Sensor magazine,1999,

[160] J. Reswick, D. Perry, D. Antonelli, N. Su, and C. Freeborn, "Preliminary evaluation of the vertical acceleration gait analyser (VAGA)," *Proceedings of the 6th Annual Symposium of Advances in External Control of Human Extremities*, 1978.

[161] G. Uswatte, W. H. R. Miltner, B. Foo, M. Varma, S. Moran, and E. Taub, "Objective measurement of functional upper-extremity movement using accelerometer recordings transformed with a threshold filter," *Stroke*, vol. 31, pp. 662-667, 2000.

[162] Stayhealthy: www.stayhealthy.com, 2005.

[163] MCRoberts: www.mcroberts.nl, cited July, 2005.

[164] IM Systems: www.imsystems.net, cited July, 2005.

[165] R. Dai, R. B. Stein, B. J. Andrews, K. B. James, and M. Wieler, "Application of tilt sensors in functional electrical stimulation," *IEEE Transactions on Rehabilitation Engineering*, vol. 4, pp. 63-71, 1996.

[166] X. Yun, E. R. Bachmann, A. Kavousanos-Kavousanakis, F. Yidiz, and R. B. McGhee, "Design and implementation of the MARG human body motion tracking system," *Proceedings of the IEEE International Conference on Intelligent Robots and Systems (RSJ)*, Sendai, Japan, 2004.

[167] E. R. Bachmann, R. B. McGhee, R. H. Whalen, R. Steven, R. G. Walker, J. R. Clynch, A. J. Healey, and X. Yun, "Evaluation of an integrated GPS/INS system for shallow-water AUV navigation (SANA)," *Proceedings of the IEEE SYmposium on Autonomous Underwater Vehicle Technology*, Monterey, CA, 1996.

[168] O. Perrin, P. Terrier, Q. Ladetto, B. Merminod, and Y. Schutz, "Improvement of walking speed prediction by acceleormetry and altimetry, validated by

satellite positioning," *Medical and Biological Engineering and Computing*, vol. 38, pp. 164-168, 2000.

[169] J. A. Paradiso, E. Hu, and K. Hsiao, "The cybershoe: a wireless multisensor interface for a dancer's feet," *Proceedings of the International Dance and Technology*, Tempe, Arizona, 1999.

[170] J. Doscher, "ADXL105: A lower noise, wider bandwidth accelerometer rivals performance of more expensive sensors," Analog Devices, www.analog.com, (cited May 2005) 1999.

[171] Honeywell: www.honeywell.com, cited July, 2005.

[172] KVH Industries, Inc: www.KVH.com, cited July, 2005.

[173] G. Wu and Z. Ladin, "The study of kinematic transients in locomotion using the integrated kinematic sensor," *IEEE Transactions on Rehabilitation Engineering*, vol. 4, pp. 193-200, 1996.

[174] Q. Ladetto, V. Gabaglio, and B. Merminod, "Combining gyroscopes, magnetic compass and GPS for pedestrian navigation," *Proceedings of the International Symposium on Kinematic Systems in Geody, Geometrics and Navigation (KIS)*, Banff, Canada, 2001.

[175] H. Rehbinder and X. Hu, "Drift-free attitude estimation for accelerated rigid bodies," *Proceedings of the IEEE International Conference on Robotics and Automation*, Seoul, Korea, 2001.

[176] W. H. Press, B. P. Flannery, S. A. Teukolsky, and W. T. Vetterling, *Numerical Recipes*: Cambridge University Press, 1986.

[177] H. J. Luinge and P. H. Veltink, "Inclination measurement of human movement using a 3-D accelerometer with autocalibration," *IEEE Transactions on Neural Systems and Rehabilitation Engineering*, vol. 12, pp. 112-121, 2004.

[178] C. Verplaetse, "Inertial proprioceptive devices: self motion sensing toys and tools," *IBM Systems Journal*, vol. 35, pp. 639-650, 1996.

[179] R. B. McGhee, E. R. Bachmann, and M. J. Zyda, "Rigid body dynamics, inertial reference frames and graphics coordinate systems: a resolution of conflicting conventions and terminology," Naval Postgraduate School, Technical report NPS-MV-01-002, 2000.

[180] J. M. Cooke, M. J. Zyda, D. R. Pratt, and R. B. McGhee, "NPSNET: Flight simulation dynamic modelling using quaternions," *Presence: Teleoperators and Virtual Environments*, vol. 1, pp. 404-420, 1992.

[181] D. Titterton and J. Weston, *Strapdown inertial navigation technology*, 2nd ed: IEE, 2004.

[182] A. A. Santiago, "Extended kalman filtering applied to a full accelerometer strapdown inertial measurement," masters of science in *Aeronautics and Astronautics*, Massachusetts Institute of Technology (MIT): Massachusetts, 1992.pp. 114

[183] J. B. Kuipers, *Quaternions and rotation sequences: a primer with applications to orbits, aerospace and virtual reality*. New Jersey, US: Princeton University Press, 1998.

[184] J. Craig, *Introduction to robotics mechanics and control*: Addison-Wesley, 1989.

[185] S. Emura and S. Tachi, "Sensor fusion based measurement of human head motion," *Proceedings of the 3rd IEEE International Workshop on Robot and Human Communication*, Nagoya, 1994.

[186] E. R. Bachmann, I. Duman, U. Y. Usta, R. B. McGhee, X. Yun, and M. J. Zyda, "Orientation tracking for humans and robots using inertial sensors,"

Proceedings of the Symposium on Computational Intelligence in Robotics and Automation, Monterey, US, 1999.

[187] J. L. Marins, X. Yun, E. R. Bachmann, R. B. McGhee, and M. J. Zyda, "An extended kalman filter for quaternion-based orientation estimation using MARG sensors," *Proceedings of the IEEE International Conference on Intelligent Robots and Systems (RSJ)*, Maui, Hawaii, 2001.

[188] R. G. Brown and P. Y. C. Hwang, *Introduction to Random Signals and Applied Kalman Filtering*, Second ed: John Wiley & Sons, Inc, 1992.

[189] M. S. Grewal and A. P. Andrews, *Kalman filtering: theory and practice using MATLAB*: John Wiley & Sons, 2001.

[190] M. S. Grewal, L. R. Weill, and A. P. Andrews, *Global positioning systems, inertial navigation, and integration*: John Wiley & Sons, 2001.

[191] J. M. Roberts, P. I. Corke, and G. Buskey, "Low-cost flight control system for a small autonomous helicopter," *Proceedings of the Australasian Conference on Robotics and Automation*, Auckland, 2002.

[192] G. Wu and Z. Ladin, "The kinematometer - an integrated kinematic sensor for kinesiological measurements," *Journal of Biomechanical Engineering*, vol. 115, pp. 53-62, 1993.

[193] msi sensors: www.msiusa.com/sensors/acceleration_ac.asp, cited June, 2005.

[194] G. Kulwanoski and J. Schnellinger, "The principles of piezoelectric accelerometers," Sensors,2004,

[195] Entran: www.entran.com/egax.htm, cited June, 2005.

[196] H. Xie and G. K. Fedder, "Integrated microelectromaechnaical gyroscopes," *Journal of Aerospace Engineering*, vol. 16, pp. 65-75, 2003.

[197] S. Nasiri, "A critical review of MEMS gyroscopes technology and commercialization status," Invensense www.invensense.com 2003.

[198] A. M. Madni, "A micromachined quartz angular rate sensor for automotive and advanced inertial applications," Sensors,1999,

[199] NEC/Tokin: www.nec-tokin.com/english/, cited June, 2005.

[200] Bosch: www.europractice.bosch.com/en/mst/, cited June, 2005.

[201] Silicon Sensing Systems: www.spp.co.jp/sssj/silicon-e.html, cited June, 2005.

[202] Analog Devices: www.analog.com/UploadedFiles/Data_Sheets/732884779ADXRS300_b.pdf, cited July, 2005.

[203] F. Ayazi and K. Najafi, "Design and fabrication of a high-performance polysilicon vibrating ring gyroscope," *Proceedings of the 11th IEEE International Workshop on Micro Electro Mechanical Systems*, Heidelberg, Germany, 1998.

[204] S. Tanaka, Y. Mochida, S. Sugimoto, K. Moriya, T. Hasegawa, K. Atsuchi, and K. Ohwada, "A micromachined vibrating gyroscope," *Proceedings of the Proceedings of the Eighth IEEE International Conference on Micro Electro Mechanical Systems (MEMS)*, Amsterdam, Netherlands, 1995.

[205] Operation Manual of Gyrostar: www.murata-europe.com/, (cited June 2005), 1999.

[206] G. J. Borse, *Numerical methods with MATLAB. A resource for scientists and engineers*. Boston: PWS Publishing Company, 1997.

[207] P. M. Whelan and M. J. Hodgson, *Essential Principles of Physics*, 2nd ed: BPCC Hazell Books, 1987.

[208] J. Crawshaw and J. Chambers, *A concise course in A level statistics*, 3rd ed: Stanley Thornes (Publishing) Ltd, 1994.

[209] N. P. Linthorne, "Analysis of standing vertical jumps using a froce platform," *American Journal of Physics*, vol. 69, pp. 1198-1204, 2001.

[210] Kistler: www.kistler.com/mediaaccess/9287B___000-159m-07.00.pdf, cited June, 2005.

[211] M. F. Bobbert, H. C. Schamhardt, and B. M. Nigg, "Calculation of vertical ground reaction force estimates during running from positional data," *Journal of Biomechanics*, vol. 24, pp. 1095-1105, 1991.

[212] J. A. DeLisa, "Gait analysis in the science of rehabilitation," Department of Veteran Affairs Research and Development http://www.vard.org/mono/gait/soutas.htm, (cited June 2005), 1998.

[213] Kionix: www.kionix.com/Product%20Sheets/KGF01%20Series.pdf, cited July, 2005.

[214] Silicon Sensing: www.siliconsensing.com/, cited July, 2005.

[215] Bosch GmbH (InvenSense): www.invensense.com/Products.html, cited July, 2005.

[216] VARTA: www.varta-microbattery.com/en/mb_data/documents/printing_material_oem/FOLDER_P oLiFlex_en.pdf, cited July, 2005.

[217] W. W. Manges, G. O. Allgood, and S. F. Smith, "It's time for sensors to go wireless. Part 1: technological underpinnings," Sensors Magazine,1999,

[218] A. Mero, P. V. Komi, and R. J. Gregor, "Biomechanics of sprint running," *Sports Medicine*, vol. 13, pp. 376-392, 1992.

[219] P. Luhtanen and P. V. Komi, "Mechanical factors influencing running speed," in *Biomechanics VI-B*, E. Asmussen and K. Jorgensen, Eds. Baltimore, Maryland: University Park Press, 1977, pp. 23-29.

[220] P. Moravec, J. Ruzicka, P. Susanka, E. Dostal, M. Kodejs, and M. Nosek, "The 1987 international athletic foundation/IAAF scientific project report: time analysis of the 100 metres events at the 2nd world championships in athletics," *New Studies in Athletics*, vol. 3, pp. 61-96, 1988.

[221] M. Ae, A. Ito, and M. Suzuki, "The men's 100 metres," *New Studies in Athletics*, vol. 7, pp. 47-52, 1992.

[222] R. Mann, "Biomechanical analysis of the elite sprinter and hurdler," in *The Elite Athlete*, N. K. Butts, T. T. Gushiken, and B. Zarins, Eds.: Spectrum Publications, 1985, pp. 43-80.

[223] H. Kunz and D. A. Kaufmann, "Biomechanical analysis of sprinting: decathletes versus champions," *British Journal of Sports Medicine*, vol. 15, pp. 177-181, 1981.

[224] L. E. Armstrong and S. M. Cooksey, "Biomechanical changes in selected collegiate sprinters due to increases velocity," *Track and Field Quarterly Review*, vol. Summer, pp. 10-14, 1983.

[225] R. Mann and J. Herman, "Kinematic analysis of olympic sprint performance: men's 200 metres," *International Journal of Sport Biomechanics*, vol. 1, pp. 151-162, 1985.

[226] W. Sinning and H. Forsyth, "Lower limb actions whilst running at different velocities," *Medicine and Science in Sports*, vol. 2, pp. 38-43, 1970.

Appendix A: PCB Layouts and circuits

In this appendix, the PCB layouts for boards 1 and 2 that comprise the inertial sensor system are presented. These circuits along with the schematics displayed in chapter 3 are constructed using the package, Easy PC.
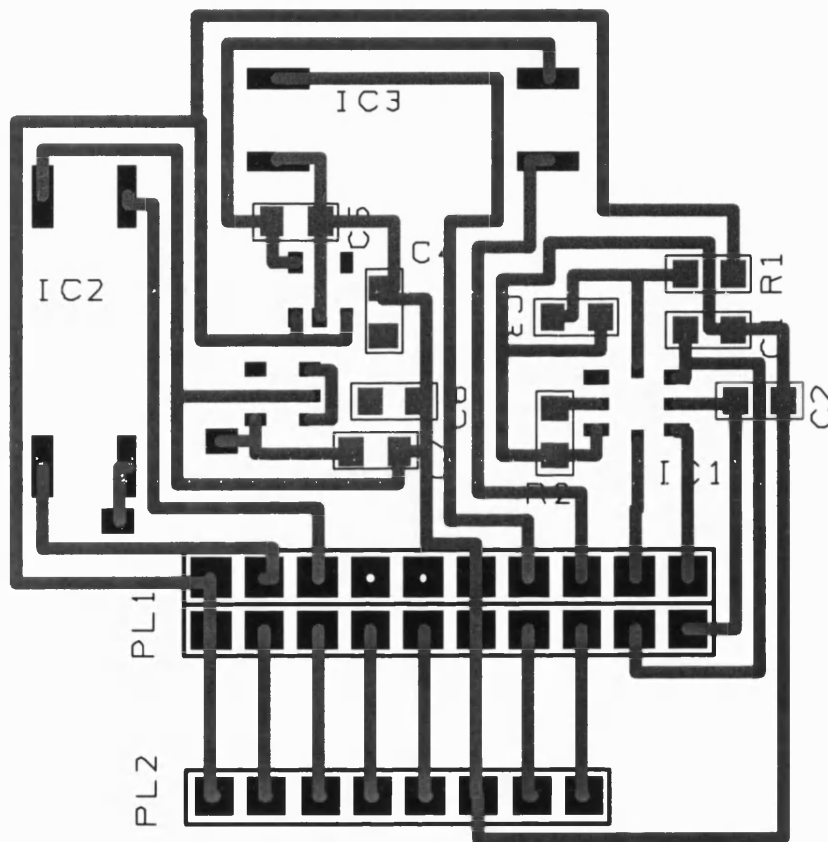

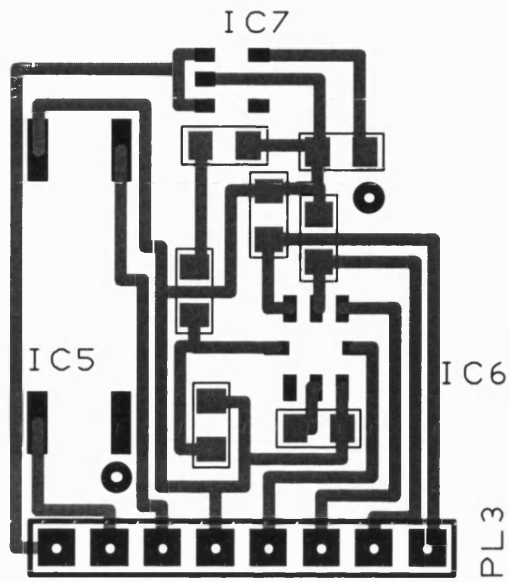**Figure A- 1 PCB layout for Board 1 (not actual size)**
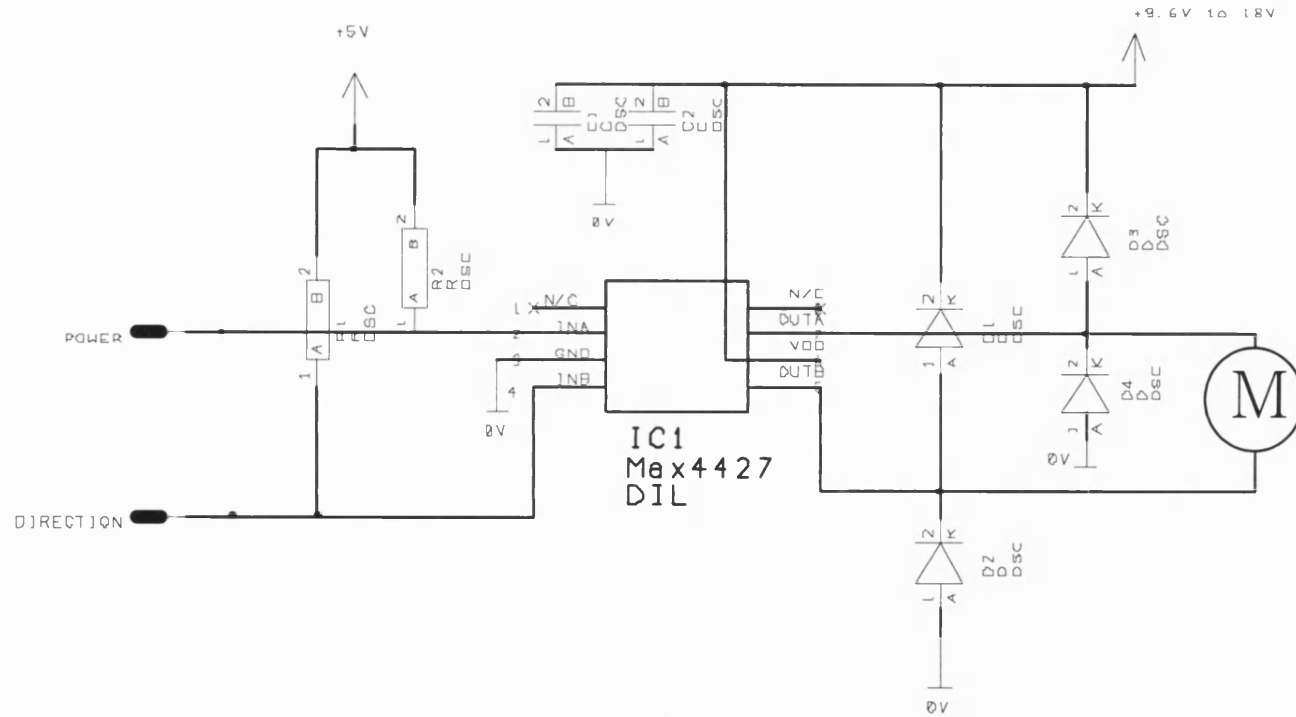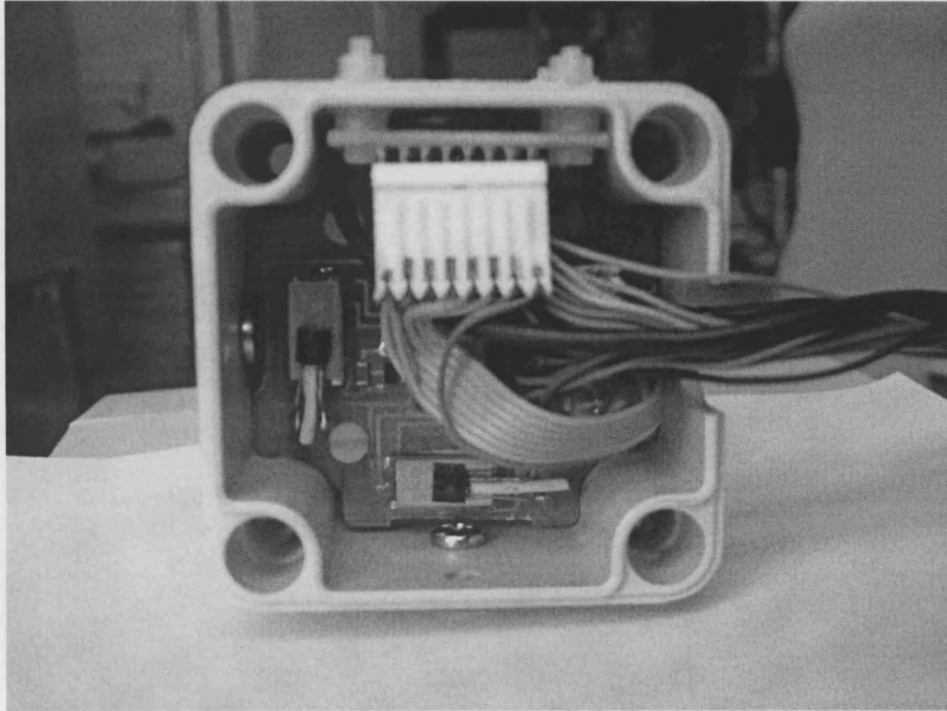
Figure A- 2 PCB layout for board 2 (not actual size)

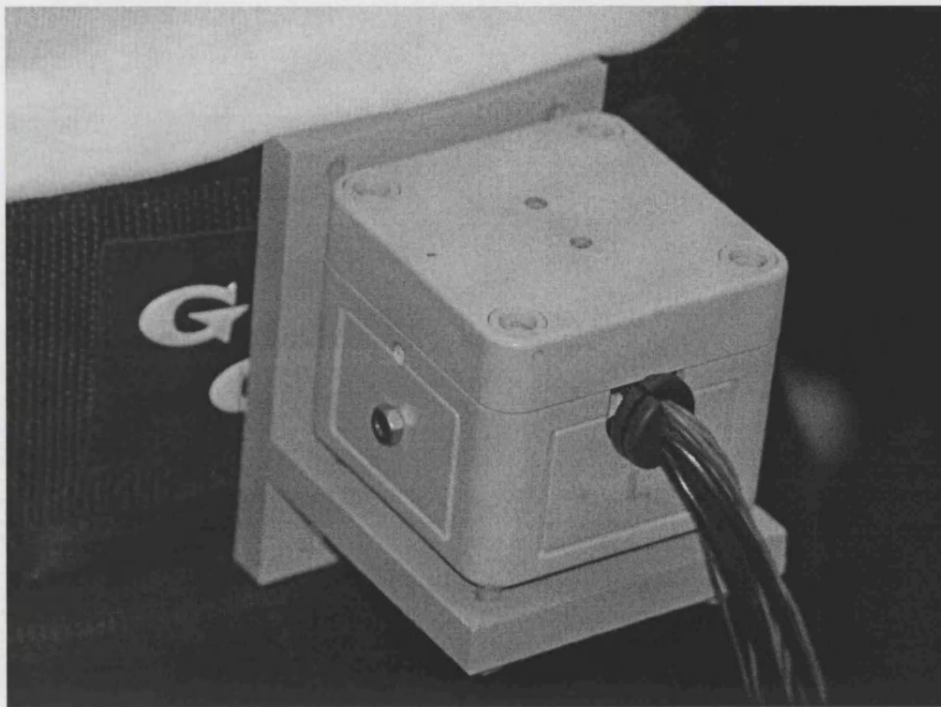**Figure A- 3 H Bridge MOSFET Driver Circuit**

Appendix B Photo Gallery

In this appendix, a collection of photographs of the inertial sensor system is presented.
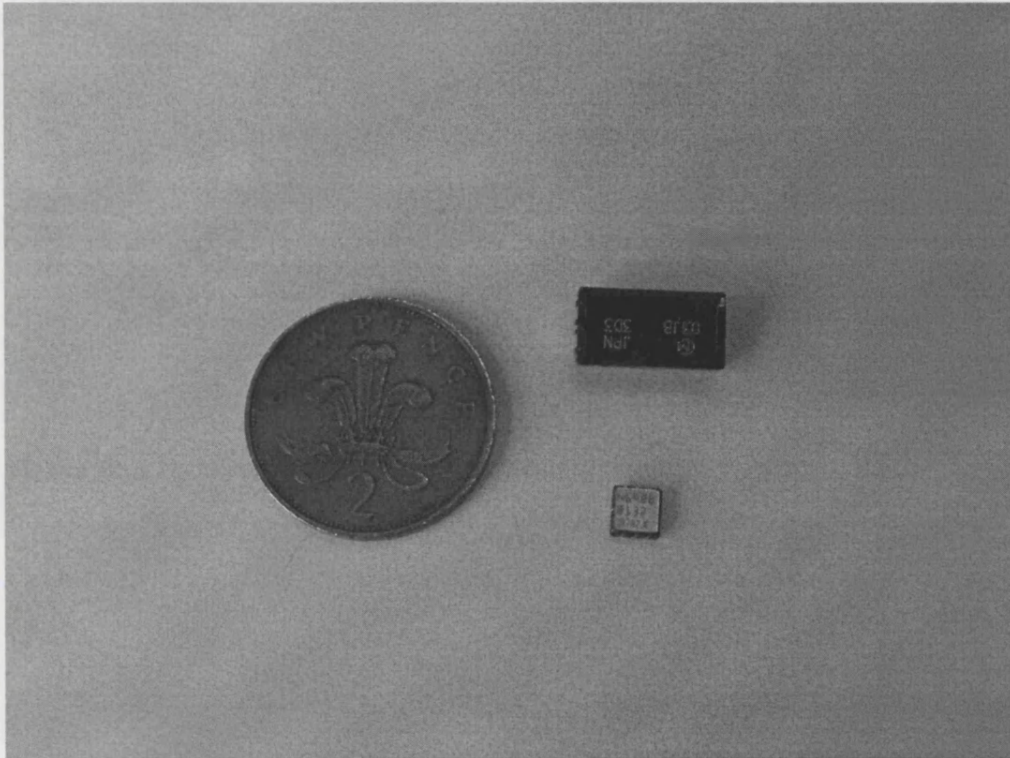
Figure B- 1 The inertial sensors used in the inertial sensor system. At the top is the gyroscope (Murata) and underneath is the accelerometer (Analog Devices)
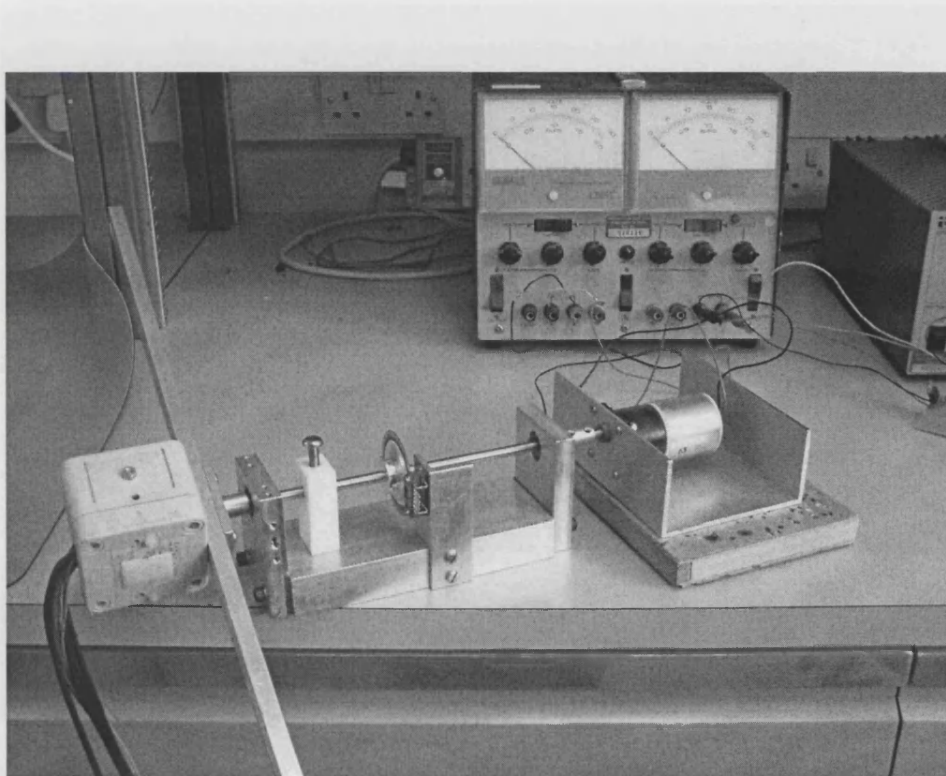
Figure B- 2 Inside the inertial sensor system

Figure B- 3 The casing of the inertial sensor system and the method of attachment to the T-shaped plastic and then onto the belt.
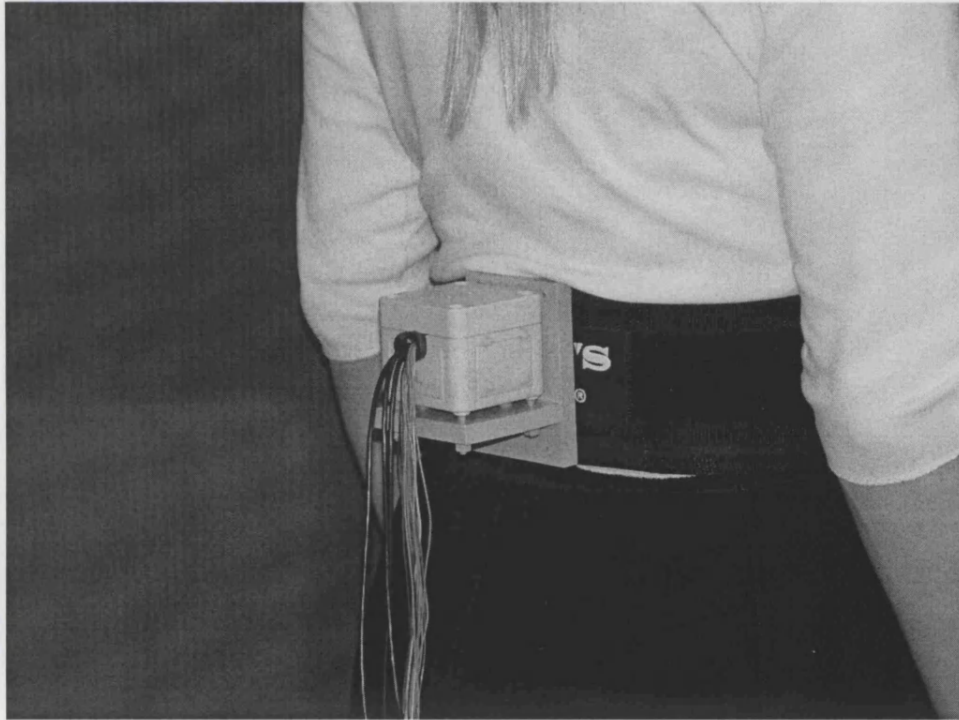
Figure B- 4 The point of attachment (assumed representative point of the CoM) of the inertial sensor system.
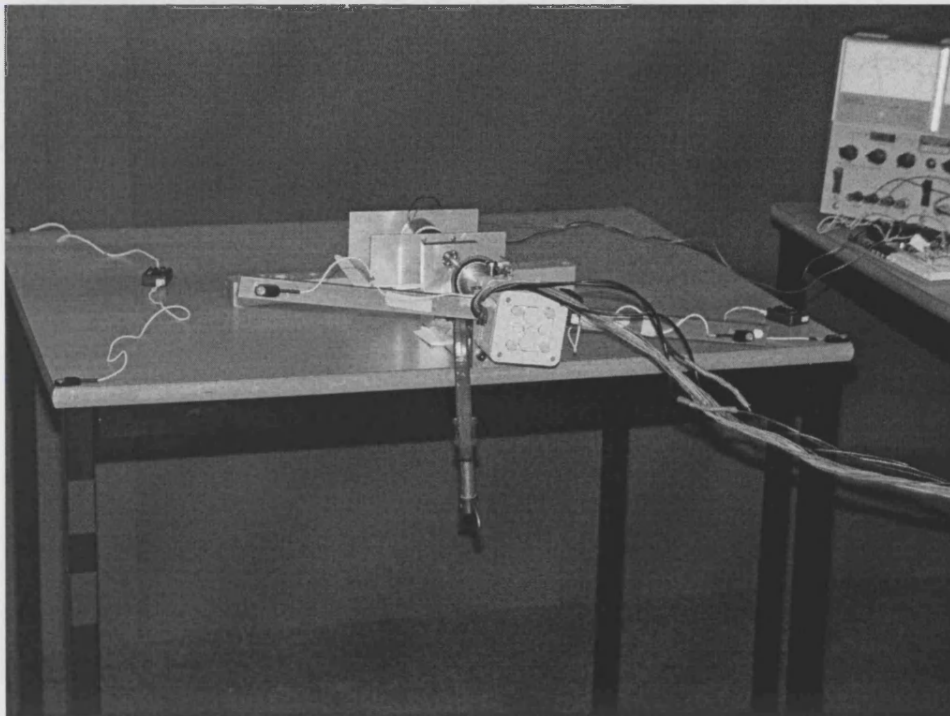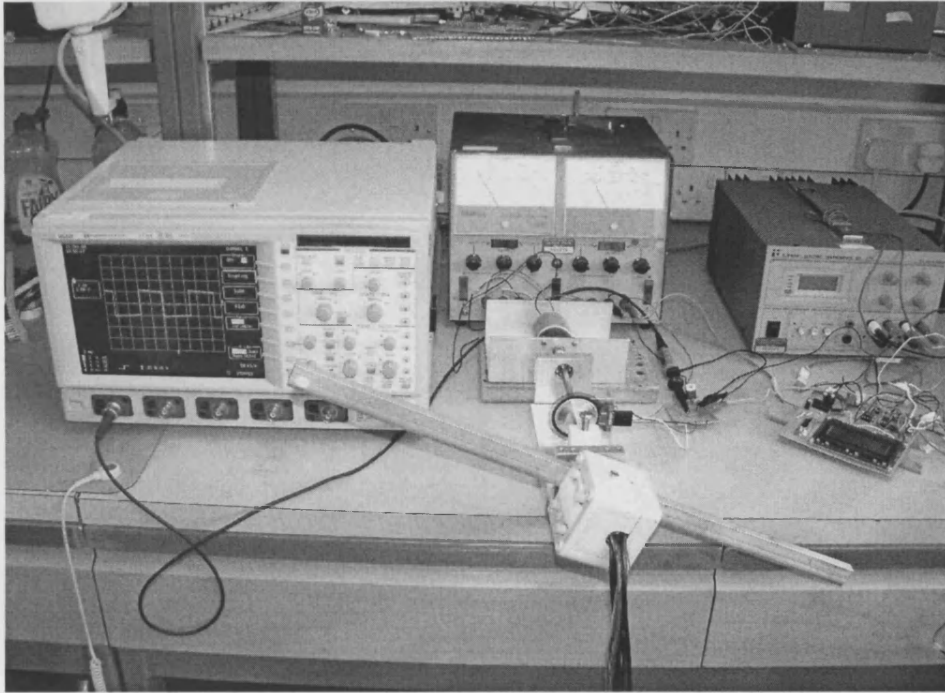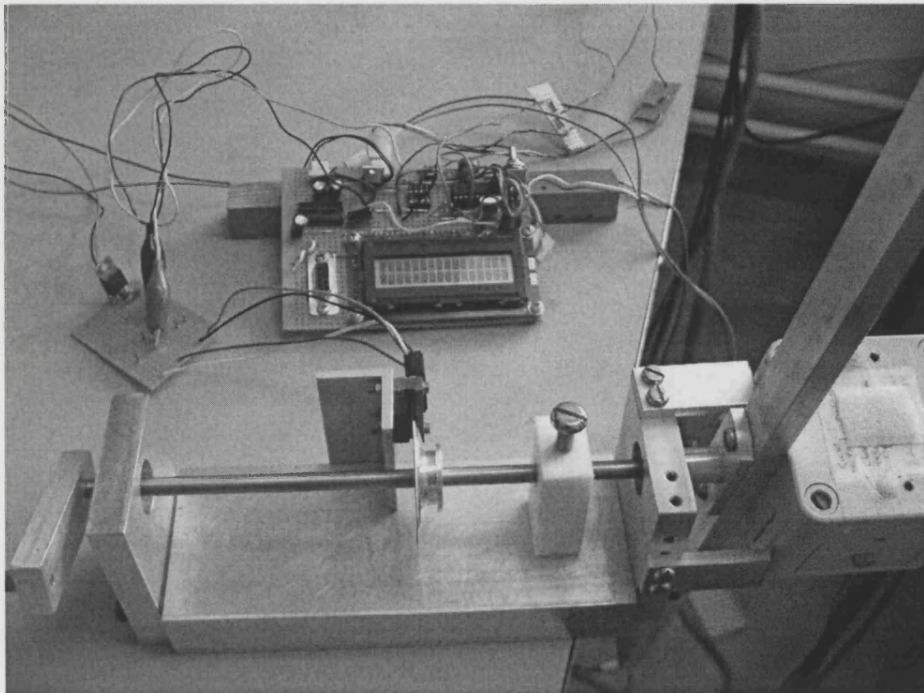

Figure B- 5 The rotating arm mechanism.
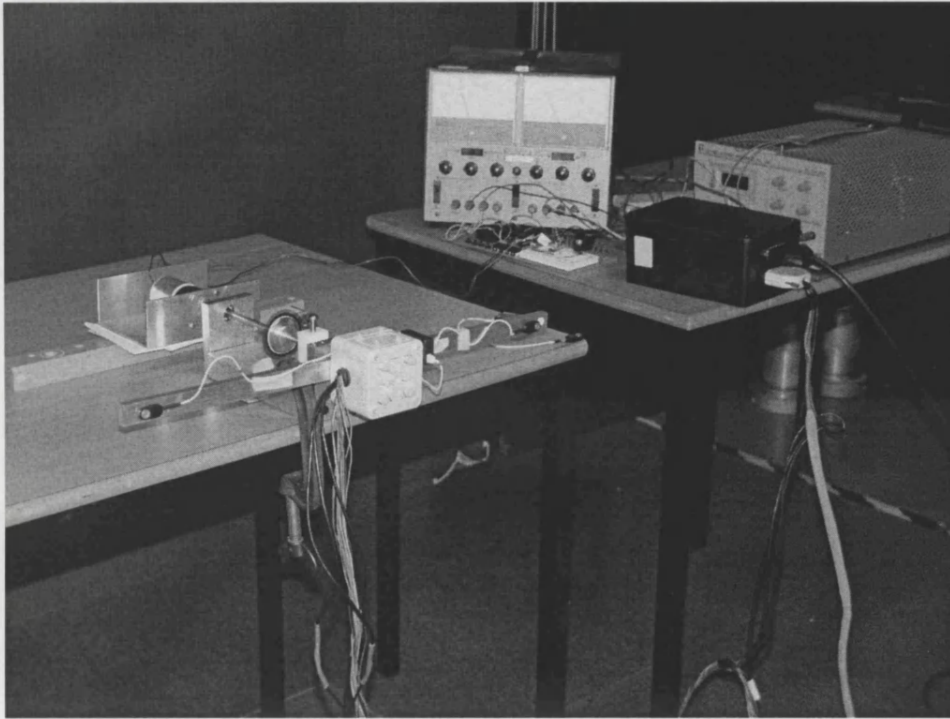
Figure B- 6 The calibration experiment.

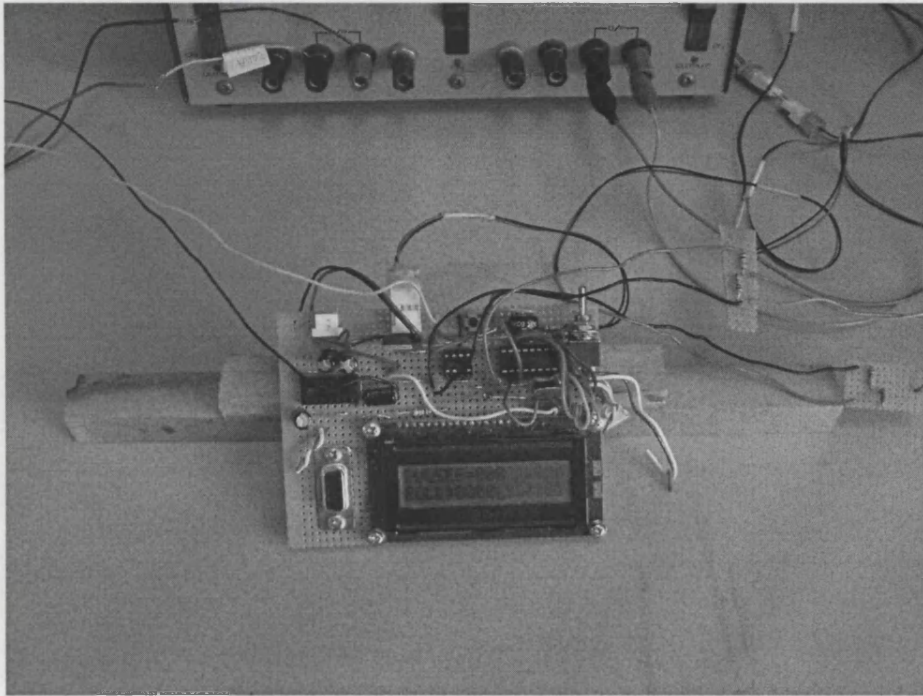**Figure B- 7 The positions of the CODA markers during the calibration Experiment.**

Figure B- 8 The verification experiment to validate the gyroscope scale factors.

Figure B- 9 The verification experiment to validate the angle estimates from the
accelerometers and gyroscopes. The stoppers have been added to
restrict the movement of the arm.

Figure B- 10 A close-up of the PIC pulse counter circuit.

Figure B- 11 A simulation of the running experiments conducted in the
Biomechanics Laboratory over the Force plate.

Figure B- 12 The running experiments on the track.